INFRARED STUDIES OF CLASSICAL NOVAE AND THE RECURRENT NOVA RS OPHIUCHI.

CATERINA MARIA CALLUS

SUBMITTED FOR THE DEGREE OF DOCTOR OF PHILOSOPHY

1987

ACKNOWLEDGEMENTS.

There are lots of people too numerous to mention that have helped me with this thesis whom I would like to thank (I'm sure you know who you are). However there are two people without whom I would not have even got past the first page. They are my supervisor Dr. A. Evans and my husband Steve: thank you.

ABSTRACT

This work is concerned with new observations, within the 1-100μm infrared wavelength range, of novae and with models to explain these and existing observations of these objects.

The first half is concerned with the classical novae. Some of these objects have long been known to be copious producers of dust during outburst. We investigate a possible formation mechanism for this dust - namely nucleation on ions, and we discuss whether such a model can reproduce the observational characteristics of individual novae. IRAS observations of classical novae are also reported. Together with the available ground based observations of these objects the IRAS observations provide valuable information on the nature of such novae. The infrared observations of the nova GQ Mus 1983 are interpreted in terms of free-free radiation from a freely expanding gas shell and a model is constructed in an attempt to reproduce these observations.

The second half is concerned with RS Ophiuchi. This star is a recurrent nova that has undergone five recorded outbursts, the most recent in 1985 January. Extensive photometric and spectroscopic infrared observations were taken during this outburst. These are presented and we attempt to model the observations in terms of a gas shell expanding into a preoutburst circumstellar envelope of material, presumably formed by the wind of the secondary star.

INFRARED STUDIES OF CLASSICAL NOVAE AND THE RECURRENT NOVA RS OPHIUCHI.

CHAPTER 1

CHARACTERISTICS OF NOVAE

1.1 Introduction

The term 'nova' in its broadest definition applies to a star that rapidly undergoes an increase in brightness. This encompasses a whole range of objects from supernovae (those objects possessing the greatest luminosity at maximum) to the dwarf novae (those which possess the least luminosity at maximum). This work is concerned with the classical novae and the recurrent nova RS Ophiuchi. A classical nova is one in which the luminosity may increase by 10 mags or more. It is thought that these novae are members of close binary systems, the primary being a white dwarf star and the secondary being a late type main sequence star (Williams, 1981). About 10 - 15 classical novae are thought to occur each year in our galaxy and they are thought to recur every 10^5 years or so. Recurrent novae, on the other hand, tend not to have as large an outburst amplitude as classical novae, contain (at least the majority do) a late type giant as their secondary and have recurrence times of 10 - 15 years. There are about 6 recurrent novae known in our galaxy.

In the remainder of this chapter we will describe the observational characteristics of classical and recurrent novae and briefly consider the theories concerning the nature of these objects.

1.1.1 Speed Class

The speed class of a nova is defined as the time taken to decline through a specified number of magnitudes from maximum brightness (usually 2 or 3) in magnitudes per day. Payne-Gaposchkin (1957) classifies nova speed class in terms of the rate of decline through 2 mags (see Table 1.1) whilst McLaughlin (1960) defines speed class in terms of the rate of decline

through 3 mags (see Table 1.2).

The speed class of a nova is often used as the initial means of differentiating between types of novae.

1.2 Observational Characteristics of Novae

The light curve and spectrum is individual to each nova, but there are particular stages of development that all novae will go through in one form or another.

1.2.1 The Light Curve

McLaughlin (1960), in his classic paper on novae described a very general light curve for these objects. He divided the light curve up into nine segments (noting that for some of the faster novae it was difficult to distinguish between each segment of nova development). Fig. 1.1 shows these nine segments (this work was based on the earlier work of Payne-Gaposchkin). The nine segments he identified were:

1. The prenova stage. The star may be constant in light for many years or may vary irregularly through 1 or 2 mags (RR Pic 1925 had constant brightness whilst the recurrent nova T Pyx was variable). On the other hand some stars (e.g. V533 Her 1963, LV Vul 1968 and V1500 Cyg 1975) showed a significant rise in brightness for 1 to 5 years prior to the outburst.

2. The initial rise. Brightening from minimum to ~ 2 mags below maximum takes place within 2 or 3 days even for slow novae. V1500 Cyg, a very fast nova, completed this intial rise in less than a day.

3. Pre-maximum halt. In many novae, about 2 mags below maximum, the brightening may cease and there is a pause ranging from a few hours in fast novae to a few days in slow novae. Novae have even been known to fade during this stage. The nova V603 Aql 1918 exhibited a pause 2.2 mags below maximum.

Table 1.1

Definition of nova speed class.

Speed Class	Definition	Rate of Decline (mag d^{-1})
Very fast	2 mags in $\leq$ 10 days	> 0.2
Fast	2 mags in 11 - 25 days	0.18 - 0.08
Medium fast	2 mags in 26 - 80 days	0.07 - 0.025
Slow	2 mags in 81 - 150 days	0.024 - 0.013
Very slow	2 mags in 151 - 250 days	0.013 - 0.008

Reproduced from Payne-Gaposchkin (1957).

Table 1.2

Definition of nova speed class in terms of t_3.

Speed Class	t_3	Rate of Decline (mag d^{-1})
Very fast	12 days	> 0.25
Fast	30 days	0.10
Slow	100 days	0.03

t_3 is time taken to decline through 3 mags from maximum.

Reproduced from McLaughlin (1960).

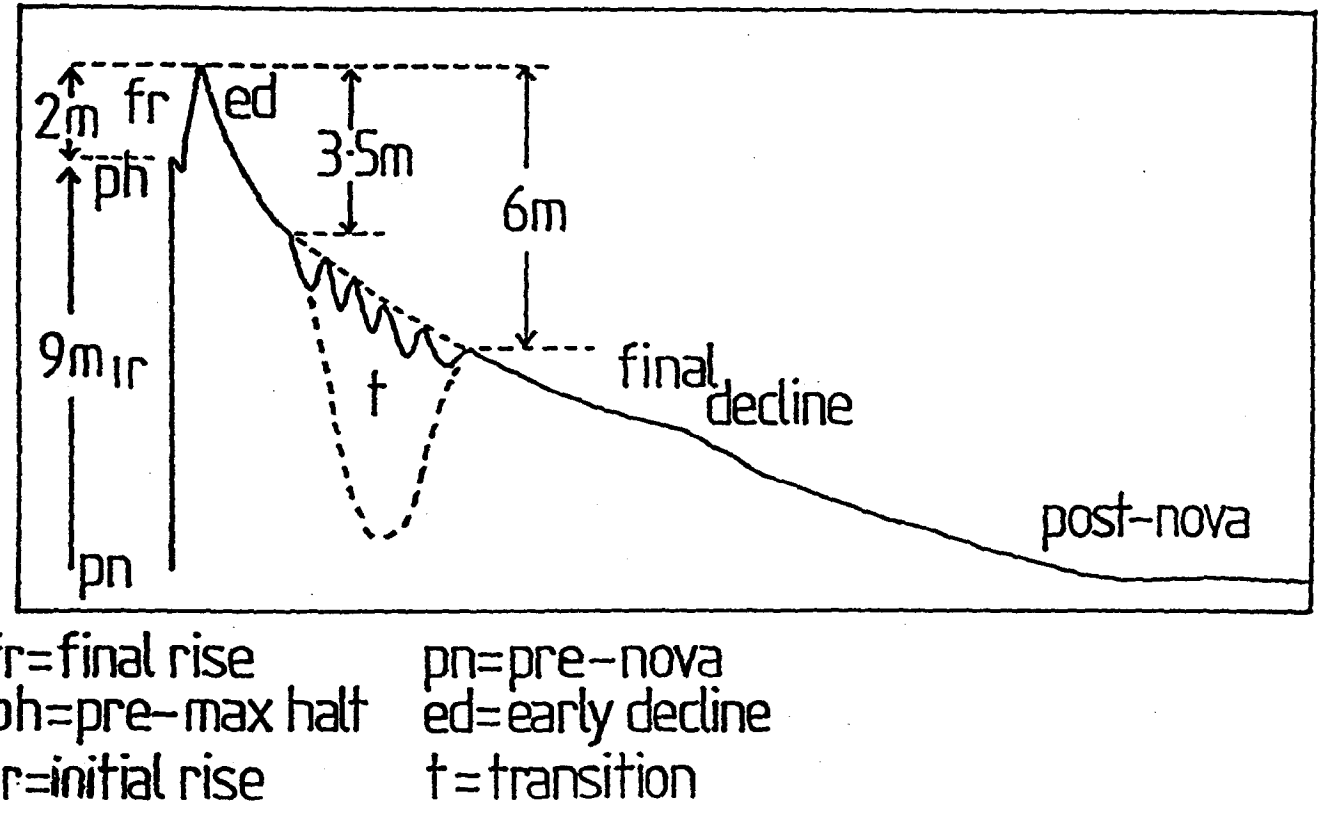

Figure 1.1. Schematic light-curve of a nova. Three types of behaviour during the transition are illustrated. Reproduced from McLaughlin (1960).

4. The final rise. The star again brightens reaching (visual) maximum in 1 day for fast novae and several weeks for the slowest. (The fast nova CP Lac 1936 went through this stage in 1.4 days).

5. Maximum. The principal rise of a fast nova lasts only a few hours or at the most 1 day. Even slow novae tend to last at maximum for only a few days.

6. Early decline. The most rapid novae fade rather smoothly through 3 or 4 mags whilst the slower usually show oscillations of brightness of a few tenths of a magnitude. The slowest novae show variations on timescales 1 - 20 days and amplitudes up to 2 mags. A smooth decline was shown by the novae CP Lau and XX Tau 1927, whilst DQ Her 1934 exhibited an oscillatory behaviour.

7. Transition. It is when the novae are about 3 - 4 mags below maximum light that they show the greatest variation in behaviour. The light may fade smoothly or strong oscillations may occur. Finally in this transition region a deep minimum of light may occur ranging from 1 to several mags, followed by a recovery after several weeks. The transition phase ends with the completion of the recovery or the stopping of the strong fluctuations at about 6 - 7 mags below maximum. The nova DQ Her exhibited a deep minimum, V476 Cyg 1920 showed a change of slope in its light curve at this stage and GK Per 1901 underwent large oscillations.

8. The final decline. After transition most novae will decline smoothly to minimum light. If there are any fluctuations in the light curve these will be smooth.

9. The postnova. This stage is equivalent (in most cases) to the prenova stage, in that some stars remain constant after reaching minimum and others vary irregularly through a few mags (CP Lac showed constant brightness at this stage whilst GK Per was variable).

1.2.2 Spectral Developement

As with the light curve, the spectral development of all novae follow the same basic stages. Payne-Gaposhkin (1957), McLaughlin (1960) and Hoffmeister (1985) have extensively described these stages in the optical whilst Friedjung (1987) and Kitchin (1982) describe the ultraviolet counterpart to such development; their work is summarized below. The spectral evolution of novae is usually divided into six stages but each stage begins before the end of the previous one, so that several spectral states can exist simultaneously.

1. The premaximum spectrum. The spectra of the novae that have been obtained premaximum (usually around the time of the premaximum halt) are strongly dominated by blue-shifted broad diffuse absorption lines. These lines can be displaced by upto 1000 km s^{-1} to shorter wavelengths due to the Doppler effect. Spectral types at this stage are usually in the range B-F with the earliest spectral type observed being B0 for V1500 Cyg 1975 and the latest F2 for the nova RR Pic 1925. In these spectra the lines of carbon, nitrogen, and oxygen are much stronger than those in normal supergiant spectra, which is probably due to the overabundance of these elements (see section 1.3.1). Helium may also be overabundant when compared to the cosmic value. V1668 Cyg 1978 was caught before maximum in the ultraviolet (Kitchin, 1982). Its spectra show that the flux falls very steeply to shorter wavelengths, and that the main features are due to neutral, singly and doubly ionized metals. This premaximum stage lasts at most a few days until shortly after peak luminosity when it disappears. Such premaximum spectra have been interpreted as a phase of uniform expansion of an optically thick cooling envelope.

2. Maximum (or Principal) spectrum. This spectrum appears at maximum visual light, and resembles that of the supergiants of class A-F with enhancements of carbon, nitrogen and oxygen, although the nova Vl148 Sgr 1943 possessed a K type spectrum. This spectrum is again displaced to shorter wavelengths and possesses a greater negative velocity than the premaximum spectrum. The faster novae have velocities of ~ - 1300 km s^{-1} and the slowest have velocities of ~ -350 km s^{-1}. At maximum this spectrum consists of a system of bright (emission) lines widened symmetrically about their rest positions and flanked on their violet sides by strong absorption lines i.e. a P Cygni structure. The strongest lines are those of hydrogen, CaII, NaI and FeII in the optical whilst in the ultraviolet most emission lines arise from the resonance and lowest lying intercombination lines connected to the ground states of the abundant elements. The spectrum at wavelengths less than 2000A is very faint. A few days after maximum the continuum diminishes rapidly in intensity and emission lines of [OI] and [NII], followed by [OIII], dominate the optical spectrum. In the ultraviolet lines of MgII and FeII appear. The physical explanation of this spectrum concerns the further expansion of the shell of ejected material. The approaching half of the shell gives rise to the violet wing of the lines and the receding portion to the red wing, while those parts that are moving tangentially to the observer produce the peak emission. The emission features are wide because they arise from the whole of the still transparent, but expanding, shell. When this shell becomes tenuous enough the density is such that the forbidden lines can then appear.

3. Diffuse enhanced spectrum. When the star has faded by ~ 1 mag over a period of 1 - 20 days (for fast to slow novae) a third absorption system appears although the maximum spectrum is still prominent. The lines are displaced to shorter wavelengths by about twice the velocity of the displacement of the maximum spectrum, ranging from ~ 2300 km s^{-1} in fast novae to ~ 800 km s^{-1} in the slowest ones. The lines are usually wide and

diffuse at first and are due mainly to hydrogen, CaII, MgII, FeII, NaI and OI (with maybe TiII and CrII); these lines later intensify and become narrower. Again P Cygni profiles are common - those of the diffuse enhanced system underlying those of the principal spectrum. This stage in spectral development usually lasts for about 2 weeks in very fast novae and can last for more than 100 days in the slowest ones. After this the lines fade and often, in a few days (a time less than or equal to t_3) they disappear. This spectrum is thought to be the result of strong turbulence in the expanding gas cloud.

4. Orion spectrum. This spectrum appears as the enhanced spectrum reaches its maximum and usually when the nova has declined ~ 2 mags from maximum light. It is so named as this spectrum closely resembles that of the 'Orion stars' i.e. the class B stars that are found in the Orion association. Thus the spectrum consists of the absorption lines of HeI, OII, NII and CII which are diffuse in character, and also wide and diffuse emission lines which are most prominent at subsidiary minima in the light curve; in addition the Balmer series of hydrogen is missing. The velocities characteristic for this spectrum are ~ -3000 km s^{-1} in the fast novae to ~ -800 km s^{-1} in the slowest. Hence in most cases the lines are shifted to greater values than in the diffuse enhanced spectrum. These velocities become even greater before the Orion spectrum disappears just after transition. The trend throughout this spectrum is for the excitation and the ionization to increase with time. The emission lines associated with this spectrum are broad and grow in relative prominence as the nova declines and the other absorption systems decrease in strength. However the most noticeable characteristic of this Orion spectrum is that during this stage the emission of some elements become extremely strong giving rise to 'flashes' or 'flares'. Nitrogen flaring, the '4640', stage is the best example of this exceptional line enhancement. It involves the rapid brightening of the NIII multiplet at 4640A as well as other NII and NIII

lines, and appears midway during the Orion stage, often lasting into the next stage of spectral development. This is thought to be caused by L_β trapping and resonance fluorescence and is more common in the faster novae.

5. Nebular spectrum. During the end of the Orion stage any residual of the principal spectrum weakens steadily, although the associated bright lines appear strong as the continuum fades. When the last absorption lines are gone and the emission lines of NIII near 4101A and 4640A are prominent the nebular lines of [OIII], followed by [NeIII], make their appearance and strengthen relatively to the permitted lines. This is the 'nebular stage' of spectral development as now the spectrum closely resembles that of a planetary nebula except for the large Doppler broadening of its lines. In the optical there are emission lines of hydrogen, HeI, HeII and some forbidden lines all having the same width as the absorption lines in the principal stage. In the ultraviolet intercombination lines of OIII], OIV], NIII] and CIII] are important together with lines of NV, CIV, [FeVIII], [FeX], [FeXI] and [SVIII]. In the infrared, HeI, OI and [OII] lines appear along with the strong OI 8446A emission that is thought to arise through selective fluorescence with the L_β line. This spectral stage arises when the gaseous shell ejected by the nova has dissipated sufficiently. The very high levels of ionization are thought to be caused by gas that has been shocked to a temperature of $\sim 10^6$K by supersonic chaotic motions as in the case of V1500 Cyg, or by the expansion of a photoionized expanding shell as seen in nova CrA 1981. This stage usually lasts until the transition stage is past.

6. Postnova spectrum. When the nova is in its final decline to minimum light the nebular spectrum fades with the bright lines weakening more rapidly than the continuum. In a few cases some nebular lines are still visible in the early postnova spectrum as with the novae DQ Her and GK Per, and lines of hydrogen and HeII may persist for many years. Near minimum, as with the prenova stage, the spectrum exhibits an early spectral type

indicating a high stellar temperature. Table 1.3 combines the light curve and spectral development of a typical nova.

1.3 The Physics of the Outburst

Before going on to describe the currently held views on the physical reasons for the nova outburst some earlier ideas, purely of historical interest, will be mentioned. One of the first ideas was that the outburst was caused by the passage of a very faint or dark star through a dense cloud of interstellar medium, thus causing the rapid heating of the outer layers of the star to incandescence (Seeliger, 1892). This idea was supported by the appearance of most novae along the boundaries of the Milkly Way where cosmic dust clouds were expected. However as this is the easiest part of the sky for us to observe we would expect the majority of novae to be seen here. Another theory attempting to explain the outburst was the head on collision between two faint or dark bodies which resulted in the total destruction of the two stars. This theory was discounted when it was realised that the probability of two such objects colliding was extremely small (Glasby, 1968). Massive meteorites plunging into the atmosphere of a dim star could also produce the required effect (Stratton, 1928); however calculations showed that the total mass of such a meteor swarm would have to be exceptionally high to reproduce the observations.

Finally explanations of the nova phenomenon were developed that related to the stars' constitution rather than any external influence. Biermann (1939) regarded the prenova as a hydrogen poor subdwarf that had contraction as its main source of energy and attributed the outburst to the release of energy from ionization in a zone of instability. In this model 10% of the stars mass is ejected thus producing the required energy; however this mass seems too large and the requirement of hydrogen deficiency is probably not fulfilled. Hoyle (1946, 1947) considered the rotational instability of a star as a means of producing the outburst.

Table 1.3

Absorption and emission systems in novae.

Absorption System	Emission System	Duration mags. from max.	Part of Light-Curve
Premaximum	Premaximum	*	Rise (early decline).
Principal	Principal	0.6 - 4.1	Early decline
Diffuse enhanced	Diffuse enhanced	1.2 - 3.0	Early decline
Orion	Orion (hazy bands)	2.1 - 3.3	Early decline
Nitrogen (Orion)	'4640' (Orion)	3.0 - 4.5	Transition
	Nebular (principal)	4.0 - 11	Transition to final decline.
	Postnova stellar	8.0 to min	Final decline and postnova.

Reproduced from McLaughlin (1960). * This is not uniform from nova to nova.

Here, when the star has exhausted its hydrogen supply a collapsing stage is reached and, dependent upon the star's angular momentum, rotational instability will be reached and thus cause the explosion (the larger the angular momentum, the sooner the instability is reached). Schatzman (1948, 1949) developed the hypothesis that a shock wave propagating within the star could produce the required energy for a nova outburst. He calculated that 0.22g of hydrogen per gram of ejected material must be converted into helium and thus envisaged the outburst as a type of 'hydrogen bomb'. This theory of shock waves as a mechanism of nova outbursts seemed the most promising until Kraft (1963) published his now classic paper on the binary nature of nova systems.

1.3.1 The Thermonuclear Runaway Model For Novae Outbursts

The nova system is considered to be a close binary with the primary a white dwarf and the secondary companion a late type main sequence star (or giant in the case of some recurrent novae). This configuration is shown in Fig. 1.2. The companion fills its Roche lobe and material from it is gravitationally attracted to the white dwarf. This material collects around the white dwarf to form an accretion disc (thus implicity suggesting that the white dwarf in these systems is not highly magnetic; $B < 2 \times 10^7$ G at the surface of the white dwarf), although a fraction of the material may spill out of the Roche lobe and cause a continuous mass loss (Kitchin, 1982). The interaction zone between the infalling material and the disc forms a hot spot (Flannery, 1975).

The nova outbursts arise from thermonuclear runaway (TNR) reactions at the surface of the white dwarf which is enriched in the elements carbon, nitrogen and oxygen as a result of hydrogen and helium burning (Gallagher & Starrfield, 1978). The accreted matter (from the secondary) is mostly hydrogen and when it reaches the surface of the white dwarf it forms a layer which will become compressed to densities $\sim 10^4$ g cm^{-3} as more mass

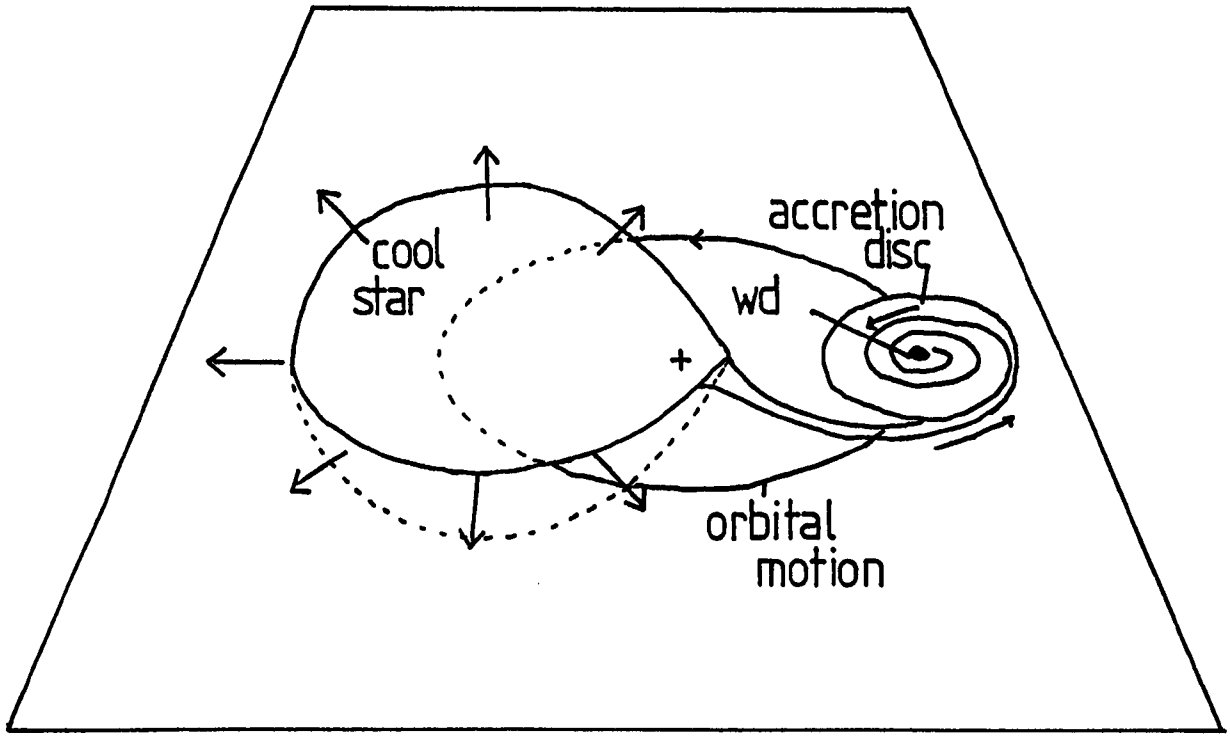

Figure 1.2. This shows the processes that lead to the nova outburst. The nova binary system is here represented schematically from above the plane of the orbits. The cross is the centre of rotation of the white dwarf primary and late type main sequencee secondary.

reaches the white dwarf surface. When ~ $10^{-4} M_0$ has accumulated on the white dwarf the density and temperature will be high enough for the nuclear burning of hydrogen and it is this that will give rise to the nova outburst (Truran, 1982). However for the CNO cycle to be initiated in a truly explosive manner it would be advantageous if the accreted hydrogen did not remain on the surface of the white dwarf but were mixed into the deeper carbon rich layers by convective processes (Lamb & Van Horn, 1975).

At first, just after the start of the nuclear burning, the temperature will rise rapidly without a corresponding pressure rise as the material is degenerate and the hydrogen shell will not be disrupted (Sparks et al., 1977). However the rates of nuclear reactions are very sensitive to temperature and as this reaches ~ 10^8K the degeneracy will be lifted and this will lead to the final explosion which completely disrupts the hydrogen shell around the white dwarf. The ejected shell is then driven outwards by shock waves, gas pressure and radiation pressure (Truran, 1982).

This is the basic mechanism of outburst for all speed classes of novae and by varying some of the intial parameters the observational characteristics of most type of novae can be reproduced. Theoretical calculations show that it is extremely difficult to initiate a thermonuclear explosion on a low mass white dwarf ($\leq 0.5\ M_0$; Koretz & Prialnik, 1985). The more massive the white dwarf and the higher the initial luminosity the less mass has to be accreted before a thermonuclear reaction begins (Truran, 1982). Fast and slow novae can thus be modelled by varying both the mass of the white dwarf and the enrichment in carbon, nitrogen and oxygen; so the greater the mass of the white dwarf and the CNO abundance, the more likely a fast nova is to be produced (Starrfield et al., 1978).

This thermonuclear model appears to explain most of the features of novae outbursts although it does have its problems. The major one is that

the decline from maximum light, in theory, should take place on the cooling timescale of the white dwarf; however it is observed to be much shorter than this timescale (MacDonald et al., 1985). Another problem arises in that the TNR requires an over abundance of carbon, nitrogen and oxygen in the white dwarf thus implying it must be a carbon-oxygen white dwarf (Starrfield et al., 1974) whereas theories of the evolution of close binaries indicate that it will be a helium white dwarf (Paczynski, 1971). Other mechanisms for the cause of the nova outburst have thus been suggested such as an episode of runaway mass accretion onto the primary which will cause a brightening of the whole disc (Gallagher & Starrfield, 1978). This mechanism could produce sufficient energy for the outburst by material falling onto the white dwarf although calculations show that it could not reproduce the rapidity of the outburst (Kitchin, 1982).

The possibility of a single star being responsible for the outburst has also been explored (Truran et al., 1977). In this case the single star would be a white dwarf upon which interstellar matter accumulated so giving rise to the required TNR. For this to occur the white dwarf would need to pass through a very large and dense interstellar gas or dust cloud. The probability of such a situation is very low but not totally negligible, but the TNR model occuring in a binary system is still considered to be the most likely explanation for the novae outbursts.

1.4 Recurrent Novae

As mentioned previously recurrent novae appear to be classical novae that have undergone more than one recorded outburst (i.e. their recurrence time is relatively short). Table 1.4 lists the known recurrent novae and some of their characteristics. These novae are categorized by speed class as with the classicals (cf. Tables 1.1, 1.2). Indeed the similarities between classical novae light curves and spectra to those of the recurrents are so great that it is not possible to tell from a nova's first outburst

Table 1.4

Observational parameters of recurrent novae.

Name	Maximum mag.	Amplitude A	Year of outburst	Interval (mean)	Type	Spectrum of secondary
T CrB	2.0 mags	8.6 mag	1866, 1946	80 yrs	fast	gM3
RS Oph	4.3	7.2	1898, 1933 1958, 1967 1985	22	fast	gM6(?)
T Pyx	7.0	7.1	1890, 1902 1920, 1944 1966	19	slow	dwarf (?)
V1017 Sgr	7.2	7.1	1901, 1919 1973	36	slow	G5III
U Sco	8.7	10.6	1863, 1906 1936, 1979	39	fast	dwarf(?)

Reproduced from Hoffmeister et al. (1985).

whether or not it will be a recurrent. The decay times of recurrents cover the entire range of decay times for classicals i.e. 6 days $\leq t_3 \leq$ 280 days, although the outburst amplitudes are slightly smaller than the average amplitudes of the classicals. This is no doubt caused by the fact that three of the known recurrents have giant stars (rather than main sequence stars) as their secondaries and if the luminosities of these stars were taken away the amplitude range would indeed be the same as for the classical novae. The only major differences between recurrents and classicals is in their inferred binary periods and their velocity profiles after outburst (Friedjung, 1986). For the classical novae their orbital periods P are < 0.6 day (with the exception of GK Per which has a period of ~ 2 days; Friedjung, 1986), whereas the recurrents RS Oph and T CrB may have periods of 230 days and 227 days respectively. However the small known group of recurrents are very heterogeneous and the periods for T Pyx and U Sco are considered to be $\leq$ 6 hours (Vogt, 1987). With regard to the velocity profiles found in novae, in classicals the highest velocities are to be found in the centre of the ejected envelope. This is exhibited by the fact that each progressive stage of spectral evolution is characterized by greater velocites (see section 1.2.2) which can be explained if there is continued mass ejection after optical maximum (Friedjung, 1986). On the other hand, in at least RS Oph and T CrB, the velocities are lowest at their centres. Friedjung (1986) interpreted this by a model of an inhomogeneous envelope ejected nearly instantaneously with the parts having the lowest velocity closest to the centre i.e. no continued mass ejection after optical maximum.

Due to the great similarities between the classical and recurrent novae the mechanism of outburst for these objects are both considered to be a TNR. However the problem with a TNR occuring in recurrents is: can enough mass fall onto the primary star in the interval between outbursts, ~ 30 years (on average)? Livio et al. (1986) think not and propose an

alternative model for the outbursts of the novae RS Oph and T CrB. They propose a model in which the outbursts follow an episodic accretion event. For RS Oph the direct impact of the accretion stream with the primary, which is assumed to be an expanded main sequence star, will cause the outburst (see Chapter 7). In the case of T CrB, disc formation and decay is allowed as the accreting star in this system is thought to have accreted much less matter than in RS Oph and thus has not yet evolved into a bloated state as a result of the mass accretion. However, the ultraviolet data of the last (1985) outburst of RS Oph as observed by Snijders (1986) throws doubt onto the Livio et al. model (see Chapter 7). Recently Starrfield et al. (1985) have calculated that a white dwarf with mass 1.38 M_0 and an initial luminosity of 0.1 L_0 could reproduce the short recurrence times of these novae and lead to an ejected mass of $\sim 8 \times 10^{-7}$ M_0. This amount of ejected mass has been observed in the recurrent nova U Sco (Williams et al., 1981). This implies that part of the reason for the much longer recurrence times in classicals is a result of lower white dwarf mass and luminosity (typically ~ 1 M_0 and 0.01 L_0 respectively; Kovetz & Pralink, 1985). Also the mass transfer rates indicated in the Starrfield et al. (1985) model were $\sim 10^{-8}$ M_0 yr^{-1} whilst those calculated for classical novae are $\sim 10^{-9}$ - 10^{-11} M_0 yr^{-1} (Kovetz & Prialnik, 1985). This must be due to the fact Starrfield et al. used a giant star for the secondary in their model of the reccurent novae (as found in some of these systems; cf. Table 1.4) whereas classical novae have main sequence stars for their secondary. Indeed Bath & Shaviv (1978) had already suggested that the red giant secondary in recurrent novae systems would produce a higher mass transfer rate and hence a shorter recurrence time. Further Shara (1980) suggested that a TNR could be aided in recurrents if the material from the red giant was enriched in ^{3}He. Unfortunately no entirely satisfactory mechanism for the cause of the outbursts in recurrent novae has been suggested.

1.5 Conclusion

In this chapter we have considered two types of novae: classicals and recurrents. We have seen how these novae show the same general characteristics in their light curve and spectra. Indeed they are considered to be the same type of object as all classical novae are thought to be recurrent but on a much longer timescale than the recurrent novae. The mechanism for their outbursts is thought to be a thermonuclear runaway as material from an accretion disc spirals down on to the primary white dwarf component of the nova system. This scenario causes a problem for the recurrents as some consider that mass accretion will not occur on a fast enough basis to trigger the outburst. An alternative model proposed for the outburst of RS Oph (see previous section) suggested a bloated main sequence star as the accreting star. Thus it is important to look for spectral evidence for such a star in this system.

In regards to the rest of this work, chapters 2 - 6 are concerned with the near and far infrared properties of classical novae, whilst the remainder deals with the infrared light curve and spectra of the recurrent nova RS Oph which underwent its last outburst at the end of 1985 January.

CHAPTER 2

DUST IN NOVAE

2.1 Introduction

One of the most interesting developments in the studies of novae over the past few decades is the discovery of dust in their ejecta a few months after outburst. This discovery was made possible with the advent of infrared astronomy, when some novae were found to have a rising infrared light curve simultaneously with a decline in the optical light. Obviously some obscuring medium was needed to explain these observations and obscuration by dust grains appeared to do this.

This chapter starts some thirty years before the advent of infrared astronomy and describes some of the ideas for explaining the deep minima seen in some novae at this time. The infrared is then introduced and infrared observations of novae seen since 1970 are described. Finally the various formation mechanisms for the formation of the dust are reviewed with particular emphasis on the 'rapid grain growth model' and the 'pre-existing grain' model.

2.2 Deep Minima In Novae

The light curve of nova Herculis 1934, DQ Her 1934, began as a 'normal' light curve of a typical slow novae (see Chapter 1 for speed class definitions); it reached maximum brightness on 23 Dec 1934, and then slowly faded, with small fluctuations at about one magnitude per month. However on 31 March 1935 its visual flux declined, from 4.4 mags, at a rate of one magnitude per day for the next four days. After this the star declined at a slower rate until it reached a minimum of 13.4 mags on 3 May 1935. Eventually the nova began to rise in brightness until it reached 7th magnitude in early July 1935, oscillating about that magnitude for the rest

of the year (see Fig. 2.1). This behaviour had been recorded previously for the nova T Aur 1891 and subsequently for the novae V732 Sgr 1936 and V450 Cyg 1942 (see Fig. 2.2). However it was the behaviour of DQ Her that first lead to the suggestion that dust was connected with nova outbursts. McLaughlin (1935) noticed that as this nova faded the red components of the emission bands weakened relatively to the violet components. The violet components then subsequently brightened a few weeks after the visual minimum and later when the nova recovered from deep minimum, the red components appeared and increased toward equality with the violet ones. Hence McLaughlin suggested that this behaviour could be explained by the formation of a cloud of dust (or other continuously absorbing medium) roughly coextensive with the gaseous shell. Hence greater absorption of light from the far side (receding gas) could account for the relative weakening of the red components of the band. Further, when the cloud dissipated the light of the receding components would then shine through again and the red components would strengthen relatively as was observed.

Grotrian (1937) however had an alternative explanation for the light curve of DQ Her, based on mass loss from the nova system. Grotrian surmised that, at the beginning of the nova outburst, the mass ejection would occur on a rapid timescale. This mass ejection would establish an extended, optically thick gas shell, the pseudophotosphere. If the mass ejection rate remained constant the gas density at any point in the shell would also remain constant. But the optical depth at that point as seen by an external observer would increase giving an overall effect of an increasing pseudophotospheric radius. The effective temperature would hence drop as the observer would now see the outer cooler regions of the star (assuming constant bolometric luminosity). However if the mass ejection rate, instead of remaining constant, decreased with time then the pseudophotosphere would appear to be shrinking and the external observer would see an increase in effective temperature as one sees into the hotter

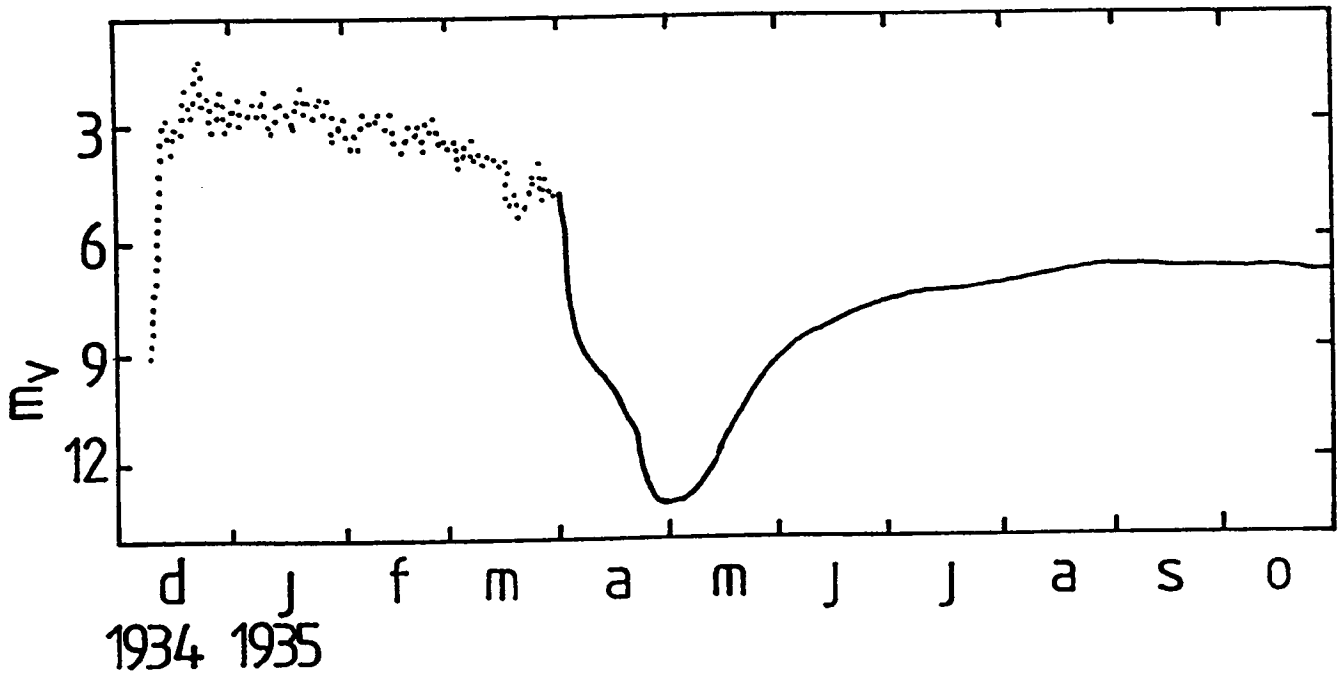

Figure 2.1. Visual light curve of DQ Her 1934. Reproduced from Grotrian (1937).

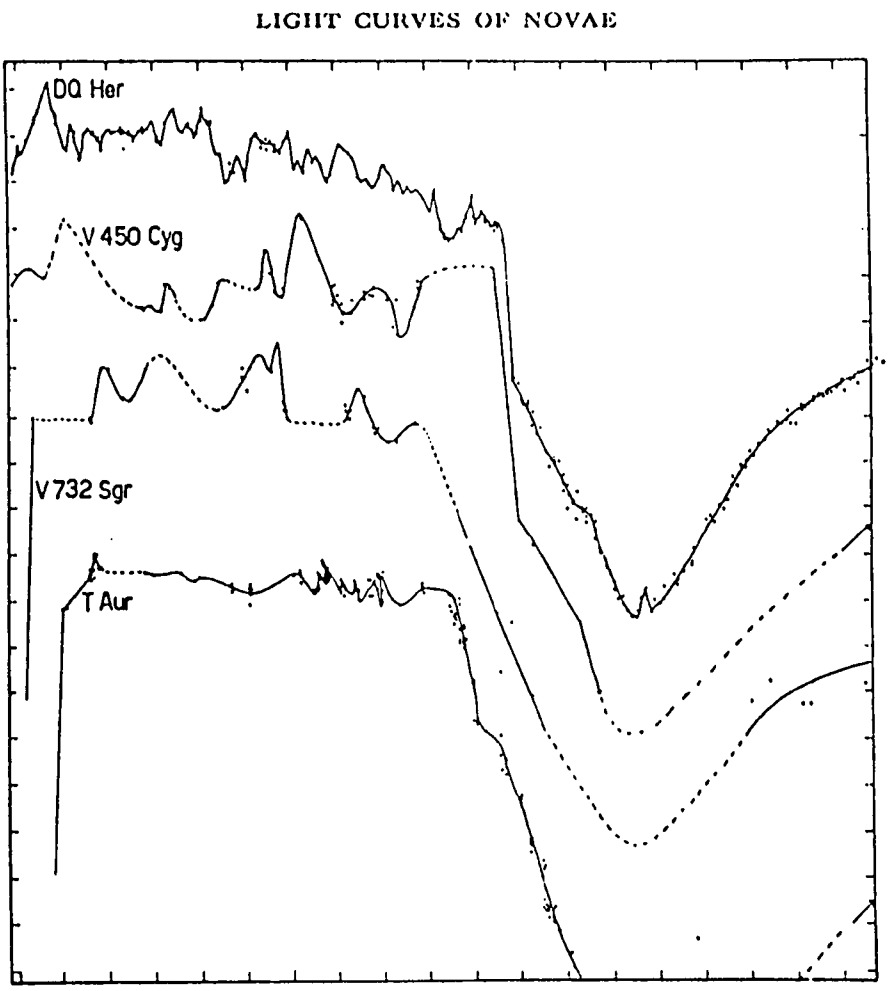

Figure 2.2. Visual light curves of four of the 'DQ Her 1934' type novae. Abscissae and ordinates are marked at intervals of 10 days and 1 mag, respectively. Reproduced from Payne - Gaposchkin (1957).

inner regions of the star. This increase in effective temperature would lead to most of the radiation from the star being emitted in shorter wavelength regions than the visual and hence a decrease in the amount of optical light. This scenario taken to its extreme, i.e. a cessation of mass loss completely, would then give rise to the observed deep minimum in DQ Her. The subsequent recovery, according to Grotrian, was due to an increase of brightness (flux) of the emission bands (lines) of the nebula because of the harder energy distribution of the continuum from the central star. Much later Bath & Shaviv (1976) were to extend this model when they demonstrated that the bolometric luminosity of novae, some time after outburst, did indeed appear to remain constant.

Stratton (1946) suggested that the deep minimum was caused by an opaque molecular cloud forming inside the outer shell of the nova, and which passed across the central star obscuring both it and the inner shells. The evidence for this was the vanishing of the the absorption lines and the weakening of the continuous spectrum that happened at the time of minimum. Furthermore because of the spectroscopic identifications of CII, NII, OII, He and H and the presence of CN bands just after the nova's maximum brightness, Stratton suggested that the cloud was of a molecular nature. ter Haar (1946) elaborated on this hypothesis and suggested that molecules were formed at the moment when the distance from the nova to the inner edge of the outermost shell corresponded to the radius of the HII region. In the HI region the much smaller radiation density would then make the formation of molecules possible. He explains the recovery of the light curve in terms of decreasing density as the shells expanded, as molecular formation is sensitive to density variations. This also explained the oscillations in brightness of some novae, especially if the degree of ionization was also not constant.

Having been one of the first to suggest some type of obscuring medium McLaughlin later changed his mind (McLaughlin, 1949). He examined

Stratton's hypothesis and found it improbable. He argued that the presence of CN bands was irrelevant to the discussion as they were only present for a few days after maximum and had never been observed again. He also pointed out that if molecules did form they were more likely to form in the inner regions of the principal shell where the density was the highest. The strongest evidence however against the formation of a molecular cloud was the lack of any appearance of molecular bands crossing the continuous spectrum early in the fading stage. He also dismisses his suggestion of the sudden formation of a cloud of dust, but on the basis of lack of understanding of the formation mechanism of dust grains rather than on any observational criteria. Grotrian's explanation appeared more satisfactory as it could explain most types of novae behaviour i.e. a smooth light curve, an oscillating light curve, and deep minima in terms of the same phenomena.

The question of what phenomena caused deep minima in novae was not addressed for a long time after McLaughlin (1949) and it was not until the advent of infrared astronomy that this question was re-examined.

2.3 The Arrival of the Infrared

With the arrival of the infrared Hyland & Neugebauer (1970) obtained infrared photometry of FH Ser 1970. In doing so these authors were the first to directly observe dust in a nova. Fig. 2.3 shows their infrared photometry taken ~ 2 months after outburst. They reported that the light curve of this nova was 'reminiscent' of that of DQ Her in that a few months after outburst they both underwent a steep visual decline. More importantly they noted that at the onset of the visual decline the infrared flux was increasing. Hence dust had appeared in the nova system as it would give the required visual obscuration while radiating in the infrared. Geisel et al. (1970) also observed this nova. They saw a weak infrared excess peaking at 5μm at about 19 days. This decayed however and after 90

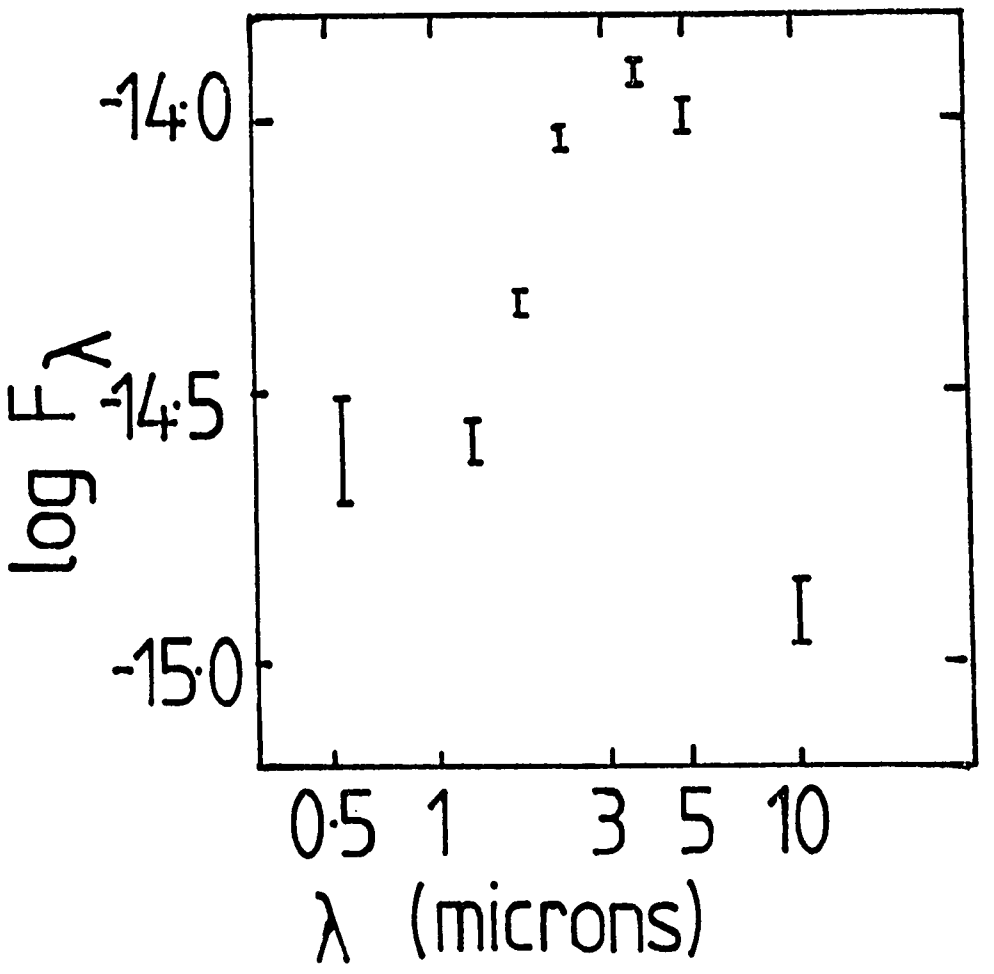

Figure 2.3. Photometry of FH Ser 1970 from 1.2 to 10.1μm on the nights 1970 April 23, 24. The visual magnitude on April 23 is also shown. Reproduced from Hyland & Neugebauer (1970).

days the infrared continuum started to rise rapidly. Putting a blackbody curve through this continuum a temperature of 900 K was estimated, implying dust. During the next observations the dust appeared to be cooling and the infrared emission started to decay with an approximate half life of 100 days. From these observations they suggested that large-scale mass loss leads to the formation of circumstellar envelopes which emit thermal radiation from dust. The timescale for the formation of grains in the ejected material was only a few days or less.

Ultraviolet observations by Gallagher & Code (1974) of this object showed that the early visual decline was indeed due to the shifting of the radiation to harder wavelengths, as Grotrian had suggested; however the overall bolometric luminosity (including the infrared) remained constant (see Fig. 2.4). Thus the intial decline in visual wavelengths was compensated for by a rise in the ultraviolet flux, whilst the subsequent rise in the infrared flux coincided with the rapid decline of the visual light curve. Eventually the radio emission reached a peak some 18 months after outburst as emission from other wavebands was fading (Hjellming et al., 1979).

Later infrared observations (Mitchell et al., 1985) confirmed that the bolometric luminosity remained constant until ~ 200 days after outburst. At times later than this the infrared energy distribution divided into two components. These authors suggested that the hot component arose from a quasistatic dust shell produced by an extended period of steady mass loss following the main nova event, and that the cool component came from the expanding cooling shell formed from material ejected during the main outburst.

After the outburst of FH Ser there were some fragmentary observations of subsequent novae which showed infrared excesses, namely V1301 Aql 1975; Vrba et al. (1977) and V4021 Sgr 1977; Hatfield & Brodzik (1977). However the next nova to be given extensive infrared coverage was NQ Vul 1976. Ney

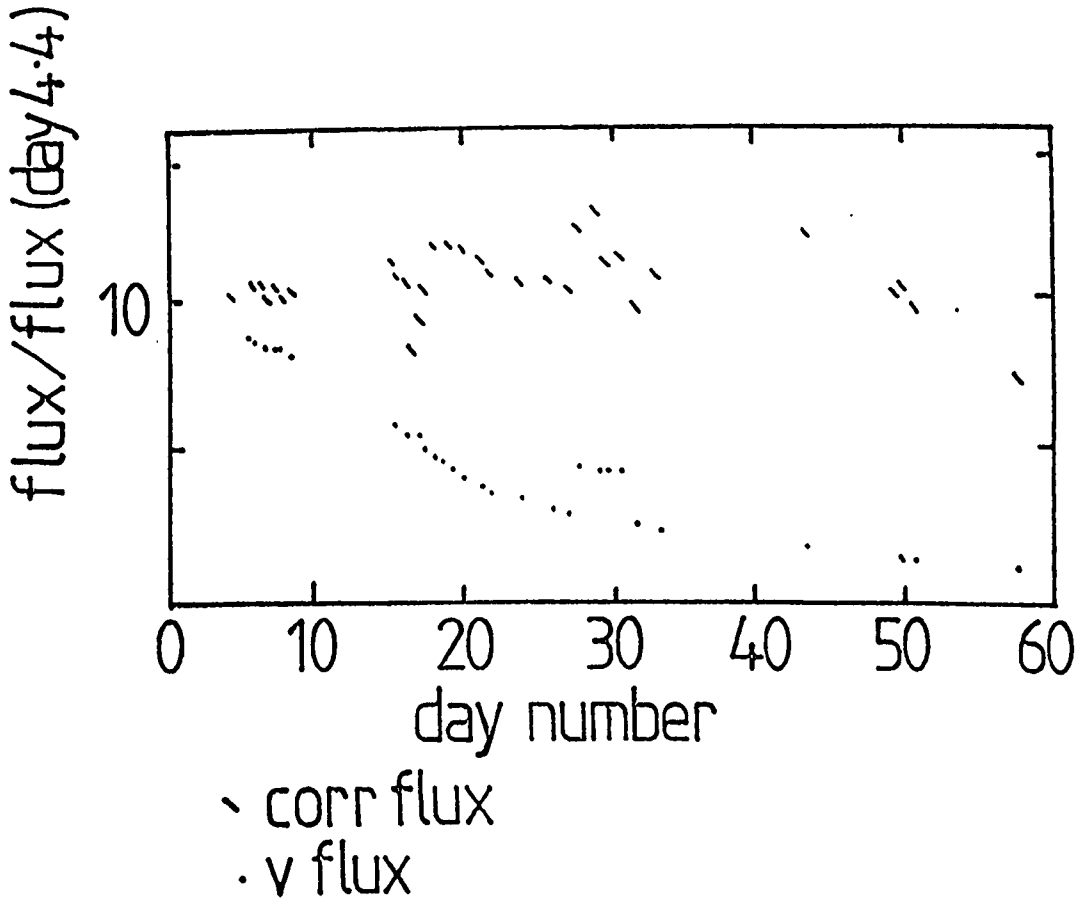

Figure 2.4. Integrated total flux from FH Ser 1970 as measured between 1550 and 5460A. Also plotted is the visual light curve. The x-axis gives days after outburst. Both sets of data have been arbitrarily normalized by the flux on day 4.4. Reproduced from Gallagher & Code (1974).

& Hatfield (1978) followed this nova with broad-band photometry at wavelengths of 0.5 to 12.5μm for day 3 to day 235. They identified three phases of infrared developement. An expanding pseudophotosphere was followed by an optically thin free-free phase, which was followed by dust condensation. During the free-free phase an infrared excess was observed near 5μm (cf. FH Ser). This led to the suggestion that as C_3 molecules may produce this feature they could be the condensation nuclei for subsequent grain formation.

Although the initial energy developement of NQ Vul was similar to that of FH Ser (ie. a visual minimum coinciding with an infrared maximum at about the same stage after outburst) the later developement was different. After 90 days, instead of reaching nearly constant luminosity and cooling, the infrared source in NQ Vul maintained constant temperature (900±50 K) whilst the infrared luminosity decreased exponentially with time. Ney & Hatfield interpreted this 'isothermal' infrared emission as evidence for continuous dust formation in a stellar wind. Another feature which was exclusive to this nova was that on ~ day 78 the blackbody temperature of the dust underwent a minimum before entering into the 'isothermal' stage (see Fig. 2.5). Subsequent to these observations Ferland et al. (1979) published 1.6 - 2.2μm spectra of this nova. These spectra indicated the presence of the first overtone vibration-rotation emission bands of CO at 2.3μm observed 19 days after outburst. On the basis of these spectra it was suggested that the 5μm excess observed by Ney & Hatfield could be emission in the stronger fundamental CO bands centred at 4.8μm, and not C_3 molecules. Due to the absence of any silicate feature (~ 10μm) the dust forming material was thought to be carbon.

LW Ser 1978 was observed in the wavelength ranges V - 19.5μm by Gehrz et al. (1980a). Like FH Ser and NQ Vul, LW Ser was a moderate speed nova. This nova also underwent three infrared phases, beginning with the free-free expansion phase which lasted from day 6 to day 26. During this

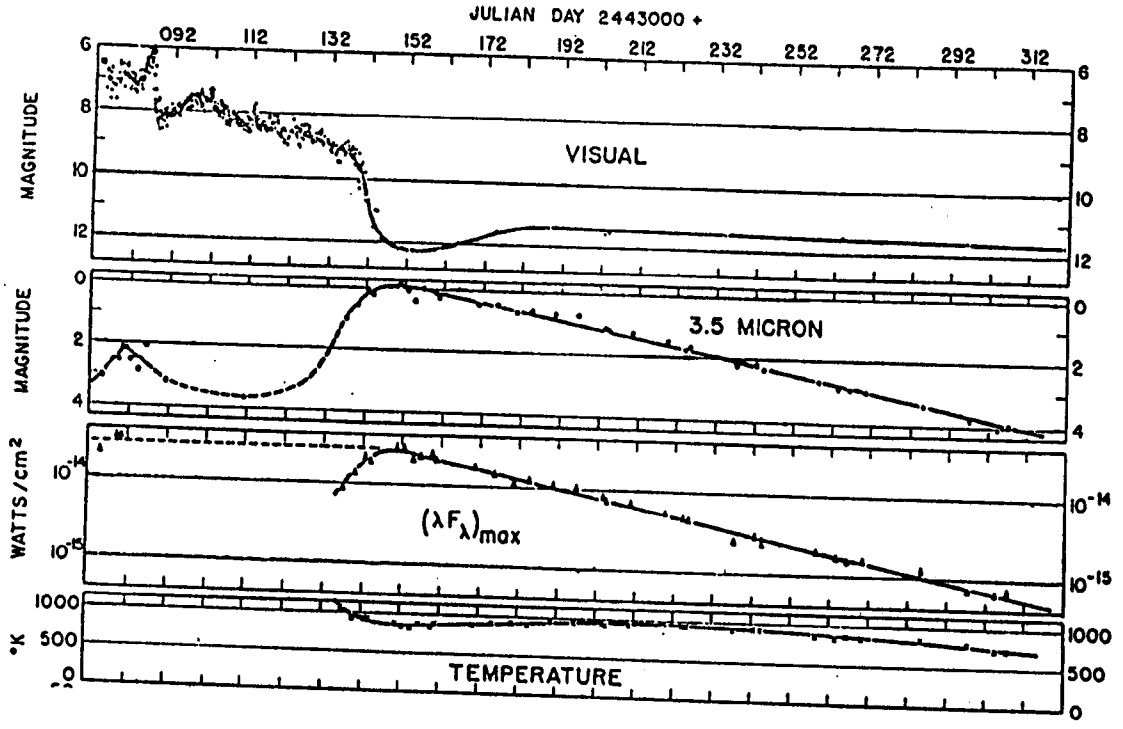

Figure 2.5. The temporal evolution of NQ Vul 1976. The top figure shows the visual light of the nova whilst the one below displays the light curve at 3.5μ. Note the brightening of the 3.5μ light curve as the visual magnitude dims representing the dust condensing. Reproduced from Ney & Hatfield (1978).

phase the infrared flux decayed at 0.1 mag day^{-1} and the 5μm feature was observed on days 16 and 19. The second phase was one of thick dust shell development which started about day 34. At this time the infrared luminosity of the dust shell was equivalent to the outburst luminosity as inferred at maximum visual light. At the same time the visual light was fading and the deep visual minimum ($m_V \sim +14.6$) during the transition phase was coincident with the infrared maximum. The final phase in the dust shell development was characterized by a gradual decline in the shell infrared luminosity, which Gehrz et al. (1980a) interpreted as due to the ending of grain growth and dispersal of the shell. The dust shell effective temperature also exhibited an isothermal stage, in which the dust temperature stayed at ~ 1000 K between days 36 - 127 (Szkody et al., 1980).

A little after the outburst of LW Ser, the nova V1668 Cyg 1978 underwent outburst. This nova differed from the aforementioned novae in that it did not show a break in the optical light curve, hence there was little optical evidence for the presence of dust in this nova. However infrared observations of this nova Gehrz et al. (1980b) indicated that an optically thin dust shell did form. They saw four major stages of shell development. The first stage was an optically thick hot pseudophotosphere which expanded until day 6. The photosphere became optically thin at 10 - 20μm by days 8 - 10. During the second stage the free-free radiation from the optically thin shell decayed as t^{-2}. There then followed a phase of dust condensation, during which the (inferred) carbon dust condensed at a temperature of 1000 - 1100 K (see Fig. 2.6). Infrared maximum was around day 60, after which the fourth phase began; a phase in which the grains were no longer growing but moved away from the star at constant velocity. Piirola & Korhonen (1979) obtained polarization data on V1668 Cyg and also came to the conclusion that dust had formed in the ejecta. Phillips et al. (1979) similarly observed a blackbody excess with temperature ~ 1200 K. Also present in this nova was the 5μm feature which appeared rather later,

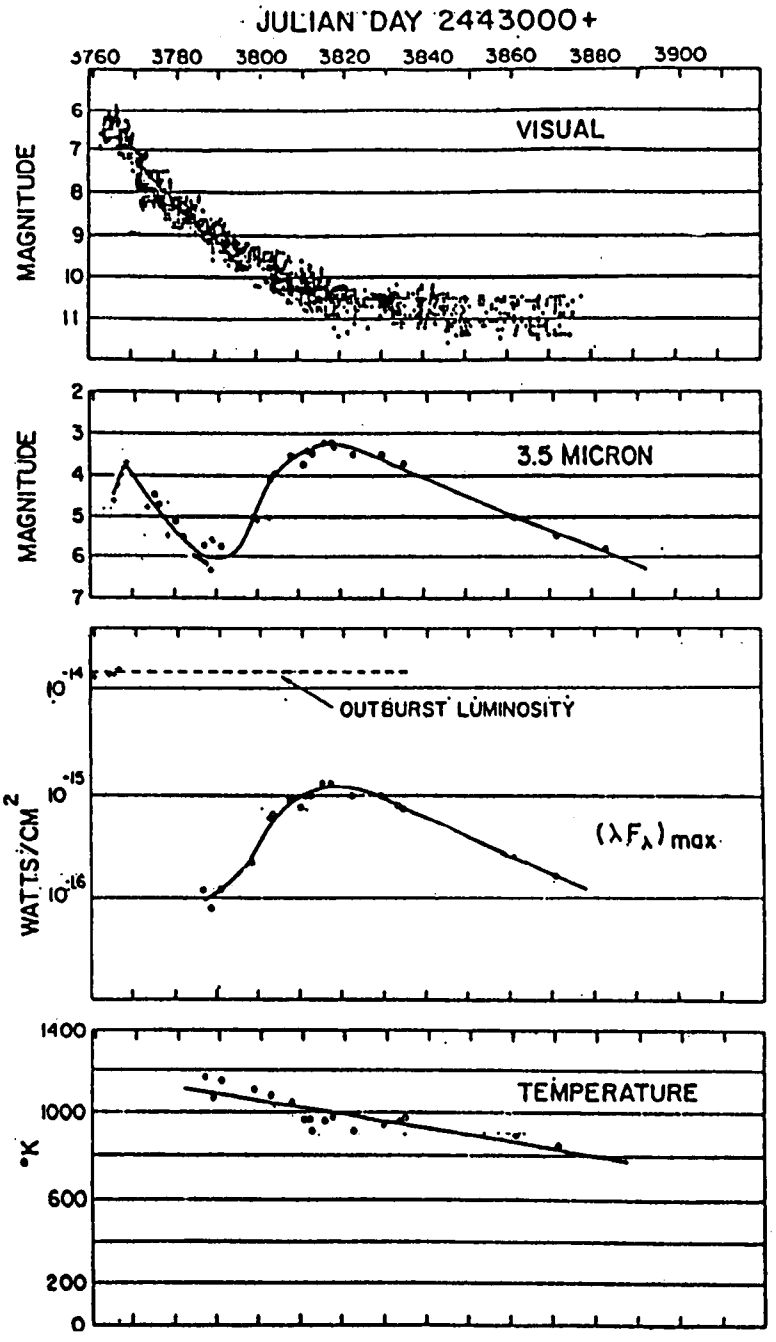

Figure 2.6. The temporal evolution of the circumstellar shell of V1668 Cyg 1978. The visual light curve (top) shows no transition phase as condensing dust causes the 3.5μm infrared flux to rise (lower figure), thus this nova produced an optically thin dust shell. Reproduced from Gehrz et al. (1980b)

day 117, than in the previous dusty novae.

Nova Coronae Austrinae 1981 was the next nova to undergo outburst, in April of that year. Observations were not particularly extensive but just enough that some definite conclusions could be drawn. This was a fast nova declining 3 magnitudes in 12 days (Shylaya, 1984), and which did not appear to undergo a drop in the optical light curve (Williams et al., 1979). JHKL observations taken 6 - 80 days after outburst showed a constantly decreasing flux (Catchpole et al., 1985). Spectroscopic observations by Shylaja (1984) in the near infrared ie. 6000A - 8000A, taken at the end of May 1981 showed emission lines which appeared to be sitting on a blackbody continuum at ~ 1000 K. Shylaja attributed this to the appearance of a dust component, suggesting that its dust shell was optically thin at visual wavelengths comparable with that of V1668 Cyg (see Fig. 2.7).

A different type of behaviour was recorded when nova V1307 Aql 1982 erupted early in January of that year. This nova was a fast one with a visual decay rate of ~ 0.3 mags day^{-1}. Gehrz et al. (1984) reported that it appeared to undergo a visual light transition at day 27 and a shell optical depth of about $\tau = 1$ at visible wavelengths was reached at about day 70 (see Fig. 2.8). Infrared observations reported by Williams & Longmore (1982) 37 days after discovery indicated an infrared excess with a blackbody temperature ~ 1000 K. Subsequent observations about three months after outburst in the 2 - 4μm range by Bode et al. (1984) also showed an excess with a temperature of ~ 1050 K. These authors reported the shell to have cooled from 1100 K on day 37 to ~ 800 K by day 156.

That this nova produced substantial amounts of dust so soon after outburst was unusual for a fast nova, which theoretically was not expected to have dust condensing until after day 80 (Bode & Evans 1982a). However the uniqueness of the nova was in the 10μm emission feature, first reported by Gehrz et al. (1982), that appeared during the dust shell development stage (see Fig. 2.9). Gehrz et al. (1984) tentatively attributed this

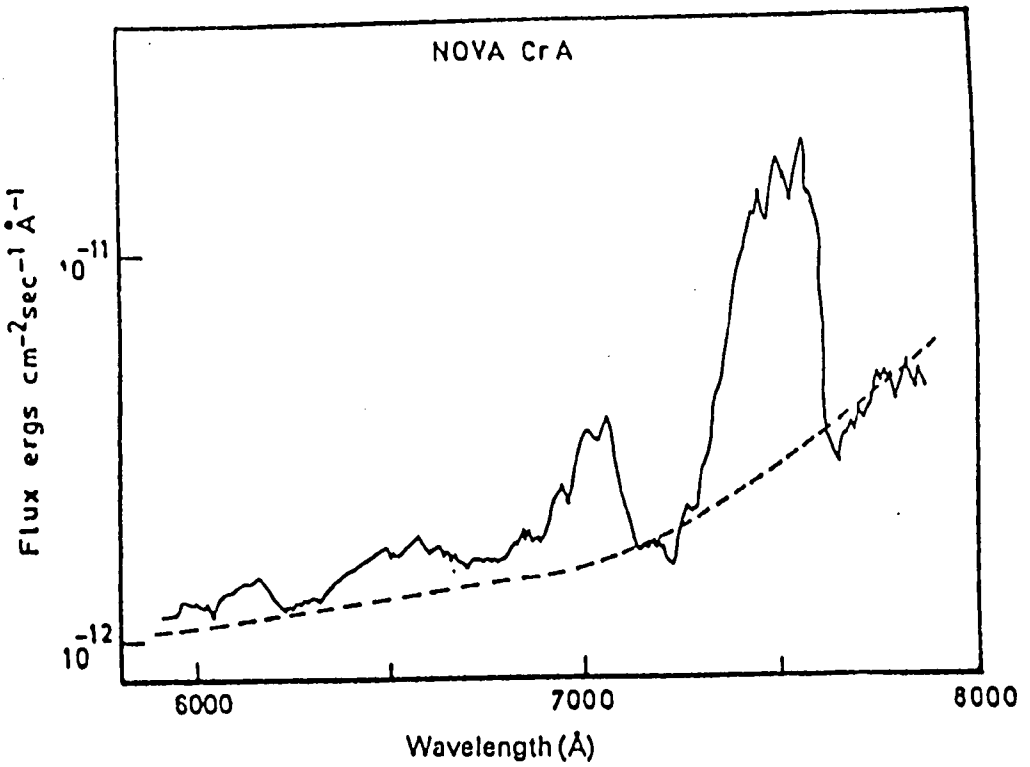

Figure 2.7. The red spectrum of nova CrA 1981 taken on 1981 May 25. A 1000K blackbody distribution (normalized at 6000A) is also shown. Reproduced from Shylaja (1984).

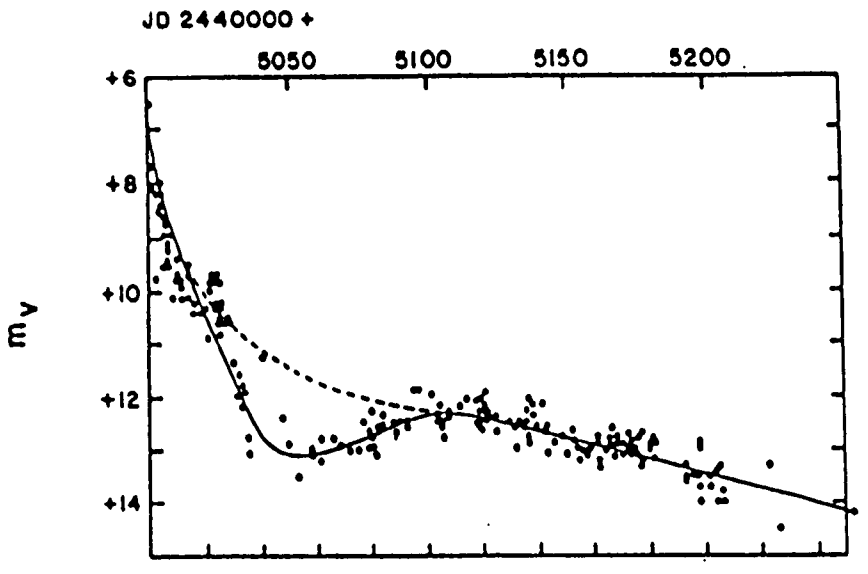

Figure 2.8. The visual light curve of nova V1301 Aql 1982. Reproduced from Gehrz et al. (1984).

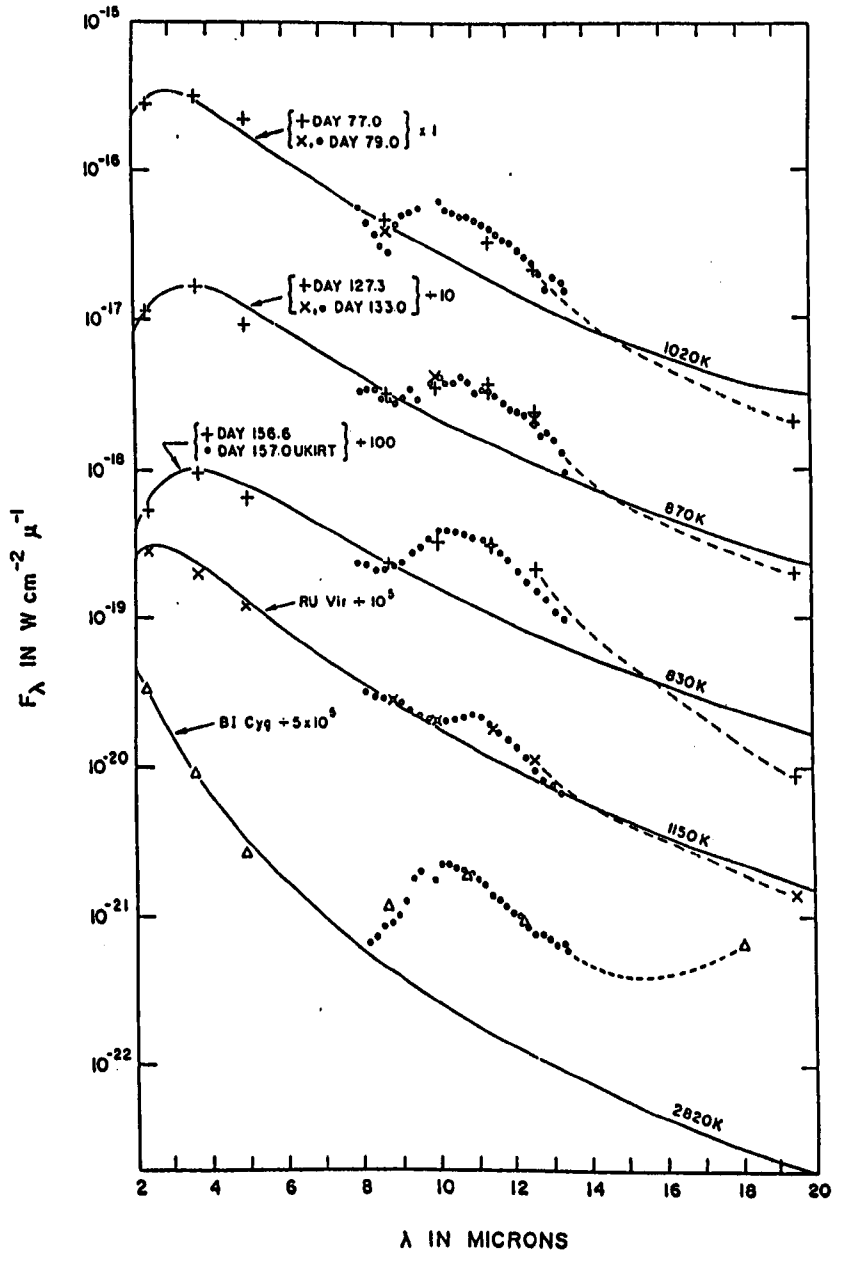

Figure 2.9. The 2.3 - 19.5μm energy distribution of V1301 Aql 1982. Shown for comparison are the energy distributions of BI Cyg, a typical oxygen-rich silicate emission star, and RU Vir, a typical carbon-rich SiC emission star. Reproduced from Gehrz et al. (1984).

feature to SiC, although its 10μm feature was larger than those observed in the SiC rich shells of carbon stars. Roche et al. (1984) disagreed with this identification and suggested an alternative identification of silicate, which has a broad feature centred on 9.7μm. Evidence for this was suggested in the fact that the observed feature was closer to 10μm than 11μm, the SiC feature peaking at 11.3μm. One thing was clear however; V1307 Aql as well as producing carbon grains, consistent with previous dusty novae, had also produced some grain material that could be identified with silicate or silicon carbide.

Observations of V4077 Sgr 1982, which underwent maximum on 1982 Oct 15 are unfortunately not very extensive. The visual light curve did undergo a transition phase in late October (Iljima & Rosino, 1983) but as the light curve oscillated so much it was difficult to interpret what the speed class of nova this was (Mazeh et al., 1985). Infrared observations taken almost simultaneously at SAAO and by IRAS suggest that this nova did form a dust shell (see Chapter 4).

The nova PW Vul 1984 was discovered on 29.95 July 1984 reaching maximum 5 days later. This was a fairly slow nova declining at 0.035 mag day^{-1}. The visual light curve as composed of all observations from the IAU circulars shows oscillations in parts of the curve but no noticeable transition break. Infrared data obtained at UKIRT some three months after outburst in the 2 - 4μm range suggest little evidence of any excess. However dust was detected in the following May (Gehrz et al., 1985), with a 10μm excess; the dust is thought to be silicate (see Chapter 5).

A second nova was detected in Vulpeculae during 1984. It was discovered in late December three days before maximum brightness. It took about 30 days to fall 3 magnitudes, i.e. $m_V \sim 0.1$ mag day^{-1} (Collins, 1984; Franciosi, 1985). This would put it on the boundary between the fast and intermediate speed classes of novae (Bode & Evans, 1983). Its light curve showed variations of tenths of magnitudes but no evidence of dust.

Infrared observations by Gehrz et al. (1985a) ~ 140 days after outburst reveal a free-free continuum upon which is superposed an extremely strong emission feature at 12.8μm, a factor of 60 above. This is attributed not to dust but to [NeII]. However Gehrz et al. (1985b) did report that both the 10μm and 20μm silicate features were present in infrared spectra taken 230 and 240 days after outburst. They suggested that silicate grains had been formed in the ejecta and noted that the 12.8μm [NeII] feature was also present on these dates.

Of the novae that underwent outburst post 1970, not all were observed to produce substantial amounts of dust. The nova V1500 Cyg 1975 showed significant departure from the dusty nova phenomenon. V1500 Cyg was the most spectacular of 'modern' classical novae, reaching an apparent visual magnitude of 1.6 mags on 30.8 Aug 1975. It was also the fastest having an initial optical decline rate greater than a mag day^{-1}. The subsequent decline rate was also smooth and 680 days after maximum the nova was 12.5 magnitudes fainter (Tempesti, 1979; see Fig. 2.10). This rather uninteresting behaviour in the visual was to some extent mirrored in the infrared. Infrared observations by Gallagher & Ney (1976) for the first 50 days after dicovery showed that intially the flux distribution closely resembled that of a blackbody, whilst after 1 Sept 1975 the flux distribution became more complex (see Fig. 2.11). A $F_\nu = 1$ flux distribution evolved suggesting some type of thermal bremsstrahlung emission. Polarization measurements taken at around this time by McLean (1976) and Arsenijevic & Vince (1977) showed little evidence for an intrinsic polarized component to the light coming from this nova.

Longer term infrared observations of this nova up to one year after maximum by Ennis et al. (1977) confirm the free-free nature of the nova spectrum. However after ~ 300 days they observed an excess at wavelengths greater than 10μm which the authors attributed to thermal radiation from dust (see Fig. 2.12). Ferland & Shields (1978a) disagree with this

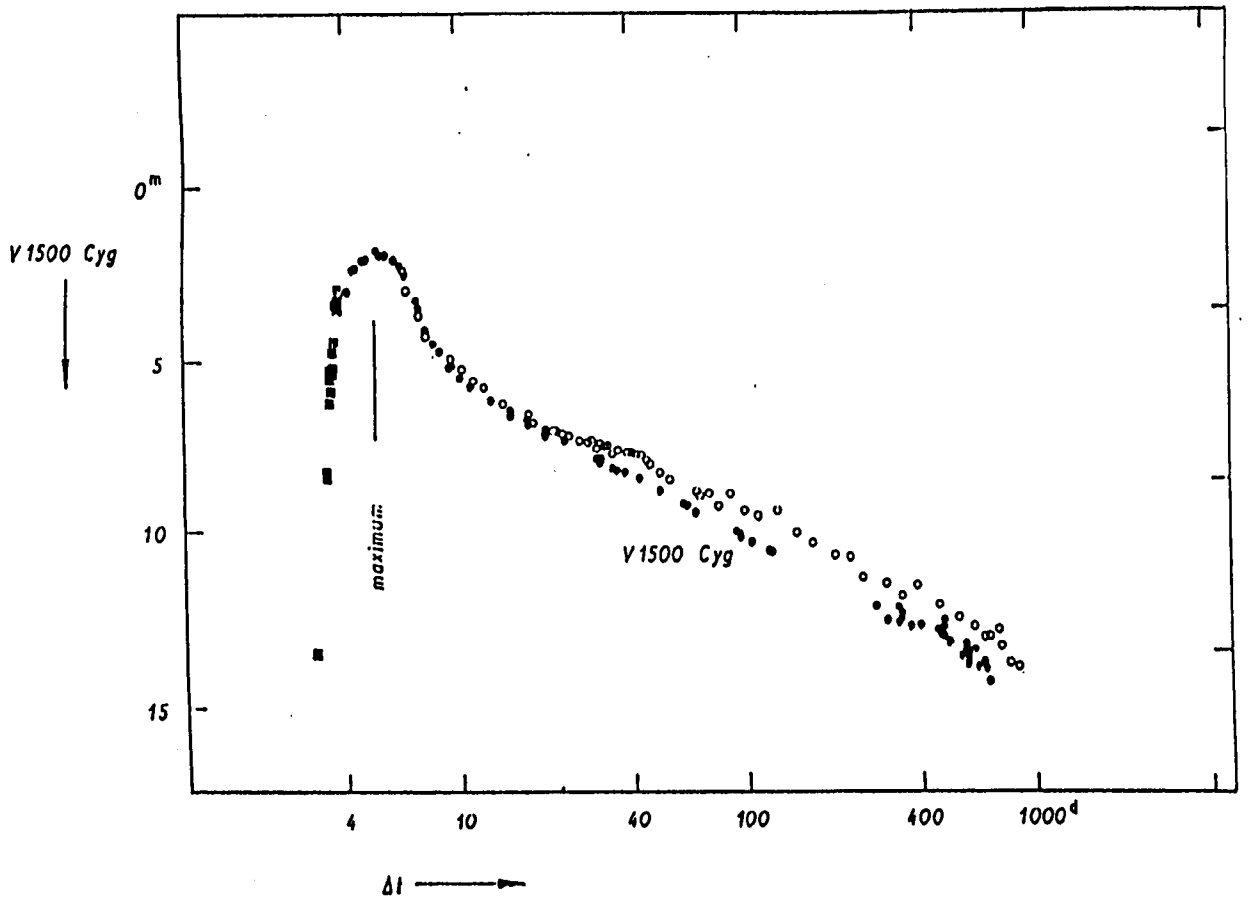

Figure 2.10. The visual light curve of V1500 Cyg 1975. Squares show prediscovery observations, dots show photoelectric observations and circles show visual observations. The x-axis gives the number of days after outburst. Reproduced from Tempesti (1975).

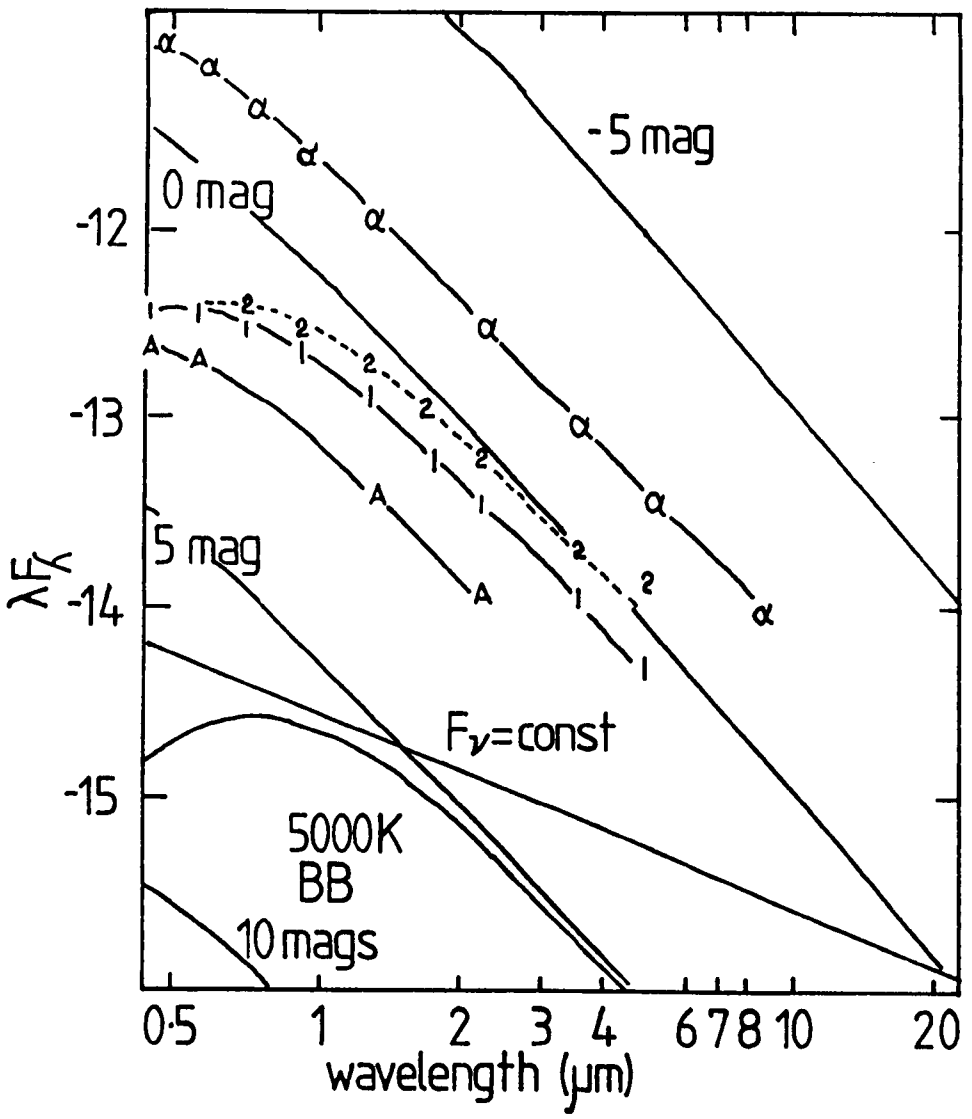

Figure 2.11. Energy spectra for V1500 Cyg 1975 near maximum light. Observations A, 1 & 2 correspond to 0.8, 1.4 and 3.2 days after outburst. In each case the spectra are well fitted with blackbodies. For comparison photometry of α Cyg (α), shifted by -2.5 mags, is also shown. Reproduced from Gallagher & Ney (1976).

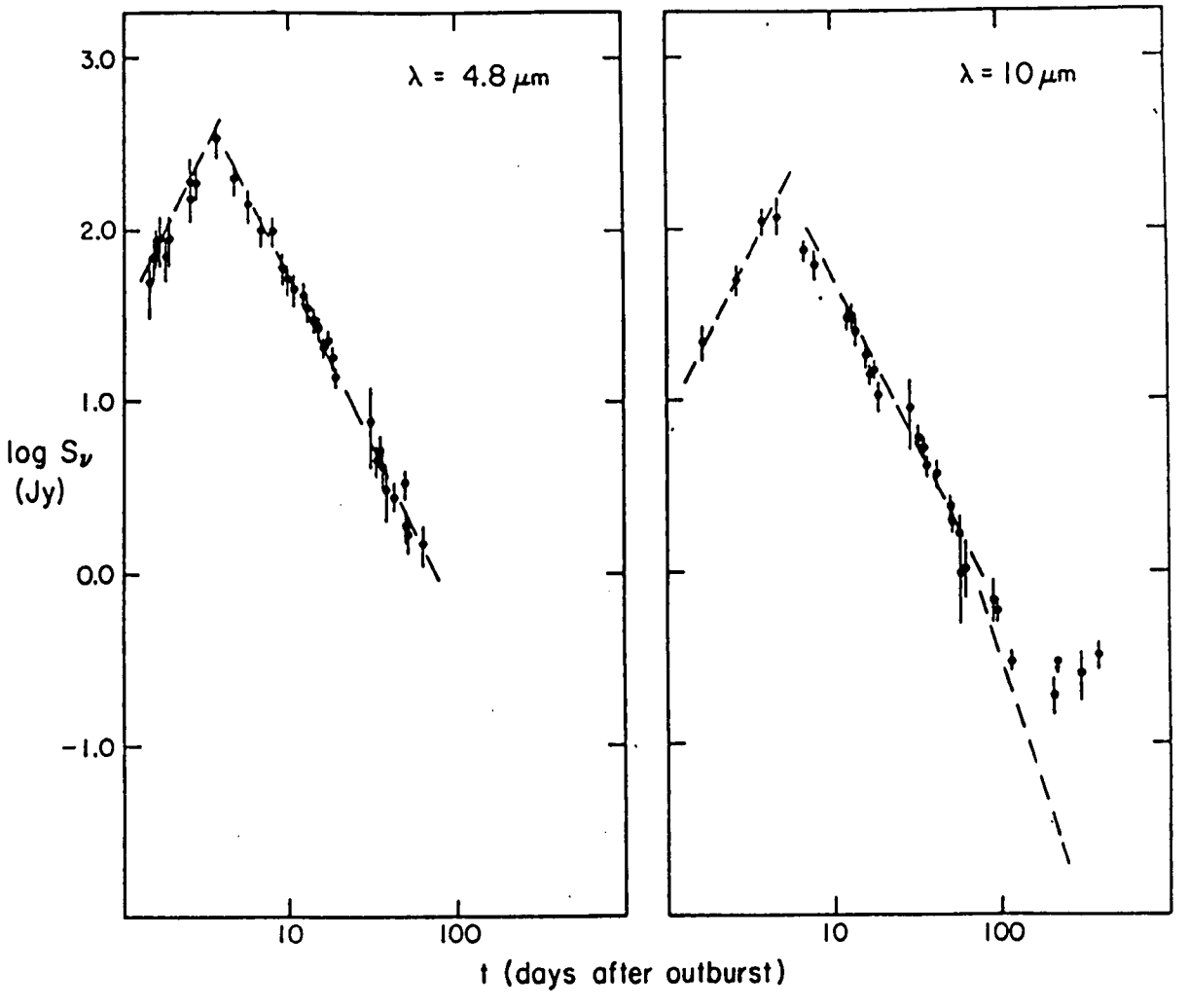

Figure 2.12. 4.8μm and 10μm flux curves of V1500 Cyg 1975. Note apparent 'excess' at 10μm at late times. Reproduced from Ennis et al. (1977).

intrepretation arguing that the fine structure line emission of [NeII] at 12.8μm could account for this excess. Yet other authors, noticeably Szkody (1977), appeared convinced that dust was present citing the obvious excess at L that developed a year after maximum. A novel approach to this problem was put forward by Bode & Evans (1985) who interpreted the 10μm data in terms of the heating of grains that were in the vicinity of the nova at the time of outburst.

So although this nova was first thought of as the prototype of dustless novae; Bode & Evans (1983) put it in class Z (a class of very fast dustless novae), there is still a small doubt as whether it was or not. The only conclusion to be drawn is that if dust was present it did not make its presence known until ~ one year after maximum.

Whereas nova V1500 Cyg was an exceptionally fast nova and its apparent lack of dust could be understood in terms of its speed class (Bode & Evans, 1982a), the nova GQ Mus 1983 which had its maximum on 18 Jan 1983 was a slower nova and hence a more likely dust producer. However (so far) this nova has not shown any unambiguous signs of dust formation. (In Chapter 3 we attempt to give an explanation for its non-production of dust).

This nova's light curve has been very difficult to interpret. Initially it fell by 2 magnitudes in 11 days which would put it in the fast nova category; however after 196 days it had only faded by 3.8 mags suggesting that its speed class was more intermediate in nature (see Fig. 2.13; Whitelock et al., 1984). Looking at the light curve in greater detail there were daily variations of a few tenths of magnitudes and a brightness flare by mid Febuary. There was a small increase in May after which the brightness of the nova remained nearly constant for ~ 5 months at V = 10.6 - 10.7 mags. Around September there was a brightening by about 1 mag (Krautter et al. 1984). So although this nova had an unusual visual light curve there was nothing about it to suggest the presence of dust.

The infrared light curve (Whitelock et al., 1984; Krautter et al.,

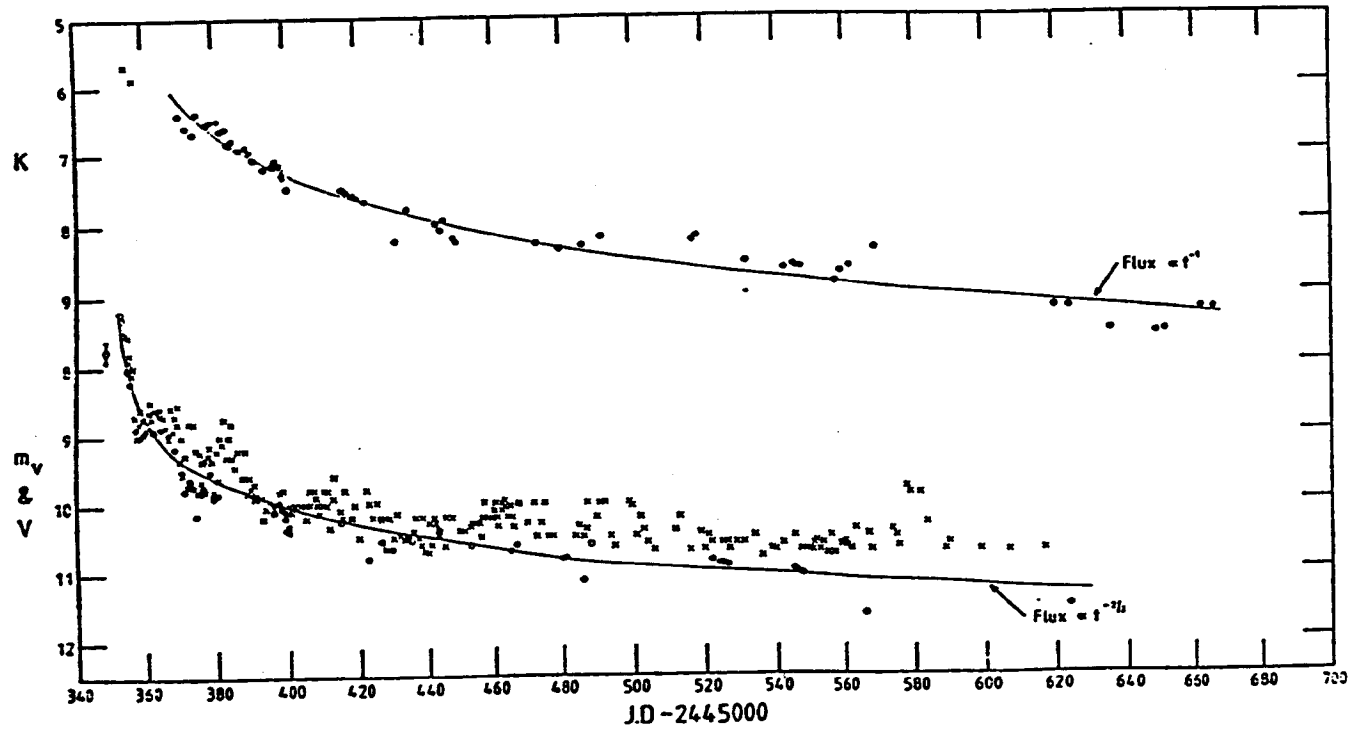

Figure 2.13. K light curve and visual light curve of GQ Mus 1983. Reproduced from Whitelock et al. (1984).

1984) decreased in flux with slight magnitude variations from the overall declining pattern. Krautter et al. (1984) note a detection of a 3.5μm feature observed between 31 Jan - 10 Feb 1983 (see Fig. 2.14). This they identify as a molecular feature, perhaps ultraviolet excited formaldehyde (Blades & Whittet, 1980). They argued that this could be evidence for emission from the molecules in grain mantles i.e. dust formation has taken place. This assignment is very much doubted as the formaldehyde feature as identified by Blades & Whittet (1980) is very heavily asymmetrical, not symmetrical as indicated by Krautter et al. (1984).

GQ Mus was the first classical nova to be detected in X-rays past maximum (Ogelman et al., 1984). It was detected by EXOSAT on 20 April 1984 with the low energy telescope (the LE). The origin of these X-rays is debatable although the above authors suggest that they could come from shock heated circumstellar gas as the nova ejecta plough through it, or from the primary white dwarf component of the nova system. IRAS data on this nova indicate that the infrared emission from this nova can be explained by a free-free radiation model (see Chapters 4 and 6).

Nova MU Ser 1983 was dicovered on 21.8 Feb 1983 (Wakuda, 1983). This was a fast nova, falling by 3 magnitudes in the first four days after maximum (Wakuda et al., 1983). Unfortunately there are few observations available of this nova and although IRAS searched for it the nova was not seen by the satellite (see Chapter 4). No evidence for dust has been observed.

2.3.1 Concluding Remarks on Infrared Novae

There have been other novae discovered since 1970 but observations of these have been extremely sparse and little can be learnt about their dust forming ability.

To summarize what has been found using the techniques of infrared astronomy, is that some novae have formed dust in their ejecta some time

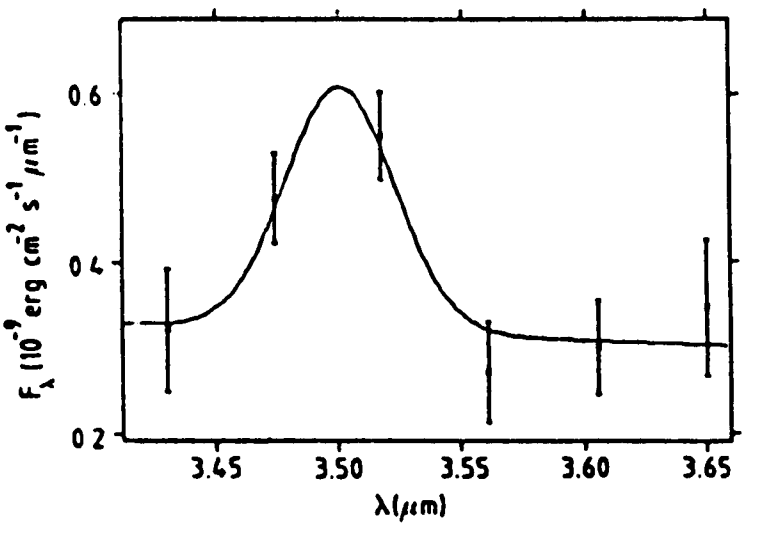

Figure 2.14. The 3.5μm 'feature' in GQ Mus 1983 fitted with a line having the instrumental width. Reproduced from Krautter et al. (1984).

after outburst. (The general trend appears to be ~ 60 days after outburst). This dust has mainly been carbon based dust although at least 3 novae have exhibited spectral phenomena that can be attributed to silicate based dust.

On the basis of the novae that we do know about after 1970 we can say (very generally) that the novae of intermediate speed class appear more capable of forming substantial amounts of dust than do those of other speed classes. Reasons for this must be based on the mechanism of dust formation which will now be discussed.

2.4 Models Of Dust In Novae

2.4.1 Introduction

Soon after unambiguous evidence for the presence of dust in novae was presented, many authors began work discussing how this dust was formed and thus how it affected the visual and infrared light curve evolution. There were two main schools of thought. Firstly that dust quickly condensed from material in the outflowing ejecta, (the rapid grain growth model), and secondly that dust had been present preoutburst and that it was only when certain criteria were met during the nova eruption that it would reveal itself (the pre-existing grains model).

2.4.2 Rapid Grain Growth

The first attempt to quantify the mechanism of grain formation was in novae was made by Clayton & Hoyle (1976) when they attempted to model the behaviour of FH Ser using a 'storage and release' mechanism. They suggested that radiation was stored throughout a large cavity, due to the high visual opacity of a shell of grains, which released this radiation as the opacity fell (see Fig. 2.15). To store enough infrared energy this model requires that the grains form in quickly moving ejecta so that they

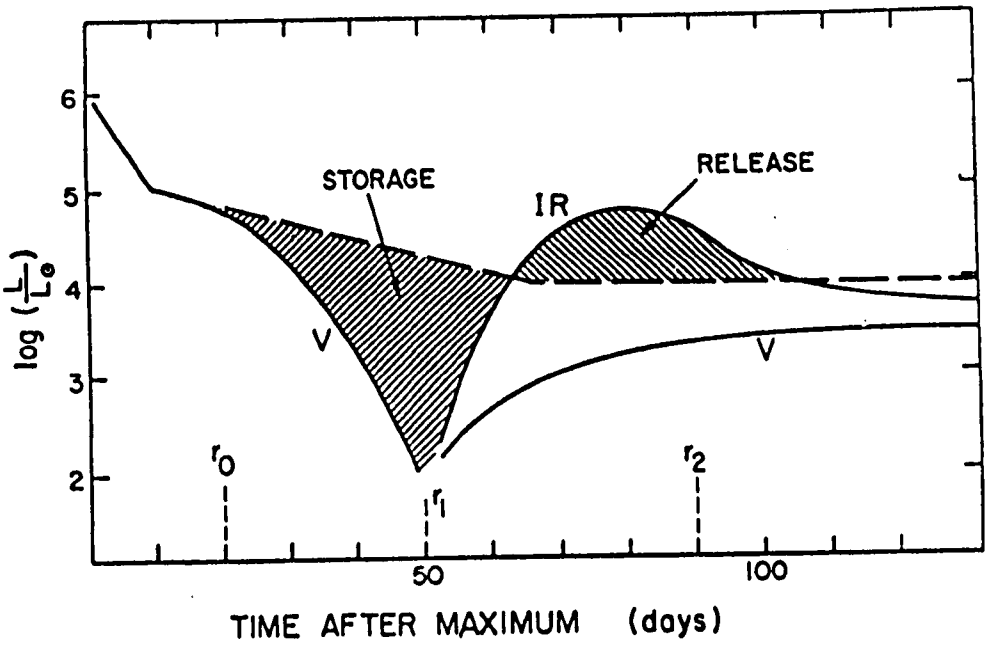

Figure 2.15. The visual and infrared luminosities of the Clayton & Hoyle (1976) model (from whom this figure is reproduced) as a function of time. The total luminosity of the underlying star is shown as a dashed line joining the visual luminosity at early times. r_0 is the condensation radius, r_1 is the radius at which grain condensation ceases and r_2 is the radius at which the infrared luminosity reaches a maximum.

have sufficient volume at the time the radiation was to be released. In this model the grains form when the radius of the ejecta reaches that radius at which the temperature is the condensation temperature of graphite, ~ 2000 K (carbon based grains have been assumed here). In order to produce the rapid fall of visual light not all the carbon will condense instantaneously at the condensation radius. If this were so the opacity would become so large that the resulting holding back of the radiation from the central star would raise the effective temperature of the grains causing them to evaporate. However as long as carbon continues to be able to condense past the point at which the condensation temperature is reached the optical depth at visual wavelengths, τ, will increase. As the optical luminosity falls as $e^{-\tau}$ this will produce the required visual decline. If grains now stop forming at some radius, say r_1, it will be at that point that the visual light will be at a minimum, i.e. at time $t_1 = r_1/v_{ej}$ (where v_{ej} is the ejection velocity). When the grains stop forming the opacity decreases and hence the visual light rises. Also at this point the infrared radiation trapped within the shell would escape giving rise to an infrared maximum.

There are some difficulties with this model, the foremost being the discrepancy with the ultraviolet observations of FH Ser by Gallagher & Code (1974). This work indicated that the initial fall in the optical light was not due to dust but the shifting of the radiation to shorter (ultraviolet) wavelengths as constant bolometric luminosity was maintained (cf. Grotrian, 1937). The velocity at which Clayton & Hoyle require the ejected material to be moving is ~ 2000 km s^{-1}. This velocity was indicated by the Doppler shift of the lines of the diffuse enhanced spectrum, but not of the principal spectrum where the bulk of the material is thought to lie. (The principal spectrum indicated velocities of ~ 1000 km s^{-1}). So although this work was a start to understanding the mechanism of grain formation in novae it did have some major problems. Clayton then collaborated with

Wickramasinghe to produce a model which was to be the basis of all subsequent work on the rapid grain formation mechanism.

2.4.2.1 Clayton & Wickramasinghe, 1976 (CW)

This model is based on the proposition that the infrared development of the nova (in this case FH Ser) is controlled by the rate of growth of grain radius. Again the grain material is assumed to be largely made up of carbon.

Like the previous work they begin with the condition that nucleation and condensation of graphite particles start when the equilibrium temperature of a condensation nucleus falls below the condensation temperature of graphite (T ~ 2000 K). This grain temperature occurs at a distance r_0 defined where the fraction of the stars luminosity intercepted by a grain is equal to the energy emitted by that grain, thus

$$\pi a_0^2 L/(4\pi r_0^2) Q(T_*, a_0) = 4\pi a_0^2 \sigma T_g^4 Q(T_g, a_0) \tag{2.1}$$

Here T_* is the temperature of the central star, a_0 is the radius of a condensation nucleus, T_g is the grain temperature and σ is Stefan's constant. Q(T,a), the Planck averaged absorption efficiency, is given by

$$Q(T,a) = \int Q_{abs}(\lambda,a) B(\lambda,T)\, d\lambda / \int B(\lambda,T)\, d\lambda \tag{2.2}$$

$Q_{abs}(\lambda,a)$ is the absorption efficiency of a graphite sphere of radius a for radiation of wavelength λ and $B(\lambda,T)$ is the Planck function. When $Q \ll 1$, (which is the case for grains having $a \leq 10^{-4}$ cm)

$$Q(a,T) \simeq 3.22a(T/10)^{1.65} \tag{2.3}$$

Now defining the equivalent temperature T_{rad} of a black sphere at distance r by

$$L/(4\pi r^2) = 4\sigma T_{rad}^4 \tag{2.4}$$

and using equations (2.1) and (2.3) then

$$T_g = (T_*^{1.65}\ T_{rad}^4)^{1/5.65} \tag{2.5}$$

Thus $T_g > T_{rad}$ and

$$r_o = 7.73 \times 10^{14}(L/5\times10^4 L_o)^{1/2}(T_*/10^4 K)^{0.825}\ \text{cm} \tag{2.6}$$

where $t_o = r_o/v_{ej}$, the waiting time before grain growth on a large scale can begin.

Nucleation occurs by a series of binary reactions in the gas phase so the dominant factor determining the nucleation rate will be the number density of carbon n_c. CW took the density to fall following an inverse square relationship so that

$$n_c = (n_c)_o(r_o/r)^2 = (n_c)_o(t_o/t)^2 \tag{2.7}$$

and J (rate of nucleation) $\propto (t_o/t)^4$ (2.8)

Such a steep decline of nucleation with time implies that the total number of condensation nuclei is established almost instantaneously at $t = t_o$, which is in contrast with the previous work of Clayton & Hoyle (1976).

It is now that the development of the infrared luminosity becomes governed by the rate of growth of grains. We have

$$da/dt = \alpha\, n_c/s\, (KTm_c/2\pi)^{1/2} \tag{2.9}$$

where α is the sticking probability, s is the density of solid graphite, T is the gas temperature and m_c is the mass of a carbon atom. (This assumes no depletion of carbon so that $n_c(t)$ is always given by equation 2.7). Assuming $T = T_{rad}$ and using equations (2.4) & (2.5)

$$da/dt = A(n_c)_0(t/t_0)^{-9/4} \tag{2.10}$$

and $A = 5.05 \times 10^{-20}(T_*/10^4)^{-0.206}\ cm^4 s^{-1}$ (2.11)

Integrating equation (2.10) this gives

$$a = a_0 + a_\infty(1 - (t/t_0)^{-5/4}) \tag{2.12}$$

where a_∞ is the final grain radius when grain growth is completed. Thus from equation (2.12) we can see that intially the grains grow rapidly. Grain growth saturates because of the expansion of the shell, which leads to a falling density n_c. As grains continue to increase in radius equation (2.5) ceases to be valid as an approximation to the grain temperature.

To calculate the grain temperature at any time CW used the condition that the radiation absorbed from the central star must equal the radiation emitted by the dust grains (see equation 2.1). They found that while the grain radius a(t) was rapidly growing, the grain temperature fell more slowly, due only to the expansion of the ejecta. Thus in this model the change in the slope of the temperature curve may be taken as observational evidence of an effective cessation of a period of rapid grain growth.

The total infrared flux at any instant is equal to the short wavelength radiation absorbed by all the grains. This infrared flux will escape if

the dust is optically thin to infrared radiation. CW found, for a_∞ = 2×10^{-4} cm (that which most closely fitted the data on FH Ser), that the infrared spectrum over all observed wavelengths approximated to that of a blackbody of temperature T_g immediately after grain growth stopped. Now assuming that the infrared radiation exactly equals the absorbed radiation at all times

$$L_{ir} = \min[N_g F_{abs}, L] \tag{2.13}$$

where N_g is the total number of grains and F_{abs} is the radiation absorbed from the central star. This means that $L_{ir}(t)$ can be calculated for given values of N_g, $(n_c)_o$, v_{ej} and t. Intially L_{ir} is zero until grain growth begins at time t_o. As a(t) grows the absorbing area and the absorption efficiency increase whilst the incident flux decreases due to radial expansion. For small particles where $Q(a) \propto a$, the infrared curve initially grows as $L_{ir} \propto a^3(t)/t^2$. This relationship is continued if the nebula remains optically thin and the particles small. In the thin nebula case the maximum in L_{ir} occurs at $t_{max} = 2.33t_o$ (see equation 2.12).

If $(n_c)_o$ is sufficiently high the grains will become large enough that the absorption efficiency $Q(T_*,a)$ saturates at unity long before the infrared maximum is reached. In a thin nebula this means $L_{ir} \propto a^2(t)/t^2$ and t_{max} will occur at $1.91t_o$. When $Q(T_*,a)$ reaches unity on the rising infrared curve (here $a = a_I$), the luminosity will then grow more slowly for the absorption efficiency can no longer increase with increasing grain size. So in thin nebulae the dust luminosities will behave as:

$$L_{ir} = Ca^3(t)t^{-2} \qquad a < a_I \tag{2.14}$$

$$L_{ir} = Ca_I a^2(t)t^{-2} \quad a \geq a_I \tag{2.15}$$

(where C is a constant), and there will be a discontinuity in the slope at $t = t_I$.

When comparing this model with the observational data on FH Ser, CW found t_0 = 45 days, consistent with the time of the observed upturn in the infrared flux. Taking $T_* = 10^4$K and $L = 1.9 \times 10^4 L_0$ results in $v_{ej} = 1.226 \times 10^8$cm s^{-1}. The grain temperature of $\leq$ 900 K observed after 90 days pointed to a model with $a_\infty = 2 \times 10^{-4}$cm and L_{ir} peaked at ~ 90 days which is in strong agreement with $t_{max} = 1.91t_0$ i.e. 86 days.

2.4.2.2 Departure From The CW Model

Whereas CW considered that grains grow simultaneously in the whole shell, Yamamoto & Seki (1979) take a different view. They find that the growth timescale of a grain will be about 1 day. This is much shorter than the observed time taken for the infrared luminosity to rise. To explain this contradiction they propose a situation in which, as the outer surface of the expanding gas shell cools to the condensation temperature, condensation will begin at the outer edge of the shell. Then as the shell continues to expand the dusty region advances to the inner region of the gas shell as it too passes the condensation distance. Finally the dusty region dominates the whole shell. So whilst individual grains complete the growth (almost) instantaneously within the narrow boundary between the dusty and gaseous region, not all grains are being formed at the same time. This process accounts for the rise time of the infrared luminosity accompanied with the decline of visual luminosity. Comparison with infrared data on NQ Vul does indeed give some of the observational characteristics of this nova (see Fig. 2.16). In order to explain the observed 'isothermal' phase in this nova the authors calculate the

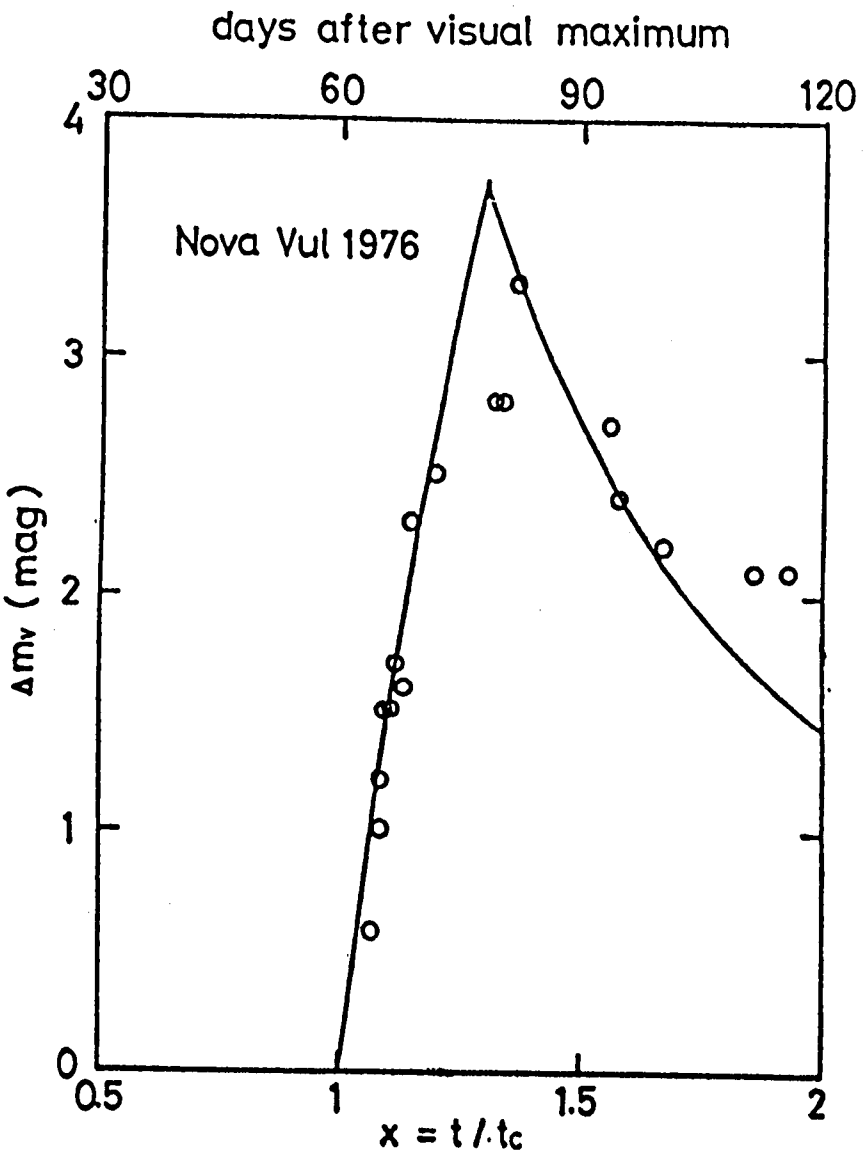

Figure 2.16. The visual decline Δv as a function of time in nova NQ Vul 1976, for which the time of intial condensation t_c = 60 days and the relative shell width $1/r_c$ = 0.3. Reproduced from Yamamoto & Seki (1979).

temperatures at the inner and outer radii of the dust shell (assuming the dust shell expands at a constant velocity maintaining constant width). They find, in this case, that the relative width of the temperature distribution becomes small at times > $1.3t_o$ thus accounting for the temperature uniformity in the later stages after the infrared maximum.

2.4.2.3 Models Involving Ionizational State

A different approach to dust formation in novae was made by Gallagher (1977). He suggests that it is the ionizational state of the gas in the nova ejecta that governs dust production (cf. Chapter 3). As this is a consequence of the luminosity of the system it is the ambient radiation field that controls the formation of grains.

Gallagher begins by assuming (borne out by observations) that there is a universal postvisual maximum constant luminosity phase in a 'normal' nova. This constant luminosity level he takes to be

$$L_{cl} \sim L_{peak} \tag{2.16}$$

in slow and medium speed class of novae, and

$$L_{cl} < L_{peak} \tag{2.17}$$

in fast novae. In doing this he is the first to imply that nova speed class is linked with grain formation.

So using this L_{cl} as a crucial parameter together with the usual conditions for the beginning of grain nucleation he finds that

$$T_g \sim 2(L_{cl}/4\pi\sigma r^2)^{1/4} \tag{2.18}$$

and the time t_d at which the dust becomes observable is

$$t_d = 2/T_o(L_{cl}/4\pi\sigma)^{1/2}1/v_{ej} \tag{2.19}$$

Assuming the condensation temperature is the same for all novae that produce grains (he uses 1300 K as a 'reasonable' value), then

$$t_d = (320/v_{ej})(L_{cl}/L_o)^{1/2} \text{ days} \tag{2.20}$$

Why then do fast novae not produce dust, as on the basis of equation (2.20) V1500 Cyg 1975 should have produced dust within ~ 75 days? Gallagher maintains that it is the ionizational state of the ejecta in fast novae that stops grains forming. For if ionization occurs rapidly enough, then the gas in which nucleation might occur will become optically thin to high energy ($h\nu \geq 13.6$eV) photons. These photons will then disrupt any of the nucleation clusters that are attempting to begin the grain formation process. Taking this one step further, if the gas is fully ionized before nucleation clusters have formed, then coulomb repulsion will inhibit the formation of any nucleation centers.

Gallagher calculates that the radius r_i of the ionized region in the nova envelope will be approximated by

$$r_i = [q_h/(4/3\pi n_h n_e \alpha_b(T)]^{1/3} \tag{2.21}$$

where q_h is the number of hydrogen ionization photons per second, $\alpha_b(T)$ is the case B hydrogen recombination coefficient and n_h the number density of hydrogen which is approximately equal to n_e the number density of electrons. We have

$$n_h = M_{ej}/(4/3\pi(v_{ej}t)^3 m_h) \tag{2.22}$$

assuming an uniform density. The ejecta are completely ionized when $r_i = v_{ej}t_i$ so

$$t_i = 2.2 \times 10^6/v_{ej}(L_{cl}/L_o)^{1/3} \tag{2.23}$$

Setting $t_i = t_d$, so that a critical luminosity L_{crit} is defined such that novae with $L_{cl} > L_{crit}$ are expected not to form substantial amounts of dust, Gallagher found numerically that $L_{crit} = 4 \times 10^4 L_o$.

Comparing this criterion with actual observations (assuming the same value for M_{ej} and the radius of the central star for all novae) shows a general agreement to Gallagher's model (see Table 2.1). There is one notable exception though, the nova HR Del 1967. In this nova t_d is calculated to be 45 days whereas t_i is calculated as 260 days yet no dust was observed. The author explains this by suggesting that the density of possible nucleation centres in this nova could be below the threshold for growth of the grains.

Yamamoto et al. (1979) expand on Gallagher's model by placing a lower limit on the mass of the envelope before dust can grow. By taking the luminosity of the central star to be lower than the Eddington luminosity (so in keeping with the observations of Wu & Kester, 1977 who suggested that the maximum bolometric luminosity of a nova ≤ the Eddington luminosity) and equating the temperature at which dust condenses with the temperature of grains in an ionized gas they find that

$$M_{ej}/M_o = 3.7 \times 10^{-5}(1800/T_o)^3 (y/1.8 \times 10^{10})^{1/2}(Q/100)^{3/4}(M/M_o(1-\beta)/0.5 \times 0.38/\kappa)^{5/4} \tag{2.24}$$

Table 2.1

Predicted and observed dust formation time scales in novae.

Nova	Speed Class	t_d (days)	t_i (days)	t_{break} (days)
V1500 Cyg	very fast	>52	<38	none
DK Lac	fast	>87	<64	none
FH Ser	moderate	58	130	68
DQ Her	slow	131	320	110
HR Del	very slow	45	260	none

Gallagher's (1977) model applied to actual novae. On his model dust should form if t_d, the dust consendation time, is less than t_i, the hydrogen ionization time. t_{break} gives the time after outburst of the break in the visual light curve. HR Del appears to behave contrary to the model prediction (see text for more details of this model).

Here y is the ratio of the total number of Lyman photons emitted from the stellar surface to the stellar luminosity, Q is $Q(T_*,a_0)/Q(T_g,a_0)$, M is the total mass of the of the nova system, β is the ratio of gas pressure to total pressure at the white dwarf surface and κ is the opacity (thought to be mainly due to electron scattering). Thus they concluded that if $M_{ej} \geq 3.7 \times 10^{-5} M_0$ grains could grow in the nova envelope.

Mitchell & Evans (1984) considered Gallagher's (1977) paper and decided that it was more likely that the ionizational state of the grain forming monomer (they used carbon) would be the critical factor influencing grain formation and not that of hydrogen. So they calculated the times that it took to ionize the ejected hydrogen and carbon completely. They assumed a uniform gas density that decreased with time as t^{-3} (because of the expansion) and that the recombination times were small compared to the ionizational times. They also incorporated the empirical relationships between nova speed class and other nova parameters to calculate these ionization times (see section 2.4.2.5).

The results of these calculations are shown in Fig. 2.17. In general the time to completely ionize hydrogen, t_h, is about 10 times longer than the time taken to completely ionize carbon, t_c and, as expected (because of the higher bolometric luminosity and the greater rate at which T_* increases in fast novae), the ionization times for fast novae are the shortest. When comparing the speed classes of three dusty novae (FH Ser, NQ Vul & LW Ser) the authors found that $t_c \sim 3$ days whereas $t_h \sim 100$ days for an ejected mass of $10^{-4} M_0$. Hence the ionization of carbon occurs long before the appearance of an infrared excess. This implies that if carbon grain formation is responsible for this excess then the grains must have formed from an ionized gas phase monomer. The authors question whether coulomb repulsion would inhibit the homogeneous nucleation of carbon and make other (presumably non-ionized) species more energetically attractive as

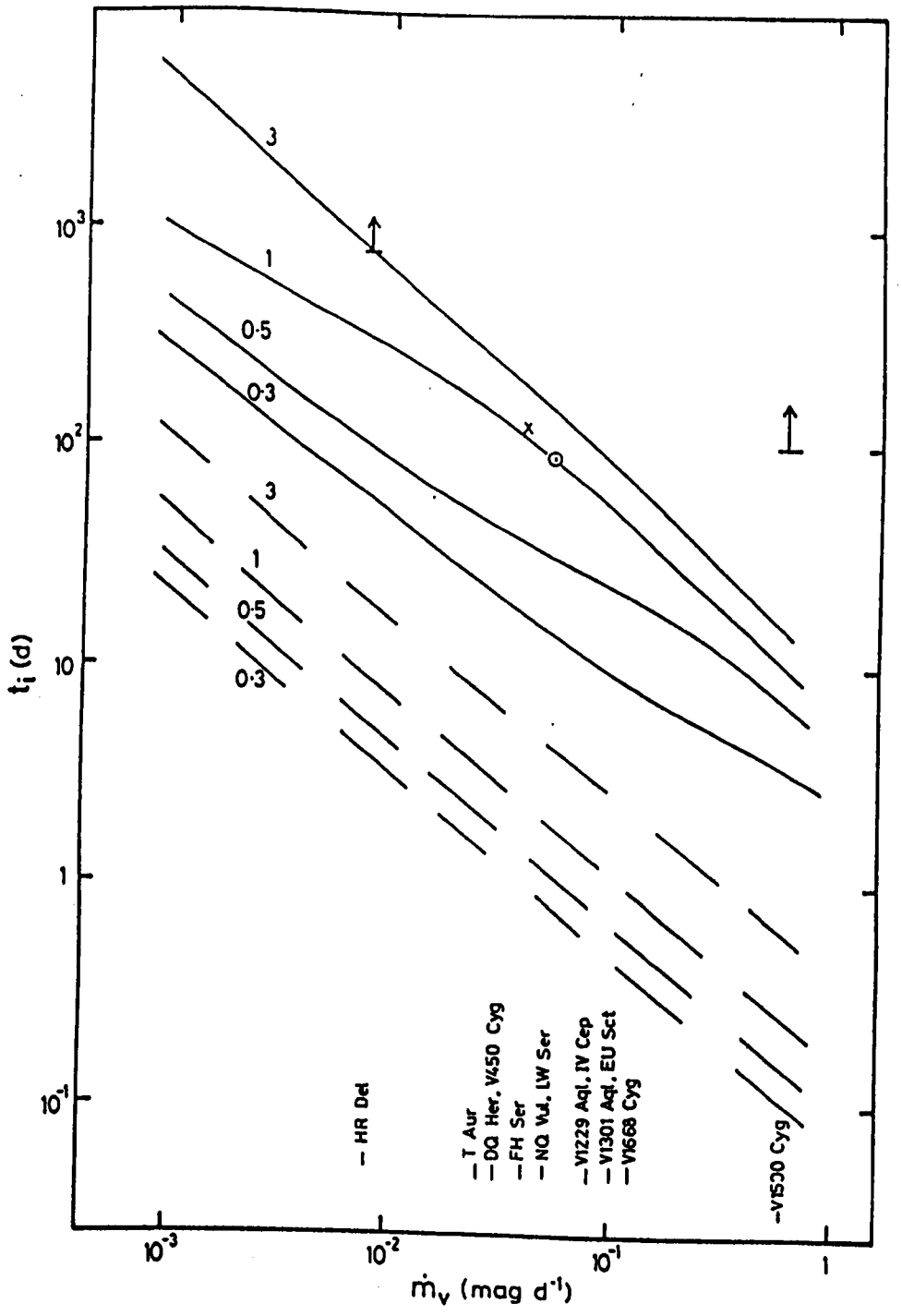

Figure 2.17. Dependence of ionizational time scale on speed class for hydrogen (solid lines) and carbon (broken lines) in the ejecta of classical novae; numbers are ejected mass in units of $10^{-4}M_{\odot}$. Grain destruction times for FH Ser 1970 (x), Nu vul 1976 and LW Ser 1978 (both o) are indicated. Reproduced from Mitchell & Evans (1984).

nucleation centres.

If the start of the grain destruction phase (as suggested by Mitchell et al., 1983, see section 2.4.2.6) is taken as just after maximum infrared flux is observed then the calculated theoretical hydrogen ionization time coincides with the start of grain destruction in the novae FH Ser, NQ Vul and LW Ser. This is explained by connecting the beginning of the grain destruction phase with the changed physical conditions in the dust shell when it is overtaken by the hydrogen ionization front.

The authors have also examined the charging of the grains during various post outburst stages of novae evolution. Soon after outburst, when carbon is ionized and hydrogen is not, is the grain growth period (see however Chapter 3). Then the proton collision rate (i.e. positive charging mechanism) is dominated by the electron collision rate (a negative charging mechanism). Thus the grains become more and more negatively charged by electron collisions until the cross section for ion collisions is sufficiently coulomb enhanced to ensure equilibrium. Calculation of the grain potential V_g at this time gives -3.5V. The authors argue that such grains are unlikely to be destroyed by grain-grain collisions when the grains are at this potential. In fact at this negative potential there will be a more frequent collision of gas phase monomers and grains so that the grain growth timescale will be reduced i.e. rapid grain growth. However when the hydrogen is also completely ionized the negatively charged grains will appear as attractive to collisions from HII as well as CII; this together with the lack of gaseous carbon (which has previously formed into grains) will halt grain growth and signal the beginning of grain destruction. This grain erosion would take the form of chemical sputtering by hydrogen and would also be helped if there were density enhancements in the ejecta, which conversely would also help to produce large grains during the rapid grain growth period.

Mitchell & Evans suggest an observational consequence of hydrogen

atoms interacting with carbon grains would be that hydrocarbon band resonances would give rise to infrared spectral features at 3.3μm and 11.3μm. Unfortunately no unambiguous evidence of such spectral features has been found yet.

These ideas were expanded on by Mitchell et al., (1986). They invoked grain charge to explain the 'isothermal' stage observed in the moderate speed novae FH Ser and NQ Vul and why infrared propeties and grain destruction phases are linked to the visual flux. They suggested that the formation of an optically thick shell may be a precondition for grain destruction. This ties in with the observations of FH Ser and NQ Vul, both of which produced optically thick shells and exhibited an 'isothermal' stage whilst the nova V1668 Cyg which produced an optically thin shell did not undergo an 'isothermal' stage.

By the inclusion of the photoelectric effect explicitly Mitchell et al. calculated that, at the start of the formation of a dust shell (i.e. optically thin stage), the grains would be positively charged by the photoelectric effect. Thus they would be less susceptible to proton attack. When the shell becomes optically thick the ultraviolet flux to the outermost grains become more negatively charged as a result of electron collisions dominating. The more negative the grains become the more proton grain collisions, and hence chemisputtering, begin to destroy the grains. In this way grain destruction is 'tuned' to the observed ultraviolet and hence visible flux. So for a shell that does not become optically thick the grains remain positively charged and grain destruction will not occur on an observable scale. Mitchell et al. note that the type of grain destruction involving charge will be critically dependent on the plasma density which controls the chemisputtering rate.

The limitation of this model is that it will only work if the photoelectric effect was to operate on the grain material. In the case of carbon it will but in the case of silicate, it will not. The nova V1307

Aql 1982 indicated silicate based grains but also underwent a visual minimum and an 'isothermal' phase (Bode et al., 1984). Clearly this mechanism cannot explain the observations of this nova as the photoelectric effect will not operate effectively on such grains.

2.4.2.4 Models Predicting Type Of Grains Formed

Soon after the CW model of rapid grain growth, Yamamoto & Nishida (1977) developed a model which predicted the type of grains formed in the nova ejecta. They started from the assumption that the abundance ratio C/O was smaller than unity. This means that carbon atoms would almost all be depleted in CO molecules and condensation into graphite grains would not take place. They found that magnesium silicate would be the first main condensate.

These authors derived a 'non- steady state nucleation formalism' which they said would be applicable to novae as the variation of temperature and density would practically be the same as the nucleation time. Firstly they calculated the number density of gas, n, in the nova envelope

$$n = M_{ej}/m_h/((4/3\pi\eta)(L_*/(4\pi\sigma T^4))^{3/2}) \qquad (2.25)$$

where M_{ej} is the ejected mass, m_h is the mass of a hydrogen atom and η is the 'geometrical factor' and is constant if the envelope expands keeping its width proportional to the outer radius.

These authors again use the same criterion as in previous work, i.e. that the onset of grain formation when the condensation temperature T_o is reached. They describe the growth of clusters of monomers as

$$d/dt(4/3\pi a^3) = \Omega C_0(t)4\pi a^2\langle v\rangle \qquad (2.26)$$

where Ω is the molecular volume of the condensate, $C_0(t)$ is the concentration of clusters at the condensation time and $\langle v \rangle$ is the mean thermal velocity of monomers.

To obtain the maximum radius of clusters equation (2.26) is integrated from $t = t_0$ to $t = \infty$ giving

$$a_{max} = 4/3 C_0(t) \Omega \tau_0 (kT_0/(2\pi m))^{1/2} \qquad (2.27)$$

(if the effect of monomer depletion is neglected). Here τ_0 is the expansion timescale of the envelope at the onset of condensation given by $\tau_0 = r_0/3v_{ej}$.

The main conclusion that the authors derive from their work (apart from the nature of the dust material) is that the condition for the appearance of grains in nova ejecta is governed by the amount of ejected mass. They found that $C_0(t_0)$ should be larger than 5×10^4 cm^{-3} by considering the formation of the molecules Mg_2SiO_4 and $MgSiO_3$ having a $a_{max} > 5A$. They did this by calculating the number of these molecules at the condensation time compared with the total number of them at different epochs in the evolution of a nova renmant. This in turn means that M_{ej} should be larger than $10^{-4} M_0$, assuming an expansion velocity of 1000 km s^{-1}. Such a condition explains the dust excess in FH Ser and the lack of dust in V1500 Cyg as the former appeared to have $M_{ej} > 10^{-4} M_0$ whilst the latter did not.

Whilst this treatment of dust formation in novae seems plausible only three novae to date, V1307 Aql 1982, PW Vul 1984 and nova Vul 1984 no. 2, have shown any evidence of silicate dust. This perhaps suggests that a C/O ratio of > 1 is to be found in the majority of nova ejecta.

Fujimoto (1980) expanded on the earlier predictions of Yamamato & Nishida (1977) when considering what type of grains would form during nova

explosions. From theoretical considerations of the evolution of CNO elements during the hydrogen shell flash on the surface of the white dwarf he concluded that the C/O ratio would be less than unity when Δm_h (mass of the accreted hydrogen rich envelope) and M_{wd} (mass of white dwarf) were small ($M_{wd} < 0.6\ M_o$) producing silicate grains. C/O would be greater than unity when Δm_h or M_{wd} ($> 0.8\ M_o$) were large, resulting in graphite type grains. This is in accordance with the results of Warner (1973) who calculated that in general white dwarfs in binary systems are up to three times as massive as those in isolation hence explaining why most dusty novae are observed to produce carbon based grains. (Fujimoto assumed normal cosmic abundance for the accreted material).

Fujimoto also found (by estimating the maximum size to which a grain must grow) the mass of the ejected envelope required for grain formation. To do this he put a condition on the minimum size a grain must be so that thermal emission would to be observed from it; this he took be 10A. The calculated minimum ejected masses were $7.1 \times 10^{-4}\ M_{wd}$ for silicate grains and $3.9 \times 10^{-5}\ M_{wd}$ for carbon grains. This puts a constraint on the recurrence period for a nova needed so that the subsequent novae outbursts would be accompanied by dust formation. Fujimoto calculated this to be $> 10^4$ years.

2.4.2.5 A Speed Class Dependent Model

Bode & Evans (1982a) attempted to explain why fast novae do not appear to produce dust. They based their explanation on the premise that the condensation time was dependent on the speed class.

The empirical relationships between nova speed class and other novae parameters that they employed were

$$v_{ej} = 2.96 \times 10^{13} m_v^{0.45} \text{ cm day}^{-1} \tag{2.28}$$

(McLaughlin, 1960) where m_v is the speed class in mag day^{-1},

$$L = 4 \times 10^{39} m_v \text{ erg s}^{-1} \tag{2.29}$$

(Shara, 1981) and

$$\Delta m = -2.5\log(1.36(15/\pi^4)(hc/(\lambda kT_*))^4 1/(\exp(hc/(\lambda kT) - 1) \tag{2.30}$$

(Bath & Shaviv, 1976).

Now following the earlier arguments of CW, they calculated the condensation distance as a function of time, and the ejecta distance with time (using $r_{ej} = v_{ej}t$). As condensation is only considered possible when $r_{ej} \geq r_0$, using equations (2.28) - (2.30) they were able to estimate when this condition was met by novae of different speed class (see Fig. 2.18). They concluded that, for novae of 'fast' speed class, the time time taken for the ejecta to reach the condensation distance is much greater than for novae of slower speed class. Taking this result into account the authors then calculated the effect that varying $(T_*)_{max}$ and the Planck mean absorption efficiency dependence on temperature would have on the condensation. Varying $(T_*)_{max}$ pointed to the straightforward conclusion that increasing this factor would lead to a later condensation time. If $Q(T) \propto T^2$ (perfectly conducting grains) Q(T) soon becomes unity and the increase of the condensation time with speed class only depends on slowly varying values of T_0 and $Q(T_0)$. Taking $Q(T) \propto T$ (impure graphite) leads to the general conclusion that novae with declines greater than ~ 0.1 mag day^{-1} may only form substantial numbers of grains $\geq$ 100 days from outburst.

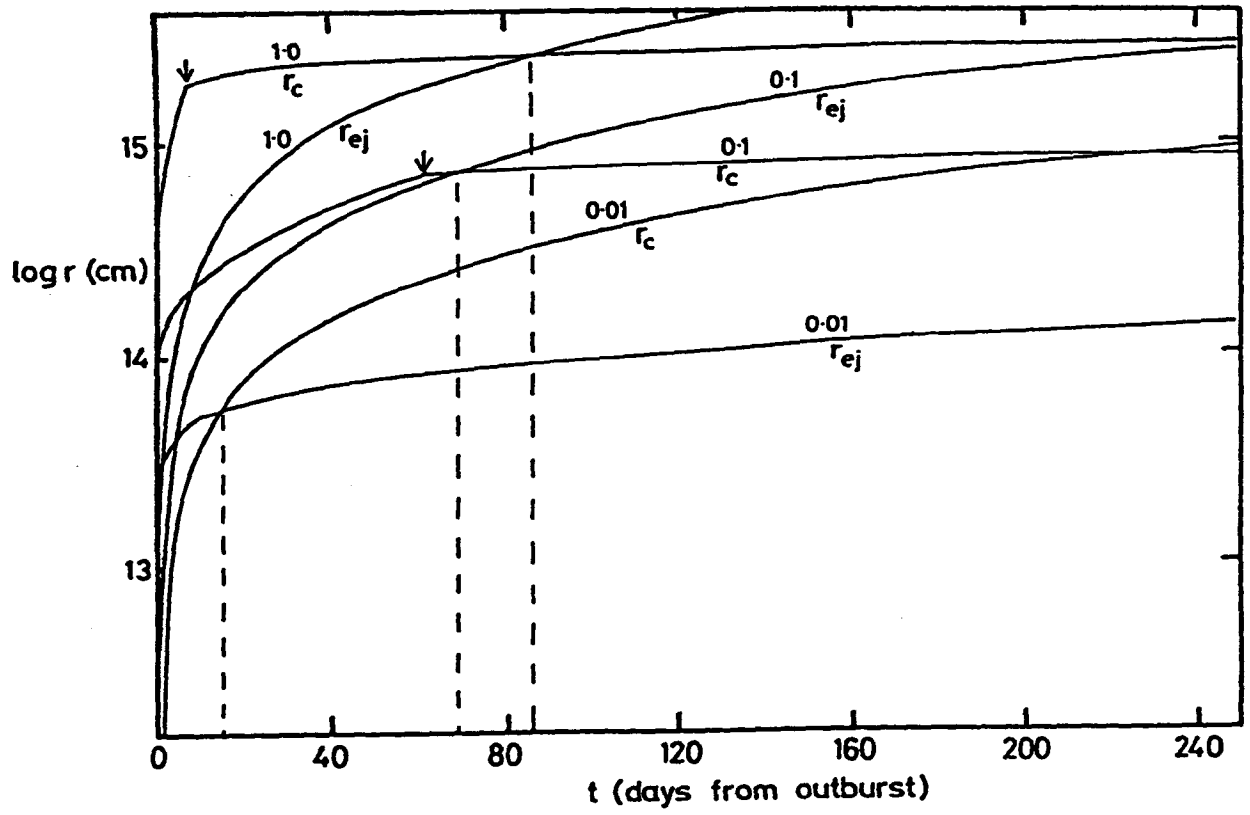

Figure 2.18. Relationship between ejecta distance (r_{ej}) and condensation distance (r_c), and time since outburst for novae with speed classes 0.01 mag d^{-1}, 0.1 mag d^{-1} and 1 mag d^{-1}. Reproduced from Bode & Evans (1982).

When considering the optical depth for novae of different speed class the authors found that (assuming the same number of nucleation centres for all novae) there is a small boundary between $m_v = 0.08$ and $m_v = 0.1$ mag day^{-1} that differentiates between those novae with substantial dust shells (the slower speed class) and those without.

When compared with the observations of different novae this model stands up well. But like the Gallagher (1977) model it does not explain why the slow nova HR Del 1967 did not form a substantial dust shell early on after its outburst.

2.4.2.6 Models For NQ Vul 1976

The nova NQ Vul 1976 was modelled in terms of its dust production by the authors Bode & Evans (1983a) and Mitchell et al. (1983). Bode & Evans (1983a) attempted to fit blackbody and pseudoblackbody functions to infrared photometry of NQ Vul and LW Ser (see Fig. 2.19). These calculations were very satisfactory fitting the data up to 20μm. If these shells were geometrically thin then $2\pi a/\lambda \geq 1$ would hold, which means the grains must be $\geq 3\mu m$.

This blackbody fitting was used by the authors to explain the behaviour of the dust temperature and the infrared light curve of NQ Vul in an analogous way to Grotrian's (1937) treatment of the visual data of DQ Her. When the ejecta reach the condensation distance grains are formed rapidly due to a high mass flow. The shell opacity will thus increase rapidly while infrared emission is great and the visual flux falls. However as the mass flow rate decreases so does the grain formation rate. As the dust shell expands the infrared and visual opacities reach a maximum and then start to decline. When the optical depth reaches this maximum the temperature is at a minimum as we are observing only the outer, cooler, layers of the dust shell. As the dust shell becomes optically thin the inner (hotter) regions become observable to us. When the shell becomes

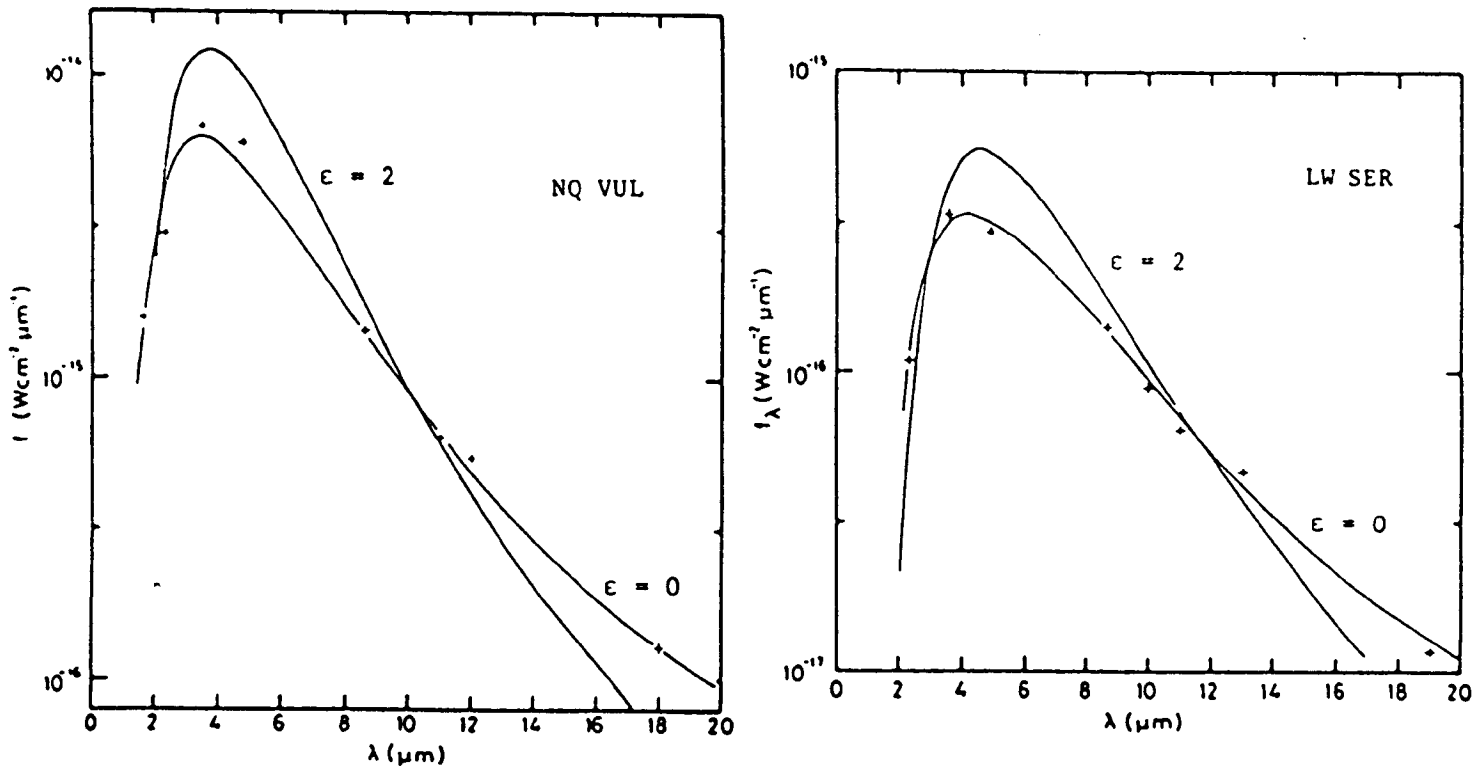

Figure 2.19. Least squares fits to the data of (a) NQ Vul 1976 and (b) LW Ser 1978 for single temperature blackbody emitters ($\varepsilon = 0$) and those whose emissivity falls away as λ^{-2} ($\varepsilon = 2$). Reproduced from Bode (1982).

truly optically thin its temperature will decrease as we observe it expanding away from the central star. In this way Bode & Evans have developed the concept of an infrared pseudophotosphere.

Such a model for the infrared evolution of a nova is examined by Mitchell et al., (1983) for NQ Vul. They consider the effects diminshing mass loss and grain growth and nucleation will have on its development.

At any distance r from the nova, the gas density ρ at time t from outburst is given by

$$\rho(r,t) \propto r^{-2}\exp(-k(t - r/v_{ej})) \tag{2.31}$$

where k is a constant. Grains will nucleate and grow once they have passed through the condensation distance $r_0 = 5.2 \times 10^{14}$ cm ($v_{ej} = 1000$ km s^{-1} and $t_0 = 60$ days from observations). In this model grains grow instantaneously once they have passed through r_0 but grain growth will go on all the time as more material passes through r_0. As $\rho = \rho(r,t)$ so the number density of grains $n = n(r,t)$ such that

$$n(r,t) \propto r^{-2}\exp(2k(t - r/v_{ej})) \tag{2.32}$$

Hence the grain size distribution will be

$$a(r,t) \propto \exp(-k(t - r/v_{ej})) \tag{2.33}$$

It is assumed that the grains are impure graphite (as this is more realistic than pure graphite and NQ Vul did not show any evidence of a 10μm feature which would suggest silicate based dust) so that,

$$Q_{abs} = \text{const} \quad (\lambda \leq 2\pi a) \tag{2.34}$$

$$Q_{abs} \propto \lambda^{-1.8} \quad (\lambda > 2\pi a) \tag{2.35}$$

Values for the bolometric luminosity of the nova 9×10^{37} erg s^{-1}, its effective temperature 5×10^{4}K and Q_{abs} were assumed constant during the period of interest and these parameters and conditions were used in a time dependent optically thick dust shell model. The equations of radiative transfer were solved for a series of quasistatic spherically symmetric models (see Fig. 2.20). Mitchell et al. found that the best fits to the data occurred when the grain size was being eroded with time. They attributed this erosion to sputtering by high velocity secondary ejecta but noted this mechanism could not account for all the erosion required (see 2.4.2.3).

All these models are variants on the suggestion that grain growth takes place rapidly in the nova ejecta soon after outburst. The next section deals with the theory that grains already existed in the system before the nova outburst.

2.4.3 Pre-Existing Grains Model

Before examining this model in great detail we will look at the reasons why the rapid grain growth model was questioned by Bode & Evans (1980), the authors who formulated the pre-existing grains model.

They began by considering the observational evidence that suggested rapid grain growth i.e. the diminishing visual flux and the reddening of the nova. As discussed earlier in this chapter (section 2.2) the visual minimum could be explained in terms of varying mass loss from the central star creating an optical pseudophotosphere (Grotrian, 1937; Bath & Shaviv, 1976). Regarding the reddening of the novae FH Ser and V1301 Aql, in both

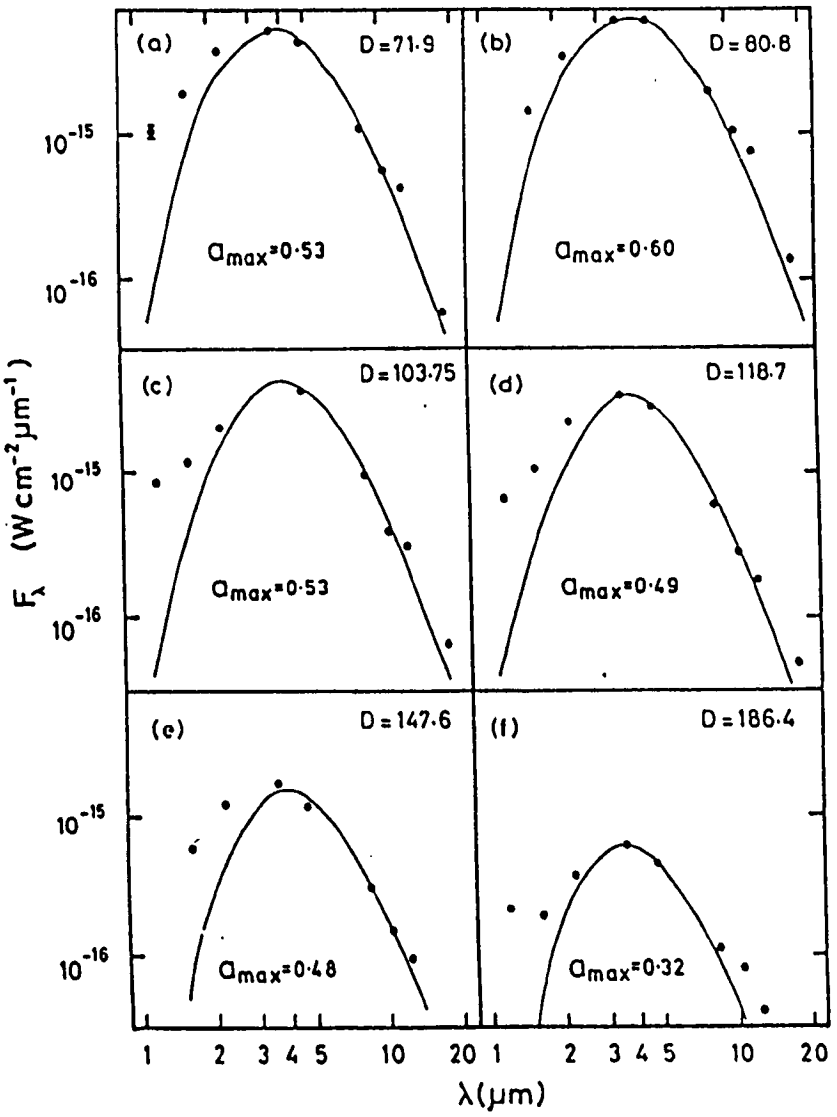

Figure 2.20. Fits to the infrared data of NQ Vul 1976 from the model of Mitchell et al. (1983) (from whom this figure is reproduced). D gives the number of days from outburst. Note the apparent changes of the maximum grain sizes.

cases the increase in (B-V) was accompanied by a decrease in (U-B), which is not consistent if grains are the cause of the (B-V) increase. Bode & Evans suggest this 'reddening' can be better understood in terms of the spectral behaviour of the nova system itself.

Taking the case of FH Ser; observationally (when the infrared flux started to rise) the condensation distance was reached after 45 days implying an ejection velocity ~ 2000 km s^{-1} ($v_{ej} = r_0/t_0$). However if the principal velocity is taken to contain the bulk of the material (Gallagher, 1977) then this principal velocity was observed to be ~ 650 km s^{-1}, so grains would then form after ~ 225 days much later than the 45 days observed.

The hostility of the post nova environment is one of the major drawbacks to the rapid grain growth model. Taking into account temperatures of ~ 10^4K and the presence of shocks in such an environment, it is very suprising that grains could form at all. The CW model requires that the conversion of carbon into graphite grains is nearly 100% efficient. Bode & Evans do not consider this requirement at all reasonable.

Gehrz et al., (1980a), when considering the production of the optically thick dust shell in LW Ser on the rapid grain growth model, required that the mass should be ejected in a thin shell in a fairly short time scale ($\leq$ 8 hours). However this assumption of instantaneous ejection is contrary to the findings of Shara (1981), who shows that 85% of the mass ejection occurs while the nova declines 3 magnitudes from maximum, which in the case of LW Ser would be ~ 60 days.

If, in the light of these suggestions, we accept the rapid formation of grains does not occur in novae, is there any evidence to suggest that the dust is pre-existing? The work of Zellner (1971) and Malakpur (1977) does indeed suggest pre-existing grains. Zellner obtained polarization data on HR Del 120 days after outburst. He observed an intrinsic

polarization averaging 0.6% in red light and declining sharply towards the ultraviolet and infrared. He explained this by scattering from highly absorptive grains (perhaps graphite or iron) of radius ~ 0.1μm (see Fig. 2.21). However Zellner remarks that such grains could not give rise to the infrared excess observed in HR Del as the polarization data was taken long before the excess was seen and such grains do not radiate very efficiently as a blackbody. He thus concluded that the 0.1μm grains were pre-existing, maybe left over from previous outbursts or perhaps scoured from surfaces of asteriodal or planetary bodies which were swept out with the nova ejecta. So Zellner suggests that there were two types of grains and that the pre-existing ones provide condensation nuclei for those of radius ≥ 1μm which ultimately would give rise to the observed infrared excess. Malakpur came to the same conclusion about pre-existing 0.1μm grains in HR Del by considering the time variation of the Balmer decrement. He likewise considered them to act as nucleation centres for ultimately larger grains.

How then does the observed visual and infrared evolution come about assuming pre-existing grains? Bode & Evans (1980) define what they call the 'heating function' as

$$H(t) = \int L_\nu Q^*_{abs}(\nu)\, d\nu \qquad (2.36)$$

Thus it is the time dependence of H(t) that is responsible for the time dependent heating of circumnova grains. In order to determine the time dependence of the heating function the frequency dependence of Q^*_{abs} for the grains surrounding the nova and the time dependence of the nova's short wavelength emission must be known. Assuming that the total bolometric luminosity of a nova remains constant the decrease in visual magnitude below maximum is given by equation (2.30), λ_V = 5500A. This defines the time dependence of the effective temperature of the nova and thus in part the time dependence of H(t).

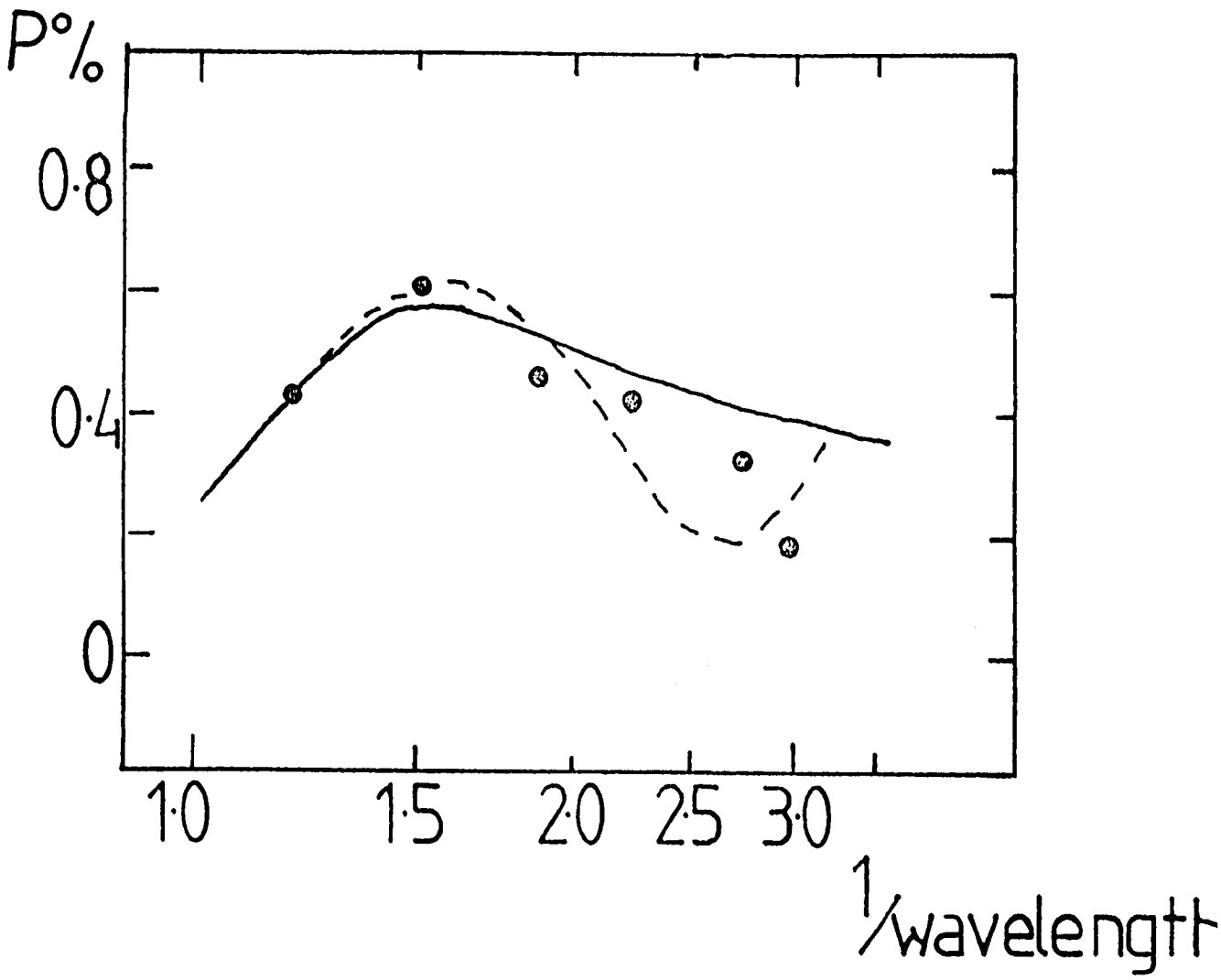

Figure 2.21. Intrinsic polarization against wavenumber in μm^{-1} for HR Del 1967. The dashed curve is for graphite grains with radius 0.10μm, and the solid curve is for iron grains of the same radius. Reproduced from Zellner (1971).

Bode & Evans (1980) determine H(t) for FH Ser by solving equation (2.30) iteratively. They assume spherical graphite grains of constant 0.01μm radius throughout the infrared developement of this nova and calculate the frequency dependence of Q^*_{abs} using the Mie formulae. They also assume the nova system has $L = L_{eddington}$, mass = 1 M_o and that the dust envelope is unchanging throughout the outburst. The results of these calculations (see Fig. 2.22) shows H(t) to have three distinct phases:

i)firstly in the time between outburst and transition. The grains will be heated increasingly by H(t) but this heating will be at an insignificant level;

ii) at transition the heating of the grains will rise rapidly as the Planck spectrum of the nova meets the peaks in the $Q^*_{abs}(\nu)$ curve;

iii) after transition H(t) will decay following roughly an exponential law as the still shifting Planck function passes away from the Q^*_{abs} maxima leaving behind an ever decreasing Rayleigh-Jeans tail. H(t) was thus approximated by:

$$H(t) = 0 \quad (t \leqslant \Delta t) \text{ phases (i) \& (ii)}$$
$$H(t) = H_o \exp(-\omega t) \quad (t \geqslant \Delta t) \text{ phases (ii) \& (iii)} \qquad (2.37)$$

where Δt is a fiducial time near the onset of transition. H(t) may be also be written as (for a blackbody distribution)

$$H(t) = L\, Q^*_{abs}(a, T_e) \qquad (2.38)$$

where L is the constant bolometric luminosity. This underlines the difference between the pre-existing grains model and that of CW in that here a is constant whilst T_e is changing which is the opposite to the latter model. During phase (iii) when the Planck function can be approximated by the Rayleigh-Jeans limit equation (2.38) becomes

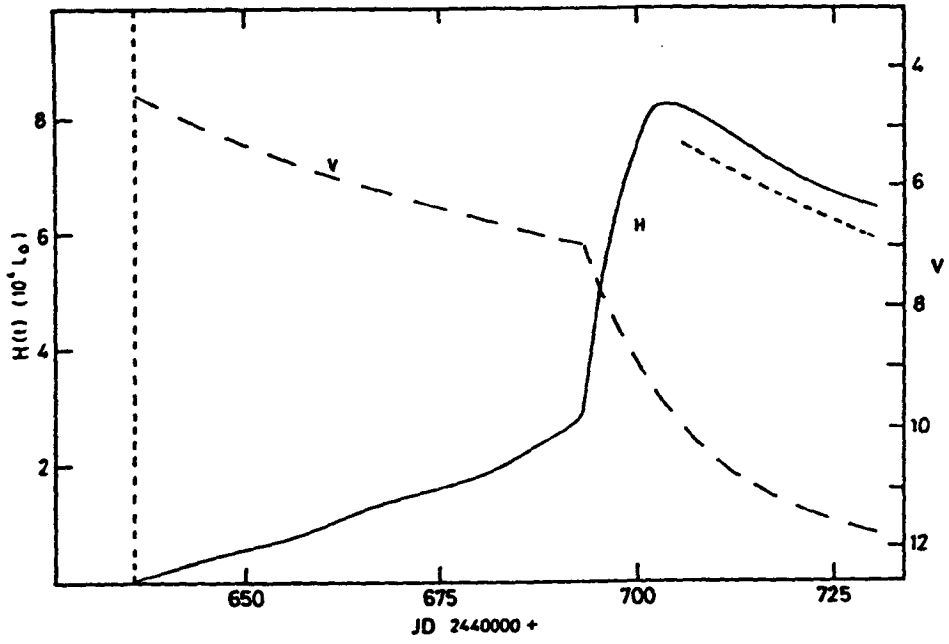

Figure 2.22. 'Heating function' H(t) for Nova FH Ser 1970. Main broken curve is visual light curve. Broken vertical line is time of maximum visual flux. Broken curve at upper right is exponential decline with decay constant $0.01d^{-1}$. Reproduced from Bode & Evans (1980).

$$H(t) \sim \text{const} \times f(\text{vis.cont.}) \qquad (2.39)$$

the continuum flux density in the visual.

The authors fitted their model to various novae. For FH Ser (see Fig. 2.23) the best fits occur for a uniform dust distribution. At times $<\Delta t$ the model does not appear to work but then the infrared flux may be due to the nova photosphere and/or spectral features. The slight rise of the infrared flux shortly before transition was attributed to early heating of the grains by H(t). For V1301 Aql the best fit to the model is obtained if the dust distribution has a degree of central condensation. The value of Δt that gives the best fit is $\Delta t = 9$ days after discovery. This is consistent with Vrba et al., (1977) whose observational data run from day 10, hence covering the period after transition.

Bode & Evans (1981) elaborate on the pre-existing grains model and explain in more detail how the observational evidence need not point towards rapid grain formation. They note that the visual light curve oscillations that occur during transition are difficult to explain by using the condensation of dust but can be explained by irregular mass loss rate or density variations in the envelope. The visual light curve recovery is best explained as being due to the increasing contribution of emission lines during the nebular stage.

When considering spectral phenomena, the correlation of outflow velocity with light curve fluctuations may be due to fluctuations in the ejection velocity and/or mass loss rate. And the correlation of the excitation of spectral features with the light curve decline is evidence of the hardening radiation field not of rapid grain formation.

Again Bode & Evans use the heating function as a means of calculating the effect small pre-existing grains will have on the nova's development. (Here they use $H = H(a,t)$ but they still only consider constant a). They

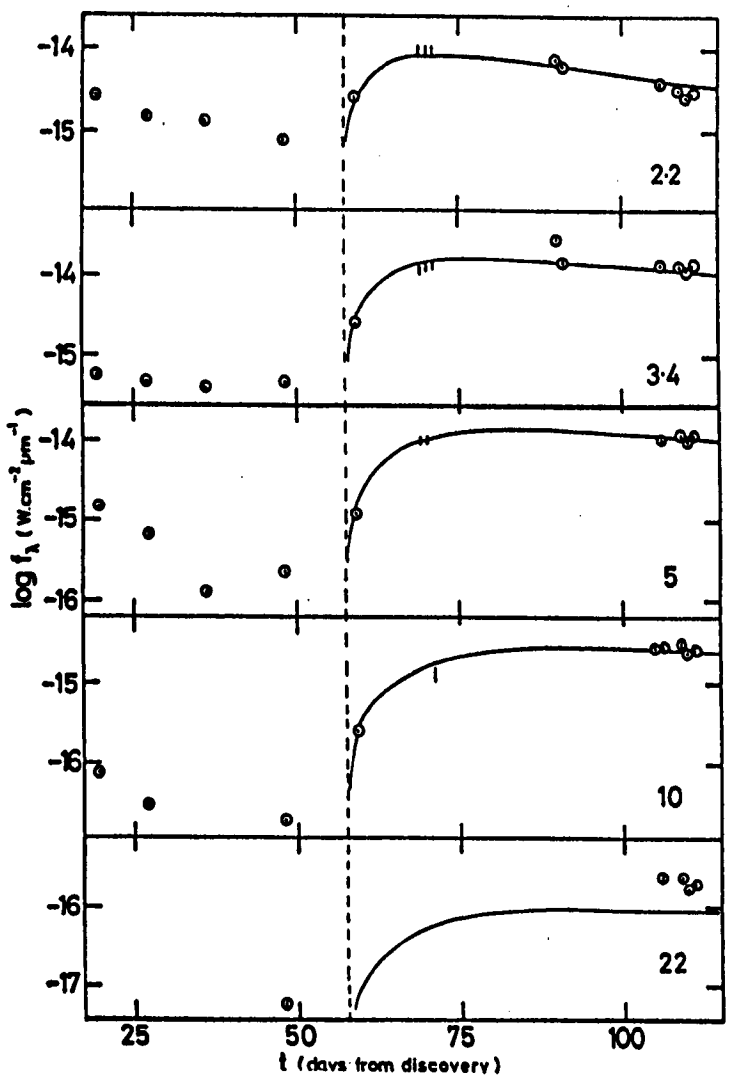

Figure 2.23. Fits of model light curves to observational data for FH Ser 1970. Numbers are observing wavelengths in microns. Δt is time from discovery. Reproduced from Bode & Evans (1980).

plot the dependence of H(a,t) on Δm for graphite grains of constant radius (see Fig. 2.24). For very large grains H(a,t) becomes the constant bolometric luminosity of the nova. The most effective heating of grains occur at 4-6 magnitudes below maximum and also the sharp decline of the visual photospheric continuum at transition will only give rise to instantaneous heating of grains if they are small. Hence for grains ≥ 0.1μm the effect of H(a,t) at infrared wavelengths would be unnoticeable. Graphite grains of a ~ 0.01μm have peak absorption efficiency at 800A. These grains would be effectively heated when the nova's photospheric temperature reaches 3.6×10^4K and the corresponding visual continuum falls by ~ 4 magnitudes. This accounts for the coincidence of the transition break in the visual light curve (which occurs at ~ 3.5 magnitudes after maximum) with the rapid rise of infrared emission. Maximum infrared emission might then be expected to occur when Δm = 4, but taking into account the light travel time (ie. the time for the shell of pre-existing grains to receive this heating radiation) this will occur about four days later (this is confirmed by observations).

Considering the optical depth at short wavelengths $\tau^*(t)$ through the entire shell of radius R,

$$\tau^*(t) = -\ln(1 - L_{ir}/L_0) \tag{2.40}$$

where L_{ir} and L_0 are the dust infrared and primary luminosities. On the pre-existing grain model there would be no expected changes in $\tau^*(t)$; L_0 changes form as the pseudophotosphere shkrinks and $\tau^* = \tau^*(\nu)$ for this model thus is:

$$\tau^*(t) = -\ln((1 - L_{ir}(t))/H(a,t)) \tag{2.41}$$

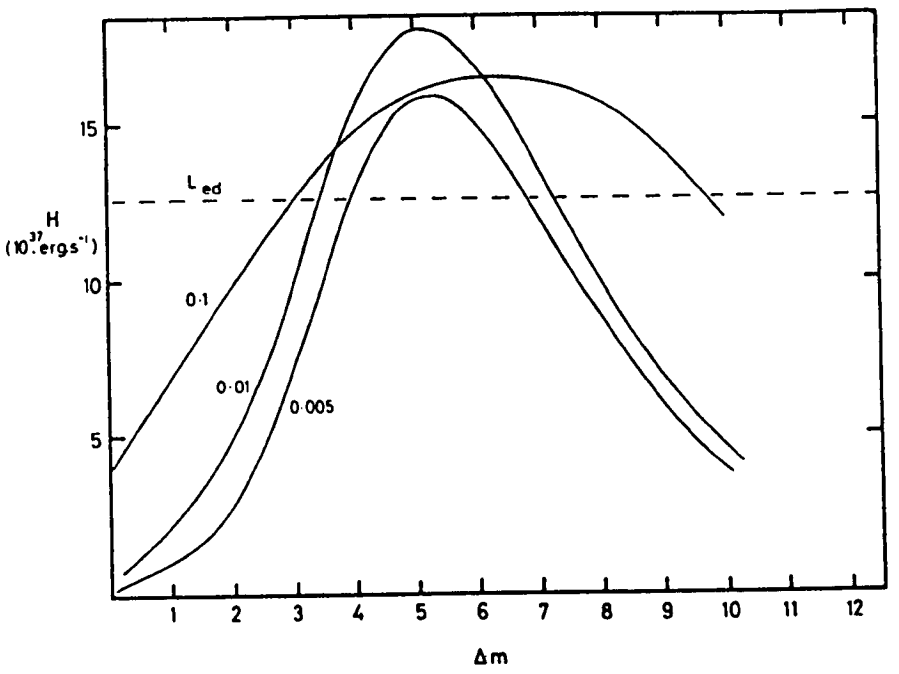

Figure 2.24. Dependence of heating function H(a,t) on Δm, the fall in the visual continuum from maximum. Curves are labelled by grain radius, in microns. Reproduced from Bode & Evans (1981).

where the optical depth has been averaged over frequency. When the light travel time is neglected the dependence of $H(a,t)$ and $L_{ir}(t)$ on time is identical, so that τ^* is indeed constant. Thus there is no contradiction between the apparent increase in τ^* and a static pre-eruptive dust shell. Bode & Evans point out that by using the above, it is possible to distinguish between the two models. As for the rapid grain growth model L_{ir} and τ^* should coincide, whilst on their model this need not be the case when the light travel time is included.

Bode & Evans (1982) calculate the extinction optical depth for different grain models as they examine the changes that may be expected in the λ2200 feature in the two models. The results of these calculations are for rapid grain growth, the extinction around 2200A is essentially neutral (apart from a very brief period near transition) whereas for the pre-existing grains model a prominent λ2200 will be formed. However if the pre-existing grains are unchanging the resultant static λ2200 feature could be misinterpreted as the rapid growth neutral feature with interstellar λ2200 superposed. Unfortunately observations of this feature have not given any conclusive evidence either way.

The origin of these pre-existing grains was considered by Bode & Evans (1981) and they suggested they could form through a gradual leakage of material that was lost from the nova system interoutburst as inferred in some dwarf novae.

Although this pre-existing grain model does appear plausible it is the rapid grain growth model that is presently in favour. This is because the latter can begin to explain a relationship between novae speed class and grain formation and why there is an 'isothermal' phase seen in some novae, neither of which the pre-existing model can do.

Recently however one nova has prompted the suggestion that the pre-existing grain model might explain the observations; it is the nova

V1307 Aql (Bode et al., 1984). Within 37 days of discovery infrared observations showed the presence of a substantial dust shell. This would mean that if dust did condense in the outflowing ejecta it must have started to form well before this time. From theoretical calculations for a nova of speed class 0.3 mag day^{-1} (the speed class of this nova) graphite grains could only begin to form $\geq$ 80 days from outburst. That this nova produced silicate based grains may have some bearing on this apparent contradiction, but it is clear that the process of grain formation is not known in this case.

2.5 Conclusion

We have discussed in this chapter the observations of deep minima in novae that first lead to the suggestion of the presence of dust in the nova systems, the infrared observations that confirmed this suggestion and the models to explain this phenomenon.

It is clear that whilst the rapid formation of grains appears to explain the observations of a falling visual light curve simultaneously with the rising infrared light curve it becomes too easy to quote this explanation in all cases. Indeed it has been shown that, in some novae, that the initial decline in the visual light is not due to dust but due to the redistribution of this visual light to harder (ultraviolet) wavelengths as the nova maintains a constant bolometric luminosity for the first 50 days or so after outburst. The alternative suggestion of pre-existing grains also has its problems; the biggest being that it cannot explain any relationship between nova speed class and grain appearance. So although we have come a long way from McLaughlin's first suggestion of dust in the nova DQ Her even now, some 50 years later, the mechanism of grain formation is not fully understood.

CHAPTER 3

NUCLEATION IN NOVAE.

3.1 Introduction

In the previous chapter the evidence for the presence of dust in nova ejecta and the various formation mechanisms to explain the origin of this dust were reviewed. At present the rapid formation of grains in the nova ejecta is the model that appears the most plausible. Here we accept that this model is viable and discuss a method of grain nucleation. We suggest that the nucleation centres for the grains are ions and determine which ions are available and most likely to act as nucleation centres. We examine how different ejected masses and various elemental abundances affect the availability of nucleation centres.

In doing this we are able to establish some basic trends differentiating between those novae capable of forming dust and those which will not. We find that novae of moderate speed classes (roughly $0.01 < m_v < 0.08$ mag d^{-1}) are the most likely to produce dust, thus the model has some observational confirmation. As the majority of dust forming novae have been observed to produce a carbon based dust we assume this condition in the model.

3.2 Nucleation Rates.

The condition for the formation of grains is that the partial pressure of the monomer gas, P, exceeds the saturated vapour pressure of the grain forming material P_{sat}, (Bode & Evans, 1982a), i.e.

$$nkT_c > p_0 \exp(-T_0/T_c) \qquad (3.1)$$

Here k is Boltzman's constant, n is the number density of the condensing monomer, T_c is the condensation temperature and p_0 and T_0 are constants, which for carbon are 1.66×10^{14} dyne cm^{-2} and 88880 K respectively (Lefevre, 1979). It is generally considered that $T_c \sim 2000$ K (Clayton & Wickramasinghe, 1976) and at this temperature the carbon number density required for grain condensation is $\sim 3 \times 10^{7} cm^{-3}$ (see Fig. 3.1). For condensation at lower temperatures equation (3.1) reveals that the carbon number density need not be so high, but we consider (for simplicity) that this temperature and number density will signal the onset of grain condensation.

Observationally we are able to estimate the nucleation rate by calculating the number of grains formed by the time all the nova ejecta has passed through the condensation distance. When assuming a uniform outflow and a density dependence of r^{-2} the nucleation rate J becomes

$$J = 2L_f/(\pi a_0^2 v_{ej} \Delta t^2) \qquad (3.2)$$

where L_f is the fraction of infrared luminosity compared to the total luminosity, a_0 is the intial grain radius, v_{ej} the ejection velocity and Δt the ejection time. On putting 'average' numbers for typical dusty novae i.e. $v_{ej} \sim 1000$ kms^{-1} (Gallagher & Starrfield, 1978), $\Delta t \sim 60$ days (Shara, 1981), $a_0 \sim 0.01\mu m$ (Bode & Evans, 1983) we obtain $J \simeq 10^{-10} cm^{-3} s^{-1}$ as $L_f \simeq 1$.

Donn et al. (1968) considered the conditions for the formation of graphite grains in cool stars by using classical nucleation theory. Assuming that this theory will describe nucleation in novae (at least to a first approximation) we calculate the theoretical nucleation rates. Donn et al. (1968) give the nucleation rate for homogeneous nucleation as

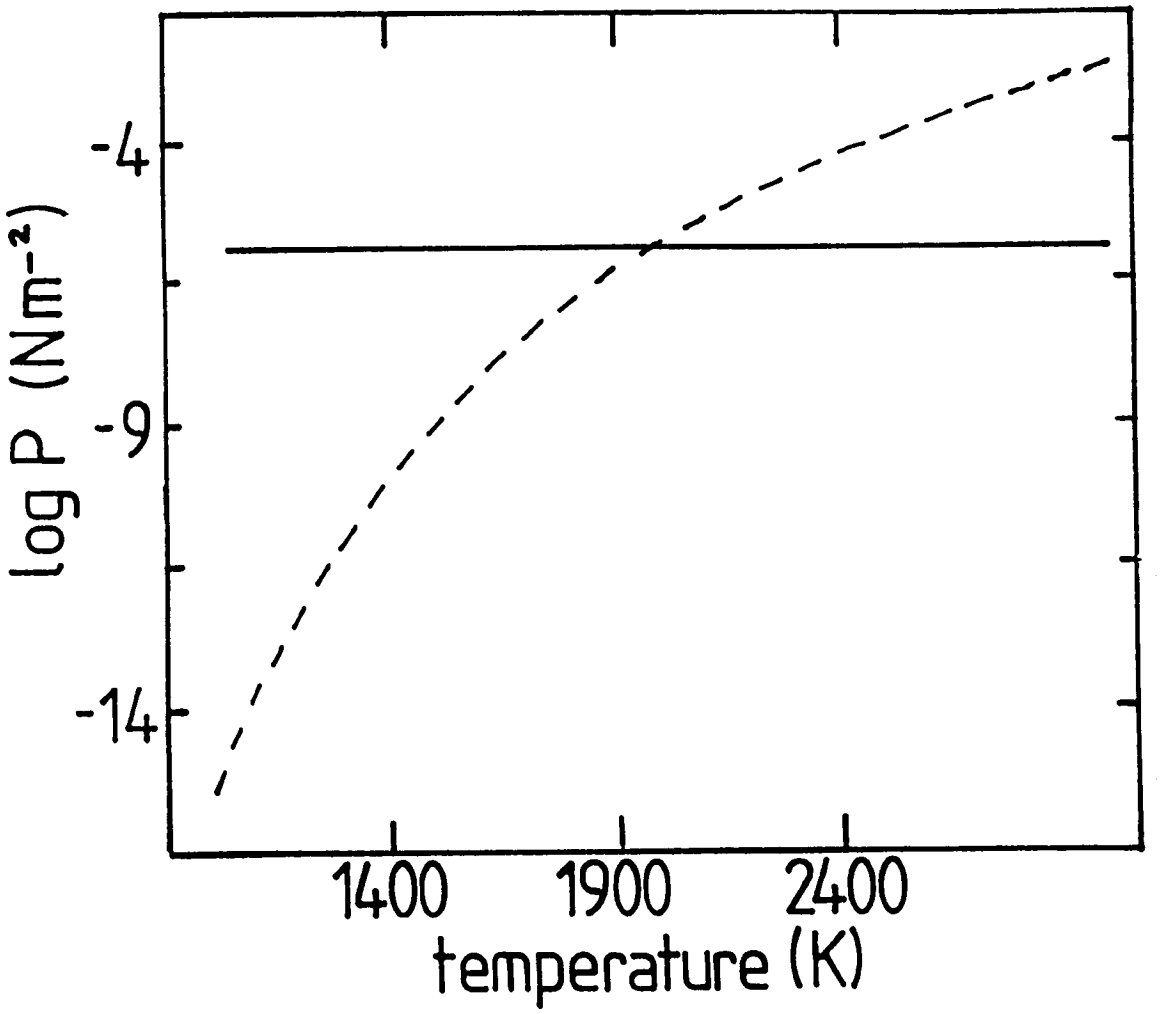

Figure 3.1. Graph to show the solution of equation (3.1) at a carbon number density of $3 \times 10^{7} cm^{-3}$, i.e. the temperature at which the partial pressure of the carbon gas (solid line) reaches its saturated vapour pressure (dashed line).

$$J_{hom} = \alpha(4\pi r^{*2})P/(2\pi mkT_c)^{1/2} \times (Zn_c \exp(-\Delta G_i^*/(kT_c))) \quad (3.3)$$

where α is the sticking coefficient for vapour impinging on the cluster, $4\pi r^{*2}$ is the surface area of the 'critical-sized' cluster, $P/(2\pi mkT_c)^{1/2}$ is the impingement rate of single carbon atoms on unit area of the cluster, ΔG_i^* is the Gibbs free energy of formation of a cluster and n_c is the number density of carbon. Also

$$r^* = -2\sigma/\Delta G_v; \quad (3.4)$$

here σ is the surface free energy and ΔG_v is the change in volume free energy accompanying condensation and is found from the expression

$$\Delta G_v = -kT/\Omega \ln(P/P_{sat}) \quad (3.5)$$

where Ω is the volume per molecule. Lastly

$$\Delta G_i^* = 16\pi\sigma^3/((3(\Delta G_v)^2). \quad (3.6)$$

Hence combining equations (3.3 - 3.6) we obtain

$$J_{hom} = 2.56 \times 10^{-9} n_c^2 Z\alpha(\sigma/1000\text{erg s}^{-1})^2 (T_c/2000K)^{-3/2} \exp(-65.7(\sigma/1000\text{erg s}^{-1})^3 (T_c/2000K)^{-3})) \quad (3.7)$$

If $\ln(P/P_{sat}) = 1$, and $\Omega = 9.09 \times 10^{-24}\text{cm}^{-3}$ then $J_{hom} \sim 5 \times 10^{-24}\text{cm}^{-3}\text{s}^{-1}$ (we put Z=0.01, α=1, after Donn et al., 1968 and $n_c = 8 \times 10^7\text{cm}^{-3}$, which is the value required if $\ln(P/P_{sat}) = 1$ and T_c=2000 K). Thus an extremely slow nucleation rate is attained by this method.

For nucleation on clusters around pre-existing ions the nucleation

rate is given by (Donn et al., 1968)

$$J_{ion} = \alpha(4\pi r^{*2})/(2\pi mkT_c)^{1/2} x\ (Pn_i Z\exp(-\Delta G_i^*/(KT_c))) \tag{3.8}$$

where n_i is the number density of avaliable ions and ΔG_{ion}^*, the critical free energy for this case is given by

$$\Delta G_{ion}^* = 4/3\pi\sigma(r^{*2}-r_1^2) - 2/3e^2(1-1/\varepsilon)(1/r_1-1/r^*) \tag{3.9}$$

Here e is the charge on an electron and ε is the dielectric constant of the cluster which is taken to be infinite (thus assuming a perfect conductor). r_1 is the size of the stable cluster about an ion and is given by

$$r_1 = (e^2/(16\pi\sigma))^{1/3}. \tag{3.10}$$

Hence combining equations (3.4), (3.5), (3.8 - 3.10) we obtain

$$J_{ion} \sim n_i\ x\ (2.06 \times 10^{-3}\exp(-35.84)) \tag{3.11}$$

assuming the same numerical values as for the homogeneous case where appropriate. Hence if $n_i \sim 1 \times 10^8 cm^{-3}$ equation (3.11) reduces to $J_{ion} \sim 5.6 \times 10^{-11} cm^{-3} s^{-1}$.

From these estimates we can see that it is unlikely that homogeneous nucleation is important in the case of novae because of its extremely low nucleation rate but the heterogeneous nucleation of carbon onto ions could indeed be a possibility considering the nearness of the ionic nucleation rate to that observed.

3.3 Nucleation On Ions.

When considering the type of ions onto which carbon could nucleate we require an element that would be ionized when carbon is still neutral (i.e. of a lower ionization potential) and a species that is abundant enough to provide adequate numbers of nucleation centers. Looking at a table of nova elemental abundances (Table 3.1) we see that the elements sulphur, silicon, iron and magnesium fit both our requirements. What we now need to know is the time at which the radius of the Stromgren sphere for species i, 'r_i', 'catches up' with the radius of the ejecta r_{ej}, as it is at this point when the element i will be completely ionized. We follow the method used in Mitchell & Evans (1984) to calculate r_i, thus

$$r_i = (3S_i/(4\pi n_t^2 \alpha_i f_i^2))^{1/3} \tag{3.12}$$

(e.g. Spitzer, 1978) where S_i is the rate of emission of ionizing photons, α_i is the recombination coefficient to excited levels and f_i the abundance by number of species i (relative to the total number abundance of all the constituents of the ejecta).

The total number density n_t at time t is given by

$$n_t = 3M_{ej}/(4\pi v_{ej}^3 t^3 m_h (f_h + 4f_{he})) \tag{3.13}$$

where M_{ej} is the ejected mass, m_h the mass of a hydrogen atom, f_h is the number abundance of hydrogen and f_{he} is the number abundance of helium. Here we have made the approximation that the nova ejecta is composed primarily of hydrogen and helium, which will be a valid approximation in the cases that we study. Equation (3.12) assumes a uniform density throughout the Stromgren sphere thus giving the 'asymptotic radius'. However Mitchell & Evans consider it a valid approximation to assume that

Table 3.1

Novae Abundances.

	solar	V1500 Cyg	V1668 Cyg(D)	CrA 81(D)	Aql 82(D)
H	10000	10000	8000	-	2500
He	1000	1000	1000	1000	1000
C	5	110	70	5	120
N	1	100	180	75	320
O	8	50	140	100	180
Ne	1.5	20	<6	110	1100
Na	0.02			0.9	
Mg	0.4			4	18
Al				2	
Si				1	2
S					280
Fe	0.5				5

The above abundances are taken from Snijders et al. (1984) and are based on data obtained with the IUE satellite. The abundances are by number, relative to He = 1000; D = dusty nova.

the Stromgren spheres adjust instantaneously to changes in the ambient environment.

The velocity of the ejecta can be related to the speed class m_v of a nova by using

$$v_{ej} = 2.96 \times 10^{13} m_v^{0.45} \text{ cm day}^{-1} \tag{3.14}$$

(after McLaughlin, 1960) and we take the radius of the ejecta to be given by

$$r_{ej} = v_{ej} t. \tag{3.15}$$

Thus by solving equations (3.12) - (3.15) by calculating the time at which $r_i \geq r_{ej}$ we are able to find the time at which a given species is totally ionized. We do this using different ejected masses and solve for various speed classes of novae. (Before we go on to discuss the results of these calculations we will briefly describe the calculation of S_i and of the condensation time t_c).

3.3.1 Calculation of S_i.

S_i, the rate of emission of ionizing photons, is a crucial factor in this problem as the Stromgren radius r_i is time dependent not only because of n_h but also because of the time dependence of S_i. This quantity is calculated using the fact that the bolometric luminosity of the nova is constant until after the grain growth period (Bath & Shaviv, 1976). S_i takes the form

$$S_i = S_{oi} m_v x_i^{\beta} \exp(-x_i) \text{ s}^{-1} \tag{3.16}$$

(Mitchell & Evans, 1984), where S_{0i} and β are constants for a given ion, $x_i = h\nu_i/kT_*$, $h\nu_i$ being the ionization potential of species i. The speed class may be related to the time in terms of decline Δm from visual maximum and hence T_* is defined as $T_* = T_0 10^{\Delta m/7.5}$ (Bath & Shaviv, 1976), where T_0 is a constant.

Mitchell & Evans calculate S_i for hydrogen and carbon obtaining for the latter

$$S_c = 1.17\times10^{49} m_v x_c^{3.5} \exp(-x_c)\ s^{-1} \tag{3.17a}$$

Fig 3.2 shows fittings to equation (3.16) for sulphur, silicon, iron and magnesium and thus

$$S_s = 4.7\times10^{48} m_v x_s^{3.6} \exp(-x_s)\ s^{-1} \tag{3.17b}$$

$$S_{si} = 4.3\times10^{49} m_v x_{si}^{2.95} \exp(-x_{si})\ s^{-1} \tag{3.17c}$$

$$S_{fe} = 4.5\times10^{48} m_v x_{fe}^{3.4} \exp(-x_{fe})\ s^{-1} \tag{3.17d}$$

$$S_{mg} = 2\times10^{48} m_v x_{mg}^{3.8} \exp(-x_{mg})\ s^{-1} \tag{3.17e}$$

These curves have been calculated assuming all the photons with energies between the ionization potential of two elements will ionize that element with the lowest potential; for example all photons with energies between 11.3eV and 13.6eV (the ionization potentials of carbon and hydrogen respectively) will all go into ionizing carbon. Clearly this is not absolutely true as photons with this energy will also be able to ionize sulphur, silicon, iron and magnesium, all of which have a lower ionization potential than carbon. What we now need to know is the fraction of these

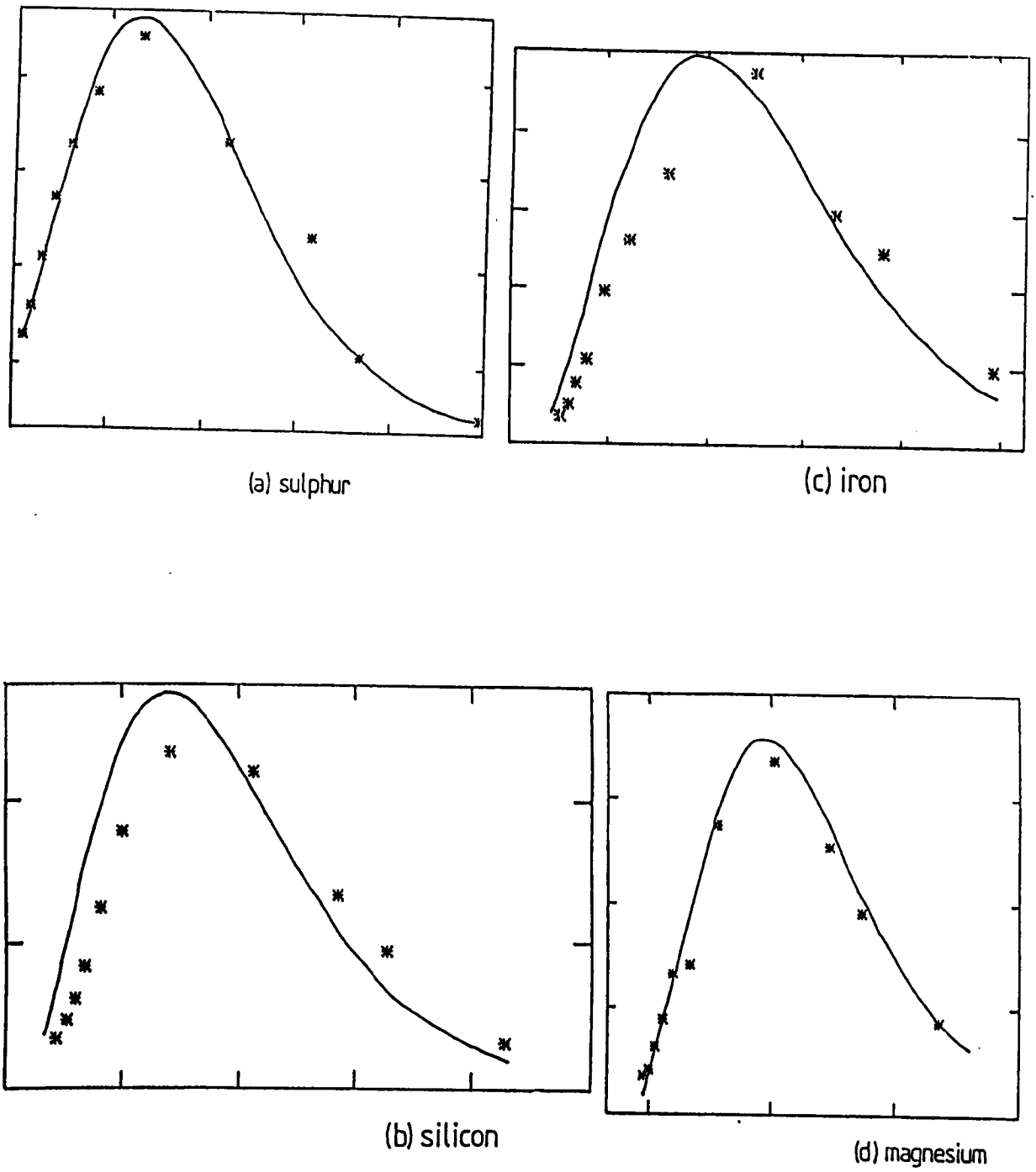

Figure 3.2a-d. Fittings of the curves for the rate of emission of ionizing photons for different elements. Plotted on the x-axis is $h_\nu/(KT_*)$ and on the y-axis is $S_{oi}x_i^{\beta}\exp(-x_i)$ (see text for details).

photons that will ionize each element. We suggest that

$$R_1/R_2 \sim n_1\eta_1/(n_2\eta_2) \tag{3.18}$$

where R_1/R_2 is the ratio of the number of photons in a given range that will ionize species 1 and 2, n_1 and n_2 are the number densities of species 1 and 2 whilst η_1 and η_2 are the photoionization cross sections of these species. Hence using equation (3.18) we are able to calculate S_i with greater accuracy.

3.3.2 The Condensation Time.

We also need to know the condensation time for novae having different characteristics as, regardless of the ionizational state of the ejecta, it is only after this time is reached that grains can begin to condense.

From Clayton & Wickramasinghe (1976) r_c is given by

$$r_c = (L\langle Q(T_*)\rangle/(16\pi\sigma\langle Q(T_c)\rangle T_c^4))^{1/2} \tag{3.19}$$

where L is the bolometric luminosity of the central source, σ is Stefans constant, T_* is the pseudophotospheric temperature of the nova and Q(T) is the Planck mean absorption efficiency for the condensation nuclei at temperature T, which is given by

$$\langle Q(T)\rangle = \min[1, 3.22a(T/10)^{\delta}]; \tag{3.20}$$

here a is the grain radius and δ is a constant. Using δ=1 and $T_*=10^5$K (Bode & Evans, 1982a) and $L = 4 \times 10^{39} m_V$ erg s^{-1} (Shara, 1981) equation (3.19) reduces to

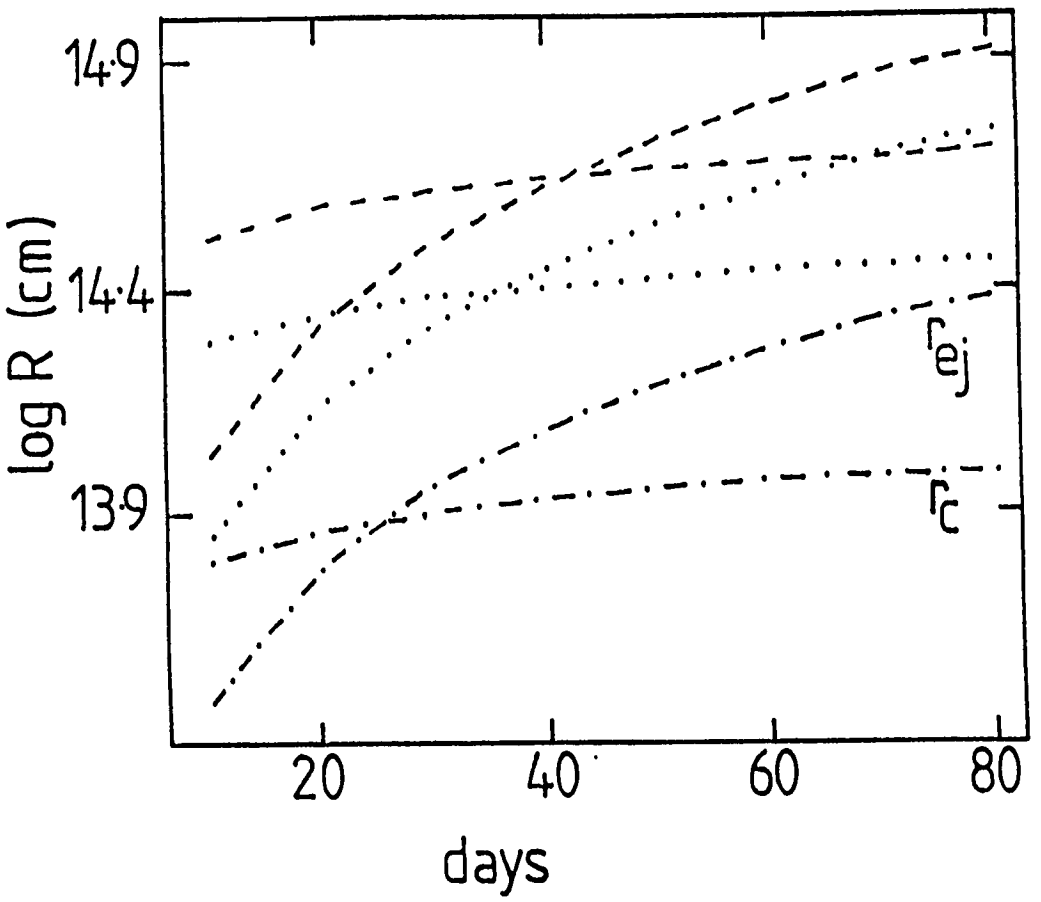

Figure 3.3. Evolution of r_{ej} and r_c for different nova speed classes showing the time at which the nova ejecta outpaces the condensation distance and thus indicating the time at which grain condensation can begin. (Dashed lines indicate m_v = 0.1, dotted lines m_v = 0.01 and dot-dash lines m_v = 0.001, in mag d^{-1}).

$$r_c \sim (10^{44} m_v/(4\pi\sigma T_c^5))^{1/2} \tag{3.21}$$

Rewriting equation (3.13) such that

$$n_c = f n_t \tag{3.22}$$

where f is a fraction we can solve equations (3.1), (3.21) and (3.22) to find when carbon $r_{ej} \geq r_c$ and hence when condensation can begin. Fig. (3.3) illustrates three such solutions of this problem for novae of three different speed classes all having an ejected mass of $4 \times 10^{-4} M_o$ and $f = 0.015$.

3.4 Results.

Table 3.2 shows the times for the complete ionization of the elements carbon, sulphur, silicon, iron and magnesium in novae with different ejected masses, speed classes and elemental abundances. It also shows the condensation time for novae with the same characteristics. Figs 3.4. graphically represent some of these results.

We see that the greater the mass of the ejecta the longer it takes all these elements to completely ionize. This is to be expected for the greater the abundance of a species in a nova ejecta, the longer it will take a nova of the same speed class to ionize it (i.e. the same number of ionizing photons are distributed amongst a greater number of neutral atoms).

Taking into account the elemental abundances as given in Table 3.1, sulphur was taken as the most abundant element with a lower ionization potential than carbon. The results indicate that sulphur is ionized before carbon when the carbon abundance is equal to, or greater than, the sulphur abundance. This is also what we would expect as the more sulphur there is

Table 3.2

Results of ionization model.

This table gives the time (in days) in which the elements carbon (t_c), sulphur (t_s), silicon (t_{si}), iron (t_{fe}) and magnesium (t_{mg}) in novae ejecta of various masses and compositions are completely ionized. The nova speed class $\dot{m}_v$ is given in terms of log(mag d^{-1}) and the nova abundances by number. Some elements are never completely ionized and the starred quantities represent their time of maximum ionization.

Table 3.2a H=2500 C=170 S=85 Si=15 Fe=7 Mg=55

					$M_{ej} = 1.3\times10^{-4}M_o$	
log m_v	t_c	t_s	t_{si}	t_{fe}	t_{mg}	t_{cond}
-2.2	118.9	77.7	17.1	88.8	39.9	27
-1.8	55.5	36.6	8.2	41.8	19.4	31
-1.4	25.9	17.1	4.0	19.3	9.3	37
-1.3	21.2	14.2	3.3	16.2	7.7	38
-1.0	12.1	8.0	1.9	9.1	4.5	43
					$M_{ej} = 5.5\times10^{-4}M_o$	
-2.2	253.6	169.6	42.5	190.2	99.2	23
-1.8	118.6	79.5	20.4	88.6	47.7	28
-1.4	55.8	37.2	9.7	41.2	22.8	33
-1.3	46.3	30.7	8.1	33.9	19.0	34
-1.0	26.4	17.4	4.7	19.1	11.0	38
					$M_{ej} = 13\times10^{-4}M_o$	
-2.2	402.6	266.3	71.0	293.2	166.7	21
-1.8	195.6	125.6	33.8	136.7	80.5	25
-1.4	100.5	59.8	16.1	63.6	38.8	30
-1.3	88.2	49.7	13.4	52.5	32.4	32
-1.0	75.0*	28.9	7.6	29.7	18.9	39

Table 3.2b H=8000 C=120 S=60 Si=10 Fe=5 Mg=40

$\log m_v$	t_c	t_s	t_{si}	t_{fe}	t_{mg}	t_{cond}
					$M_{ej} = 0.9\times10^{-4}M_o$	
-2.2	63.4	44.4	7.9	39.6	19.0	29
-1.8	29.7	18.9	3.9	21.1	9.2	35
-1.4	14.1	8.8	1.9	10.0	4.5	41
-1.3	11.6	7.4	1.6	8.3	3.7	42
-1.0	6.6	4.2	0.9	4.7	2.2	49
					$M_{ej} = 4\times10^{-4}M_o$	
-2.2	139.5	90.3	20.6	101.4	48.2	26
-1.8	65.0	42.9	9.8	47.9	23.3	31
-1.4	30.1	20.1	4.8	22.3	11.2	36
-1.3	24.9	16.6	4.0	18.4	9.3	38
-1.0	14.0	9.4	2.3	10.4	5.4	44
					$M_{ej} = 9\times10^{-4}M_o$	
-2.2	215.5	144.2	34.9	159.4	81.5	24
-1.8	100.3	67.5	16.8	74.6	39.2	28
-1.4	46.7	31.4	8.0	34.7	18.8	33
-1.3	38.7	25.9	6.7	28.7	15.7	35
-1.0	22.0	14.7	3.9	16.1	9.0	39

Table 3.2c H=10000 C=120 S=60 Si=10 Fe=5 Mg=40

$\log m_v$	t_c	t_s	t_{si}	t_{fe}	t_{mg}	t_{cond}
					$M_{ej} = 0.9\times10^{-4}M_o$	
-2.2	55.5	34.9	7.0	39.6	16.5	30
-1.8	26.5	16.4	3.4	19.0	8.0	35
-1.4	12.3	7.8	1.7	9.0	3.9	41
-1.3	10.4	6.6	1.4	7.6	3.2	43
-1.0	5.8	3.7	0.8	4.3	1.9	48
					$M_{ej} = 4\times10^{-4}M_o$	
-2.2	123.6	80.8	17.8	91.9	41.8	26
-1.8	58.1	37.9	8.6	43.0	20.3	31
-1.4	26.9	17.8	4.2	20.1	9.7	37
-1.3	22.2	14.8	3.5	16.8	8.1	38
-1.0	12.5	8.3	2.0	9.4	4.7	43
					$M_{ej} = 9\times10^{-4}M_o$	
-2.2	191.8	128.4	30.4	144.2	71.0	24
-1.8	89.6	59.9	14.6	67.7	34.2	29
-1.4	41.7	27.9	7.0	31.4	16.4	34
-1.3	34.3	23.2	5.9	26.0	13.7	36
-1.0	19.4	13.1	3.4	14.5	7.9	40

Table 3.2d H=2500 C=170 S=390 Si=30 Fe=7 Mg=250

$\log m_v$	t_c	t_s	t_{si}	t_{fe}	t_{mg}	t_{cond}
					$M_{ej} = 1.3\times10^{-4}M_o$	
-2.2	133.1	139.5	23.8	103.0	84.9	26
-1.8	61.8	65.6	11.5	48.7	40.9	32
-1.4	28.6	30.7	5.5	22.6	19.5	38
-1.3	23.9	25.1	4.6	18.6	16.3	39
-1.0	13.4	14.4	2.7	10.5	9.4	44
					$M_{ej} = 5.5\times10^{-4}M_o$	
-2.2	282.1	304.3	58.6	220.3	207.3	24
-1.8	131.2	142.6	28.0	101.9	100.4	28
-1.4	62.3	68.8	13.4	47.2	48.8	33
-1.3	51.9	57.5	11.1	39.1	40.9	35
-1.0	30.0	34.2	6.4	22.0	24.2	40
					$M_{ej} = 13\times10^{-4}M_o$	
-2.2	456.4	513.5	97.0	337.6	365.1	22
-1.8	227.1	283.9	46.1	157.0	186.7	26
-1.4	189.2*	185.3*	21.9	73.1	103.5	31
-1.3	149.6*	147.6*	18.1	60.5	91.6	32
-1.0	74.6*	74.0*	10.3	34.1	60.4	36

Table 3.2e H=8000 C=120 S=280 Si=20 Fe=5 Mg=180

$\log m_v$	t_c	t_s	t_{si}	t_{fe}	t_{mg}	t_{cond}
					$M_{ej} = 0.9\times10^{-4}M_o$	
-2.2	76.1	80.8	12.4	58.6	45.3	30
-1.8	36.0	37.9	5.9	27.9	21.8	35
-1.4	16.8	17.8	2.9	13.1	10.5	41
-1.3	14.0	14.8	2.4	10.8	8.7	42
-1.0	7.9	8.3	1.4	6.1	5.0	48
					$M_{ej} = 4\times10^{-4}M_o$	
-2.2	164.8	175.9	31.1	130.0	111.3	26
-1.8	77.0	82.0	15.0	60.8	53.4	31
-1.4	35.9	38.4	7.2	28.1	25.6	36
-1.3	29.5	31.7	6.0	23.4	21.3	38
-1.0	16.7	18.0	3.5	13.1	12.3	43
					$M_{ej} = 9\times10^{-4}M_o$	
-2.2	255.2	275.8	52.6	201.3	186.7	24
-1.8	119.3	129.3	25.1	93.7	90.1	29
-1.4	56.0	61.5	12.0	43.5	43.6	34
-1.3	46.5	51.3	10.0	35.7	36.4	35
-1.0	26.7	29.9	5.7	20.1	21.4	40

Table 3.2f H=10000 C=120 S=280 Si=20 Fe=5 Mg=180

$\log m_v$	t_c	t_s	t_{si}	t_{fe}	t_{mg}	t_{cond}
					$M_{ej} = 0.9\times10^{-4}M_o$	
-2.2	68.2	71.3	10.8	52.3	39.6	30
-1.8	32.2	33.4	5.3	24.7	19.1	36
-1.4	15.1	15.8	2.6	11.6	9.2	42
-1.3	12.4	13.2	2.1	9.6	7.7	43
-1.0	7.0	7.4	1.2	5.5	4.4	48
					$M_{ej} = 4\times10^{-4}M_o$	
-2.2	149.0	158.5	27.6	115.7	97.6	27
-1.8	68.8	73.8	13.3	54.4	47.0	31
-1.4	32.3	34.4	6.4	25.4	22.5	37
-1.3	26.5	28.5	5.3	21.0	18.7	39
-1.0	14.9	16.1	3.1	11.8	10.8	43
					$M_{ej} = 9\times10^{-4}M_o$	
-2.2	229.8	245.7	46.6	180.7	164.2	25
-1.8	106.6	115.5	22.3	84.2	79.0	29
-1.4	50.0	54.5	10.7	38.9	38.0	35
-1.3	41.3	45.1	8.9	32.1	31.7	36
-1.0	23.5	26.0	5.1	18.1	17.5	41

H=2500 C=170 S=85 Si=15 Fe=7 Mg=55

Mej=5.5

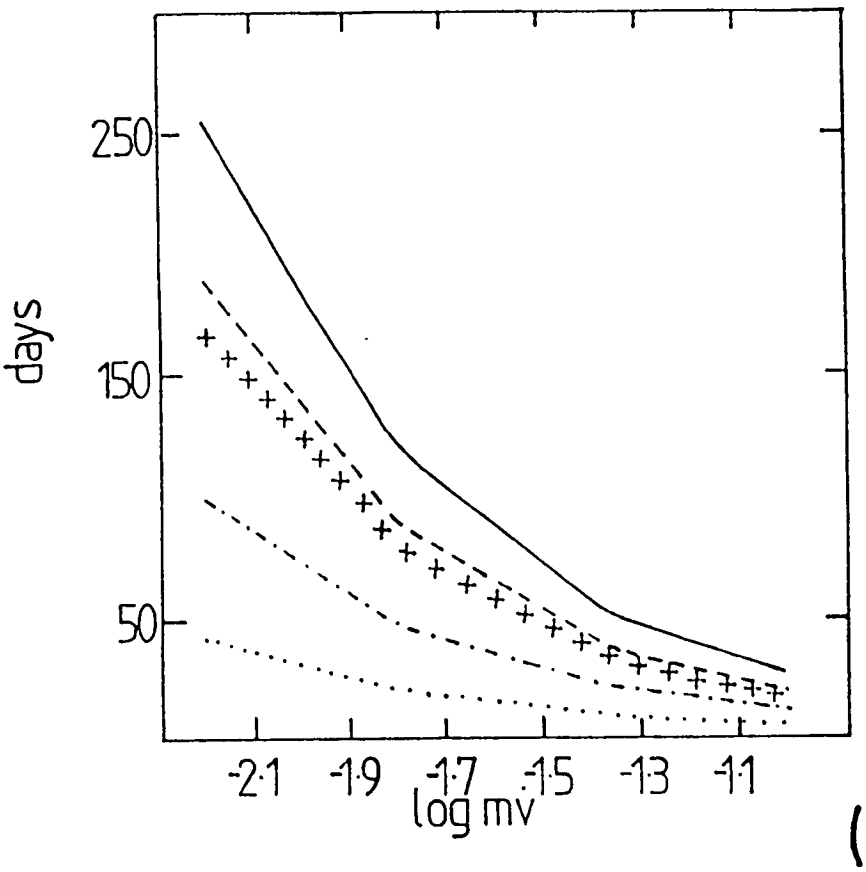

(a)

H=2500 C=170 S=85 Si=15 Fe=7 Mg=55

Mej=13

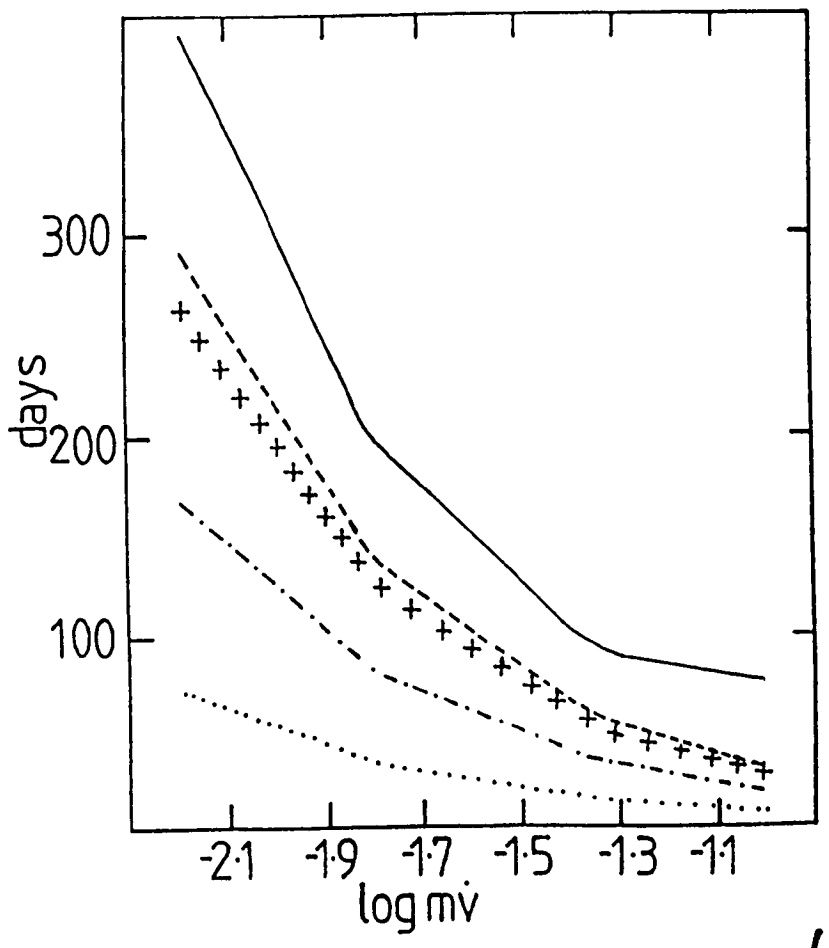

(b)

H=8000 C=120 S=280 Si=20 Fe=5 Mg=40
Mej=0·9

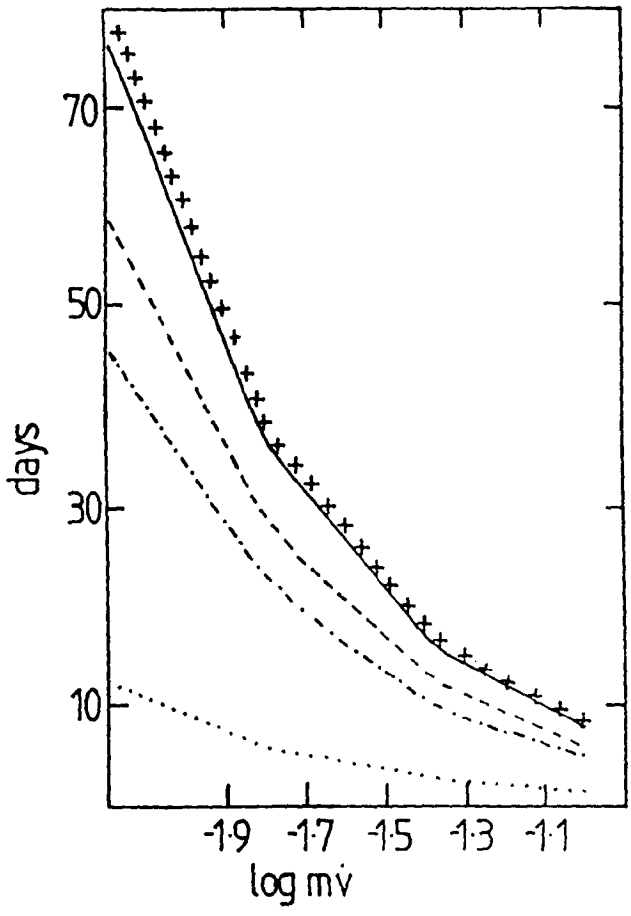

(c)

H=8000 C=120 S=280 Si=20 Fe=5 Mg=180
Mej= 4

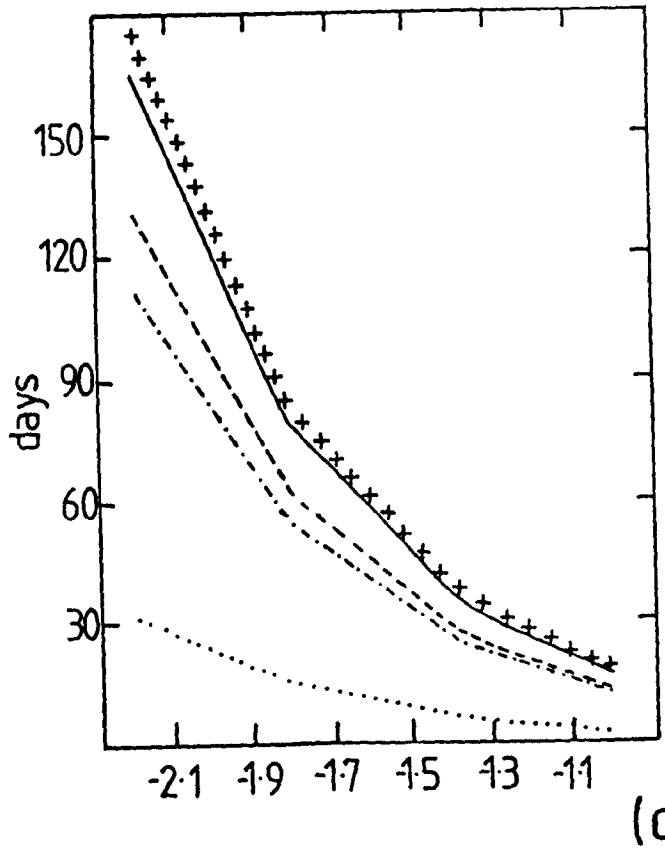

(d)

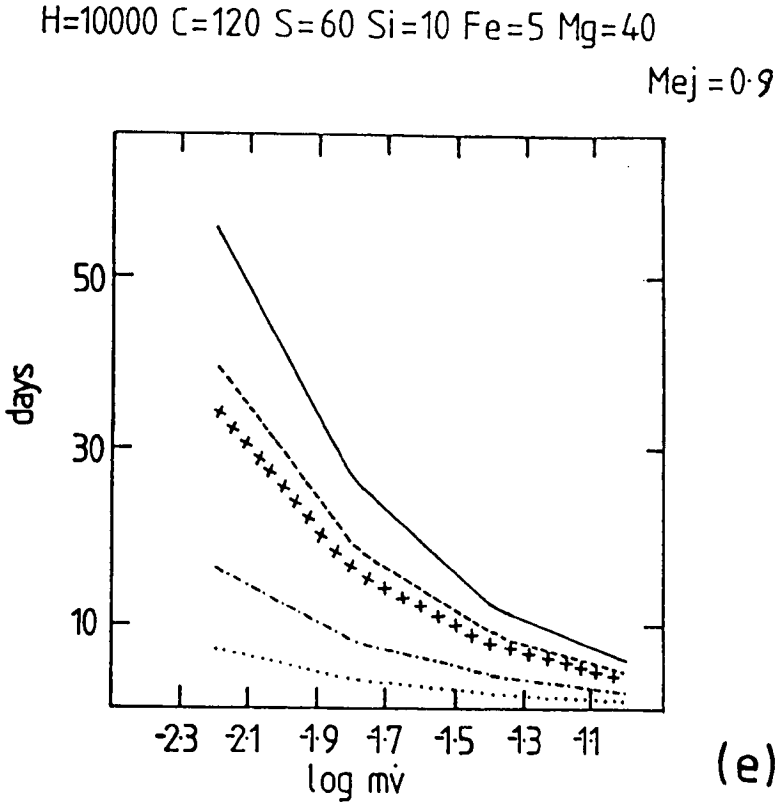

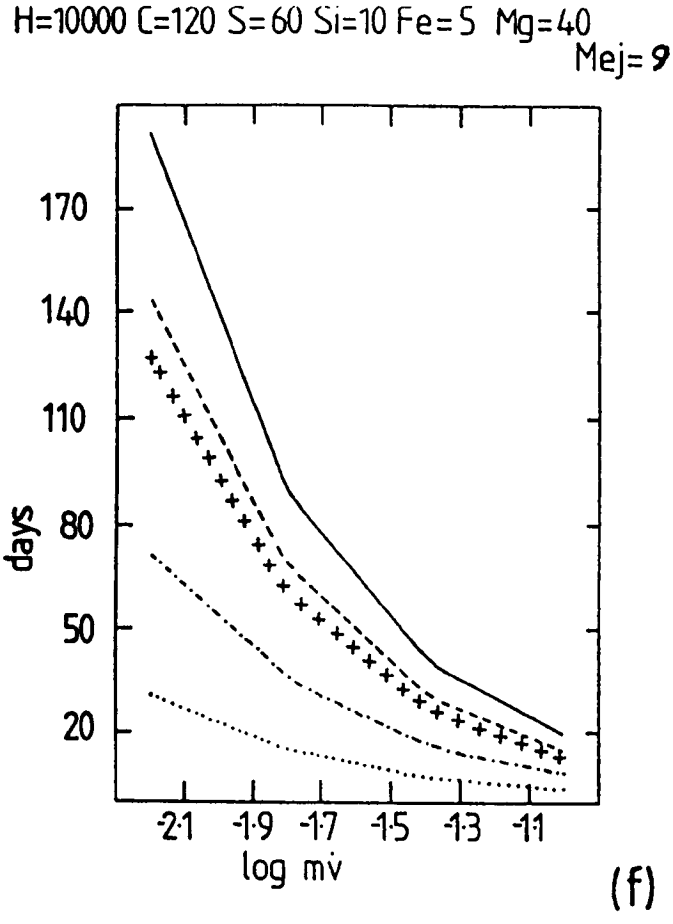

Figure 3.4a-f. Time taken for total ionization of an element in the nova ejecta (in days) against nova speed class. The values at the top of the figures represent the proportion (by number) of each element in the ejecta. The ejected mass is given in terms of 10^{-4} Mo. Represented by a solid line is carbon, by a dashed line is iron, by a dotted line is silicon, by a line of crosses is sulphur and by a line of alternate dashes and dots is magnesium.

in relation to carbon, the greater the proportion of photons of energys $\geq h\nu_C$ that is required to ionize it.

With regard to the other elements it appears that they are ionized in the order silicon, magnesium with iron either third or fourth (dependent on the carbon and sulphur abundances) on taking the range of elemental abundances that we have chosen. Silicon is ionized well before the others mainly because of its high photoionization cross section, which is about an order of magnitude higher than any of the other elements. This means that a sizable portion of the photons that could ionize either carbon or sulphur will in fact ionize the silicon instead.

One interesting point to notice is that, for the highest ejected masses and fastest speed classes, the element carbon (and sometimes sulphur) will never ionize completely. As the ejecta become further away from the central ionizing source, the rate of arrival of high energy photons will become less frequent (as a consequence of the constant bolometric luminosity but increasing effective temperature with time) and eventually the carbon Stromgren sphere begins to shrink. The time at which the carbon (and sometimes the sulphur) Stromgren sphere reaches its greatest extent is given in Table 3.2 as a starred entry.

3.5 Discussion.

How would nucleation on ions work? We propose that if there are enough completely ionized elements with some neutral carbon left in the ejecta of a nova, then carbon atoms will use these ions as nucleation centres, which will then lead to dust formation. For the purpose of this discussion we assume that ionized atoms of any element will be equally attractive to a neutral C atom, although some will be more favourable than others. For example A. P. Jones (private communication) has suggested that iron or silicon ions will be the most likely to act as nucleation centers for neutral carbon atoms. There are many factors involved in whether or

not a nova will produce dust by this method, but we first look at the novae of the fastest speed class in our range. For our choices of elemental abundances and ejected masses the elements silicon, iron and magnesium are always ionized before carbon (and in the case where the carbon abundance is greater than that of the sulphur, the sulphur is also ionized before the carbon). Thus at a first glance it would appear that novae of fast speed class could always be able to form dust as there are always ions onto which the neutral carbon atoms could nucleate. However this cannot happen in all cases as we must also take into account the condensation time, as condensation will only start when this time has passed. From Table 3.2 we can see that in the fastest novae all elements (including carbon) are ionized within the condensation time. Hence condensation is unlikely to take place in these cases as there is no neutral carbon available when the condensation distance is reached. We note that the lower the ejected mass, the more time elapses between the complete ionization of all the elements and the arrival at the condensation radius. In these cases if the carbon Stromgren sphere begins to shrink just before the ejecta radius is reached condensation may still take place, dependent upon whether the densities of the neutral carbon and ionized species are high enough.

Bode & Evans (1982a) also found that novae with the fastest speed classes were less likely to produce dust. However they suggested this on the basis that the condensation radius would outpace the ejecta at relatively large distances. This would mean smaller densities at the condensation radius and hence make it more difficult for grains to start condensing. They did not consider the ionization state of the ejecta in their model.

Turning now to the elemental abundances, the results indicate that if the sulphur abundance is greater than the carbon abundance, sulphur ions will not be available as nucleation sites for carbon atoms. This implies that the carbon atoms will have lost their greatest source of nucleation

centres (if our assumption of neutral carbon being equally attracted to any ionized element is correct) and hence little dust production. However in the examples in which the sulphur abundance is greater than that of carbon (see Table 3.2) silicon, iron and magnesium are still available as nucleation centers. The combined abundances of these elements should more than compensate for the lack of sulphur ions and some novae with these abundances should be able to produce dust. However what seems most likely in these cases is that, with competition from the neutral sulphur for the nucleation centers, any dust produced would not be pure graphite. As nova HR Del 1967 perhaps exhibited features due to MgS in the infrared (see Chapter 4), maybe in some of these cases sulphides may form.

Looking at the novae with the slowest speed classes, it appears that in all cases these should be able to form dust as the condensation distance is reached before any of the elements are completely ionized. But this apparent ease with which these novae could form dust is deceptive. In the cases of slow novae with the highest ejected masses, by the time enough suitable elements have been ionized to produce the nucleation centers, the density in the ejecta may become too low for substantial dust formation to take place (see below).

Here we have dealt with carbon based dust, although some novae have been known to produce a silicate based dust (see Chapters 2 and 5). This model might explain the reason why novae with the characteristics we have chosen produce graphite rather than silicates, as silicon is always the first element to be ionized and therefore, before total ionization, it will find few suitable ions to act as nucleation centers. However A. Jones (private communication) has suggested that ionized silicon atoms could combine with some neutral species although we will not explore this possibility here.

In summary, fast novae ($m_V \sim 0.1$ mag d^{-1}) are very unlikely to produce carbon based dust by this model as all elements are ionized before the

condensation distance is reached. The slowest novae in our range (m_v ~ 0.006 mag d^{-1}) would also have difficulty in producing dust as by the time enough elements have been ionized to produce nucleation centres required, the carbon number density will be too low for effective grain nucleation. Thus it is the novae with moderate speed classes (m_v ~ 0.01 mag d^{-1}) that seem the most capable of producing dust by this method.

3.5.1 Observational Corroboration for the Model.

From the results we see that generally novae of intermediate speed classes are the ones that are most likely to produce dust by this method of nucleation onto ions. This is what is seen observationally (Gallagher, 1977; Bode & Evans, 1982a). For these novae the model predicts that dust will be formed between ~ day 25 - day 60 after outburst and again this is what observations show (Bode & Evans, 1983). We will now attempt to explain the observational characteristics of the novae FH Ser 1970, HR Del 1967 and GQ Mus 1983.

FH Ser had a speed class of ~ 0.04 mag d^{-1} (Gallagher, 1977) and was observed to produce a substantial dust shell ~ 45 days after outburst (see Chapter 2). Yamamoto & Nishida (1977) reported that the ejected mass of this nova was > $10^{-4}M_0$. Using our results for such a speed class and an ejected mass of 9 x $10^{-4}M_0$, together with the elemental abundances given in Table 3.2b, we plot the evolution of each element's Stromgren sphere with time (see Fig. 3.5a). We note from Table 3.2b that the condensation distance is reached on day 33 and around this time (to within a day) all the elements are completely ionized apart from carbon. So between day 34 and day 47 there will be some neutral carbon available to condense onto the ions. So the minimum time that the carbon atoms will have to nucleate onto the ions is ~ 14 days. At day 34 (the time when the sulphur is completely ionized) the ejecta extend to a radius of ~ 2.36 x 10^{14}cm, so using equation (3.13) the carbon density at that radius will be ~ 2.3 x $10^{8}$$cm^{-3}$

and this is consistent with the densities required for the formation of carbon grains.

It is worth noting that the carbon itself will be completely ionized after day 47 and so no condensation of neutral carbon atoms onto ions can occur after that time, thus this is consistent with day 45 observationally being the beginning of the infrared rise, indicating the appearance of a dust shell.

The nova HR Del had a speed class somewhere between 0.009 - 0.005 mag d^{-1} (Sanyal, 1974; we take 0.006 mag d^{-1}) and on the models of Gallagher (1977) and Bode & Evans (1982a) was expected to produce a substantial dust shell, but there was no unambiguous observational evidence for such a shell. The model discussed here could perhaps explain the lack of a dust shell.

The mass of the ejected shell of HR Del has been calculated by Robbins & Sanyal (1978) to be ~ 2.9 x 10^{30}g. This is reasonably close to the value of 13 x $10^{-4}M_{\odot}$ (~ 2.6 x 10^{30}g) that has been used in some of our model calculations so this is the value we will use. The elemental abundances in this nova are closest to those tabulated in Table 3.2a (S. Starrfield, private communication) so we use these abundances and we again plot the evolution of the individual Stromgren spheres using the above initial parameters (see Fig. 3.5b). The condensation distance for such a nova is reached on day 21, well before any of the elements are completely ionized so dust should be able to form as carbon is the last element to be ionized. However the problem facing such a nova is not the availability of nucleation centers but the number density of carbon at the start of condensation. If we consider that nucleation will only begin when there are an adequate number of ions avaliable this will be after day 166 when magnesium is completely ionized. On this day the ejecta will have reached a distance of ~ 5.02 x 10^{14}cm where the number density of carbon will be ~ 7 x $10^{7}cm^{-3}$. This may be a little low for condensation to take place

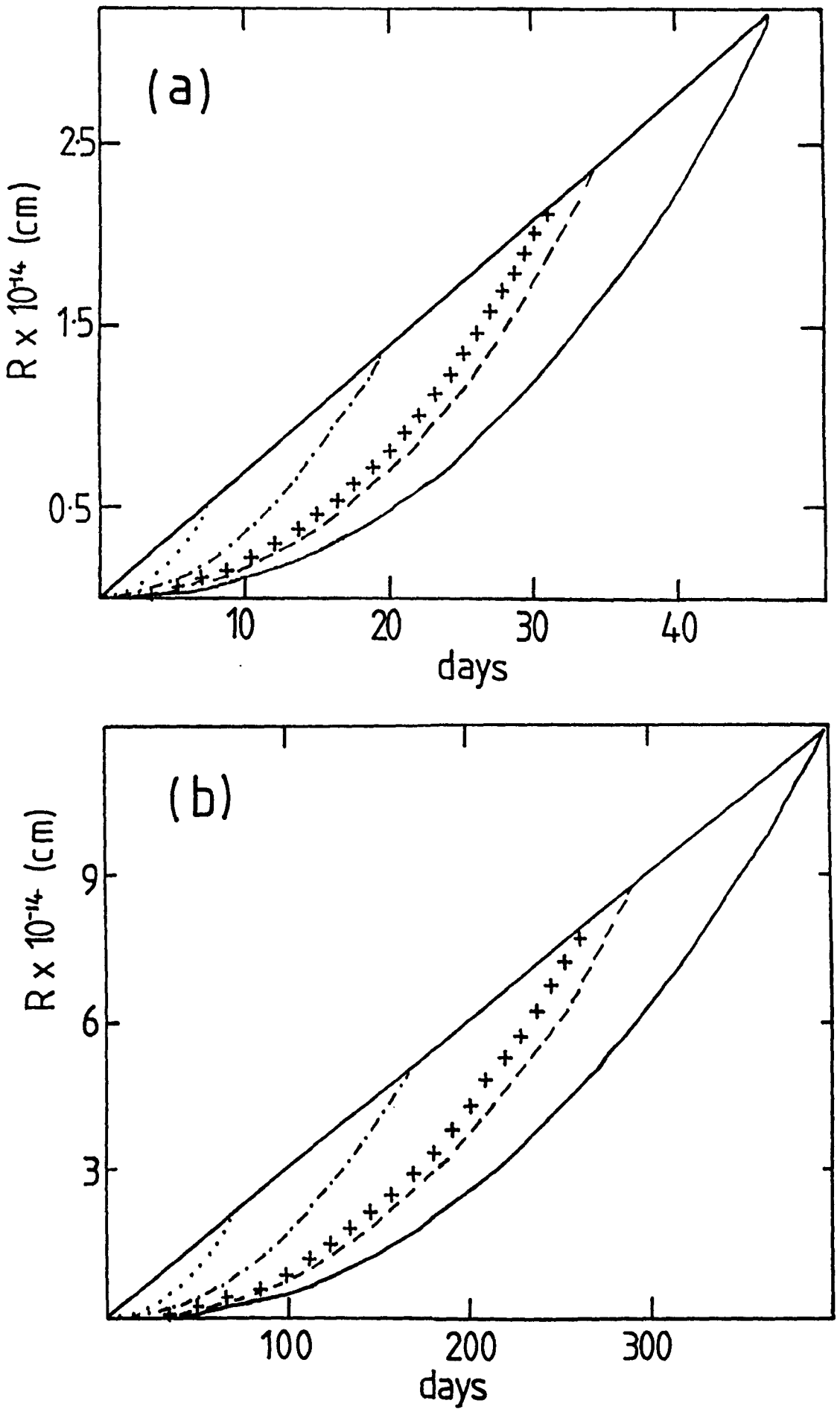

Figure 3.5a-b. Evolution of the Stromgren spheres in the nova ejecta for a 'FH Ser 1970' type nova (a) and a 'HR Del 1967' type nova (b). Also shown is the evolution of the ejected radius (r_{ej}). Values and symbols as in Figs. 3.4.

efficiently and thus on this ionizational model little dust would form in a HR Del type nova.

Another of the novae that seemed a likely candidate for dust production (in view of its moderate speed class) was the nova GQ Mus 1983 (see also Chapters 2, 4 & 6). This non-production of dust can now be explained by this model. Pacheco & Codina (1985) calculated the ejected mass to be $\sim 2.8 \times 10^{-4} M_0$, whilst the observed speed class was $\sim$ 0.05 mag d^{-1} (Whitelock et al., 1984). The abundances as determined by Krautter et al. (1984) give values close to those listed in Table 3.2b. Looking at this table for these intial parameters we see that all the elements would ionize before the condensation distance is reached and hence no dust production would be expected. (In Chapter 6 we calculate the ejected mass from this nova to be an order of magnitude down on that quoted above, however this will not affect the conclusion as ionization occurs even more rapidly for smaller masses).

3.6 Conclusion.

It has been shown that, with suitable abundances of the elements carbon, sulphur, silicon, iron and magnesium, suitable ejected masses and speed classes, it is a possibility that neutral carbon atoms will nucleate onto ions perhaps as a precursor to substantial dust formation.

Very generally the novae of intermediate speed classes are the most likely to produce dust. However the ejected mass also plays a vital role in this model with the slowest speed classes of novae able to produce large amounts of dust only if the ejected mass is in the lower range of possible values. This model can also explain the infrared observations of the novae FH Ser, HR Del and GQ Mus. And if we had more accurate values of their abundances and ejected masses this model may be able to more fully reproduce the observations concerned with the appearance (or non-appearance) of dust.

Omissions to the model include the effect that other elements in the nova ejecta would have on the photoionization rates, as elements having lower ionization potential than magnesium would also be competing for the ionizing photons. However such elements as sodium and titanium are not particularly abundant and as such would have a negligible effect on the calculations.

So although in principle this model does work, we ideally need more calculations of observed novae ejected masses and elemental abundances to apply it to individual novae. However the main problem with this is that we must observe these novae **before** dust is formed, to obtain realistic starting values for the elemental abundances. There is little use in using abundances determined after dust has formed, as the elements involved in dust production will be substantially depleted.

CHAPTER 4

IRAS - OBSERVATIONS OF CLASSICAL NOVAE.

4.1 IRAS.

IRAS, the InfraRed Astronomical Satellite (Jennings, 1980), was launched in January 1983 under the joint cooperation of the United States, the Netherlands and the United Kingdom. Its mission was to map all the sky in four wavelength bands (numbered I - IV) centred on 12μm, 25μm, 60μm and 100μm respectively. (Fig. 4.1 shows the relative spectral response with wavelength). IRAS continued functioning until 22 November 1983, when the liquid helium refrigerant ran out (Jennings et al., 1983). By that time it had successfully surveyed more than 96% of the sky.

The results of the IRAS mission have appeared in a catalogue of infrared point sources (PSC), a catalogue of extended sources smaller than 8′, a catalogue of low resolution spectra (Beichman et al., 1984), and an atlas of the absolute surface brightness images of the entire infrared sky plus several other products. In this way IRAS has collected together information on ~ 250000 point sources and ~ 20000 small extended sources.

The satellite consisted of two main parts, the spacecraft and the telescope. The telescope was an f/9.6 Ritchey-Chretien design with beryllium mirrors and 57cm aperture. The focal plane assembly (Fig. 4.2) consisted of a detector array for the survey, a low resolution spectrometer (LRS), which was basically an 'objective prism spectrograph', and a chopped photometric channel (CPC), which was used for making higher resolution maps of individual sources. (See Table 4.1 for properties of IRAS instrumentation). There were 62 infrared detectors in the main survey array covering the four wavebands and 8 visible light detectors near the sides of the focal plane assembly. The detectors in the survey array were arranged so that every source crossing the field of view was seen by at

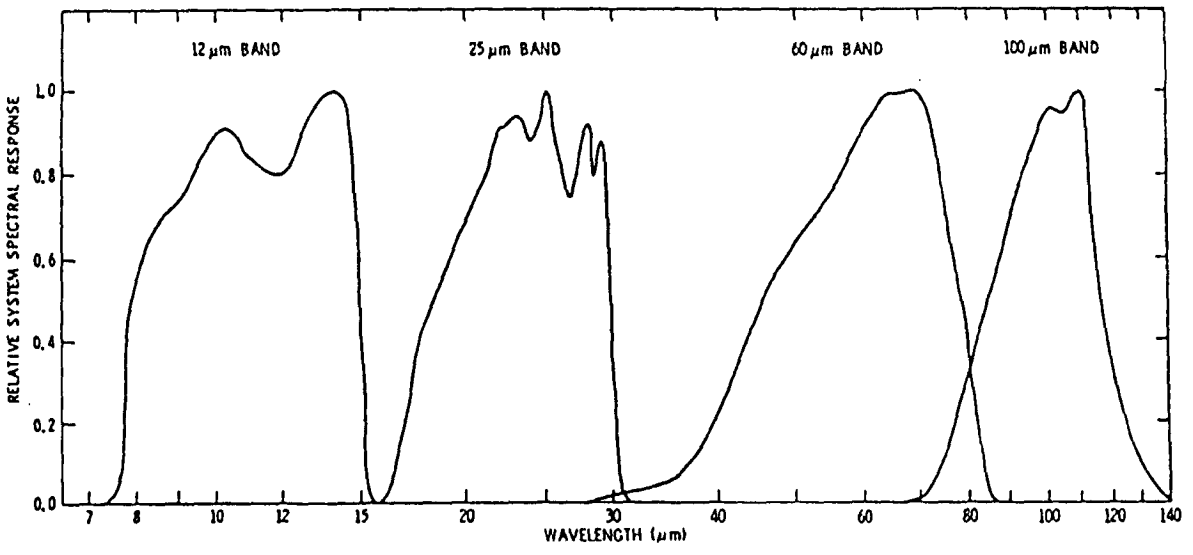

Figure 4.1. The relative system spectral response of the IRAS detectors with wavelength centered on each of the four IRAS wavebands. Reproduced from the IRAS explanatory supplement (1984).

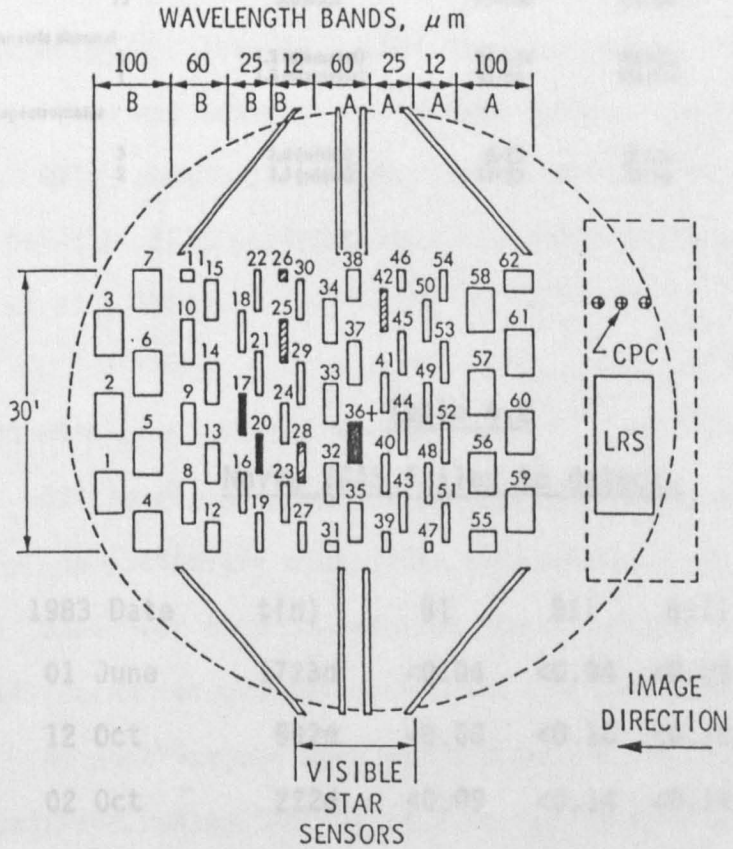

Figure 4.2. The focal plane assembly on the IRAS satellite. The rectangles in the central portion each represent a detector, filter, and field lens combination of the survey array. The shaded detectors were inoperative during the survey. Reproduced from the IRAS explanatory supplement (1984).

Table 4.1

Characteristics of the IRAS focal plane assembly.

Centre wavelength (μm)	No. of detectors	Detector field of view (arc min × arc min)	Wavelength interval (μm)	Detector material	Dwell time (ms)	Average 10 σ sensitivity (Jy)
Survey array						
12	16	0.75×4.5	8.5–15	Si:As	190	0.7
25	15	0.75×4.6	19–30	Si:Sb	190	0.65
60	16	1.5×4.7	40–80	Ge:Ga	390	0.85
100	15	3.0×5.0	83–120	Ge:Ga	780	3.0
Chopped photometric channel						
Band 1	1	1.2 (diameter)	84–114	Ge:Ga	1,000	7.0
Band 2	1	1.2 (diameter)	41–63	Ge:Ga	1,000	7.0
Low resolution spectrometer						
					Resolving power	
Band 1	3	5.0 (width)	8–13	Si:Ga	14–35	
Band 2	2	7.5 (width)	11–23	Si:As	14–35	

Table 4.2

Novae IRAS failed to detect.

Nova	1983 Date	t(d)	BI	BII	BIII	BIV
V1668 Cyg	01 June	1723d	<0.04	<0.04	<0.05	<0.25
V1370 Aql	12 Oct	592d	<0.08	<0.10	<0.10	<1.00
MU Ser	02 Oct	222d	<0.09	<0.14	<0.14	<2.00

Here 1983 Date refers to the date that the object was observed by IRAS in 1983, t(d) is the time (in days) after outburst that the nova was observed. Upper limits to detections are given in Jy.

least two detectors in each waveband (Iras Survey Team, 1983).

Further to the survey, a programme of pointed observations (AO's, additional observations) was developed using the survey array and the CPC. These observations gained sensitivity by increasing the integration time through the co-addition of repeated scans, by pointing the most sensitive detectors at the specified object and by increasing the dwell time by slower scanning. The AO's also observed sources at a higher angular resolution than was achieved during the survey. It is the results of some of these AO's that will be described later in this chapter. (For more details on the IRAS mission see the IRAS Explanatory Supplement ed. Beichman et al., 1984).

4.1.1 IRAS AO's on Classical Novae.

The additional observations on classical novae were carried out with the array in photometry mode. The type of macro (standard observational sequence) used for each observation characterized the survey speed, the number of scans across the source and the duration of the observation. Some of the observations were carried out at 1/4 of the survey speed of 3.85 arcmin/sec, using the 'best' detector in each of the four wavebands. In this instance, if 7 survey like scans were done the observation time was 437s, while for 10 survey like scans the observation time was 605s. For observations carried out at 1/2 survey speed the entire survey array was used. When 5 scans were taken the observation time was 249s and when 13 scans were taken this rose to 634s. (This compares with observation times of no more than a few seconds for objects in the standard survey). Each observation was then repeated (generally) within one day. The data obtained on each source was then coadded and analyzed and reduced by using the STARLINK software COMBINE and CONTOUR (Hirst & Cudlip, 1984). Some of the maps emerged as intensity maps whereas others had been processed by a point source filter and hence were developed as flux maps. (The PSC data

on classical novae were analysed by Dinerstein (1986) and where applicable her results will be compared to our results from the AO's).

Classical novae have long been known as sites of dust formation (see Chapter 2, Gallagher & Starrfield, 1978 and Bode & Evans, 1983). When observing in the far infrared (as with an instrument like IRAS) there is the potential of much information to be learnt about classical novae. Amongst which, with good IRAS observations and perhaps simultaneous observations at other wavelengths, are the nature of the emitted radiation (e.g. thermal bremsstrahlung), whether or not they possess a dust shell and the possible presence of infrared fine structure lines. It is worth noting for the most recent novae ($\geqslant$ 1980) that the date of the IRAS observation is crucial to the interpretation of the data. This is because the overall characteristics of the nova system a reasonable time after outburst will be time dependent (generally the nearer the IRAS observation was to outburst the more relevant is the time to data interpretation).

4.2 Results.

Unfortunately some of the novae IRAS was to search for it failed to detect. Before going on to describe successful observations of classical novae, the ones that IRAS failed to detect will be described briefly. With these the only information IRAS can give is an upper limit on the flux in each band. This limit has been taken to be the 3σ limit which is given in Table 4.2. These upper limits were based on the median noise value for the entire map and the bandwidth of each individual detector. The upper limits were correlated with the available ground based observations to see if any IRAS detection would have been expected.

4.2.1 V1668 Cyg 1978.

This nova was a fast one (see Table 4.3 for speed classes of novae) which did not undergo a visual transition break but did produce an optically thin dust shell (Gehrz et al., 1980b). A very basic extrapolation (by a least squares fit to a magnitude against time plot) of the 12.6μm and 19.5μm data of Gehrz et al. (1980b) to the time of the IRAS observations results in fluxes that are extremely low, ($\leq 10^{-4}$Jy), and hence IRAS would not have been able to detect it in any of its four bands.

4.2.2 MU Ser 1983.

A non-detection of this nova seems surprising at first, since the observations were taken only 220 days after outburst. However MU Ser was a particularly fast nova, falling by 3 magnitudes in the first four days after maximum (Wakuda et al., 1983). Assuming that this nova did not produce dust (as in the case of very fast novae like V1500 Cyg 1975) the infrared emission would then be due to a freely expanding hot gas i.e. thermal bremsstrahlung emission. Nine days after outburst Feast & Carter (1983) obtained JHK magnitudes. As both J and K points are subject to contamination from hydrogen and helium emission lines (Whitelock et al., 1984) then, to a reasonable approximation, only the H flux will be mainly due to free-free radiation. We can then use this H flux to extrapolate to the time of the IRAS observations (assuming that during day 9 - day 220 the fluxes were on the optically thin part of the free-free continuum). To do this we use the relationships between flux and time found by Ennis et al. (1977) for fast novae.

The measured flux at H on day 9 was 0.306 Jy. Now from Ennis et al.

Table 4.3

Nova speed class.

Nova	Speed class	Ref
V1668 Cyg	0.12	3
MU Ser	0.70	8
V1370 Aql	0.30	1,2
GQ Mus	0.05	6,7
V4077 Sgr	unknown	9,10
HR Del	0.008	4
DQ Her	0.03	5

Speed class is in mag day^{-1} and the references are

1. Bode et al. (1984)
2. Gehrz et al. (1985)
3. Gehrz et al. (1980b)
4. Sanyal (1974)
5. Martin, in press.
6. Whitelock et al. (1984)
7. Krautter et al. (1984)
8. Wakuda et al. (1983)
9. Iijima & Rosino (1983)
10. Mazeh et al. (1985)

$$\text{flux} \propto 1/t^2 \text{ if } 2c_s t/H << 1$$
$$\text{flux} \propto 1/t^3 \text{ if } 2c_s t/H >> 1 \qquad (4.1)$$

where t is time, H is initial thickness of the expanding shell and c_s is the sound speed in the plasma. So at t = 220 days, the flux is 5×10^{-4} Jy, in the first case, and 2.1×10^{-5} Jy in the second. Such low fluxes are well beyond the capabilities of the IRAS detectors and hence a non-detection at day 220 of this nova is inevitable.

4.2.3 V1370 Aql 1982.

This nova was undetected by IRAS 592 days after outburst. As mentioned in Chapter 2 this fast nova was unique in that it produced a silicate based dust shell, as witnessed by the 10μm feature observed by Bode et al. (1984) and Roche et al. (1985). On this basis a detection in IRAS band I might not seem unreasonable. Extrapolating the ground based 12.6μm data of Gehrz et al. (1984) (again by means of a least squares fit to flux against time), we have that the expected flux in band I would be negligible ($\leq 10^{-4}$ Jy).

4.3 Novae Detected By IRAS.

IRAS detected both dusty and non-dusty novae during its observations. In Table 4.4 the observed IRAS fluxes are given, in which t(d,y) is the time in days or years from outburst. In the case of the dusty novae the fluxes are colour corrected (those values given in brackets) as we would expect an essentially blackbody distribution (non-colour corrected fluxes for these novae have also been included). For the dustless novae the IRAS fluxes are in the form (in band flux)/bandwidth and have not been colour corrected. The 1σ errors are also given.

Table 4.4

Novae IRAS detected.

Nova	1983 Date	t(d,y)	BI	BII	BIII	BIV
GQ Mus	02 June	135d	0.33 ±0.02	0.41 ±0.02	0.42 ±0.02	<0.9
	08 June	141d	0.35 ±0.02	0.32 ±0.02	0.42 ±0.02	<0.65
	12 June	145d	0.30 ±0.02	0.33 ±0.02	0.29 ±0.02	<0.58
	16 July	179d	0.23 ±0.02	0.31 ±0.02	0.36 ±0.02	<0.43
	21 Aug	215d	0.23 ±0.02	0.29 ±0.02	0.38 ±0.02	<0.46
	01 Sept	225d	0.21 ±0.02	0.21 ±0.02	0.23 ±0.02	<0.43
V4077 Sgr	10 Oct	360d	2.17 ±0.03 (1.8)	0.84 ±0.06 (0.66)	<0.2	<2.0
	18 Oct	368d	1.96 ±0.04 (1.61)	0.75 ±0.06 (0.59)	<0.2	<2.0
DQ Her	06 March	48.3y	<0.1	<0.1	0.39 ±0.02 (0.45)	1.71 ±0.08 (1.61)
HR Del	01 May	15.4y	<0.05	0.38 ±0.03	<0.07	<0.2

Symbols are the same as in Table 4.2. Numbers in brackets are colour corrected fluxes.

4.3.1 GQ Mus 1983.

Nova Muscae was a peculiar nova in that although quite fast, theoretically it was still slow enough for the formation of dust (Bode & Evans, 1982). (See Chapter 3 for a possible explanation of why this nova did not produce any dust). However all ground based near infrared observations of this nova showed no evidence for dust being present (Whitelock et al., 1984; Krautter et al., 1984). The first AO's available of this object were taken 225 days after outburst and in 'hard copy' form (i.e. with preliminary flux calibrations). The nova was detected in bands I and II (see Callus et al., 1986). These fluxes implied a colour temperature of ~ 340 K. Such a value would indeed indicate the presence of circumstellar dust despite the contrary near infrared data (see Fig. 4.3). The properties of the infrared excess appeared consistent with shock heated dust (cf. Ogelmann et al., 1984), and perhaps could account for the observations by Krautter et al., (1984) of a possible molecular feature at 3.5μm (see Chapter 2). However when the final AO products were made available, it was discovered that IRAS had detected this object in band III as well, and such a flux distribution could not possibly follow a blackbody law. These data covered the period from 135 days to 225 days after outburst (assuming that the outburst date is that given in Whitelock et al., 1984). IRAS contour maps of GQ Mus are given in Fig. 4.4.

This more comprehensive data set showed that the infrared flux coming from this nova could be well modelled by the expansion of a hot gas, i.e. thermal bremsstrahlung. The gas parameters that best fitted the data were an electron temperature $T_e \sim 2.5 \times 10^4$K, an ejected mass $M_{ej} \sim 3 \times 10^{-5}$Mo with the gas obeying an r^{-2} density dependence, assuming spherical symmetry and uniform outflow. (For model fits to the IRAS observations see Fig. 4.5). In band III the observed fluxes appear higher than the ones predicted from this model. This could be due to fine structure lines of

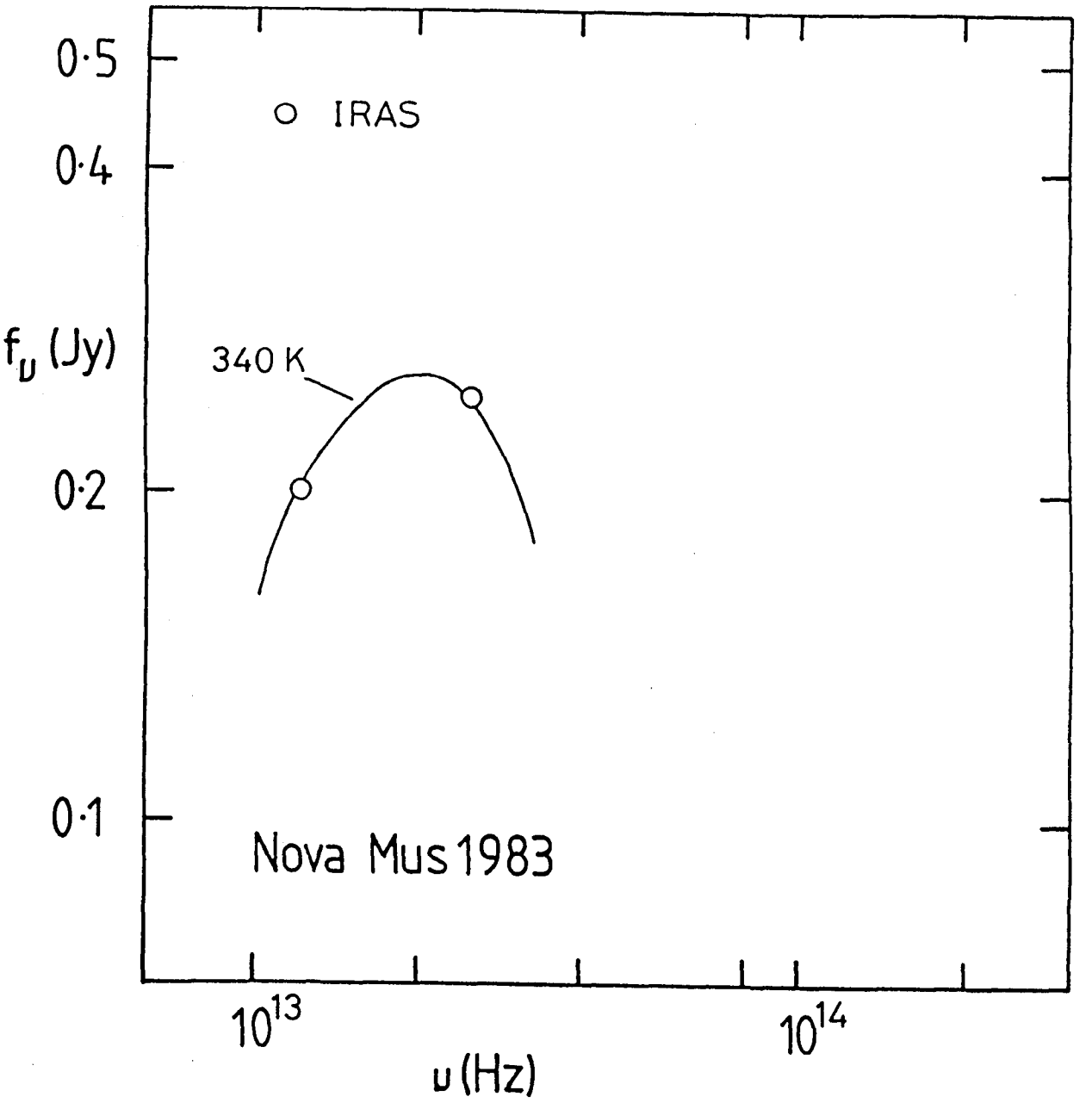

Figure 4.3. 340K blackbody fit to our first band I & II detections of the nova GQ Mus 1983.

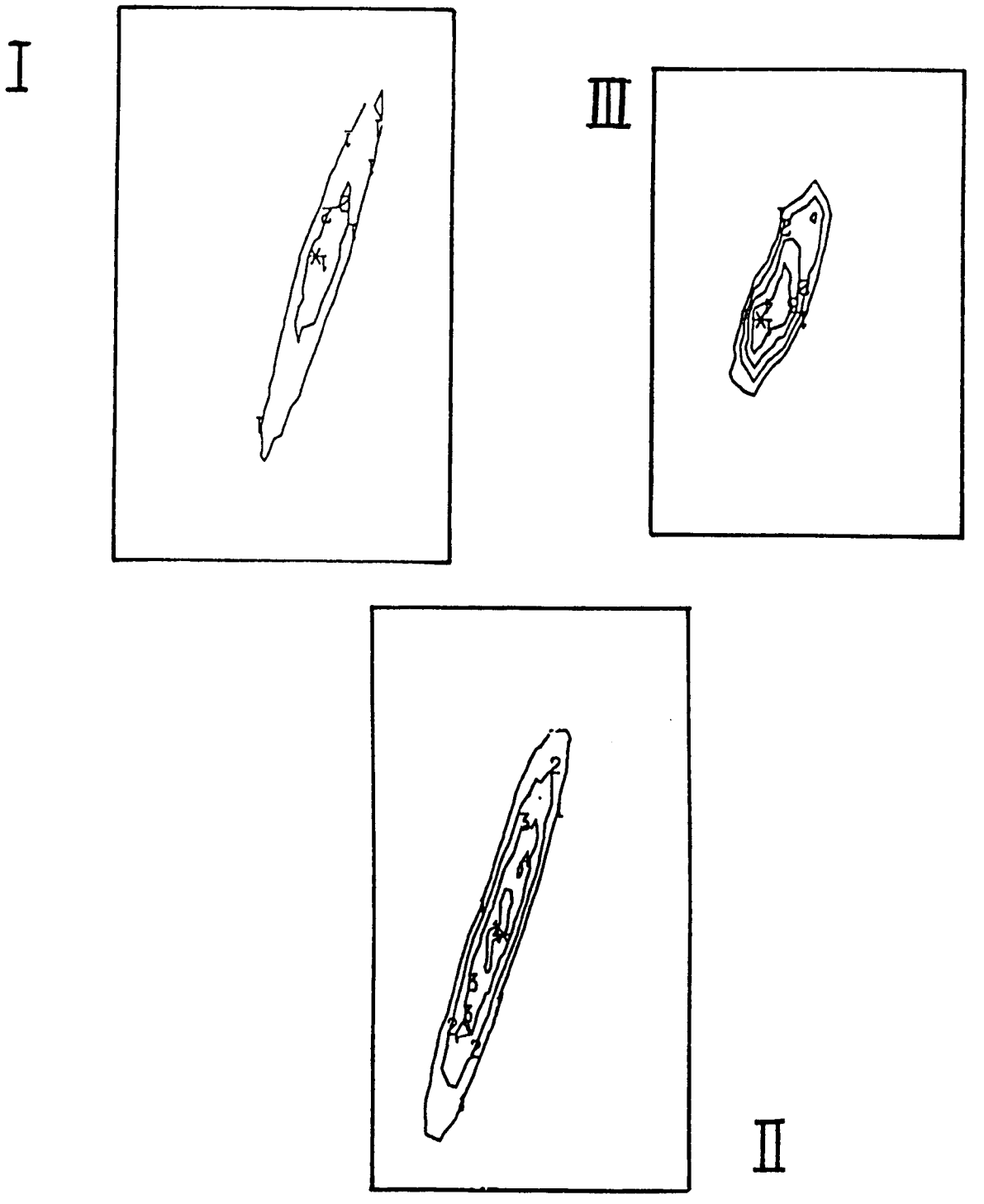

Figure 4.4a-c. IRAS contour maps of GQ Mus 1983 in IRAS bands I, II & III.

Contour levels are (in terms of 1 x 10^{-14} W m^{-2}):

Band I: 1) 1, 2) 2.

Band II: 1) 0.25, 2) 0.50, 3) 0.75, 4) 1.00.

Band III: 1) 0.4, 2) 0.45, 3) 0.5, 4) 0.55.

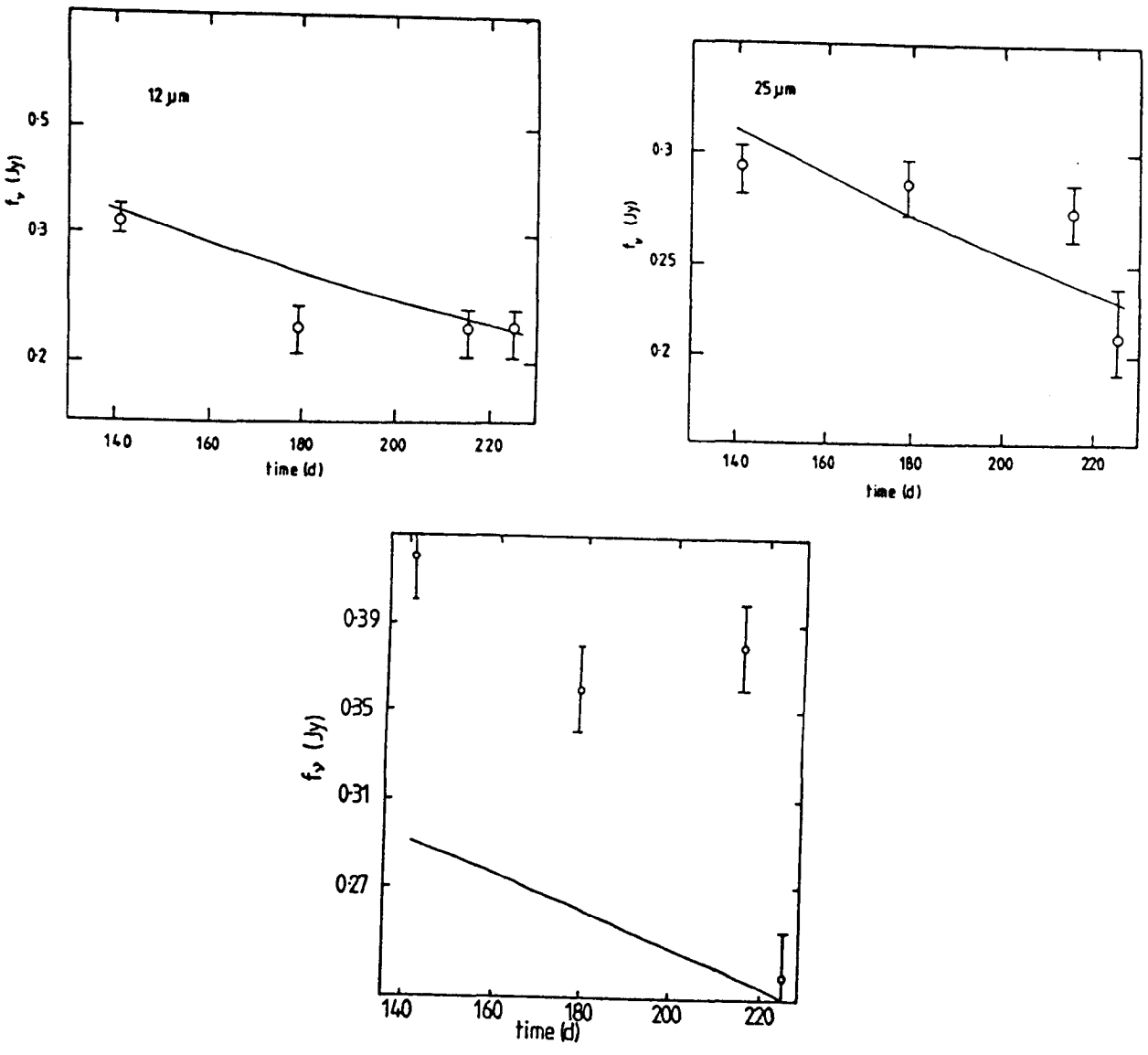

Figure 4.5. A free-free model fit to the IRAS bands I, II & III detections of GQ Mus 1983 (see chapter 6 for details of the model).

[OIII] at 52μm. If this was so then these lines would contribute ~ 30% of the flux at this waveband up to ~ day 215. The same model would also account satisfactorily for the near infrared SAAO data (for a detailed explanation of this model see Chapter 6; model fits to the SAAO data are given in Fig. 6.8).

On day 225 the IRAS band I, II and III points (to within the IRAS error bars) appear to lie on the optically thin portion of the free-free continuum (see Fig. 4.6). Unfortunately if the band IV flux had been on this part of the continuum as well it would have been just below the sensitivity of band IV detectors. However we can still get an upper limit to the electron number, n_e on this day with this information. The cutoff wavelength $\lambda_1 > 60\mu m$ (band III) therefore ν_1 (the turnover frequency) $\leq 5 \times 10^{12}$ Hz. For free-free emission the emitting gas becomes optically thick when

$$(0.02\ n_e^{\ 2}\ v_{ej}\ t)/(\nu_1^{\ 2}\ T_e^{\ 3/2}) \ f\ 1 \qquad (4.2)$$

where v_{ej} is the velocity of the ejecta. This assumes a plane geometry and a uniform homogeneous source. Thus

$$n_e < 801875\ T_e^{\ 3/4}\ (v_{ej}/1000 kms^{-1})^{-1/2}\ (t/225d)^{-1/2}\ cm^{-3} \qquad (4.3)$$

Taking $T_e \sim 2.5 \times 10^4 K$ (as in the model) we obtain

$$n_e < 1.6 \times 10^9\ cm^{-3}. \qquad (4.4)$$

This is consistent with the electron density calculated in the free-free model for day 225. (As the above is the greatest value n_e can take on day 225 a density greater than this in the model would be inconsistent with the observations).

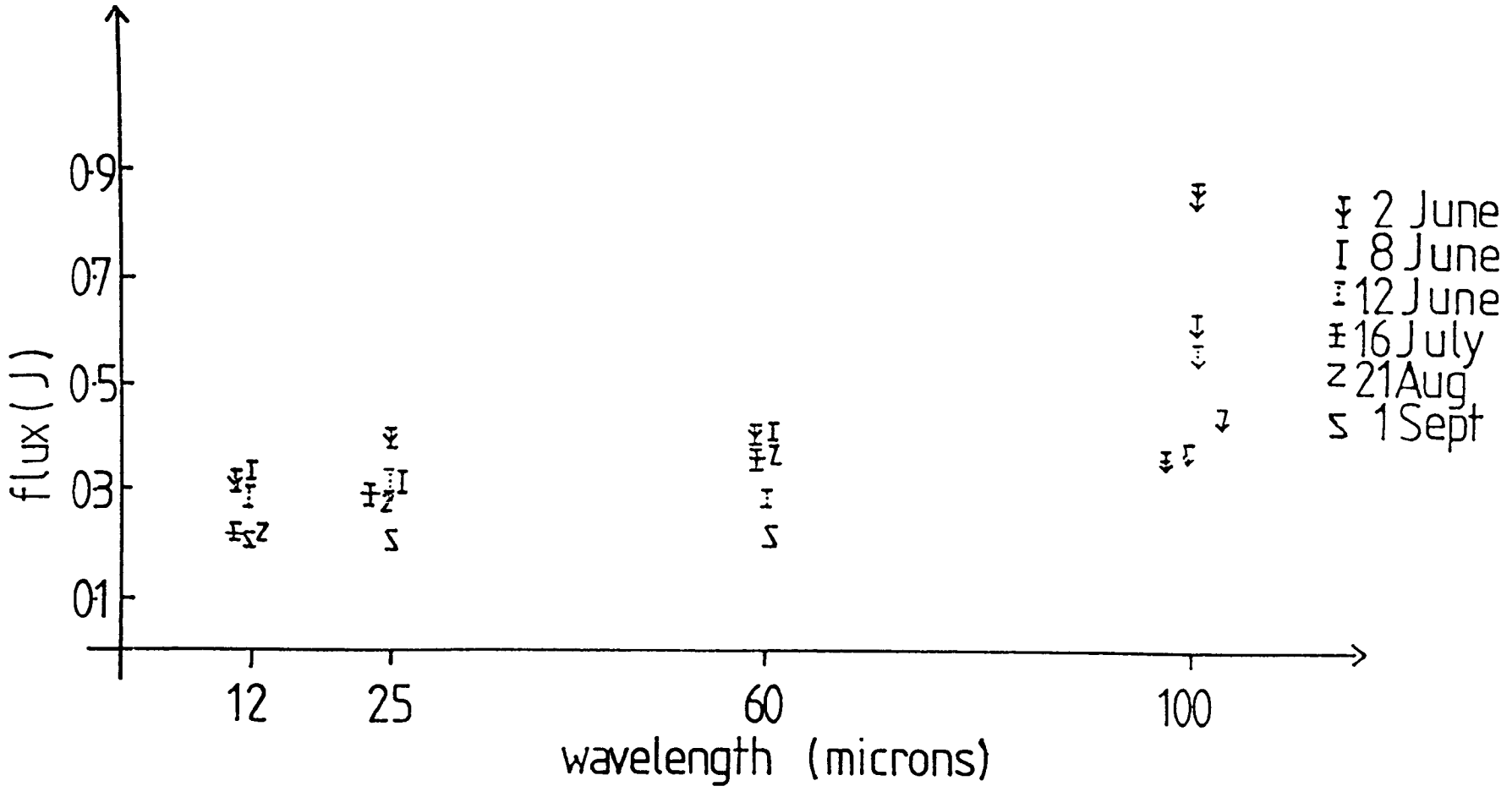

Figure 4.6. The IRAS fluxes of GQ Mus 1983 on all the different days of observation. Clearly on day 225 (1 Sept) the points lie on the optically thin part of the free-free continuum.

Now nova Mus was also detected as a X-ray source more than one year after outburst (Ogelman et al., 1984). Taking into account the IRAS results, we can try to explain the origin of these X-rays. Ogelmann et al. suggested two possible origins; either i) they could arise from the shock heating of pre- existing circumstellar material or ii) they could arise from the continued shrinking and subsequent temperature rise of the pseudophotosphere down to the surface of the white dwarf (cf. Bath & Shaviv, 1976 and Chapter 2). Any shock heated circumstellar gas would give rise to corresponding shock heated dust (if there was any). We can estimate the expected flux density that would arise from shock heated dust in bands I and II by using the results given by Draine (1981). He calculates the 'normalized' infrared emission spectrum for shocks into a gas having silicate and carbon components with a power law size distribution as proposed by Mathis et al. (1977), and defines f_λ such that the intensity normal to a shock is $(I_\lambda)_{ir}(o)$ where

$$(I_\lambda)_{ir}(o) = 21/(128\pi)\ (n_h)o\ m_h v_s^3\ f_\lambda. \tag{4.5}$$

(With this normalization, $\int f_\lambda\, d\lambda$ is just the fraction of the shock's radiant power which emerges as infrared emission from dust). In equation (4.5) $(n_h)o$ is the preshock hydrogen density, m_h is the mass of a hydrogen atom and v_s is the velocity of the shock. Thus assuming spherical symmetry we have a configuration as shown in Fig. 4.7. Thus F_λ, the observed flux at wavelength λ, is

$$F_\lambda = 2 \int (I_\lambda)_{ir}(o) \cos\theta\ 2\pi R^2/D^2 \sin\theta\, d\theta \tag{4.6}$$

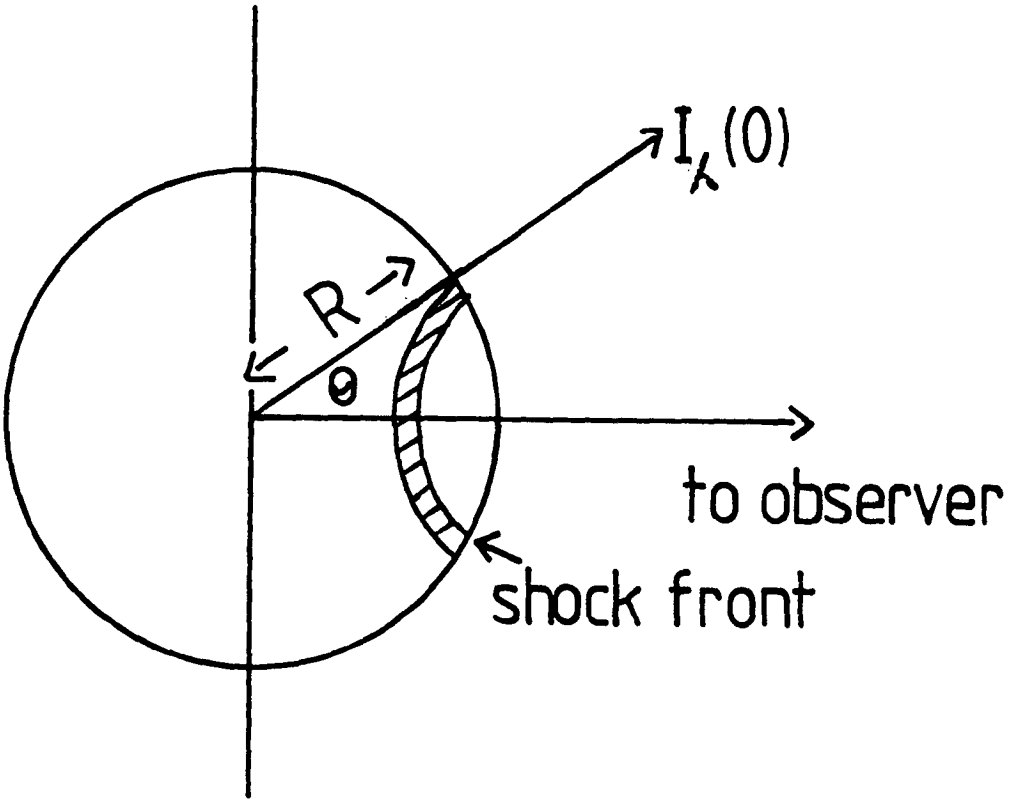

Figure 4.7. The geometry of the situation in the nova remnant of GQ Mus 1983. Spherical symmetry is assumed so that the shocked gas at a radius R imparts an intensity $I_\lambda(o)$ normal to the shock front.

where D is the distance to the source. This reduces to

$$F_\lambda = 2\pi R^2/D^2 \ (I_\lambda)_{ir}(o) \tag{4.7}$$

Now substituting in equation (4.7) we obtain

$$F_\lambda = (2\pi R^2/D^2) \ (21/128\pi) \ (n_h)o \ m_h \ v_s^3 \ f_\lambda, \tag{4.8}$$

which can be written as

$$F_\lambda = 21R^2/64D^2 \ (n_h)o \ m_h \ v_s^3 \ [\lambda f_\lambda]/\lambda \text{ ergs cm}^{-2} \text{ s}^{-1} \ \mu\text{m}^{-1} \tag{4.9}$$

Draine has graphically represented the function $[\lambda f_\lambda]$, and we assume $(n_h)o = 10^5 \text{ cm}^{-3}$, D = 3.3 kpc (as in model), v_s = 1000 km s^{-1} and $R = v_s t$ where t = 200 days so that for band I

$$F_\lambda = 4\text{x}10^{-12}((n_h)o/10^5\text{cm}^{-3})\text{x}(t/200 \text{ d})^2(D/3.3\text{kpc})^{-2}(v_s/1000\text{kms}^{-1})^5 \text{ erg s}^{-1}\text{cm}^{-2}\mu\text{m}^{-1} \tag{4.10}$$

or

$$F_\nu = 0.21((n_h)o/10^5\text{cm}^{-3}) \ (t/200 \text{ days})^2 \ (D/3.3\text{kpc})^{-2} \ (v_s/1000\text{kms}^{-1})^5 \text{ Jy} \tag{4.11}$$

thus the expected band I flux would be ~ 0.21 Jy assuming the factors in brackets are ~ 1. This value is indeed consistent with that observed in band I by IRAS (see Table 4.4). However following the same steps for band II gives

$$F_\nu = 0.02 \ ((n_h)o/10^5\text{cm}^{-3}) \ (t/200 \text{ days})^2(D/3.3\text{kpc})^{-2} \ (v_s/1000\text{kms}^{-1})^5 \text{ Jy} \tag{4.12}$$

i.e. ~ 0.02 Jy if the factor in brackets are ~ 1, which is more than one order of magnitude lower than that observed. (We could change the values in the brackets so that the predicted flux matches that observed in band II; however the band I flux would be changed as well so there would be no benefit in doing this). So Ogelmann et al's. first suggestion, shock heated circumstellar material, is not consistent with the IRAS observations or there was no circumstellar dust. This leads us to the conclusion that the observed X-ray emission was due to the pseudophotospheric effect, in fact the mechanism preferred by Ogelman et al.

4.3.2 V4077 Sgr 1982.

This nova was detected by IRAS in bands I and II on the 360th and 368th day after its outburst (see Fig. 4.8). It was also observed in the JHK and L wavebands at SAAO on day 390 (M. Feast, private communication). Mazeh et al. (1985, from whom the outburst date is taken) described the light curve of this nova in some detail and noted that its pre-maximum behaviour was characteristic of those novae having slow speed class, whereas its post-maximum decline was characteristic of faster novae despite the fact that the deep minimum in the light curve was reminiscent of the novae NQ Vul and LW Ser (see Chapter 2). The infrared light curve of such novae appear to undergo an 'isothermal' phase which has been interpreted as the destruction of grains following the initial grain growth period (Mitchell et al., 1983; 1986).

The band I/band II flux ratio gives a blackbody temperature of ~ 800 K, which is also consistent with the SAAO data (see Fig. 4.9). (The slight mismatch between the two data sets almost certainly arises from the difference in time at which the two sets were obtained). Such a temperature can only reasonably be interpreted as arising from thermal emission by dust grains. However at this temperature an observation in

NOVA SGR 1982

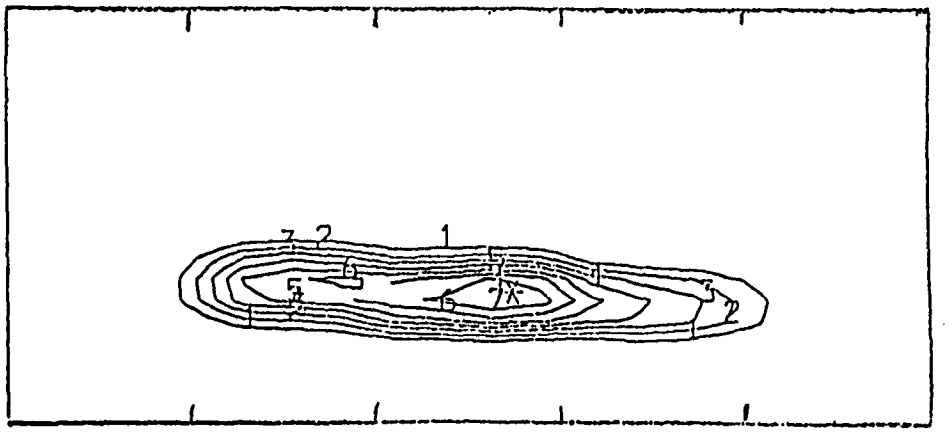

BAND 1

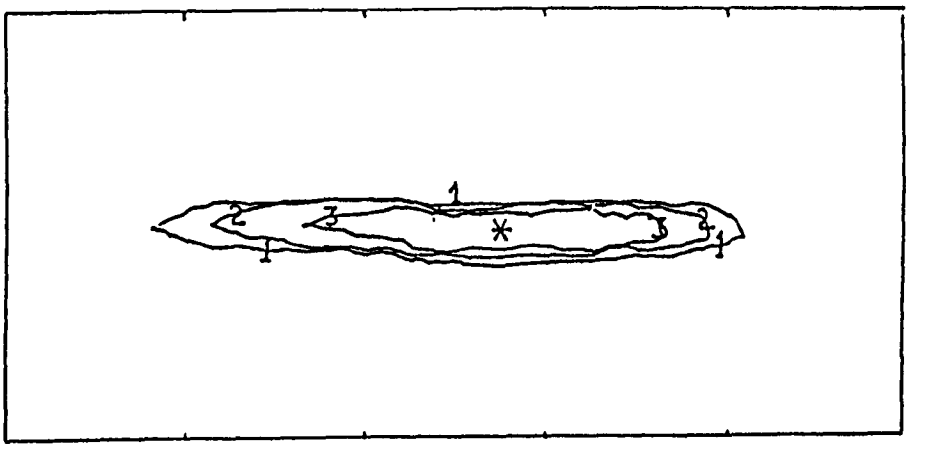

BAND 2

Figure 4.8. IRAS contour maps of V4077 Sgr 1982 in IRAS bands I & II. Contour levels are (in terms of 1 x 10^{-14} W m^{-2}):

Band I: 1) 3.0, 2) 4.5, 3) 6.8, 4) 10.1, 5) 15.2, 6) 22.8, 7) 34.2.

Band II: 1) 0.71, 2) 1.71, 3) 2.71.

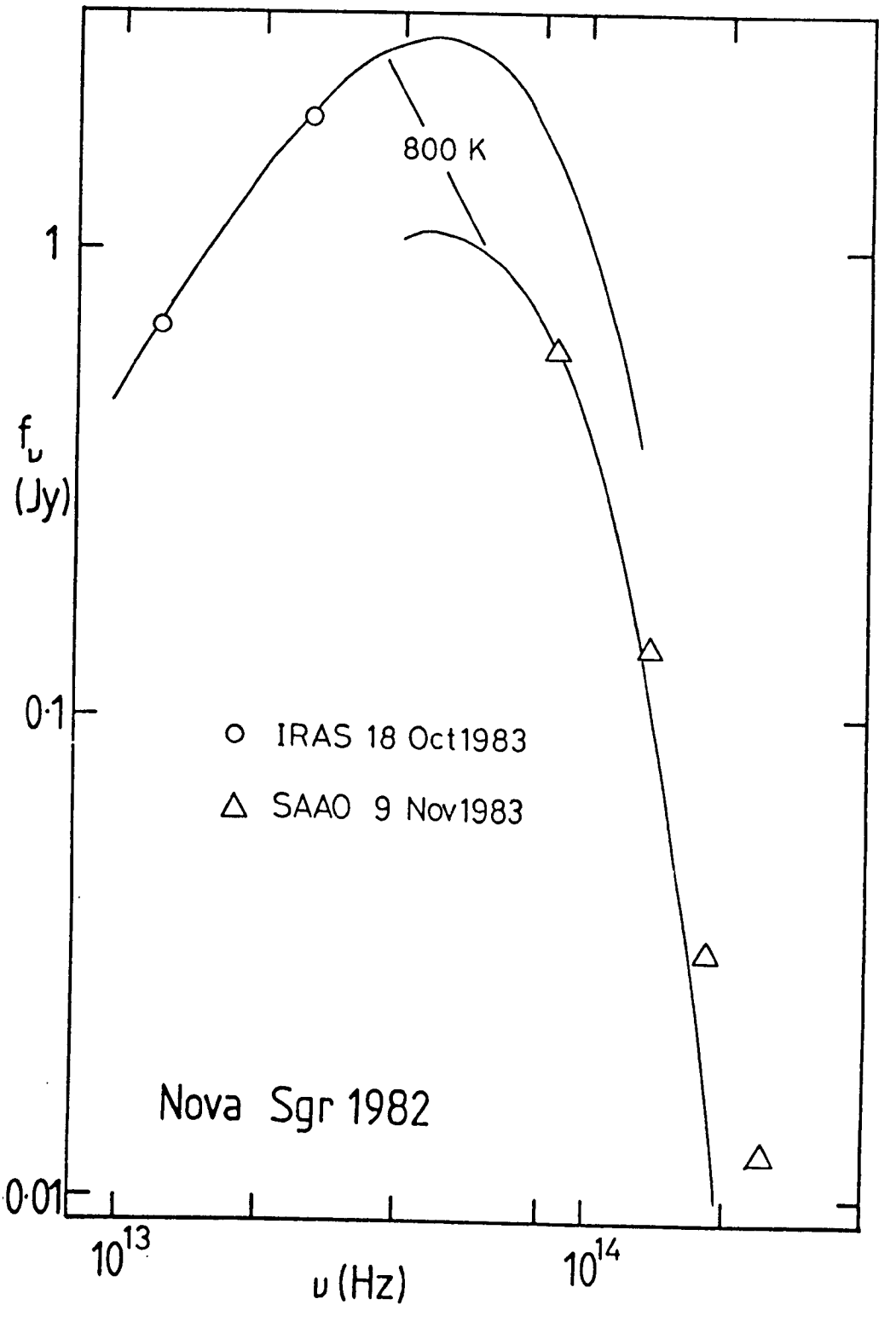

Figure 4.9. 800K blackbody fit to the IRAS band I & II detections of V4077 Sgr 1982. Also shown is SAAO near infrared data taken approximately three weeks later.

band III should have been well within the capabilities of the IRAS detectors when we extrapolate the implied 800 K blackbody to 60μm. This discrepancy was also noted by Dinerstein (1986) when analyzing the survey data of this object. She suggested that this could be understood by invoking emission by dust grains having a λ^{-1} dependence of emissivity on wavelength. However Bode & Evans (1983) note that the radial dependence of the grain density distribution also affects the form of the dust distribution longwards of peak emission, but this would tend to broaden rather than narrow the distribution. Perhaps the flux distribution is essentially blackbody in character but has emission features in band II (maybe a sulphide feature or fine structure lines; see section 4.3.4).

Although we have only obtained observations on two days the colour temperature calculated on both these dates is essentially constant. This is consistent with Dinerstein (1986) who reported that the PSC data from day 161 to day 357 gave a constant blackbody temperature of 900±200 K. This supports the view that the infrared behaviour of V4077 Sgr displayed an 'isothermal' stage.

Assuming graphite grains (there is no evidence of a 10μm silicate feature), and that the distance D to the nova is 2.5 kpc (for consistency with Dinerstein, although Mazeh et al., 1985 derive 4.7 kpc), the dust mass M_d is calculated (assuming an optically thick shell) by

$$M_d = (4D^2 f_\nu a\rho)/(3B_\nu Q_{abs}(\nu)) \qquad (4.13)$$

where f_ν is the flux at frequency ν, a is the grain radius, B_ν is the blackbody distribution and Q_{abs} is the absorption coefficient (Q_{abs}/a is tabulated by Draine, 1981). The results of dust mass from the AO's and from the survey (Dinerstein, 1986) are given in Table 4.5. Clearly from this we can see that the dust mass is continually decreasing over the period 161 - 374 days after outburst. The corresponding grain destruction

Table 4.5

Evolution of the dust shell of V4077 Sgr.

V4077 Sgr	time (days)	dust mass (M_o)
	161	2.02×10^{-6}
	169	1.63×10^{-6}
	357	1.82×10^{-7}
	360	2.64×10^{-8}
	368	2.42×10^{-8}

The first three values are given by Dinerstein (1986) where we have substituted a value of $a\rho/Q_{abs} = 0.024$ instead of 0.05 to agree with our calculations. Both set of data assume a distance of 2.5 kpc.

time is ~ 100 days which is of the same order as that required by the grain charge models of Mitchell & Evans (1984) and Mitchell et al. (1986).

The infrared luminosity L_{ir}, of the dust shell at the time of the AO's has been calculated from

$$L_{ir} = 4\pi D^2 f \tag{4.14}$$

where f is the total flux

$$f = (f_\nu \sigma T_d^4 \langle Q_d \rangle)/(B_\nu Q_{abs}(\nu)\pi) \tag{4.15}$$

σ being Stefan's constant, T_d the dust temperature and $\langle Q_d \rangle = 0.01 a T_d^2$ (in c.g.s) the Planck mean absorption coefficient of the dust. From this a lower limit on the nova luminosity can be obtained, if we assume that the dust shell is optically thick (as witnessed by the transition break), from

$$L_{ir} = L_*(1-e^{-\tau}) \tag{4.16}$$

where L_* is the nova luminosity; since $e^{-\tau}$ is negligible then $L_{ir} \sim L_*$. In this way the deduced nova luminosity $L_* \sim 1300 L_\odot$.

4.3.3 DQ Her.

This nova, often regarded as the prototype of dusty novae (see Chapter 2), was observed by IRAS in bands III and IV (Fig 4.10). These detections suggest a colour temperature of ~ 40 K which is consistent with no detections in bands I and II (A. Evans, private communication, calculated that the probability of the IRAS sources arising from an interstellar dust cloud in the same line of sight to be extremely low). We explore the possibility that this emission could be due to dust produced during the great minimum, now 'thinned out' and heated by the stellar remnant. To do

III

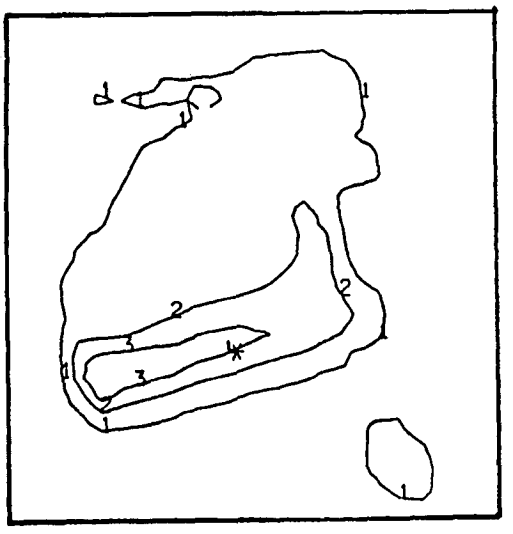

IV

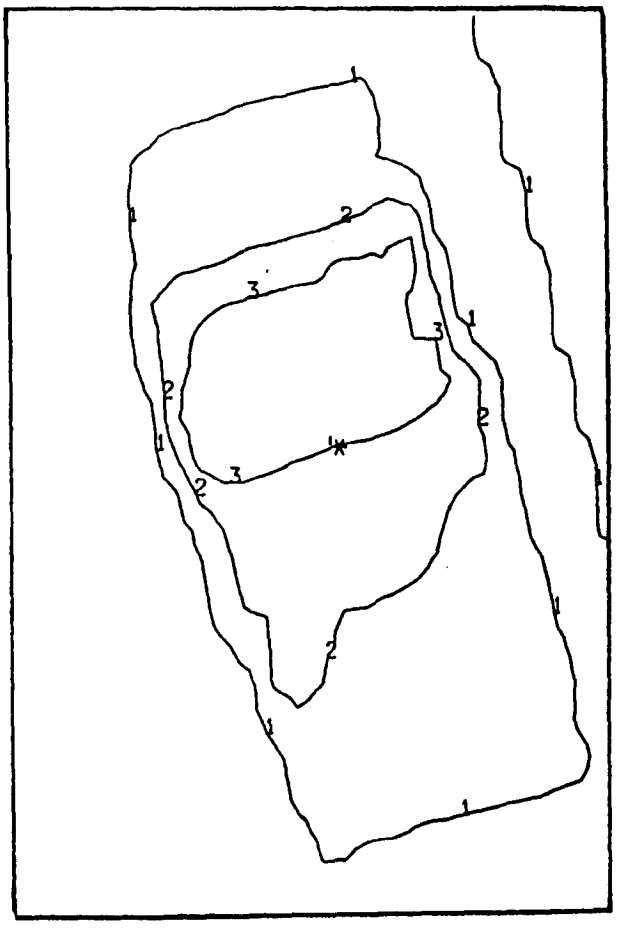

Figure 4.10. IRAS contour maps of DQ Her 1934 in IRAS bands III & IV. Contour levels are (in terms of 1 x 10^{-14} W m^{-2}):

Band III: 1) 12.7, 2) 13.0, 3) 13.2.

Band IV: 1) 11.5, 2) 12.0, 3) 12.5.

this we need to know the optical depth in the visual of the dust when the observations by IRAS were taken, knowing that the optical depth τ at light minimum in 1935 reached ~ 9. Now assuming that the density in the ejecta falls as r^{-2}, is undergoing uniform outflow and that there are no significant grain destruction processes at work, we have

$$\tau = \int N_0 \, (r/r_0)^{-2} \, \pi a^2 \, Q_{abs} \, dr \tag{4.17}$$

where N_0 and r_0 are constants; so that

$$\tau = N_0 \pi a^2 Q_{abs}(1/R_1 - 1/R); \tag{4.18}$$

hence,

$$\tau(t) = N_0 \pi a^2 Q_{abs}(1/(v_{ej}(t-\Delta t)) - 1/(v_{ej}t)) \tag{4.19}$$

where Δt is the ejection time. Now assuming instantaneous nucleation of all condensible material once it has passed through the condensation distance r_c, the maximum optical depth τ_{max} will be

$$\tau_{max} = N_0 \pi a^2 Q_{abs}(1/r_c - 1/(r_c + v_{ej}\Delta t)) \tag{4.20}$$

so that if $\Delta t = t_c$ i.e. mass ejection until transition

$$\tau/\tau_{max} = 2t_c^2/(t(t-t_c)) \tag{4.21}$$

Therefore putting t = 48.3 yrs (time of IRAS observation) and t_c = 100 days (Stratton, 1946), the optical depth τ_{iras} at the time of the IRAS observation will be ~ 5.8×10^{-4}. As this dust shell is optically thin, and assuming it acts as a blackbody we will have that

$$f_{ir} = 1.34(\lambda f_{\lambda})_{max} \tag{4.22}$$

(Gehrz et al., 1980b) where f_{ir} is the observed infrared flux. From Allen (1973), a blackbody at 40 K peaks at ~ 150μm. Solving $\delta(\nu B_{\nu})/\delta\nu = 0$ we then find the wavelength at which νB_{ν} peaks is ~ 108μm, hence we find $(\nu B_{\nu})_{max} = 1.76$ J. Converting to wavelength units (4.24) becomes

$$f_{ir} = 6.64 \times 10^{-11} \ erg \ cm^{-2} \ s^{-1} \tag{4.23}$$

Taking a distance of 420 pc to this nova (Ferland et al., 1984) we find that

$$L_{ir} = 4\pi D^2 f_{ir} = 1.4 \times 10^{33} \text{ erg s}^{-1} \tag{4.24}$$

Thus using equation (4.16)

$$L_{*} \sim 2.4 \times 10^{35} \text{ erg s}^{-1} \tag{4.25}$$

However this is more than two orders of magnitude greater than the known luminosity of the DQ Her remnant (1×10^{34} erg s^{-1}; Ferland et al., 1984). This discrepancy can be resolved if a) the extrapolated optical depth is incorrect, due to non-uniform outflow, a density distribution other than r^{-2} or changing grain radius (or a mixture of these factors), b) the dust is not currently being heated by the remnant or c) the flux from the third and fourth bands is not due to dust. In this case it is possible that the flux may be due to fine structure lines, especially those of [OIII]. However using predictions from Ferland et al. (1984) for the flux due to [OIII] at 52μm and 88μm this could not account for more than ~ 6% of the observed flux in the third and fourth bands.

4.3.4 HR Del 1967.

HR Del was an extremely slow nova having a speed class of ~ 0.008 mag day^{-1} (Sanyal, 1974). Theoretically a nova having such a speed class would be expected to produce vast amounts of dust soon after outburst (Gallagher, 1977; Bode & Evans, 1982). Unfortunately no infrared observations are available for the period just after outburst, though the absence of any deep minimum in the visual light curve suggests that large scale grain formation did not take place. However observations obtained some 3 years after outburst (Geisel et al., 1970) suggest an infrared excess with colour temperature ~ 300 K and L_{ir} ~ 30 L_o. (Also see Chapter 3).

IRAS observed this object in band II only so this would appear to rule out any thermal emission by dust. This is reinforced by extrapolation of Geisel et al.'s dust temperature to the time of the IRAS observations. Using $T_d \propto t^{-1/2}$ (Bode & Evans, 1983) we would expect a dust temperature of ~ 130 K. If the observed IRAS emission is due to blackbody dust then at this temperature detections in bands III and IV would have also been expected. However this assumes that the dust is essentially carbon based. Several sulphides have strong features in the 20μm - 30μm window (Nuth et al., 1985) and as sulphur is highly overabundant in many novae (Collin-Souffin, 1977) perhaps this nova produced sulphide condensates. In this case the dust shell would have to be optically thin at visual wavelengths to explain the absence of a deep minimum. Dinerstein (1986) suggested that the band II emission could be due to fine structure lines, perhaps of [SIII] 19, 34μm, [NeV] 24μm, [OIV] 26μm or [SiII] 35μm. High resolution spectroscopy at ~ 25μm might determine if this nova did indeed produce some kind of sulphide condensate or exhibit fine structure lines and hence explain the band II emission.

4.4 Conclusion.

In general the data from the IRAS mission on classical novae have been a valuable source of information especially when coupled with ground based observations. The fact that we now have a greater wavelength range of information has helped to confirm the origin of the infrared radiation from the novae GQ Mus and V4077 Sgr (thermal bremsstrahlung and thermal dust emission respectively). For the older novae searched for in the AO's the data have revealed that their evolution since outburst is more complicated than a simple extrapolation. For DQ Her in particular such an extrapolation from the time of the 1934 outburst to the time of the IRAS observations show great inconsistency. The emission from HR Del is most likely to be due to sulphides or fine structure lines and the AO's have shown little sign of carbon based dust from this nova, in keeping with the grain nucleation model developed in Chapter 3.

However IRAS did not detect all of the novae it searched for. It appears that from these non-detections that fast novae fade extremely quickly (or have little emission) in the far infrared (see MU Ser). Perhaps then these wavelengths are not the best studying the propeties of fast novae, except immediately after outburst.

CHAPTER 5

NOVA PW VULPECULAE 1984.

5.1 Introduction.

This nova was discovered by Wakuda on 1984 July 27.711 UT at an apparent photovisual magnitude of ~ 9.2 (Kosai, 1984). Since that time it has been observed in the optical, ultraviolet and infrared wavelength ranges. It is seen to have some intriguing characteristics which do not lead it immediately to be categorized into any particular speed class.

A short review of all the available data on this object follows, together with the results obtained from service time on UKIRT, from where we received an infrared spectrum in the wavelength range 2μm - 4μm, and service time at SAAO, from which we obtained infrared photometry in the J - L wavebands.

5.2 Observations of PW Vul.

5.2.1 The Light Curve.

The light curve of this object has been studied extensively by Noskova et al. (1985) who carried out observations at U, B and V in the period 1984 August - December. Their light curve is shown in Fig. 5.1a.

They found that this nova exhibited abrupt oscillations in brightness of differing duration which occured both on the rising branch and after maximum light. The maximum was quite difficult to pinpoint as it appears that the star spent ~ 2.5 days at maximum around August 5 when it reached a visual magnitude of ~ 6.4 mags. It then faded sharply and ~ 3.5 days later it had dropped by more than two magnitudes giving it a speed class of ~ 0.57 mags d^{-1} - a fast nova. By the beginning of September the star was fluctuating with an amplitude of up to one magnitude in a cycle of several

days with a mean visual flux of 7.8 mags. From Sept 10 to the end of the year the nova declined at a mean rate of ~ 0.02 mags d^{-1}, becoming two mags fainter after about 80 - 100 days. The nova took 85 days to drop by three mags, giving a speed class of ~ 0.035 mags d^{-1} - a slow nova, obviously the initial decline at 0.57 mags d^{-1} is not related to speed class. Noskova et al. (1985) remark that the light curve closely resembles the behaviour of the slow novae DQ Her 1934 and NQ Vul 1976 during the first 2 - 3 months after their outbursts, although there does not appear to be an obvious transition break in the light curve of PW Vul. After this time the light curve continued to oscillate for ~ 3 months (see Fig. 5.1b; this shows the light curve as composed of data from the IAU Circulars for the year 1985) and eventually steadied in ~ 1985 May whilst by 1985 December it had reached ~ 12.1 mags.

Noskova et al. (1985) also measured the colour indices B-V and U-B. They note that at the time of the initial dimming on August 6 - 10, these colours reddened significantly. Several days later the nova became bluer again, reaching B-V $\simeq$ 0.35 mags and U-B $\simeq$ -0.7 mags and until late October the colours remained practically constant. However subsequently these colours changed by a few tenths of a magnitude with B-V diminishing and U-B increasing. From an estimate of the interstellar extinction in the direction of PW Vul using 10 stars around this region the authors were able to estimate a distance of 1.9 kpc to this nova.

5.2.2 Spectroscopic Observations.

Spectroscopically this nova had been monitored from outburst by Rosino et al. (1984). They saw broad emission lines and they managed to detect hydrogen up to H_{16} (with mean widths of ~ 580 km s^{-1}). They observed many lines of FeII, and also lines due to CaII 3934A, NaI 5893A, NII, OI and TiII. All emissions were flanked by P-Cygni absorptions. They measured the mean radial velocity of this absorption system to be ~ -610 km s^{-1}.

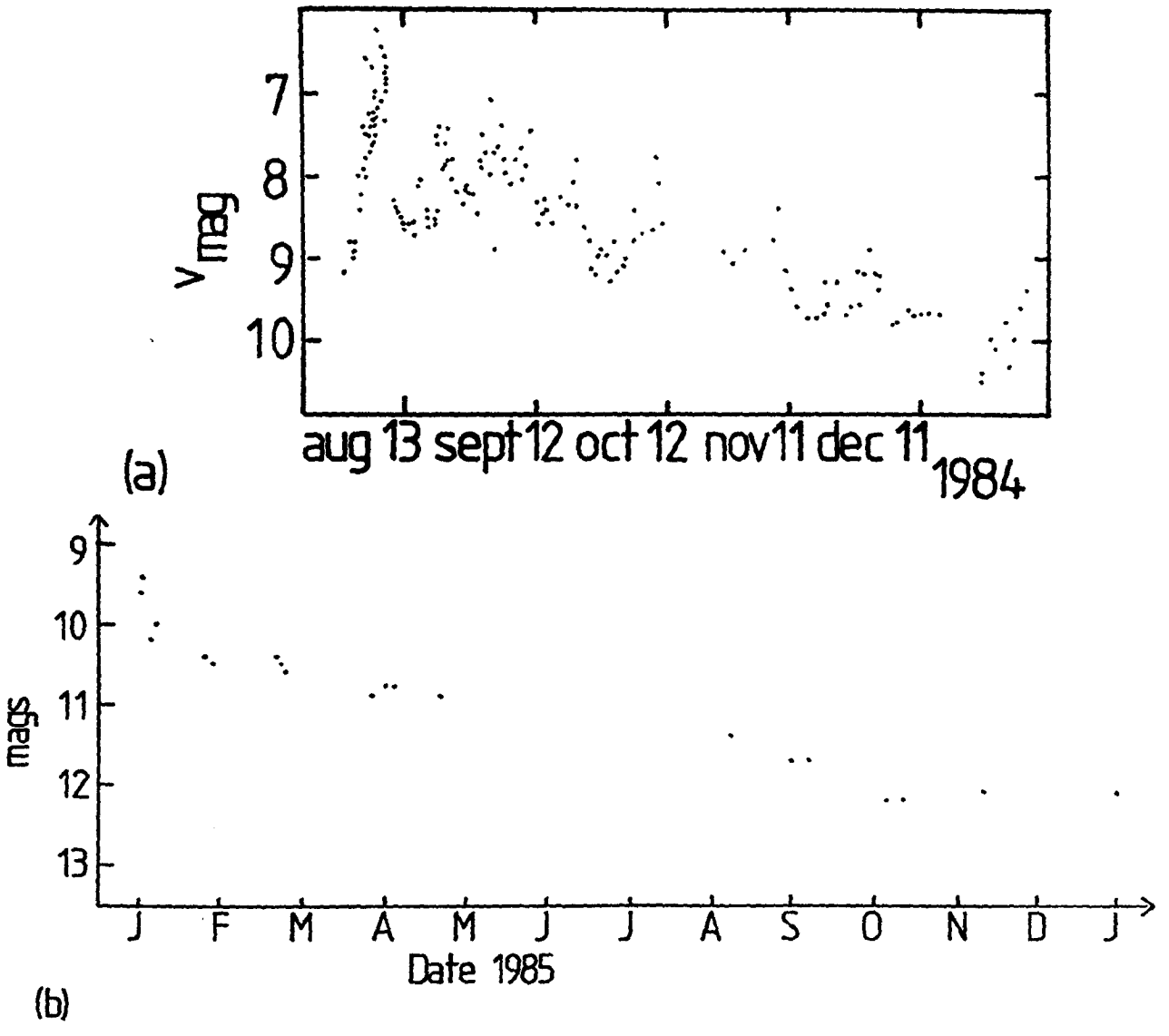

Figure 5.1. Visual light curve of PW Vul 1984. a) Reproduced from Noskova et al. (1985), b) compiled from the IAU Circulars.

Andrillat & Houziau (1984), on 1984 August 2.92, also saw broad emissions in the blue. They witnessed in addition a broad absorption component whose centre was at ~ -710 km s^{-1}. Balmer lines were seen up to H_{12} with velocities of ~ 560 km s^{-1}. The FeII lines showed the same profile but were considerably weaker. There were also seen strong CaII lines with wide K - line absorption at 3924.7A; the interstellar component was located at 3932.7A. In the ultraviolet the TiII doublet at 3759A and 3761A was conspicuous. On the following day Andrillat (1984) observed in the near infrared. She saw broad emission features, notably the Paschen series from P_7; OI λ7773 - 8446A, the CaII triplet at 8498, 8542 & 8662A and also lines of NI and CI. There were very weak lines of MgII λ7877 - 7896A that were characterized by broad absorption components shifted to -820 km s^{-1}. The expansion velocity as deduced from the total width of the emission lines was ~ 1100 km s^{-1}. A day later she observed no major changes but by August 5 the absorption components of the lines were stronger and the OI emisssion lines had decreased in intensity.

Four spectra were obtained by the IUE satellite of this nova (M.A.J. Snijders, private communication). The earliest one was taken on 2 August and hence is a pre-maximum spectrum; it was the hardest spectrum obtained. (This spectrum is only one of a few pre-maximum spectra obtained of novae and seems to reinforce the property that pre-maximum nova spectra are harder than those at maximum; Penn et al., 1984). The identified lines are FeII UV1 λ2630 in emission and absorption and the MgII λ2800 P Cygni profile. A MgII interstellar doublet (and perhaps the MgI interstellar line) were present in the high resolution spectrum.

Returning to the optical data of Rosino et al. (1984) at maximum (August 4-5), most of the emission lines weakened or disappeared whilst the absorptions became stronger. However during the following nights, while the system was in decline, the emissions lines strengthened. On August 11 the emission lines appeared distinctly split into two symmetric components

with a mean separation of ~ 580 km s^{-1}. The total width of the emission bands was ~ 1130 km s^{-1}, the red component being slightly stronger than the blue. At this time a new absorption system appeared and soon became much stronger than system I. Meanwhile in the ultraviolet a spectrum obtained on 1984 August 7 was showing lines due to C, N, O Mg and Fe in low stages of ionization. The MgII expansion velocity as measured from this spectrum was ~ 2800±300 km s^{-1} which was about 2.5 times larger than that obtained by the previous authors in the optical.

Sowell et al. (1985) obtained spectroscopy in the blue on August 12 and August 17 and in the red on August 22, each with ~ 5A resolution. The first scan showed the Balmer series, FeII lines and the CaII H & K lines, all in emission with no absorption features. However on August 17 absorption features were present. On this scan the CaII K and FeII emission lines were weaker compared to the Balmer series. Table 5.1 lists the observed lines with their measured radial velocities. The blue spectrum showed strong Hα in emission along with a very small violet absorption feature. The full width of Hα extended from -1151 to +1911 km s^{-1}.

Rosino et al. (1984) observed almost simultaneously with Sowell et al., with observations taken between August 18 - 23. They measured radial velocities of ~ -793 km s^{-1} and -1350 km s^{-1} for systems I and II respectively. The emission bands (which they still saw in two components) became wider and HeI lines emerged at 5875A, 6678A and 7065A. A near infrared spectrum taken on August 18 revealed strong emissions due to OI 7773 & 8446A, CaII 8498, 8542 & 8662A and relatively weaker emissions due to hydrogen, FeII, NI and OI.

Further ultraviolet spectra obtained on August 30 revealed the presence of FeII UV lines 1 (2630A), 2 (2374A) & 3 (2359A). From the low resolution spectrum obtained then the extinction E(B-V) was estimated to be ~ 0.3 - 0.6 using the strength of the 2200A extinction feature. A final

Table 5.1

Measured lines and radial velocities in PW Vul.

λ(lab)	Ion(mult)	August 12		August 17	
		λ(obs)	v(km/s)	λ(obs)	v(km/s)
4101.737	Hδ	4099.01	-206	4099.21	-193
4173.450	FeII (27)	4172.17	-99	4173.77	+14
4233.167	FeII (27)	4230.71	-181	4231.11	-155
4340.468	Hγ	4340.34	-16	4341.79	+82
4861.332	Hβ	4859.40	-126	4861.56	+5
4923.921	FeII (42)	4921.69	-143	4923.88	-11
5018.434	FeII (42)	5015.78	-166	5016.71	-112
5169.030	FeII (42)	5166.53	-152	5167.26	-112
5234.620	FeII (49)	5230.44	-247	5231.42	-192
5275.994	FeII (49)	5273.13	-170	5275.10	-60
5316.693	FeII (48,9)	5313.56	-184	5314.31	-143

Reproduced from Sowell et al. (1985).

set of ultraviolet spectra taken on September 30 were characterized by the dominance of emission lines and the growing in importance of semi-forbidden and forbidden lines. Lines of C, N, O, Al, Si, Fe and Mn became important in emission and the P Cygni profiles in these spectra appeared more complicated than at earlier epochs. These spectra did not seem to have many lines of high excitation and forbidden lines as is seen in the nebular stage of nova evolution. However in enhanced and Orion spectra, spectral development is characterized by narrowing absorptions with very few emission lines. It is possible that the nova was on the way to entering into the nebular stage of developement at the time of these observations and indeed information from other spectral wavebands indicate that the nebular stage was reached a few months later (see below).

Additional observations by Rosino & Iljima (1987) between mid August and November showed that the degree of excitation in the optical spectra was slowly increasing. Most of the low ionization potential lines weakened or disappeared whilst neutral helium lines emerged and strengthened. The nitrogen 'flaring' also ocurred in this time period with the appearance of NIII λ4640 and NII λ5755. In November all of the permitted lines were still flanked by the two systems of P Cygni absorption whilst in December more lines of NII and NIII appeared along with HeII λ4686. The two absorption systems by this time were blurred, forming the diffuse absorption. By the end of December the nova had reached the transition to the nebular stage which was marked in 1985 January by the appearance of the lines [OIII] λ5007, 4959, 4363 and the disappearance of all absorption features.

In the near infrared, as the nova was undergoing its transition, Rosino & Ilijima (1987) note a 'remarkable change'. All of the low excitation lines disappeared, with the exception of OI λ8446 which was still strong. [AIII] λ7135, 7751 were recorded and [OII] λ7320, 7330 became nearly as strong as OI λ8446.

Duerbeck et al. (1984) estimated the distance to this nova to be ~ 1.2 kpc, from the intensity of the interstellar CaII line; thus A_V = 1.4 mags and E(B-V) ~ 0.45 mags. The apparent maximal visual magnitude of ~ 6.3 mags thus leads to Mv(abs) = -5.5, a value they feel that is somewhat fainter than the mean absolute magnitude of a slow nova.

Kenyon & Wade (1986) obtained optical spectrophotometric data of this nova from 1984 September until 1986 April. The lines they detected and their measured fluxes are given in Tables 5.2 and 5.3. In the inital spectra taken on 1984 October 9 and 10 in the red, the nova had fallen 2 mags from maximum. The spectra were dominated by the strong Hα line which had a velocity of expansion ~ 1200 km s^{-1} (rather large for a slow nova, see Chapter 1). There was also evidence for a blue shifted absorption feature. On measurement of the velocity widths of some of the weaker emissions like HeI λ5878 and [AIV] λ7238 they were found to be comparable to that of Hα and most of these stronger lines appeared also to have blue shifted absorption components. A blue spectrum taken on 1985 March 20 (at ~ 4.2 mags below maximum) contained no blue shifted absorption features. Nebular lines [OIII] λ4959, 5007 and [NeIII] λ3869, 3967 were strong in March and the HeI lines appeared to have weakened slightly. HeII λ4541, 4686, 5411 and NV λ4603 developed into strong emission features and other high ionization lines including [CaVI λ5461 and [FeVI] λ5146, 5176, 5335 were also prominent. This slow nebular evolution of the nova continued into June, the strongest feature becoming [OIII] λ5007 which was significantly stronger than even Hα; [NeIII] lines were also fairly intense. All of the permitted lines diminished in intensity by a factor ~ 2 - 3 in the March - June period whilst most of the forbidden lines decreased by ~ 25%. The HeII λ4686/Hβ ratio increased during this time implying a higher effective temperature in June. The emission lines remained broad in March and June, the velocities of the strongest being between ~ 1000 - 1500 km s^{-1}. In the last spectrum these authors obtained

Table 5.2

Emission line fluxes* in the red spectra of PW Vul.

Identification	9/10/84	20/3/85	02/6/85
[FeVI]λ5677		0.18	0.03
[NII]λ5755	2.32	1.38	0.86
HeIλ5876	3.61	0.26	0.09
[FeVII]λ6087			0.11
[OI]λ6300	1.91		0.09
[OI]λ6364	2.33		0.05
Hα	69.3		3.64
HeIλ6678	2.9		0.03
[AV]λ7006			0.02
HeIλ7065			0.07
[AIII]λ7136			0.07
[AIV]λ7238	4.4		0.04
[OII]λ7320,30	3.1		0.39
[OI]λ7777	4.0		
λ8402	4.65		
HeIIλ8237	1.08		

Reproduced from Kenyon & Wade (1986).

*In units of 10^{12} erg $cm^{-2} s^{-1}$.

Fluxes have not been dereddened.

Table 5.3*
Emission line fluxes in the blue spectra of PW Vul.

Identification	20/03/85	2/06/85	25/04/86
OIIIλ3312	0.10		
OIIIλ3341	0.24		
OIIIλ3444	0.81	0.30	
OIIIλ3760	0.19	0.08	
H 10	0.07		
H 9	0.15		
[NeIII]λ3869	0.45	0.30	
H 8	0.29	0.24	
[NeIII]λ3967	0.35	0.16	
NIIλ3995	0.03		
[FeV]λ4071	0.07	0.07	
?[FeII]λ4084	0.05		
Hδ, NIIIλ4097	0.70	0.29	
NIIIλ4196	0.10		
[FeII]λ4244	0.03		
[FeII]λ4276	0.06		
Hγ	0.66	0.24	0.02
[OIII]λ4363	1.82	1.06	0.05
HeIλ4471	0.04	0.02	
FeIIλ4520	0.10	0.08	
HeIIλ4541	0.02		
NVλ4603	0.14	0.06	
NIIIλ4634,40	0.93	0.34	
HeIIλ4686	0.48	0.21	
Hβ	1.68	0.59	0.04
[OIII]λ4959	1.57	1.42	0.35
[OIII]λ5007	4.83	4.31	1.01
[FeVI]λ5146	0.05	0.07	
[FeVI]λ5176	0.10	0.10	
[FeII]λ5271	0.03	0.03	
[FeII]λ5297	0.13	0.04	
[FeVI]λ5335		0.02	
HeIIλ5411	0.05	0.02	
[CaVI]λ5461	0.03	0.01	
[FeII]λ5527	0.02	0.01	
FeIIλ5535	0.03	0.01	

Reproduced from Kenyon & Wade (1986).
* In units of 10^{-11} erg cm^{-2} s^{-1}.
Fluxes have not been dereddened.

on 1986 April 25 very strong [OIII] lines were dominant due to the very weak continuum. The nebular lines of [OIII] had in fact weakened by a factor ~ 4 from the previous June with the hydrogen lines declining by more than one order of magnitude in the same period.

Kenyon & Wade (1986) also made infrared photometric observations of PW Vul (included here for completeness). They took data at J, H and K on 1984 October 6 and 7, and the colours were as follows:

6 Oct K=6.58 (H-K)=0.25 (J-K)=0.39

7 Oct K=6.07 (H-K)=0.23 (J-K)=0.48

They interpreted these colours using the following model. Two thirds of the radiation at H (1.65μm) was assumed to be emitted by a 8000 K blackbody, with the remainder being supplied by optically thin material at 7000 - 9000 K (see section 5.3.3). Thus the variation at K was deemed to be due to fluctuations in the optically thin emission. But since their optical spectra, taken a few days later, show no evidence for variations in the red continuum and no variations in emission lines above the 10% level, these infrared fluctuations cannnot be verified. The total measured Bγ flux from these in infrared spectra was ~ 2% of the total Hα flux taken from the slightly later (optical) spectra.

From these data the authors were able to estimate some abundances in the nova ejecta. On 1985 March the HeII λ4686/Hβ ratio implied that $He^{++}/H^{+} \simeq 0.03$ while in June this ratio increased slightly to ~ 0.035 which was to be expected as the underlying nova remnant evolved towards higher effective temperatures (see Chapter 2). The reddening corrected HeI λ5876/Hα ratio for the 1984 October data implies $He^{+}/H^{+} \sim 0.13$ and thus a lower limit to the helium/hydrogen abundance in October was ~ 0.13. Their best estimate for the He/H ratio during 1985 June is ~ 0.11±0.01, so the helium abundance in PW Vul seemed to be fairly constant in time. This value is somewhat low for a slow classical nova and is more typical of a fast nova such as V1500 Cyg 1975 (Ferland, 1979). The oxygen and neon

abundances for different electron densities and effective temperatures are shown in Table 5.4. If T_e > 15000 K both the oxygen and neon abundances were near solar in March and June 1985; however the oxygen abundance was enhanced over solar by a factor of ~ 10 if the effective temperature was significantly lower than 15000 K. On estimating the densities using the [FeIV] lines they find the observed intensity ratio of λ5176/λ5146 in 1986 March implied the electron density $n_e \leq 8 \times 10^6 cm^{-3}$ for $T_e \geq 10000$ K whilst n_e ~ few x $10^6 cm^{-3}$ for any T_e. They estimated n_e ~ 1-4 x $10^6 cm^{-3}$ for Te ~ 10000 - 20000 K from the relative line intensities observed on June 2.

5.2.3 A Dust Excess?

Gehrz et al. (1985b) observed this nova on 1985 May 14.4 at infrared wavelengths; Table 5.5 gives the infrared magnitudes obtained. From the apparent infrared excess they deduced that dust grains had condensed in the ejecta. The dust temperature was calculated to be ~ 700 K. From the fact that these observations were taken 285 days after outburst and the inferred dust temperatures Gehrz et al. suggested that dust had probably condensed in the ejecta before this date. (We will be returning to these data in section 5.4).

5.3 The UKIRT Spectra.

We received spectra, in four wavelength ranges obtained as service observations on UKIRT on 1984 October 23. The spectra were obtained using the cooled grating spectrometer CGS2 which has a resolution of $\lambda/\Delta\lambda$ ~ 500 (i.e. medium range resolution). The spectra consisted of one in the 2 - 2.35μm K band, two in the 2.9 - 3.6μm L band and one in the 3.6 - 4.15μm L' band. The data were reduced grating position by grating position in an attempt to minimize the effect of variable clouds that unfortunately were present at the time of the observations. The data were made available in the form of const. x (target [PW

Table 5.4

Oxygen and neon abundances in PW Vul.

Date	T_e(K)	n_e(cm^{-3})	OII/HeI	NeII/HeI
20/3/85	10000	$5x10^7$	0.25	0.0051
	15000	$8x10^6$	0.016	0.00054
	20000	$5x10^6$	0.007	0.00033
01/6/85	10000	$2x10^7$	0.096	0.0018
	15000	$5x10^6$	0.006	0.00020
	20000	$3x10^6$	0.004	0.00019
25/4/86	10000	$2x10^6$		
	15000	$7x10^5$		
	20000	$3x10^5$		

Reproduced from Kenyon & Wade (1986).

Table 5.5

1985 May 14 magnitudes of PW Vul.

Waveband (μm)	magnitude
2.3	9.9
3.6	8.4
4.9	7.6
8.7	5.5
'N	5.3
11.4	5.2
Q	≥2.2

Magnitudes obtained by Gehrz et al., 1985.

Errors are ±0.05 mags at 2.3, 3.6μm and ±0.1 mags at 4.9 - 11.4μm.

Vul]/standard) x (F_λ[Planck function at the temperature of the standard]), and absolute flux values at selected wavelengths were provided so that the spectra could be calibrated. (The standard stars used were BS7615 for the K band and BS7806 for the other bands). However due to the poor weather conditions the flux calibrations were not very accurate and this is exhibited in the fact that the two spectra obtained in the L band have a maximum difference in their flux of ~ 25% even though the same standard star was used. The accuracy in the wavelength scale was ± 0.002μm for the K band and ± 0.003μm for the L and L' bands. The spectra were analysed using the Starlink routine DIPSO.

5.3.1 Line Identifications.

Figs 5.2 show the entire spectrum with identifications of the strongest lines whilst these lines are tabulated in Table 5.6. As expected, the hydrogen lines are the most prominent and dominate the spectrum. Neutral helium is also well represented and, as the major hydrogen lines appear to be blended with others it is likely that hydrogenic HeI also contributes at these wavelengths; the temperature in the nebular continuum (see section 5.3.3) would tend to exclude significant contributions from ionized helium although a weak HeII λ8237 line was observed by Kenyon & Wade (1986) on 1984 October 9.

Identifications of the lines due to CI and NI are less secure than those due to hydrogen or helium. NI and CI lines were observed as early as 1984 August 3 in the visual and in the near infrared about two weeks later (see section 5.2.2). If these identifications are correct they probably arise from the tail end of the maximum or enhanced spectrum that usually contain lines of this nature (see Chapter I).

In the L spectrum there is a noticeable feature at ~ 3.52μm. A feature also appeared in the nova GQ Mus 1983 at this wavelength and was attributed by the authors Krautter et al. (1984) to formaldehyde. However

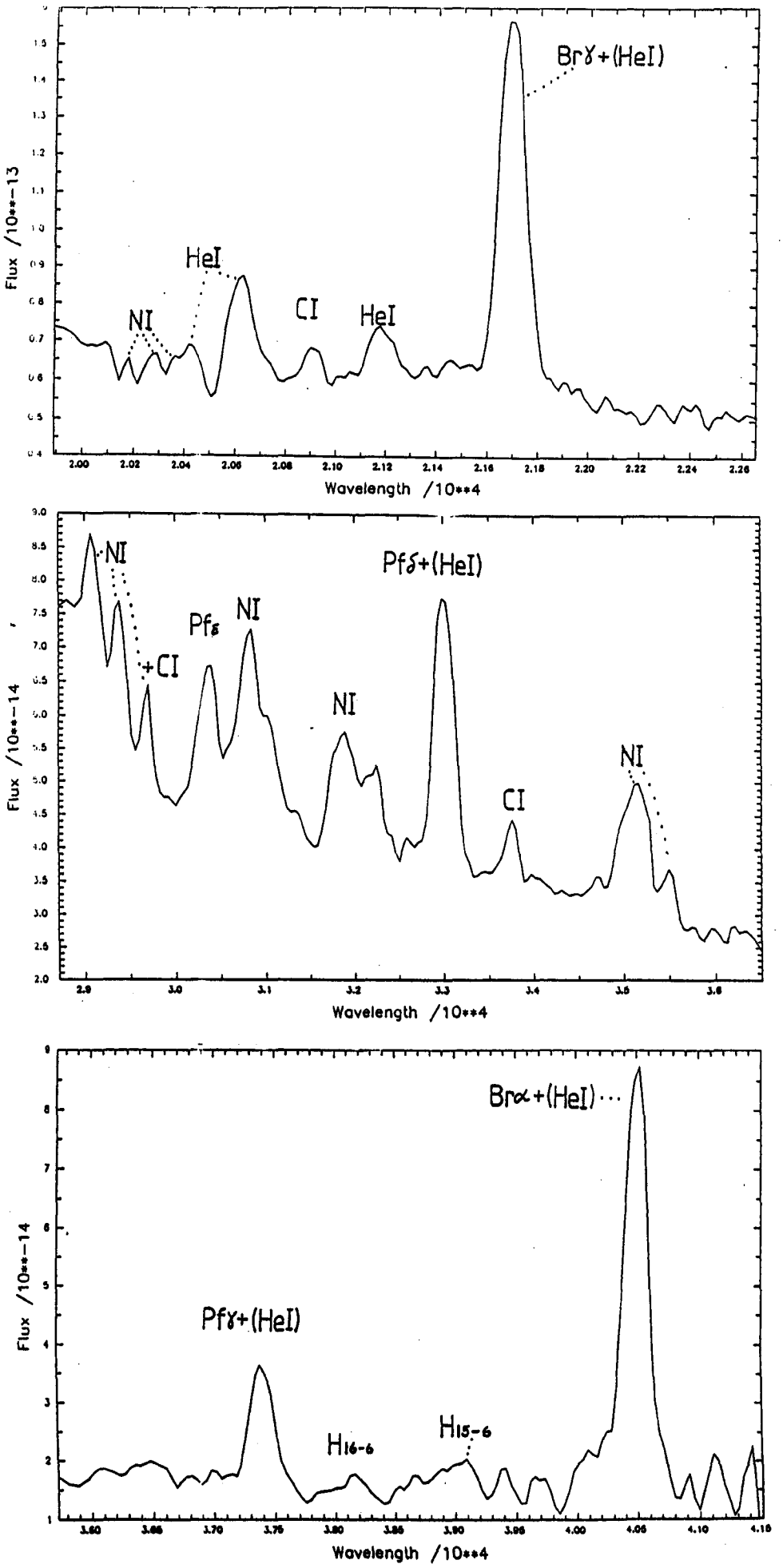

Figure 5.2a-c. The dereddened infrared spectra of PW Vul obtained from UKIRT on 1984 October 23.

Table 5.6

Line identifications in the spectra of PW Vul.

Observed λ(μm)	Identification
2.01771	NI
2.02831	NI
2.03612	NI
2.04170	HeI
2.06234	HeI
2.09024	CI
2.11702	HeI
2.16890	Brackett γ (+ HeI 7-4)
2.90628	NI
2.93640	NI
2.96653	CI + NI
3.03431	H 10-5
3.07950	(NI ?)
3.18745	NI
3.22510	?
3.29791	Pfund δ (+ HeI 9-5)
3.37322	CI
3.51381	NI
3.54895	NI
3.73724	Pfund γ (+ HeI 8-5)
3.81660	H 16-6
3.90954	H 15-6
4.05105	Brackett α (+ HeI 5-4)

(The H 14-6 line is to be located on the side of the Br α line).

this identification is suspect as the feature in GQ Mus was symmetric and not skew as is the 3.52μm formaldehyde feature in the pre-main sequence star HD97048 (Blades & Whittet, 1980). Although this feature in PW Vul was slightly antisymmetric this is likely to be due to contamination from another line and thus we reject H_2CO as the identification. This is further reinforced by the comments of Baas et al. (1983) who consider that such a molecule could not form in novae as the required grains (needed for condensation of the molecule) could not be sufficiently cold.

5.3.2 Use of Equivalent Widths to Find Temperature.

Before we go on to analyse the spectra we will briefly describe how the equivalent width of a hydrogen emission line can be used as a diagnosic to deduce the temperature of the region giving rise to that line. This is a procedure we will be using not only for the PW Vul spectra but also later for the spectra of RS Oph (Chapter 8).

As the equivalent width of a line is the width of the (hypothetical horizontal) continuum that contains the same total power as that contained in the line we have that

$$W_\nu = \int (f_{c+l} - f_c)/f_c \, d\nu \qquad (5.1)$$

where W_ν is the equivalent width expressed in frequency units, f_{c+l} is the flux in the continuum plus the emission line under consideration and f_c is the flux in the continuum only. If ε_ν is the volume emissivity, i.e. the power per unit volume per unit solid angle per unit frequency interval then

$$f_c = 4\pi\varepsilon_\nu V/(4\pi D^2) \qquad (5.2)$$

where V is the volume from where the line originated and D is the distance to the object. Since f_c is approximately independent of the frequency since the free-free continuum is flat, equation (5.1) becomes

$$W_\nu = D^2/(\varepsilon_\nu V) \times E_\nu V/(4\pi D^2) \tag{5.3}$$

where E_ν is the total energy emitted per unit volume per unit time in the line. We can approximate W_λ, the equivalent width in wavelength units, by

$$W_\lambda \simeq W_\nu \lambda^2/c \tag{5.4}$$

thus

$$W_\lambda = E_\nu \lambda^2/(4\pi\varepsilon_\nu c) \tag{5.5}$$

Thus for a line x

$$W_X = E_X \lambda_X^2/(4\pi\varepsilon_\nu(\lambda_X)c) \tag{5.6}$$

Equation (5.6) gives the equivalent width of an emission line relative to a nebular continuum provided that both arise in the same volume of the source. Now $E_\nu = N_n A_{nn'} h\nu_{nn'}$, where n' and n are the respective quantum numbers of the lower and the upper states, N_n is the number density of atoms in state n and $A_{nn'}$ is the Einstein probability coefficient for spontaneous transitions between the states n and n'. We also have that

$$\varepsilon_\nu = 8/3(2\pi/3)^{1/2} n_\nu Z e^6/(m^2 c^3)(m/(kT))^{1/2} N_i N_e \exp(-h\nu/(kT))(g(\nu,T) + f(\nu,T)) \tag{5.7}$$

(Lang 1974), where n_ν is the refractive index, N_e and N_i are the number densities of electrons and ions respectively, $g(\nu,T)$ is the free-free gaunt factor and $f(\nu,T)$ is the bound-free gaunt factor. All other symbols have their usual meanings. Thus the equivalent width can now be written as a function of temperature and density. We assume that n_ν and $f(\nu,T)$ are both equal to unity. This is not quite valid in the case of the bound-free gaunt factor, although it does not differ from unity by more than ~ 10% (Tucker, 1975). In any case at higher temperatures ($\geq 5 \times 10^4$K), the contribution from bound-free emission becomes progressively smaller (Lang, 1974) by comparison with the free-free emission, so the greatest error from this assumption will be at these temperatures. We estimate that the error in the temperature, deduced from the equivalent widths, due to the bound-free gaunt factor will be no more than ±5%. $g(\nu,T)$, the free-free gaunt factor was taken as given by Lang (1974).

The results of these calculations of the equivalent widths are displayed in graphical form of W_λ against temperature for the Paschen, Brackett and Pfund series of lines in Figs. 5.3. To use these graphs in the analysis of our spectra the equivalent width of a line is read using the 'EW' command in DIPSO and the corresponding temperature read off from Figs. 5.3.

5.3.3 The Continuum.

In this section we attempt to find the continuum on the UKIRT spectrum. Using the DIPSO procedure 'MERGE' we first combined all the four spectra. We then required a starting point by which to model the continuum. As mentioned previously, Kenyon & Wade (1986) interpreted the J, H and K colours from photometry obtained 16 days earlier than our spectrum by estimating that the H (1.65μm) magnitude could be explained if two-thirds of the radiation was emitted by a blackbody (presumably the pseudophotosphere) and the remaining third by optically thin material at

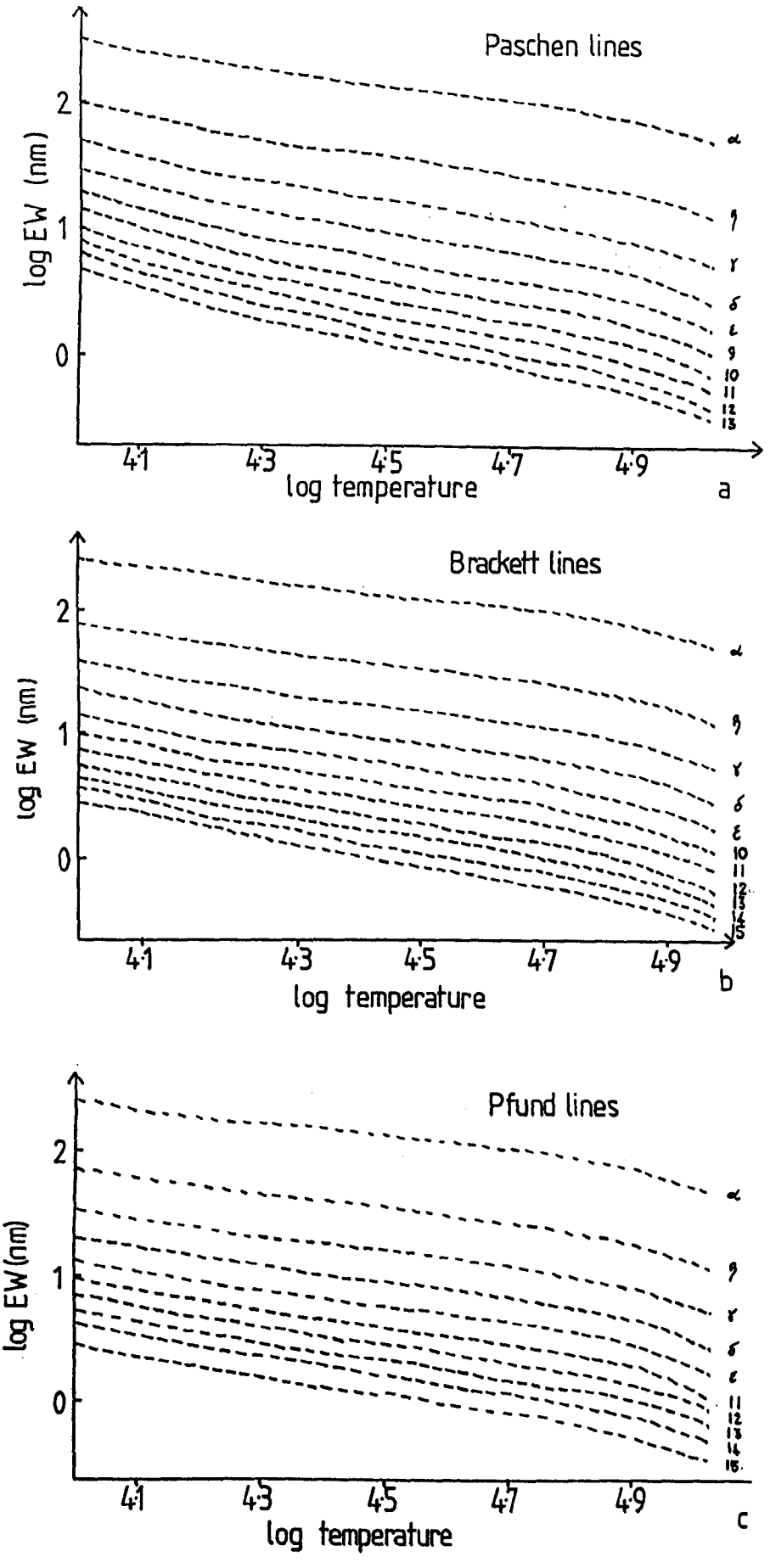

Figure 5.3a-c. These graphs show log temperature (in K) against log equivalent width (nm) for the first ten lines in the Paschen, Brackett and Pfund series of hydrogen.

7000 - 9000 K (i.e. a nebular continuum consisting of free-free and free-bound emission). They do admit however that this is just one of a range of possible solutions and indeed their value of 8000 K used for the pseudophotosphere does seem on the low side (see below).

The pseudophotospheric temperature T_* can be calculated from $T_* = T_0 10^{\Delta m/7.5}$ (Bath & Shaviv, 1976) where T_0 is a constant (15280 K) and Δm is the decline in magnitudes from visual maximum. So at the time that our spectra were obtained $T_* \sim 30000$ K (and a little less than this 16 days earlier), although the fact that the light curve was oscillating before (as well as after) maximum may affect this temperature. However as the greatest proportion of the infrared flux was deemed to originate from the pseudophotosphere we used this temperature as a first iteration in our attempts to fit the continuum to our spectra.

Using the routine 'NEBCONT' on DIPSO a nebular continuum consisting of free-free and free-bound emission can be calculated. However to use this routine we require the Hβ flux or the HeII 1640A flux at the time the spectra were obtained. The IUE spectrum of this object taken around the same time as our infrared spectra do not reveal the presence of a HeII 1640A line (M.A.J Snijders, private communication) which puts an upper limit on the temperature of the nebular continuum of ~ 10000 K. Unfortunately we do not have the flux in the Hβ line either but Kenyon & Wade (1986) do have such fluxes for three dates in 1985 (i.e. after the UKIRT spectrum was obtained). By extrapolation of these data we were able to estimate the Hβ flux on the required date (see Fig. 5.4) of $\log[f(H\beta)] = -10.44$ ergs $cm^{-2}s^{-1}$. (From Fig. 5.4 we can see that if the flux of this line declined uniformly this value is an accurate representation of the flux on October 23, however to allow for differing decline rates this value was allowed to vary between $-10.2 \rightarrow -10.7$ when fitting the data). We used an E(B-V) = 0.45 (Kenyon & Wade, 1986; Snijders, from the 1984 September 30 IUE spectrum, estimates E(B-V) =

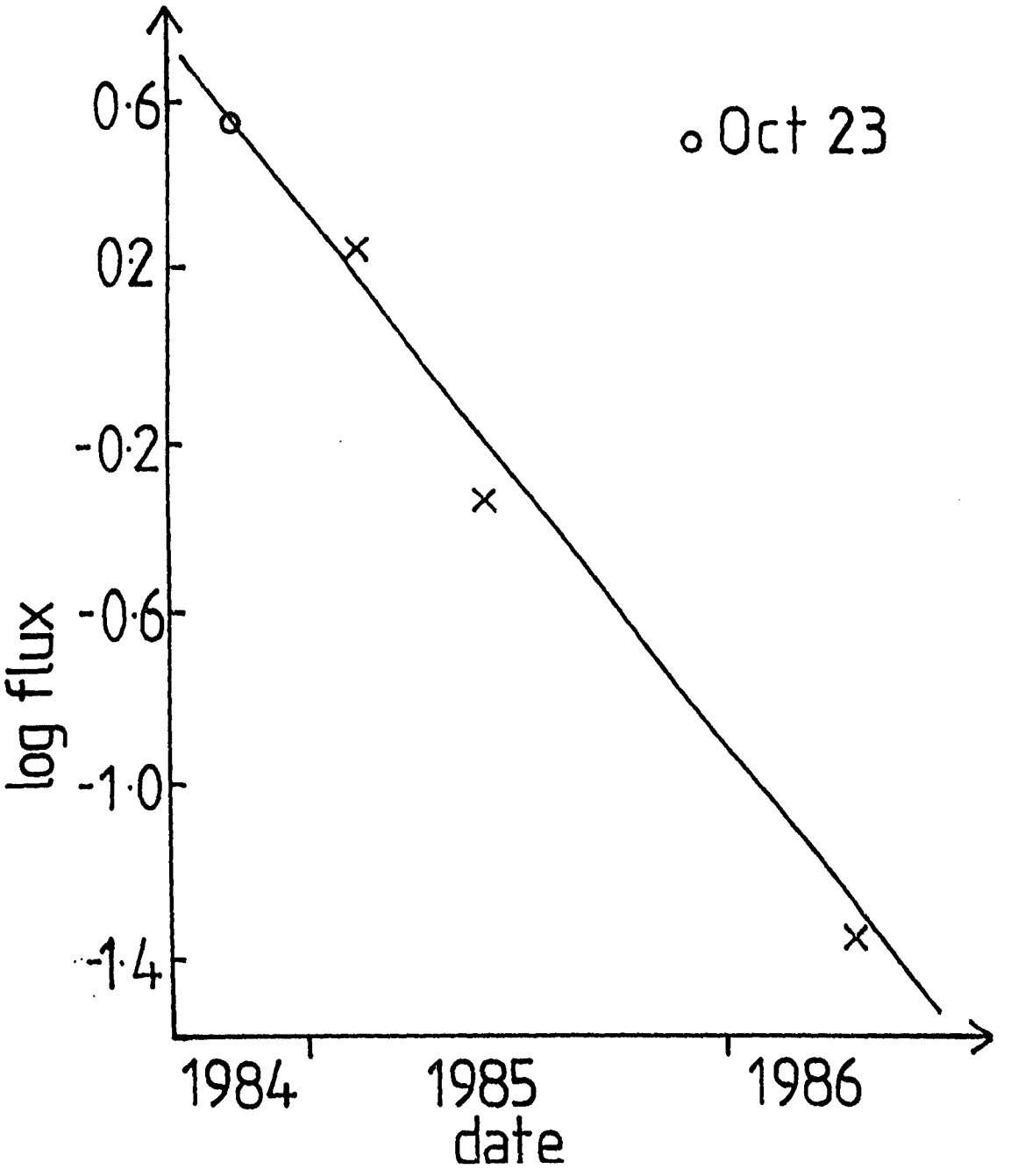

Figure 5.4. Log flux in the Hβ line plotted against time for PW Vul 1984. The o represents the extrapolated flux in this line on 1984 October 23, the date when our spectra were obtained. (Fluxes taken from Kenyon & Wade, 1986).

0.5±0.15) and an electron density of $10^6 cm^{-3}$ for the emitting region, although changes of this density by factors of one order of magnitude either way did not make any significant difference to the level of the nebular continuum. The temperature of the nebular continuum was varied between 6000 K - 10000 K to see which gave the best fit to the data, although a difference of a few thousand degrees had little effect on the level of the continuum. (Unfortunately there was no evidence of a bound-free discontinuity in the spectrum to help with fixing this temperature, but this was obviously due to the dominance of the pseudophotosphere at this point). The helium to hydrogen ratios used were in keeping with those found by Kenyon & Wade (1986), but as with the electron densities these had little effect on the continuum.

The best fit to the nova continuum was thus obtained by the addition of a nebular continuum at 9000 K, (and the above parameters) with a blackbody at 20000 K (the pseudophotosphere; see Fig. 5.5). Thus the calculated continuum of the stellar remnant was subtracted from the merged spectrum leaving only the lines and the nebular continuum.

5.3.4 Fitting the Hydrogen Lines.

The most prominent hydrogen lines i.e. Brα, Brγ and Pfγ, Pfδ, were fitted using the 'ELF' suite of commands in DIPSO with a Gaussian profile (Figs. 5.6 shows the fittings to these lines). The fitted profiles were then added back to the calculated nebular continuum of the spectra (Figs. 5.7 show the calculated line profiles plus the calculated nebular continuum) in order to find the equivalent widths of the fitted lines relative to their nebular continuum by use of the EW command in DIPSO. Thus the temperatures implied by these lines could be calculated using the procedure described in section 5.3.2.

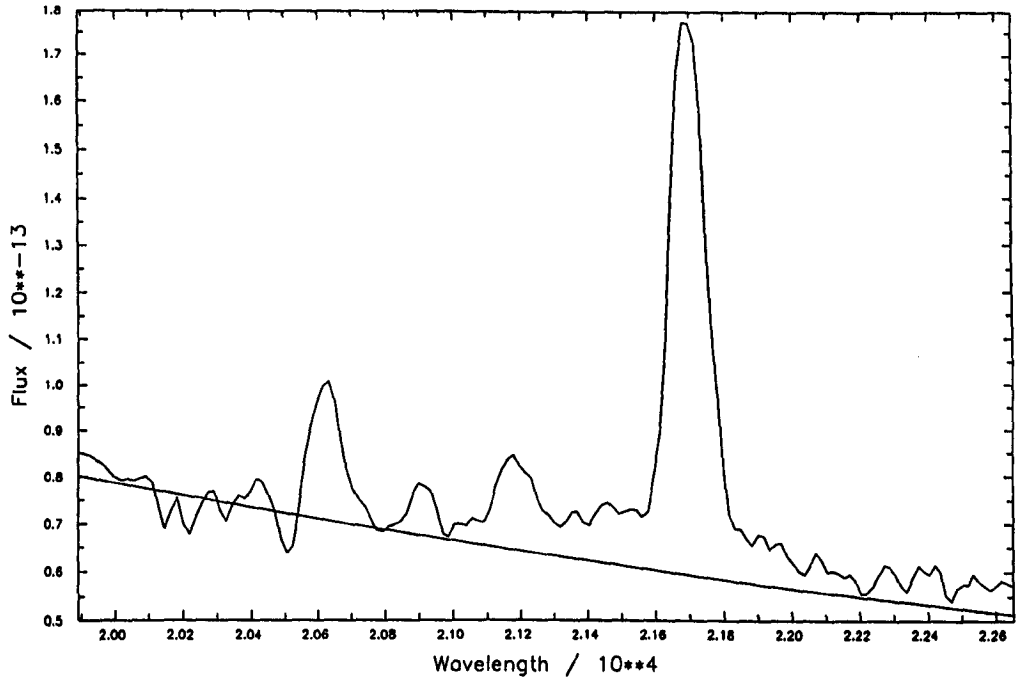
Flux / 10**-13
Wavelength / 10**4

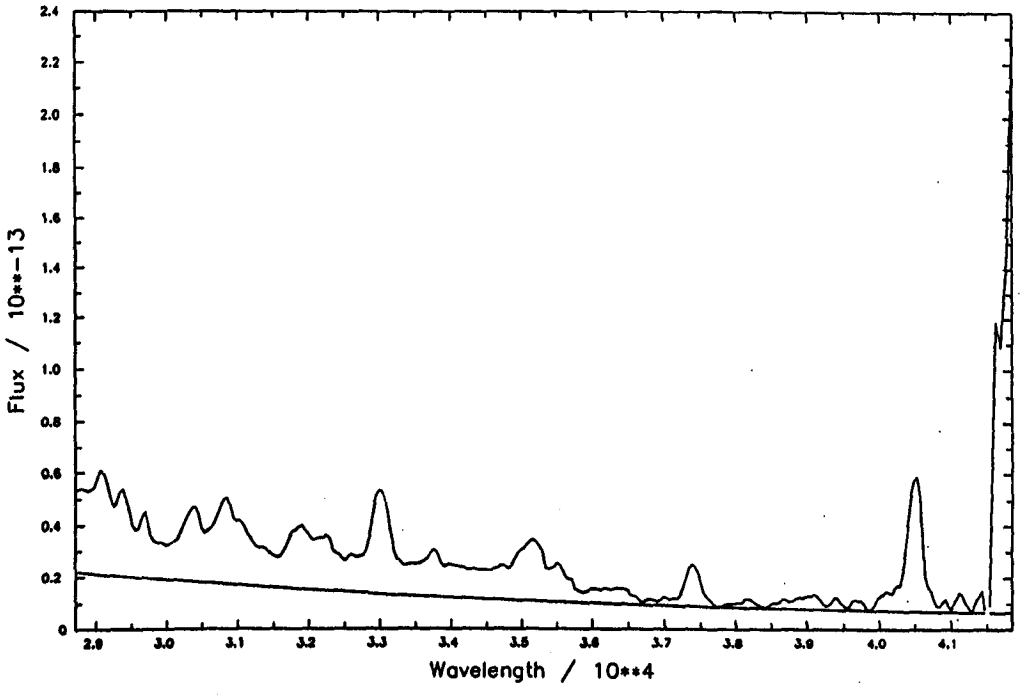
Flux / 10**-13
Wavelength / 10**4

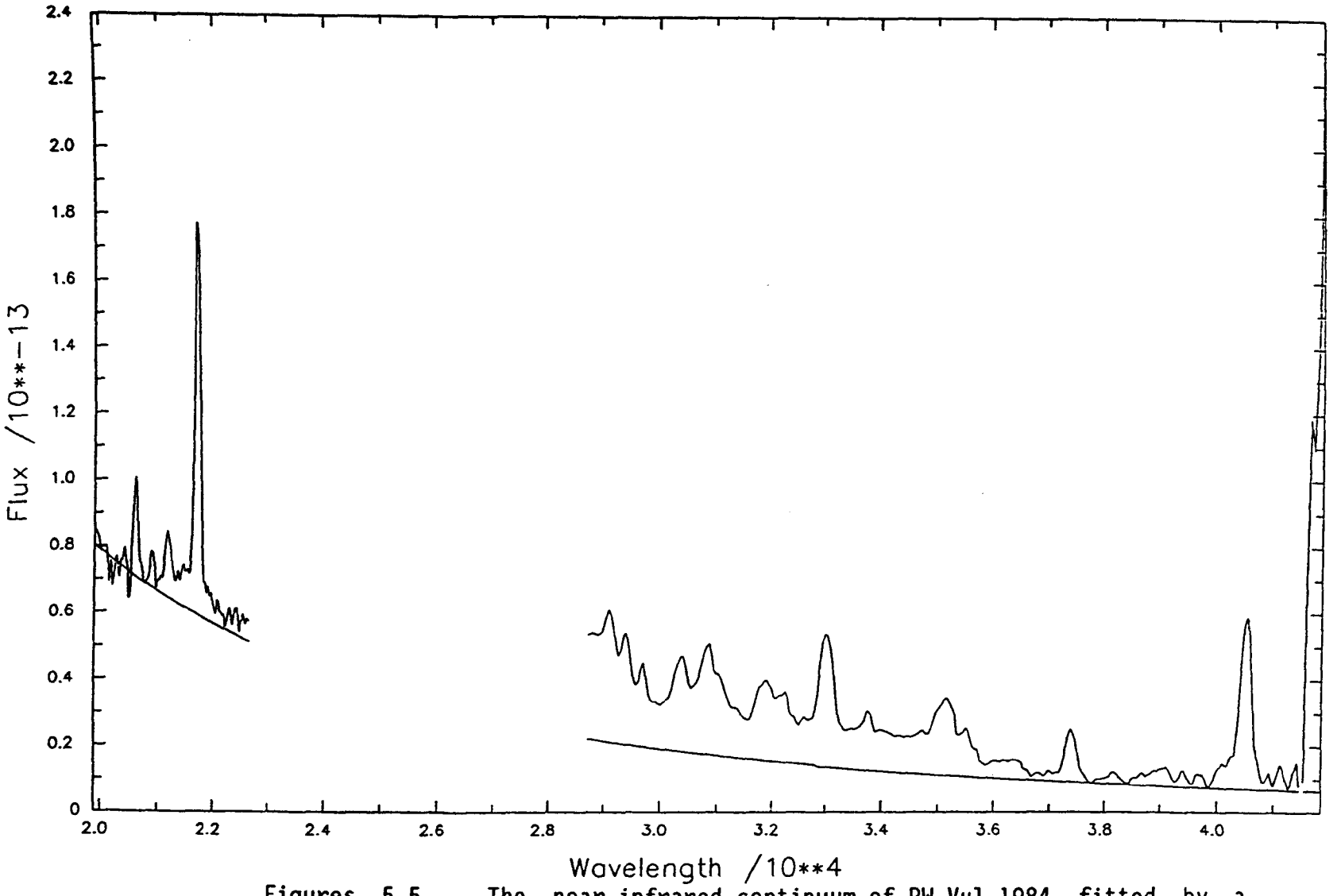

Figures 5.5. The near infrared continuum of PW Vul 1984 fitted by a blackbody continuum at 20000K plus a nebular continuum at 9000K (for details see text).

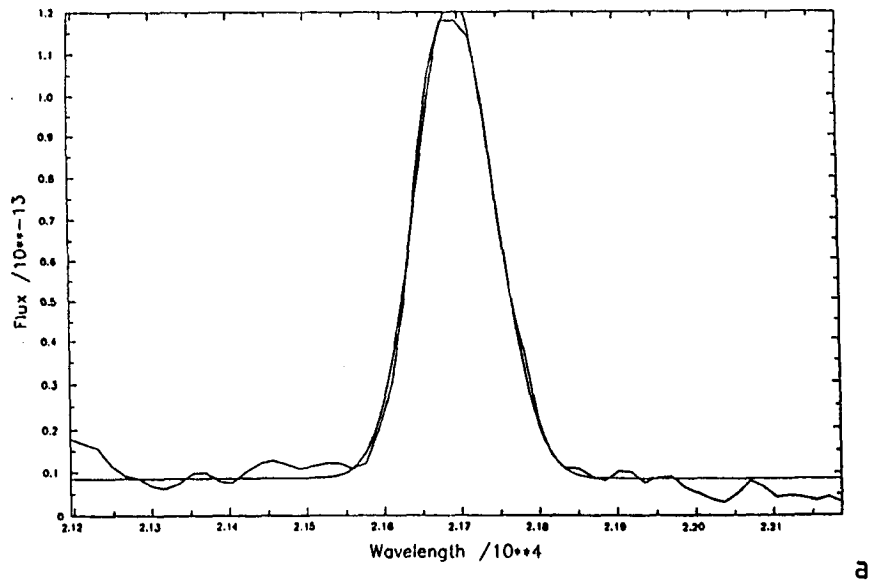

a

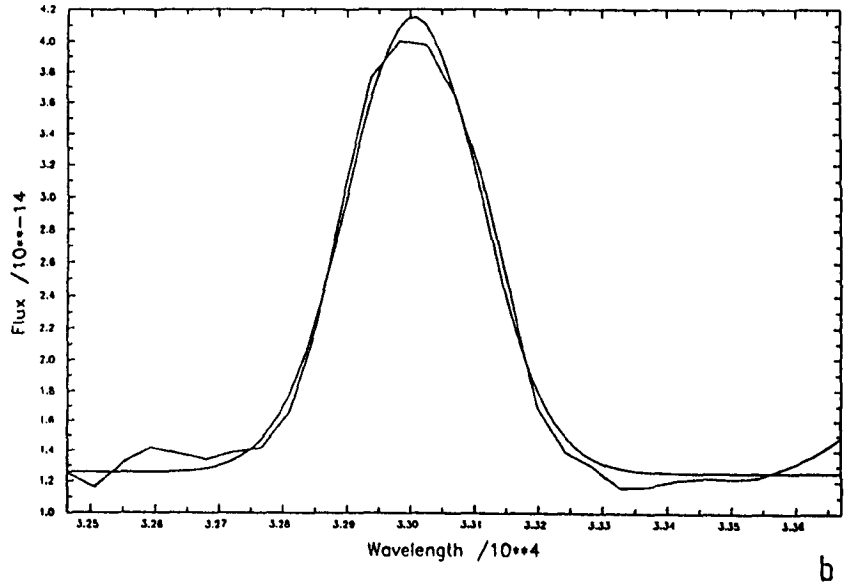

b

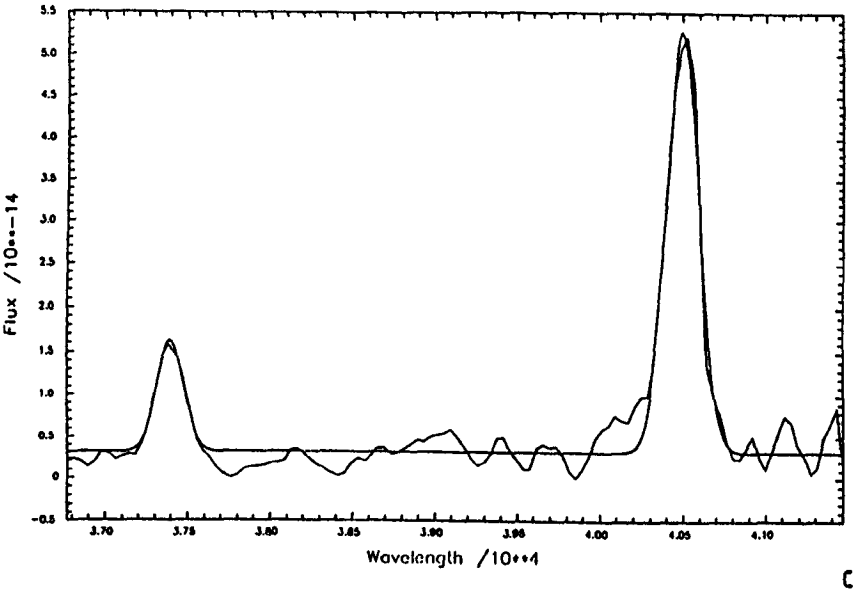

c

Figure 5.6a-c. ELF fittings to the Br α, γ and Pf γ, δ lines in the infrared spectra of PW Vul 1984. Note the the Br α and Pf γ lines appear to be a little underestimated in relation to the continuum by the ELF routine.

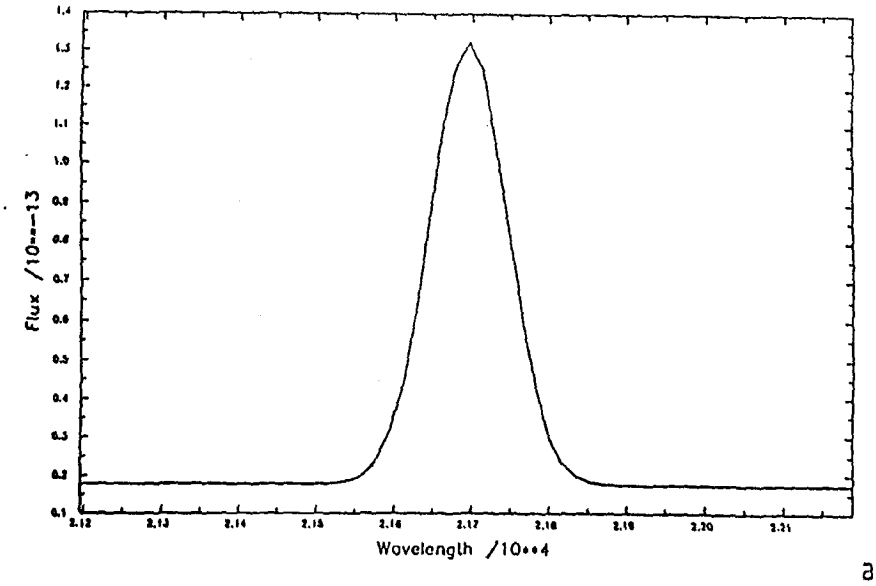

a

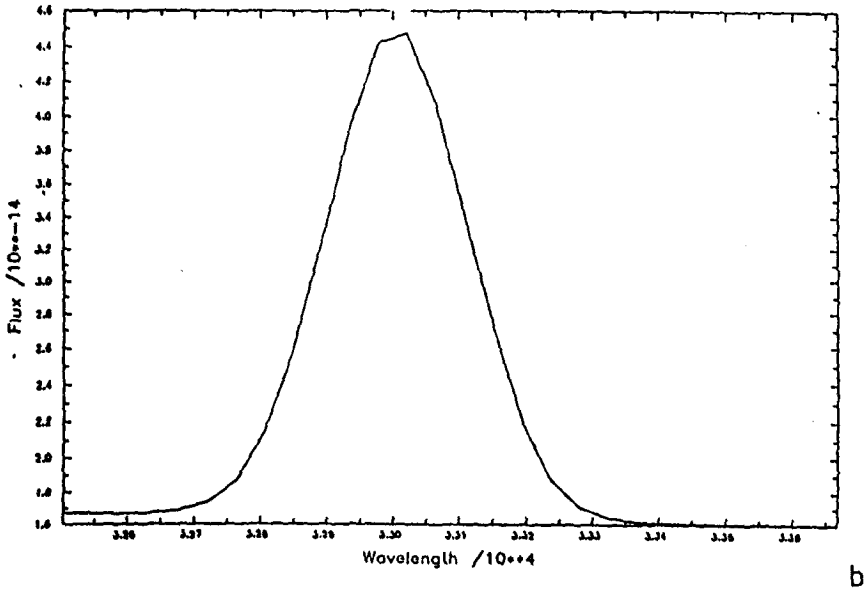

b

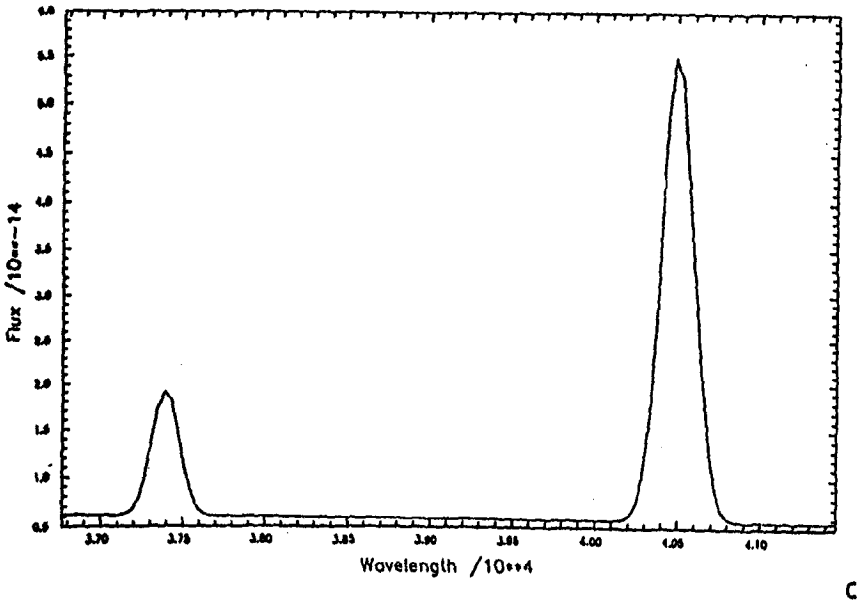

c

Figure 5.7a-c. The ELF fittings of the lines in figs 5.6 added back to the calculated nebular continuum.

5.3.5 Results and Discussion.

We can estimate the extent of the pseudophotosphere by measuring the amount that the blackbody representing it was shifted to fit the observed level of the continuum, if we assume a distance to the nova. The solid angle Ω subtended by the source will be given in terms of the source's radius R_* and its distance D as

$$\Omega = \pi R_*^2/D^2 \tag{5.8}$$

If we take a distance of 1.9 kpc (Noskova et al., 1985) we find that the pseudophotosphere is at a radius of $\sim 9.0 \times 10^{11}$cm on October 23. Bath & Shaviv (1976) link the pseudophotospheric temperature to its radius by the formula

$$R_* = 4.66 \times 10^{20} T_*^{-2} \alpha^{1/2} (M/M_0)^{1/2} \text{cm}. \tag{5.9}$$

where α is a constant ~ 1 and M is the mass of the nova system. If we take $M = 1M_0$, then $R \sim 1.2 \times 10^{12}$cm by this method so the distance to the nova can be confirmed at ~ 1.9 kpc. At this time the ejecta will have reached a distance $\sim 5.9 \times 10^{14}$cm (if $r_{ej} = v_{ej}t$ and $v_{ej} \sim 1000\text{km s}^{-1}$, the velocity of the principal spectrum; Kenyon & Wade, 1986), so these two results are consistent.

The equivalent widths of the hydrogen lines and the implied temperatures from these lines are tabulated in Table 5.7. If these lines were uncontaminated by any other lines then we would expect the temperature implied by the lines to be equal to that of the nebular continuum (9000 K) for the model to be self consistent. (There is an error of ~ ±500 K in the temperature due to uncertainities in measuring the equivalent widths using the DIPSO routine). As all the lines are contaminated with hydrogenic

Table 5.7

Temperatures in the H lines as deduced from their equivalent widths.

Line	EW (nm)	Temp (K)
Br α	192.6 (269.7)	15850 (8900)
Br γ	73.7	6700
Pf γ	41.7 (71.4)	8000 (5600)
Pf δ	42.5	7100

neutral helium the equivalent widths should give temperatures < 9000 K. This they do except for the temperature in the Brα line which is far too high. By examination of the fit to the Brα and Pfγ line it appears that the flux in the lines have been underestimated. We thus made a simple correction of extending the Gaussian fit of the lines down to the apparent observed continuum, which gave more consistent temperatures (those given in brackets in Table 5.7).

Measurement of the flux in the Brγ line and the HeI (2.058μm) line gives a lower limit to the ratio of the number density of helium to the number density of hydrogen by the use of

$$n(He^+)/n(H^+) > 0.14T_4^{-0.8}\exp(0.32/T_4)I(\text{HeI } 2.058\mu m)/I(B\gamma) \qquad (5.10)$$

(Krautter et al., 1984), where T_4 is the temperature implied by the lines in units of 10^4K and I is the observed intensity in the lines. If we use a temperature of 9000 K equation (5.10) gives n(HeI)/n(HI) > 0.07 which is consistent with the values of Kenyon & Wade (1986), and as they noted may be a little on the low side if this nova is considered to have a low speed class (Ferland, 1979).

5.4 Infrared Photometry.

5.4.1 The Light Curves.

We obtained infrared photometry from SAAO taken between 1984 August 9 - September 23 in the wavebands JHK and L (1.25μm, 1.65μm, 2.2μm and 3.5μm). These dereddened light curves are shown in Figs. 5.8 and the corresponding data in Table 5.8 (the data has been dereddened using E(B-V) = 0.45, Duerbeck et al., 1984; the errors on the data are typically ±0.02 mags for the JH & K bands and ±0.08 mags for the L band).

These curves all follow the same basic trend of oscillations

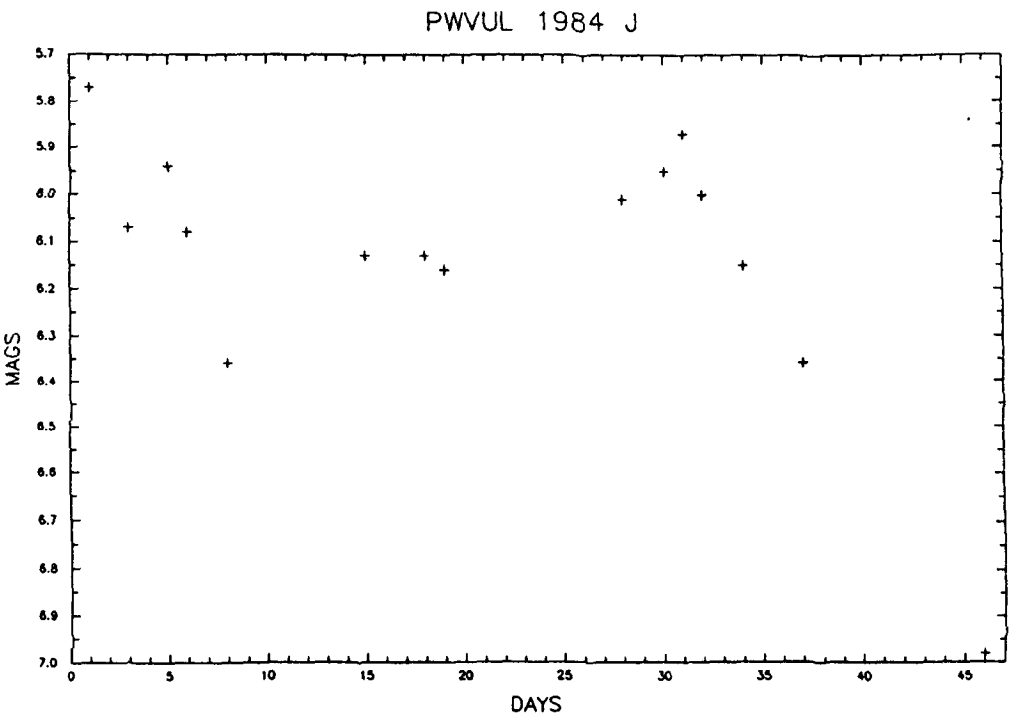
PWVUL 1984 J
MAGS
DAYS
5.7
5.8
5.9
6.0
6.1
6.2
6.3
6.4
6.5
6.6
6.7
6.8
6.9
7.0
0
5
10
15
20
25
30
35
40
45

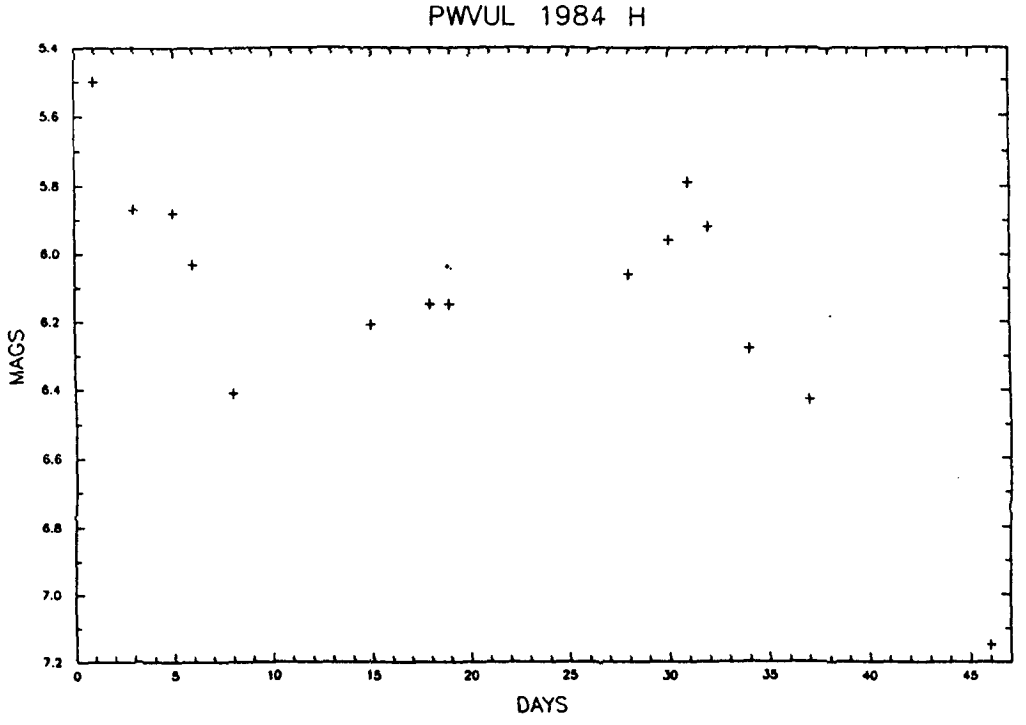
PWVUL 1984 H
MAGS
DAYS
5.4
5.6
5.8
6.0
6.2
6.4
6.6
6.8
7.0
7.2
0
5
10
15
20
25
30
35
40
45

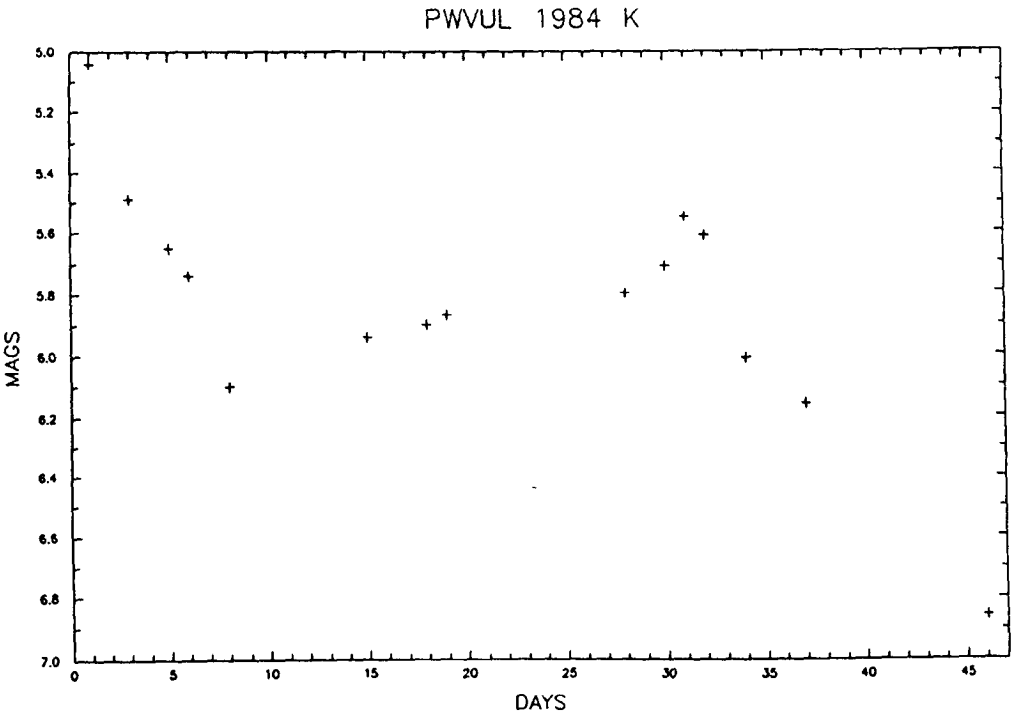

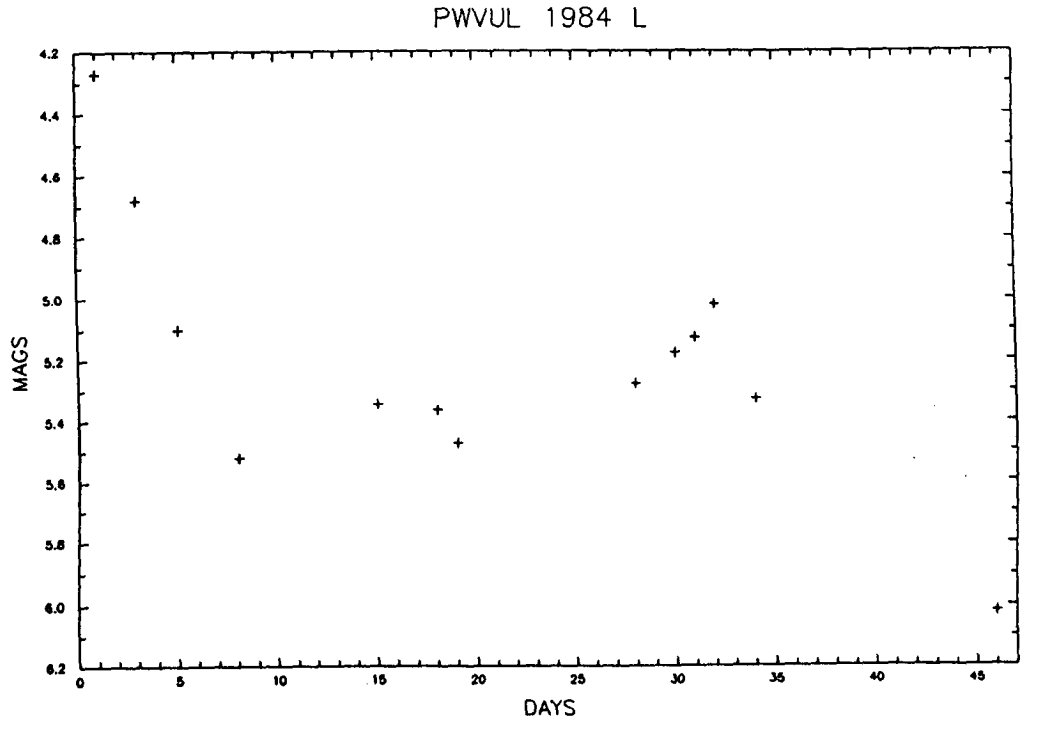

Figure 5.8a-d. The dereddened infrared light curves of PW Vul obtained from SAAO.

Table 5.8

Infrared Magnitudes of PW Vul.

Date(1984)	J	H	K	L
9 Aug	5.77	5.50	5.04	4.27
11	6.07	5.87	5.49	4.68
13	5.94	5.88	5.65	5.10
14	6.08	6.03	5.74	-
16	6.36	6.41	6.10	5.52
23	6.13	6.21	5.94	5.34
26	6.13	6.15	5.90	5.36
27	6.16	6.15	5.87	5.47
5 Sept	6.01	6.06	5.80	5.28
7	5.95	5.96	5.71	5.18
8	5.87	5.79	5.55	5.13
9	6.00	5.92	5.61	5.02
11	6.15	6.28	6.01	5.33
14	6.36	6.43	6.16	-
23	6.98	7.15	6.86	6.02

Data have been dereddened using $E(B-V) = 0.45$.

(typically of tenths of a magnitude) whilst overall slowly declining. These observations superimposed upon those of the visual light curve suggest that the infrared light curves mimic the behaviour of the nova in the visual (unfortunately we cannot be absolutely certain of this as the visual observations do not exactly overlap with those taken in the infrared; see Fig. 5.9). However if the behaviour of the visual and infrared light curves are indeed concurrent, this may be interpreted as a period of variable mass loss from the central system (c.f. Grotrian, 1937 and Bath & Shaviv, 1976).

There is no evidence in these infrared light curves to suggest the formation of a carbon based dust in the first two months after outburst and the emission is probably due to free-free and free-bound processes. Unfortunately due to the unknown form of the density variation in the nova ejecta we cannot quantitatively model this flux.

5.4.2 Dust.

Section 5.2.3 outlined the observations of Gehrz et al. (1985) which lead to these authors concluding that there was a dust excess on 1985 May 14.4. Table 5.9 lists their infrared fluxes together with those of Greenhouse (1985) and Kenyon & Wade (1986). (All these fluxes have been dereddened using E(B-V) = 0.45 and hence the errors in the infrared fluxes are calculated from the errors in E(B-V) as estimated by Snijders, private communication, as well as the systemetic errors in the magnitudes). Fig. 5.10 shows our attempt to fit a blackbody of 700 K (that temperature deduced by Gehrz et al., 1985) to the data of Gehrz et al. (1985). This is an extremely poor fit and indicates that any dust present cannot be conductive in nature i.e. there are no carbon based grains. Alternatively, silicate grains do not approximate to a blackbody but have a feature centered on 9.7μm and in the May data there does appear to be an excess around these wavelengths. The earlier data show no excesses but

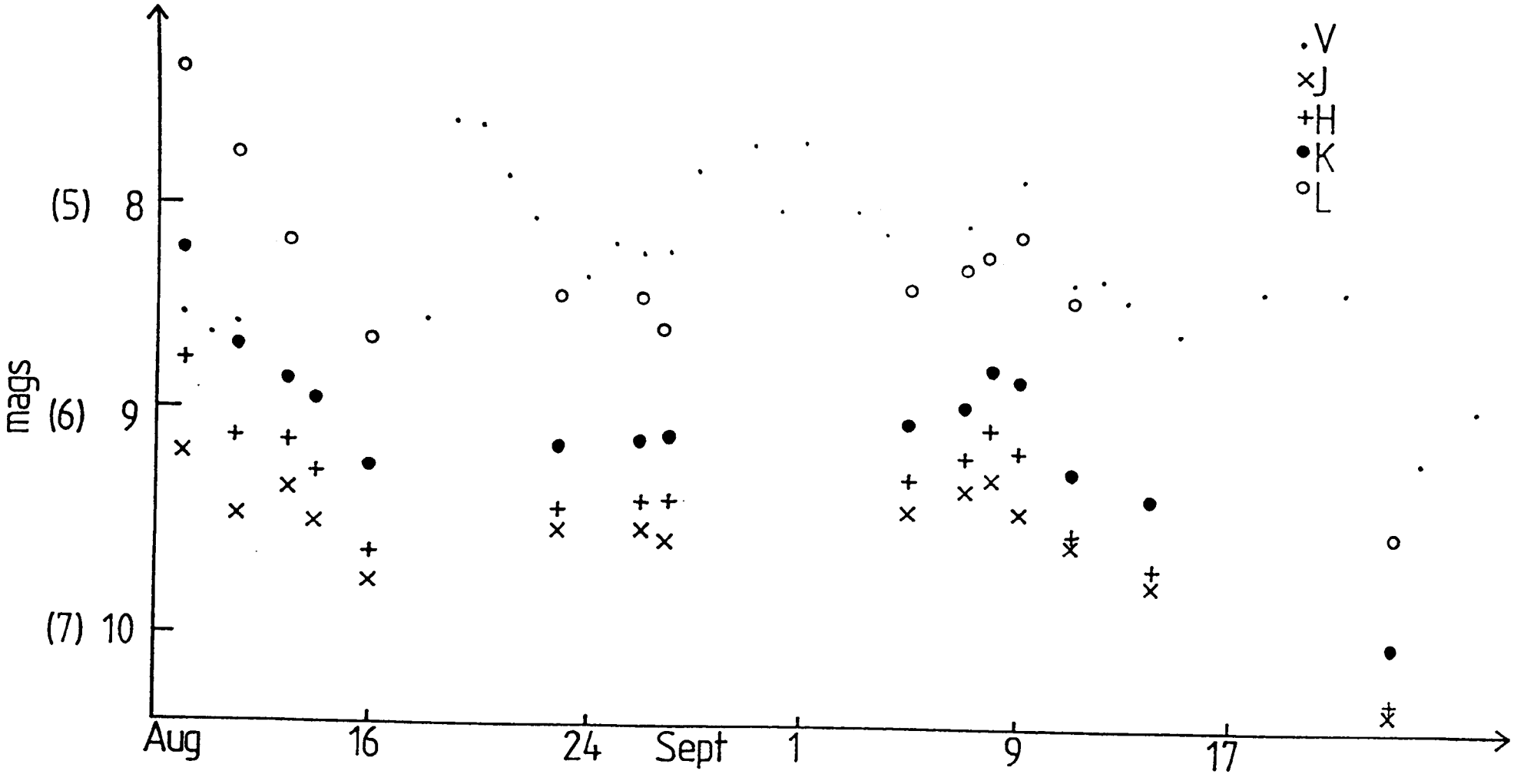

Figure 5.9. The visual and infrared light curves of PW Vul over the period 1984 August 9 - September 23. (Visual mags taken from Noskova et al., 1985, infrared mags obtained from SAAO). The ordinate gives the V magnitudes as unbracketted values, and the infrared magnitudes in brackets.

Table 5.9

Observed fluxes from PW Vul.

Date	J	H	K	L	4.9	8.7	N	11.4	
6/10/84	2.81	2.00	1.50	-	-	-	-	-	(1)
	±0.4	±0.2	±0.1						
28/04/85	0.07	0.05	0.07	0.13	-	-	-	-	(2)
	±0.01	±0.01	±0.01	±0.01					
14/05/85	-	-	0.07	0.12	0.14	0.34	0.31	0.26	(3)
			±0.01	±0.01	±0.02	±0.02	±0.02	±0.02	

This gives the dereddened flux in Jy from PW Vul in various wavebands. (1) Kenyon & Wade, 1986 (2) Greenhouse, 1985 (3) Gehrz et al., 1985

Table 5.10

Model fluxes.

Date	J	H	K	L	4.9	8.7	N	11.4
6-7/10/84	0.20	0.29	0.39	-	-	-	-	-
28/04/85	0.05	0.07	0.10	0.12	-	-	-	-
14/05/85	-	-	0.09	0.12	0.13	0.15	0.16	0.16

This shows the fluxes in Jy calculated from the free-free plus free-bound emission model.

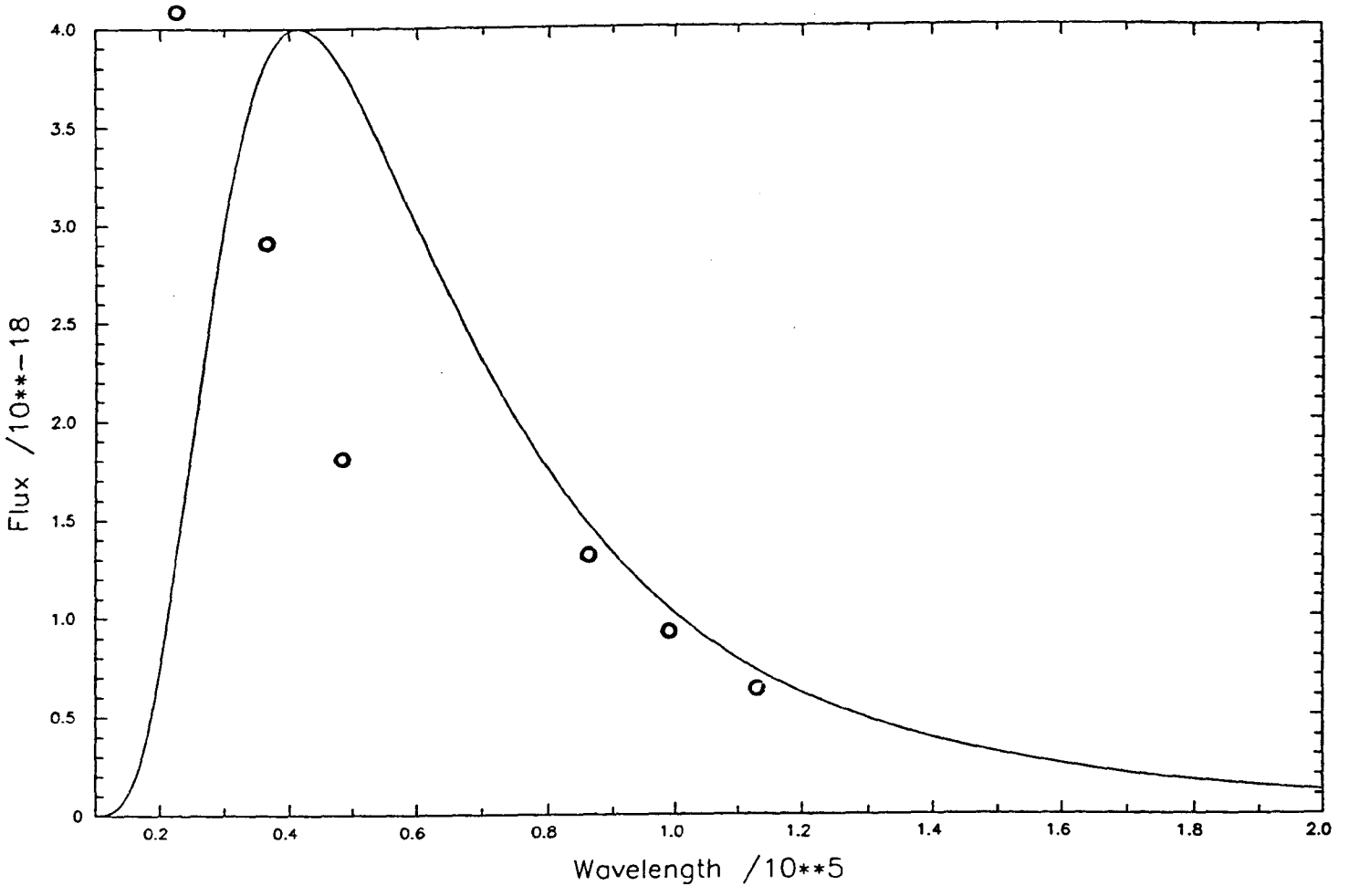

Figure 5.10. Best attempt to fit a blackbody at 700K through the (dereddened) infrared data of Gehrz et al. (1985) for PW Vul 1984 obtained 285 days after its outburst.

these data only extend to the L waveband so if silicate dust had formed it would not be expected to manifest itself at the shorter wavelengths.

We attempt to model the infrared fluxes by use of a free-free and free-bound emission model (explained fully in Chapter 6; here we include bound-free emission by adding the appropriate Gaunt factor $f(\nu,T) = 1$). The distance is set at 1.9 kpc (Noskova et al., 1985) and the number density of electrons is consistent with the value found when fitting the nebular continuum for our 1984 October spectra; again for consistency the nebular temperature is set at 9000 K. Table 5.10 gives the calculated fluxes for this model. The calculated fluxes for 1984 October 6 are too low, but this is to be expected as the pseudophotosphere contributes most of the flux at these wavelengths at this time. However as the pseudophotosphere shrinks and its temperature becomes even higher its effect on the infrared fluxes will be progressively less. This is seen in the fact that on 1985 April 28.4 the fluxes from the model fit quite well to those observed. (This is reinforced when we try to fit the excess flux at the J, H and K bands on October 6 to a blackbody of temperature $T_* \sim$ 20000 K, see section 5.3.3, they do fit satisfactorily).

The fits for the 1985 May data reveal that there is indeed an excess at the longer wavelengths. By subtraction of the model fits to those observed we can deduce how much flux is supposedly due to the silicate feature.

Fig. 5.11 shows attempts to fit this 'silicate' feature with models of silicate grains of differing radius. (This is based on a Mie theory program by A. Evans, private communication, that assumes the grain material is olivine and uses its optical properties as tabulated in Draine & Lee, 1984. However it must be noted that the interstellar silicate that Draine & Lee describe may not have the same optical properties as the silicate found in novae). Values for the absorption efficiency Q_{abs} of the grains were thus calculated. As flux $\propto Q_{abs}B_\lambda$ in the optically thin case,

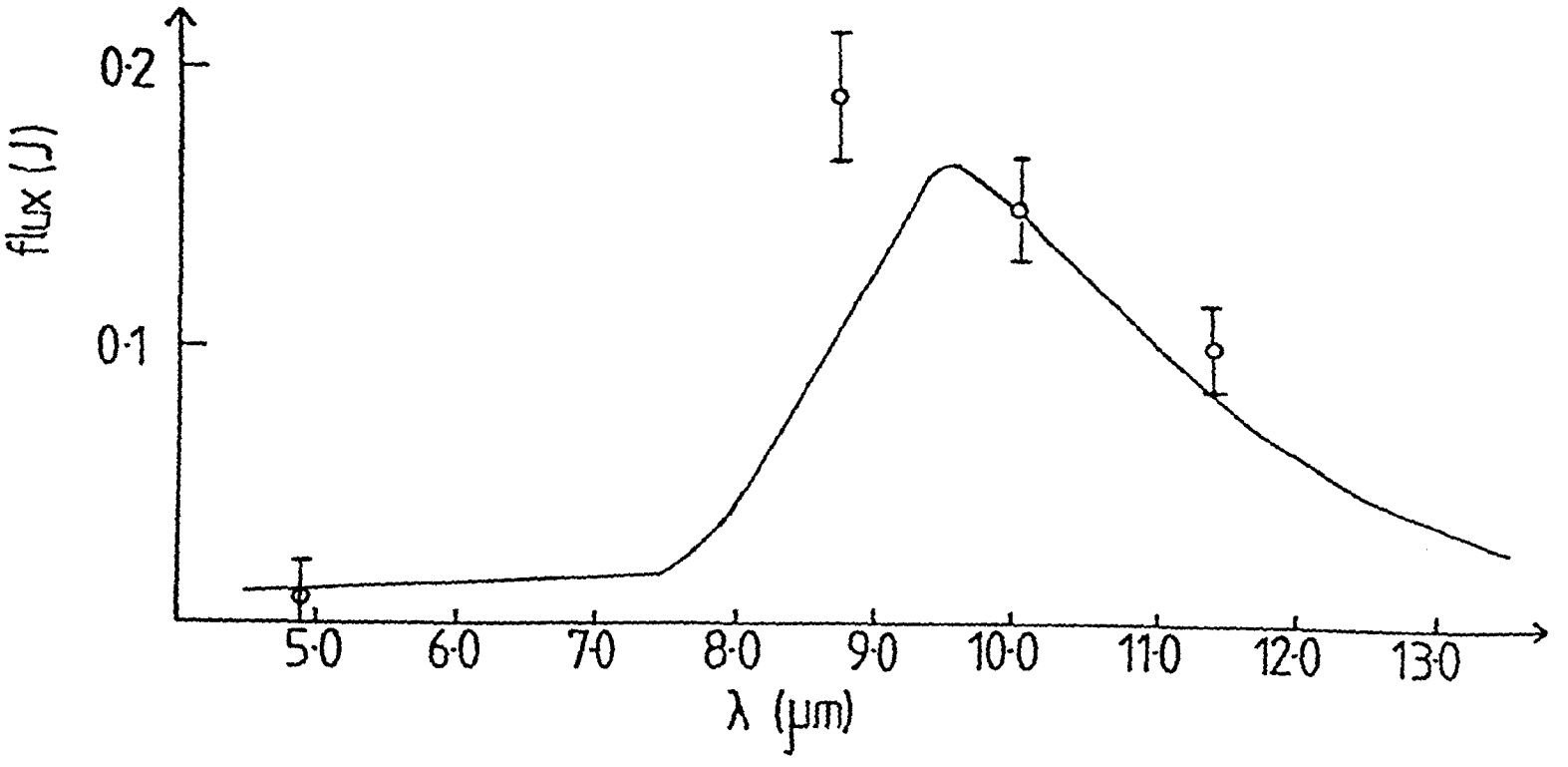

Figure 5.11. Attempt to fit the deduced 'silicate' feature of PW Vul 1984 (i.e. the deduced free-free continuum has been removed from the infrared photometry) for grains of size 0.5μm and at a temperature of 700K. (Various combinations of silicate grain size and temperature between 0.1-0.7μm and 600-800K, all result within a few percent to the fit shown).

where B_λ is the Planck function (e.g. Wickramasinghe, 1967) we can normalise the fluxes that we have obtained with $Q_{abs}B_\lambda$ (we have normalized at the N point) so obtaining the fits. For silicate grains of radius 0.1 - 0.7μm and temperatures between 600 - 800 K the fits are very good at the 4.9μm, N and 11.4μm points but they underestimate the 8.7μm point, even when taking into account the errors on the observed flux at this point. This could be due to a number of factors. Firstly the continuum due to free-free and bound-free emission may have been miscalculated, but for the flux at 8.7μm to be lower than the flux at the N point it would require the source to be optically thick at these wavelengths and this is somewhat unlikely when considering the length of time after outburst that these data were obtained. Using equation (4.2) this would imply an electron density $n_e > 4 \times 10^9$ cm^{-3} which is clearly unrealistic 285 days after outburst. Also we calculated the flux from silicate grains of one particular radius whilst in reality we will have grains with a distribution of radii in the nova ejecta. Lastly the 8.7μm point could be contaminated by line emission although no obvious elements have lines around this wavelength.

All this appears to suggest that some type of silicate was present in the ejecta of PW Vul some 10 months after outburst. Silicate condensation is thought to occur at a condensation temperature $T_c \sim 1000$ K (Yamamoto & Hasegawa, 1977). It is likely therefore that the silicate in PW Vul was produced earlier than 10 months, as we estimated its temperature at this time to be ~ 600 - 800 K. This is further reinforced by the silicate nucleation model for novae of Yamamoto & Nishida (1977; see Chapter 2) who consider that almost all the monomers of condensable elements condense into grains within several tens of days after the nova explosion. (This is of course dependent on the number density of condensible monomers). More recently Henning & Svatos (1986) considered the formation of silicate grains in circumstellar environments and suggested that, whilst small silicate grains (~ 0.01μm) could condense at ~ 1000 K, grains bigger than

these could only begin to condense at lower temperatures (500 K being the lowest temperature that they considered viable). They also suggested that the feature seen at ~ 10μm in M giants was a result of smaller grains formed at the higher condensation temperatures that had coagulated to form bigger grains. Thus it is not possible to state categorically that the silicate apparently present in PW Vul did form before its first observation at ~ 10 months, especially when taking into account the number density variability within the shell during the first few months after outburst (see section 5.4.1). (It is interesting to note that Bode & Evans, in press, remark that silicates seem to form when the white dwarf is a NeMg white dwarf rather than a CO white dwarf. Such a detection of silicate dust in PW Vul could thus indicate the nature of its primary).

5.5 Conclusion.

PW Vul is seen to be a rather interesting nova in both its photometric and spectrometric behaviour, neither of which can give a conclusive indication of the nova's speed class. The infrared spectra which we obtained from UKIRT some three months after outburst suggested that the remnant could be modelled at that phase using a nebular continuum at 9000 K combined with a pseudophotospheric continuum at 20000 K. These spectra contained hydrogen, neutral helium and (possibly) neutral metal lines, suggesting that the nova had not entered into the nebular stage which is characterized by many forbidden lines and lines of high excitation (see Chapter 1).

This nova appears to have formed a silicate based dust ~ 10 months after outburst, but there is no evidence of any carbon based dust. Of the other novae observed to produce a silicate type dust, nova V1307 Aql 1982 exhibited the 10μm silicate feature at ~ 37 days after outburst (Williams & Longmore, 1982) whilst the infrared spectrum of nova Vul 1984 no. 2 contained this feature ~ 230 days after outburst (Gehrz et al, 1985b); both

were fast novae. So PW Vul does not share any characteristics with the other two silicate producing novae (both of which exhibited overabundances of neon, whereas PW Vul, as far as we know, did not; see Kenyon & Wade, 1986).

Now that we have a few novae exhibiting silicate type dust it would be most useful to observe any subsequent novae at both the 2-4μm & 8-13μm windows so we can distinguish between the types of dust produced.

CHAPTER 6

FREE-FREE MODELLING OF NOVA GQ MUSCAE 1983

6.1 Introduction

The nova GQ Muscae 1983 (see Chapters 2 and 4) was an unusual nova in that, theoretically its speed class ~ 0.06 mag day^{-1} was such that dust production was expected on the models of Gallagher (1977) and Bode & Evans (1982a) but no detections of dust were made (Whitelock et al., 1984; Krautter et al., 1984). (See however Chapter 3 for a possible explanation of this phenomenon). Instead the form of its infrared light curve suggested that this flux was being produced by thermal bremsstralung emission from a hot gas (Krautter et al., 1985). Hence we attempt to model the infrared photometry obtained at SAAO over a period 27 days - 310 days after outburst, and also our AO data from IRAS taken from day 140 - day 225 with a free-free model.

6.2 The Model

A model is constructed in which we have the central nova remnant, consisting of a white dwarf primary and a late type main sequence secondary, surrounded by a hot gas at electron temperature T_e, which is moving at a velocity v_{ej} (which we take to be a constant during the period of interest). In Fig. 6.1 this configuration is shown where R_1 and R represent the inner and outer edges of the gas shell respectively.

For convenience the gas shell was divided into three regions (see Fig. 6.1). An observer would then see radiation coming from the inner edge of region 3, the outer edge of region 2 and the outer edges of region 1 that were facing her. The observer would also see radiation coming from the secondary, but not from the white dwarf which is obviously a negligible emitter at these wavelengths. In the model we make the assumptions of

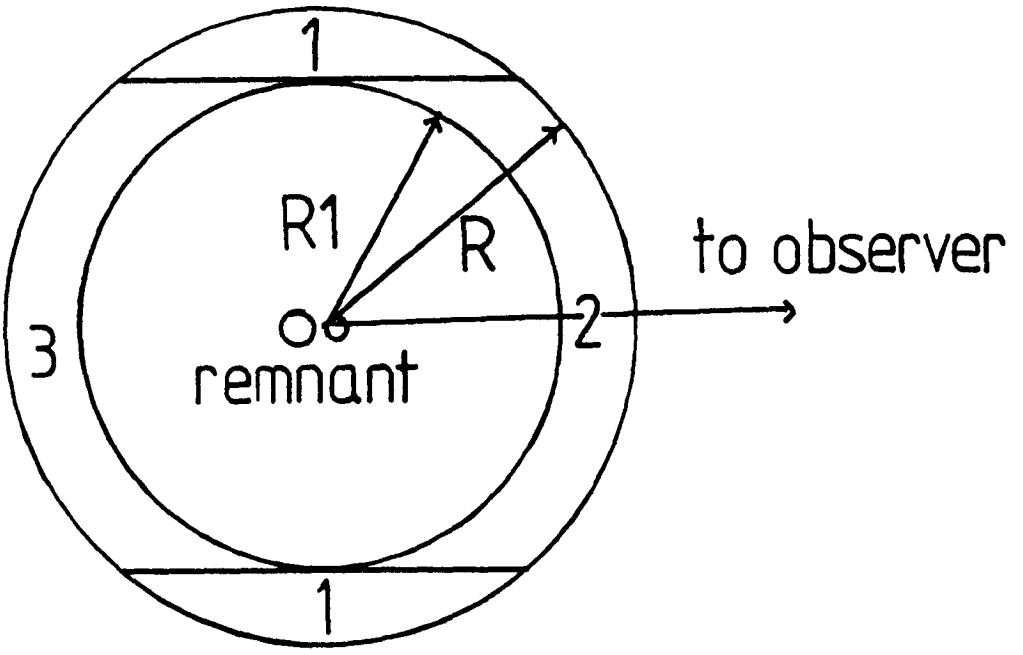

Figure 6.1. Representation of the nova remnant GQ Mus 1983. An expanding hot gas shell surrounds the white dwarf primary and the main sequence secondary (see text for details).

ignoring any free-bound radiation (Whitelock et al., 1984 find no Pfund discontinuity in their spectra which would suggest that free-bound emission is indeed negligible and that $T_e \geq 10^4 K$), treating the density distribution as an inverse square law and we treat the secondary as a point source. However all optical depth effects have been included. We begin with the equation of transfer i.e.

$$I_\nu = I_\nu(0)e^{-\tau} + \int S_\nu e^{-\tau} d\tau \tag{6.1}$$

where I_ν is the intensity at frequency ν, τ is the optical depth and the source function $S_\nu = \varepsilon_\nu/\kappa_\nu$, the ratio of the emission coefficient to the absorption coefficient. Applying equation (6.1) to the regions in the gas shell we obtain

$$I_\nu = \int S_\nu e^{-\tau_1} d\tau \quad \text{for region 1.} \tag{6.2a}$$

$$I_\nu = \int S_\nu e^{-\tau_2} d\tau + \int S_\nu e^{-\tau_2-\tau_3} d\tau + B_\nu e^{-\tau_S} \quad \text{fo r region 2.} \tag{6.2b}$$

where B_ν is the Planck function which approximates the secondary, τ_S is the optical depth in the line of sight through the shell (ie. the optical depth affecting the star as we treat it as a point source) and τ_1, τ_2, τ_3 are the optical depths for regions 1, 2 and 3 respectively.

$$I_\nu = \int S_\nu e^{-\tau_3} d\tau \quad \text{for region 3.} \tag{6.2c}$$

(Later on it will be useful to rewrite these equations in terms of distance into the shell by substituting $d\tau = \kappa_\nu\, dx$). We define angles θ and ϕ such that θ is the angle between the observer and the radius R, and ϕ is the angle between the observer and an arbitrary radius r into the gas shell (see Fig. 6.2).

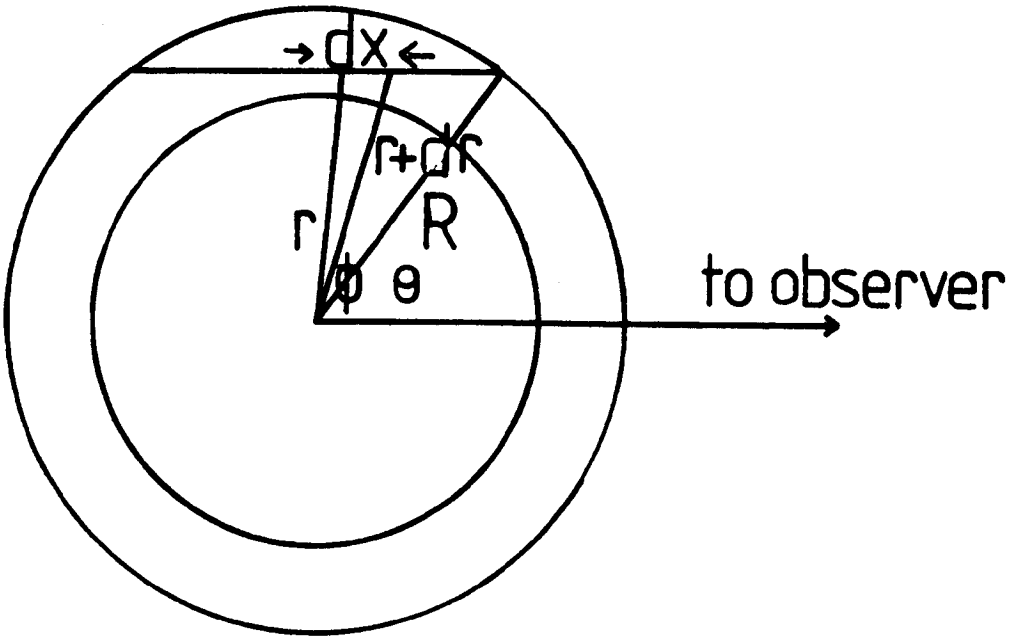

Figure 6.2. The geometry of the situation in the nova remnant of GQ Mus 1983 (see text for details).

We wish to find dx in terms of these angles (see Fig. 6.3).

We have

$$dx^2 = r^2 d\phi^2 + dr^2 \tag{6.3}$$

and, as $r = R\sin\theta/\sin\phi$, equation (6.3) becomes

$$dx = R \sin\theta \, d\phi/\sin^2\phi \tag{6.4}$$

For region 3 as we only observe flux from its inner edge, following a similar procedure to that above, we obtain

$$dx = R_1 \sin\theta \, d\phi/\sin^2\phi \tag{6.5}$$

Now

$$f_\nu = \int I_\nu \, d\Omega \tag{6.6}$$

where f_ν is flux and $d\Omega$ is the solid angle dA/D^2, the ratio of an element of area to the square of the distance from the source to the observer. The emitting area will be in the form of circular annuli (see Fig. 6.4) and are calculated as

$$dA = 2\pi R \sin\theta \cos\theta \, R \, d\theta \qquad \text{for regions 1 and 2.} \tag{6.7a}$$

$$dA = 2\pi R_1 \sin\theta \cos\theta \, R_1 d\theta \qquad \text{for region 3.} \tag{6.7b}$$

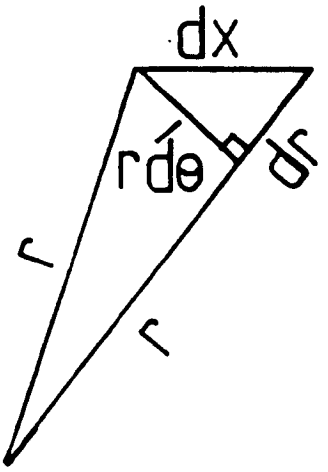

Figure 6.3

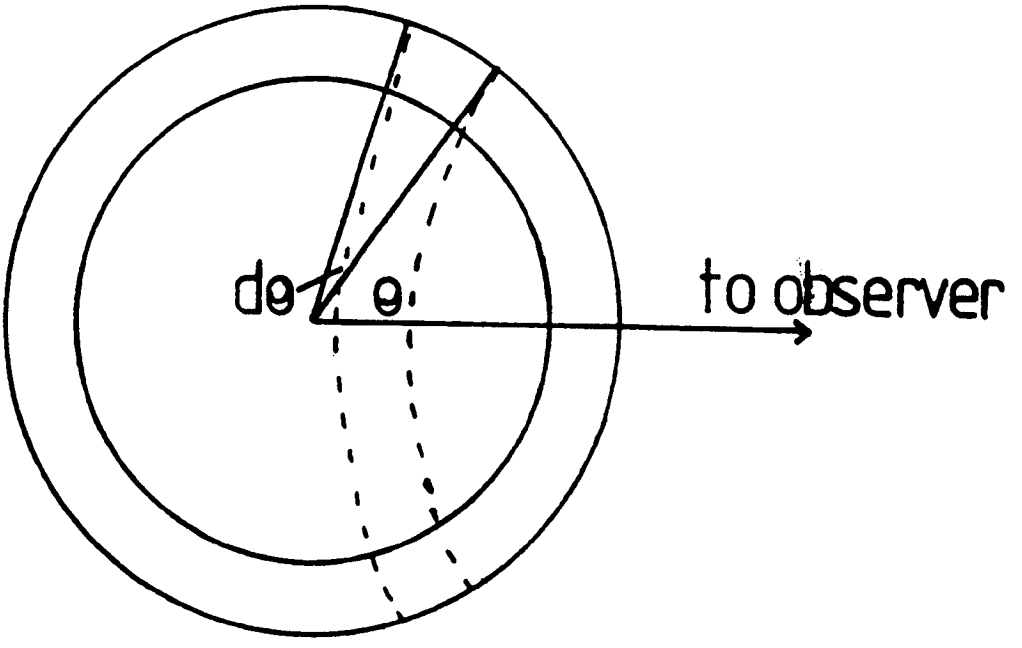

Figure 6.4. Representation of an emitting circular annulus in the nova remnant of GQ Mus 1983 (see text for details).

Hence equations (6.2) become

$$f_1 = \iint \varepsilon(\theta,\phi)e^{-\tau`(\theta,\phi)}R \sin\theta \, d\phi/\sin^2\phi \times 2\pi R^2 \sin\theta \cos\theta \, d\theta/D^2 \tag{6.8a}$$

$$f_2 = \iint \varepsilon(\theta,\phi)e^{-\tau`(\theta,\phi)} R\sin\theta \, d\phi/\sin^2\phi \times 2\pi R^2 \sin\theta \cos\theta \, d\theta/D^2$$
$$-\iint \varepsilon(\theta,\phi)e^{-\tau`(\theta,\phi)-\tau`(\theta,\phi)} \times R_1 \sin\theta \, d\phi/\sin^2\phi \; 2\pi R_1^2 \sin\theta \cos\theta \, d\theta/D^2$$
$$+\int B_\nu e^{-\tau} 2\pi R^2 \sin\theta \cos\theta \, d\theta/D^2 \tag{6.8b}$$

$$f_3 = -\iint \varepsilon(\theta,\phi)e^{-\tau`(\theta,\phi)} R_1 \sin\theta \, d\theta/\sin^2\phi \times 2\pi R_1^2 \sin\theta \cos\theta \, d\theta/D^2 \tag{6.8c}$$

where $\tau(\theta,\phi)$, the optical depth will be calculated explicity below.

Now ε_ν is given by (Lang, 1974):

$$\varepsilon_\nu = 8/3(2\pi/3)^{1/2} n_\nu (Z/m)^2 e^6/c^3 (m/kT)^{1/2} N_i N_e g(\nu,T)\exp(-h\nu/kT) \tag{6.9}$$

where n_ν is the refractive index of the plasma, Z is the charge of the ions, $g(\nu,T)$ is the gaunt factor (all of these we assume are equal to unity), N_e is the electron number density, N_i the ion number density. All other symbols have their usual meanings.

We now calculate the optical depth in each of the regions. We know that

$$\tau = \int \kappa_\nu \, dx \tag{6.10}$$

where $\kappa_\nu = \varepsilon_\nu/B_\nu$. So for all regions the general form of τ the optical depth will be

$$\tau = C \int r^{-4} \, dx \tag{6.11}$$

Here

$$C = 8/3(2\pi m/(3kT))^{1/2}(e^2/c)^3/m^2 \exp(-h\nu/kT)$$
$$(n_i)_o(n_e)_o((r_e)_o(r_i)_o)^2/B_\nu$$

(6.12)

remembering that we have assumed $N_i = (n_i)_o(r/(r_i)_o)^{-2}$ and $N_e = (n_e)_o(r/(r_e)_o)^{-2}$. Substituting for dx for the different regions equation (6.11) becomes

$$\tau = C/(2R^3\sin^3\theta)[(\phi - \sin 2\phi/2) - (\theta - \sin 2\theta/2)]$$

(6.13a)

for regions 1 and 2, and for region 3

$$\tau = C/(2R_1^3\sin^3\theta)[(\theta - \sin 2\theta/2) - (\phi - \sin 2\phi/2)]$$

(6.13b)

As we are treating the star as a point source equation (6.10) becomes

$$\tau = C\int_R^{R1} x^{-4}\, dx$$

(6.14)

which reduces to

$$\tau = C/3(1/R1^3 - 1/R^3) = \tau_*$$

(6.15)

Finally we need to determine the limits to put on equations (6.8). Referring to the Figs. 6.5 - 6.6 we have:

For region 1 ϕ varies between the

angle ABC and the angle ACD hence

$$\theta < \phi < \pi - \theta \qquad (6.16a)$$

For region 2 ϕ varies between the angle ABC and the angle ABD hence

$$\theta < \phi < \arcsin(R\sin\theta/R1) \qquad (6.16b)$$

For region 3 ϕ varies between the angle ABC and the angle ABD hence

$$\theta < \phi < \arcsin(R1\sin\theta/R) \qquad (6.16c)$$

For region 1 θ varies between the angle ABC and the angle $\pi/2$ hence

$$\arcsin(R1/R) < \theta < \pi/2 \qquad (6.17a)$$

For region 2 θ varies between the angle 0 and the angle ABC hence

$$0 < \theta < \arcsin(R1/R) \qquad (6.17b)$$

For region 3 θ varies between the angle $\pi/2$ and π hence

$$\pi/2 < \theta < \pi \qquad (6.17c)$$

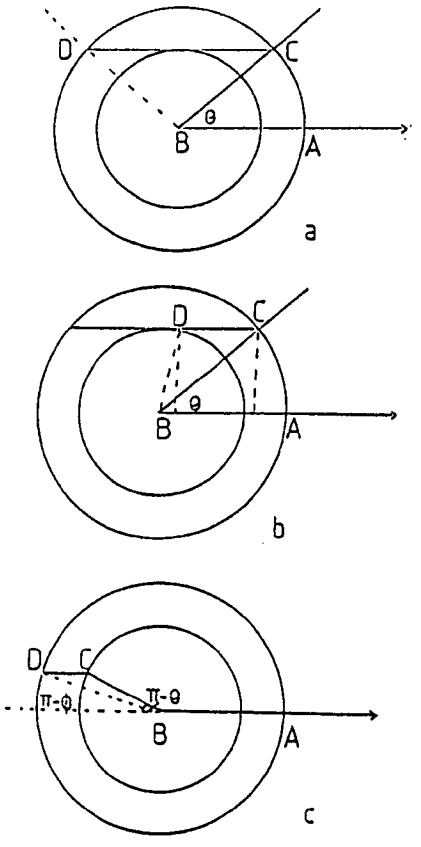

Figure 6.5a-c. Limits on the angle θ in each of the three regions of the gas shell around GQ Mus 1983.

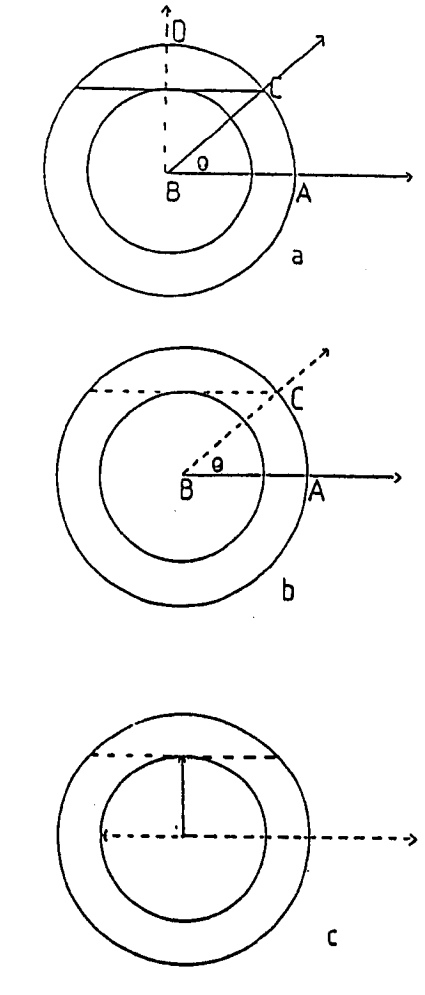

Figure 6.6a-c. Limits on the angle ϕ in each of the three regions of the gas shell around GQ Mus 1983.

Now that we have the forms of the optical depths and the limits for each region equations (6.8) can be written out in full. An ALGOL program was written to solve these equations and hence to calculate the observed infrared flux from the free-free emitting gas shell and the main sequence star. The NAG routine D01DAA was used to solve the double integral.

6.3 An Analytical Check of the Model

The equations (6.8) can be solved analytically if we ignore any optical depth effects in the gas shell. In such circumstances we will expect the analytical answers to be ≥ the answers obtained when these effects are included. For each region of the gas shell we can calculate the flux at any infrared wavelength and at any time by reversing the order of integration and thus determing the equivalents limits when this reversal has been made. Thus for region 1 we will have

$$f_1 = \int_{\arcsin \frac{R_1}{R}}^{\pi/2} \int_{\theta}^{\pi-\theta} \text{ECONST}\ 2\pi R^3/D^2 (\sin\phi/\sin\theta)^2 \cos\theta\, d\theta d\phi \tag{6.18}$$

where

$$\text{ECONST} = CB_\nu/R^4 \tag{6.19}$$

Plotting the limits out on the θ, ϕ plane gives (see Fig. 6.7a)

$$f_1 = \int_{\arcsin y}^{\pi/2} \int_{\arcsin y}^{\phi} A\,(\sin\phi/\sin\theta)^2 \cos\theta\, d\phi d\theta + \int_{\pi/2}^{\pi-\arcsin y} \int_{\arcsin y}^{\pi-\phi} A\,(\sin\phi/\sin\theta)^2 \cos\theta\, d\phi d\theta \tag{6.20}$$

where $A = \text{ECONST} \times 2\pi R^3/D^2$ and $y = R_1/R$.

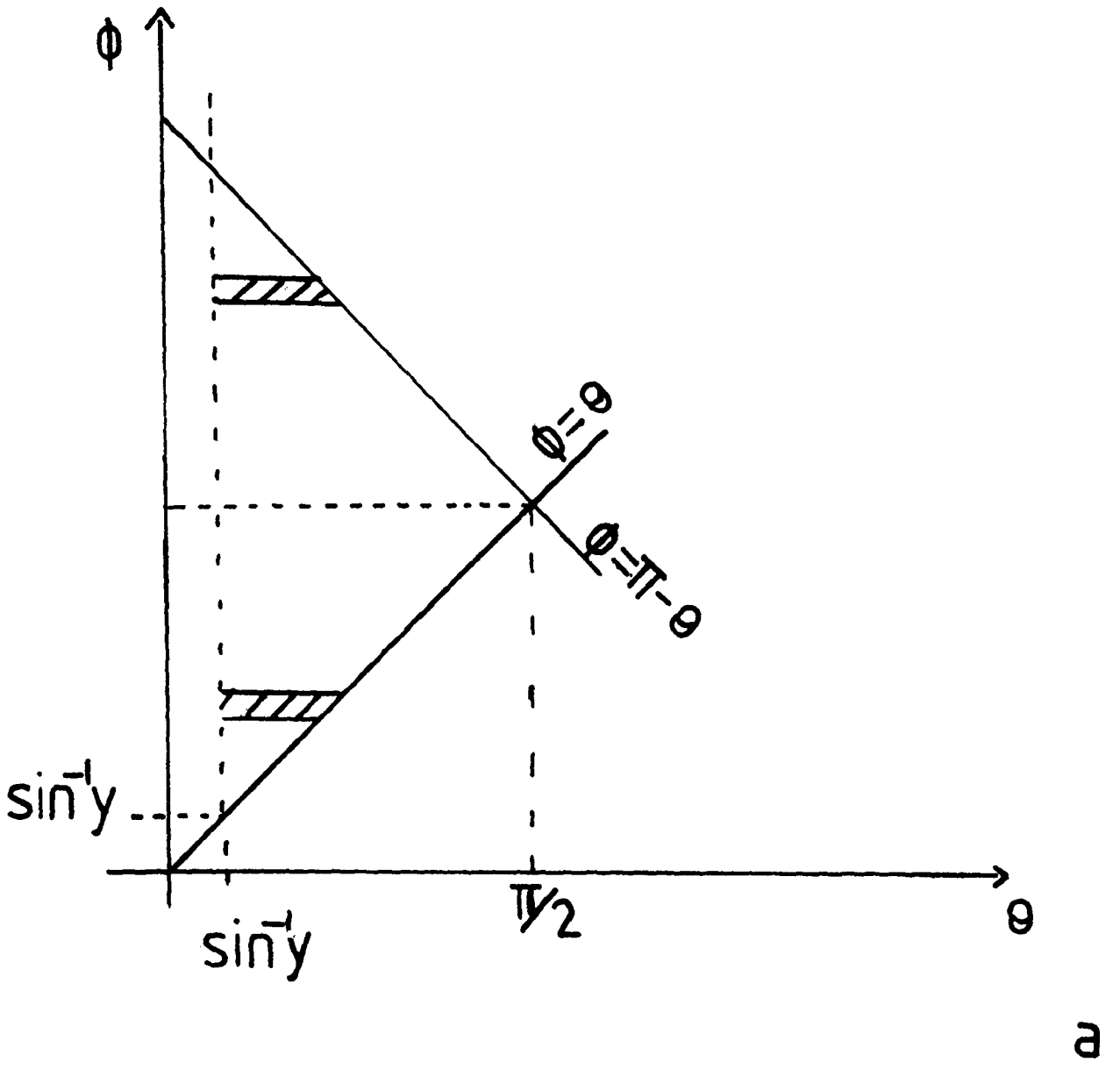

Figure 6.7a. Plotting the limits on the θ, ϕ plane for region (1) in an optically thin gas.

When integrated equation (6.20) gives

$$f_1 = A(\pi/(2y) - \arcsin y/y + 2\cos(\arcsin y)) \tag{6.21}$$

For region 2 we have

$$f_2 = A \int_0^{\arcsin y} \int_{\theta}^{\arcsin(\frac{\sin\theta}{y})} (\sin\phi/\sin\theta)^2 \cos\theta \, d\theta d\phi \tag{6.22}$$

Plotting the limits out on the θ, ϕ plane gives (see Fig. 6.7b)

$$f_2 = A \int_0^{\arcsin y} \int_{\arcsin(y\sin\phi)}^{\phi} (\sin\phi/\sin\theta)^2 \cos\theta \, d\theta d\phi + A \int_{\arcsin y}^{\pi/2} \int_{\arcsin(y\sin\phi)}^{\arcsin y} (\sin\phi/\sin\theta)^2 \cos\theta \, d\theta d\phi \tag{6.23}$$

Integrating equation (6.23) gives

$$f_2 = A(\cos(\arcsin y)/2 + 1/y - 1 - \pi/(4y) + \arcsin y/(2y)) \tag{6.24}$$

As we have neglected optical depth effects the radiation coming from the inner edge of region 3 through region 2 will be of the same form as that coming from region 3 itself. This should be equal to that from region 2 so we calculate

$$f_3 = -B \int_{\frac{\pi}{2}}^{\pi} \int_{\theta}^{\pi - \arcsin(y\sin\theta)} (\sin\phi/\sin\theta)^2 \cos\theta \, d\theta d\phi \tag{6.25}$$

where $B = A/y$. Thus plotting these limits on the θ, ϕ plane gives (see fig 6.7c)

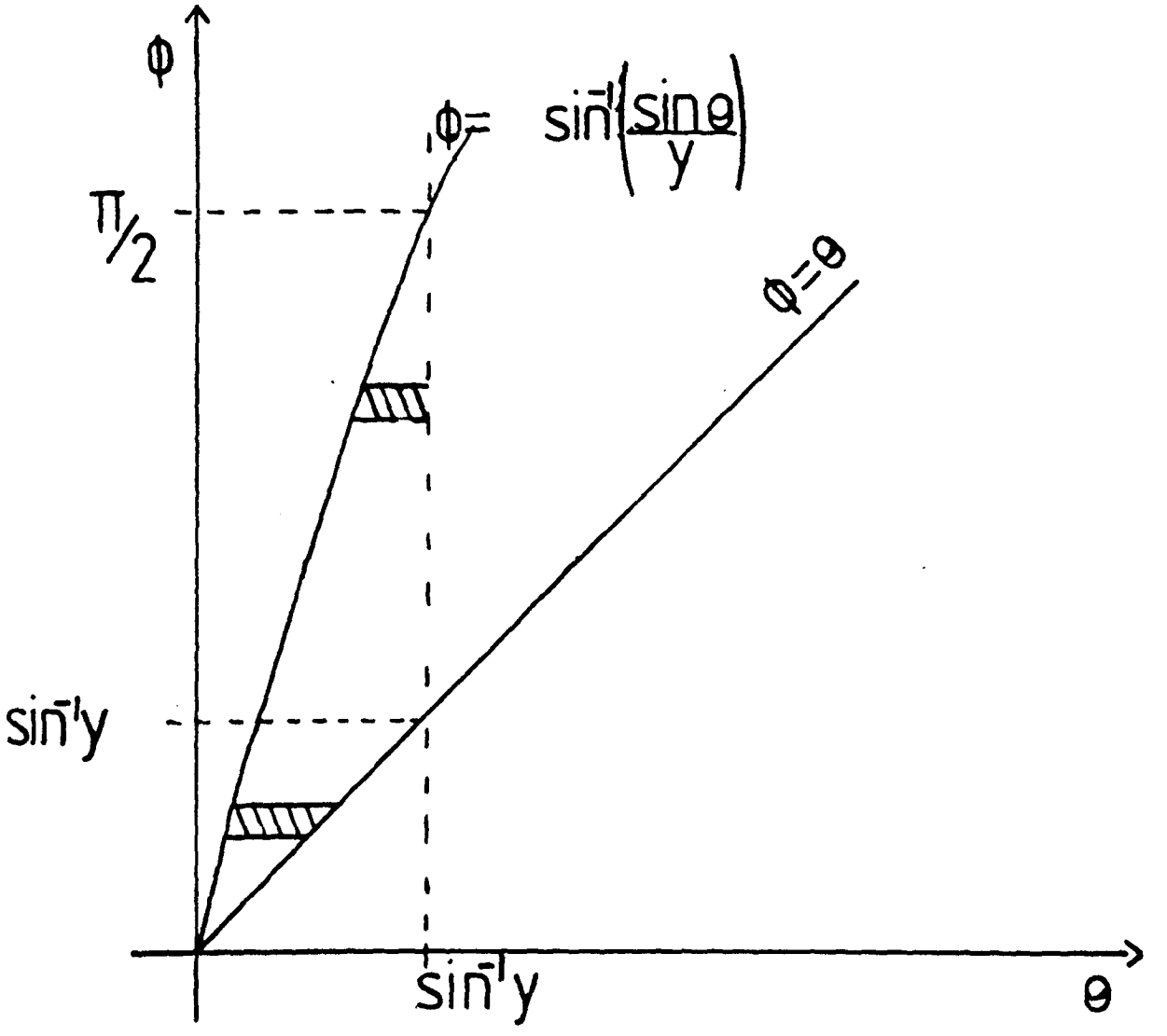

Figure 6.7b. Plotting the limits on the θ, φ plane for region (2) in an optically thin gas.

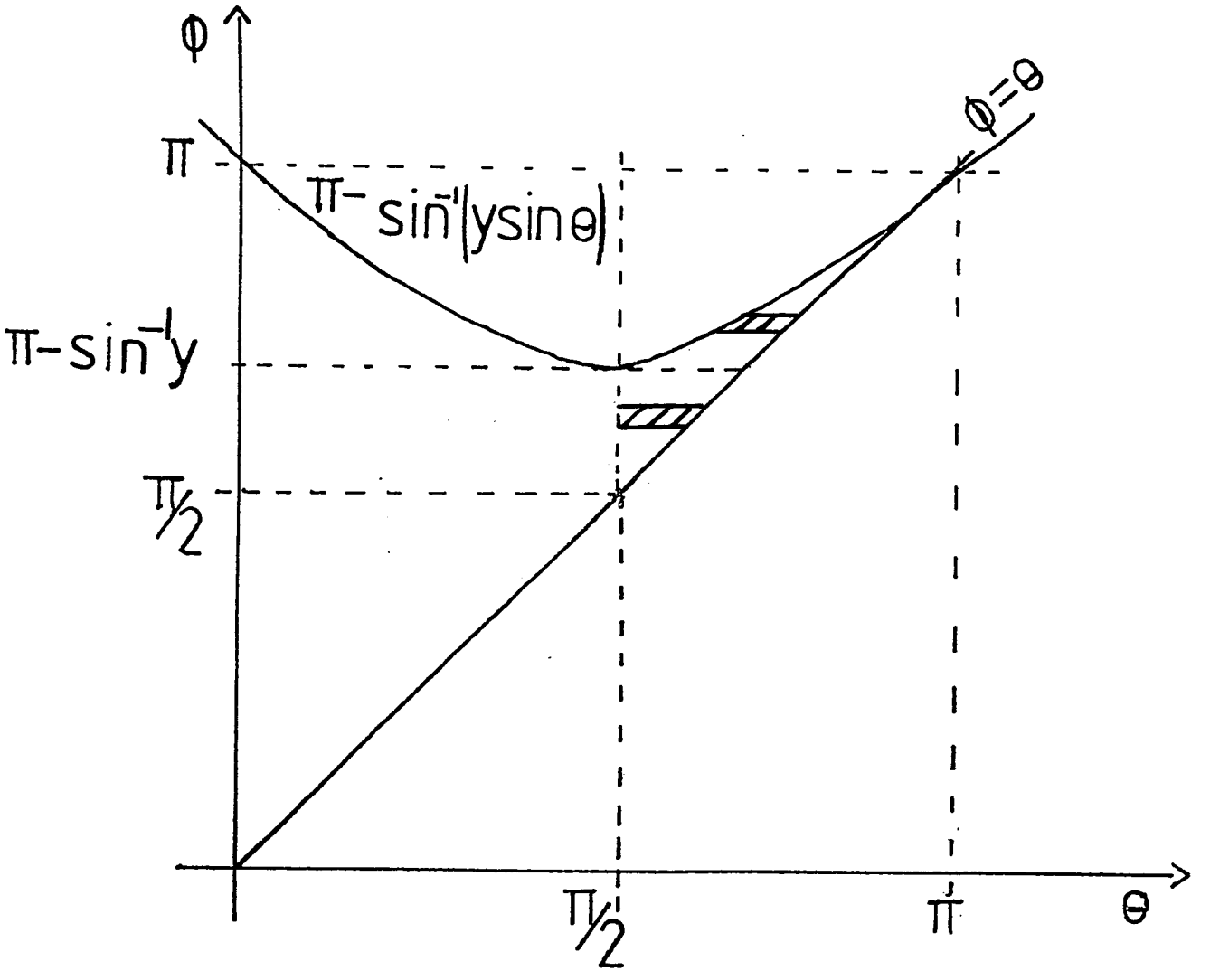

Figure 6.7c. Plotting the limits on the θ, φ plane for region (3) in an optically thin gas.

$$f_3 = -B\int_{\pi/2}^{\pi-\arcsin y}\int_{\pi/2}^{\phi} (\sin\phi/\sin\theta)^2 \cos\theta \, d\theta d\phi$$
$$-B\int_{\pi-\arcsin y}^{\pi}\int_{\arcsin(\sin\phi/y)}^{\phi} (\sin\phi/\sin\theta)^2 \cos\theta \, d\theta d\phi$$

(6.26)

Integrating equation (6.26) gives

$$f_3 = -B(\pi/4 - \arcsin y/2 + y - 1 - y\cos(\arcsin y)/2)$$

(6.27)

which is indeed equivalent to (6.24) as expected.

Now using equations (6.21), (6.24) and (6.27), the analytical fluxes can be calculated. Thus the total free-free flux, f_ν, coming from the shell is given by

$$f_\nu = f_1 + f_2 + f_3$$

(6.28)

so that

$$f_\nu = A(3\cos(\arcsin y) + 2/y - 2)$$

(6.29)

As $R_1/R \ll 1$, this can be approximated by

$$f_\nu \sim A(1 + 2/y)$$

(6.30)

Hence in this way we are able to estimate what the results of the model should be when optical depth effects are included. So these approximations essentially tell us if the program has any faults in it especially with regards to the integration procedure used.

6.4 Input Parameters

To obtain fits to the observational data values for certain parameters such as the electron density and the temperature of the plasma had to be assumed. The parameters that were inserted into the program are given in Table 6.1 and will be commented upon here.

The distance to the nova was assumed to be D = 3.27kpc. Krautter et al. (1984) find that D = 4.8kpc ± 1kpc from the interstellar extinction E(B-V) = 0.45±0.02 (derived from the interstellar 2200A feature in the ultraviolet spectrum of GQ Mus which they obtained). Whitelock et al. (1984) find the distance to be ~ 5kpc by using the M_V - t_3 (time to decline through 3 magnitudes from maximum) relationship of Schmidt (1957). Our assumed distance is therefore a little on the low side. This in part could be caused by the neglect of any free-bound emission which would increase the flux in all wavebands and thus imply a greater distance to the nova. However this free-bound emission is <<10% and so the distance would only be raised to a maximum of 3.45kpc.

The gas temperature was assumed to be 2.5×10^4K, and this was taken as a constant during the period of interest. Whitelock et al. (1984) calculate an electron temperature of $T_e > 10^4$K for day 32 after outburst from the absence of any Pfund discontinuity in the 2.3μm region therefore our temperature does not contradict these findings.

The velocity of the ejecta was taken to be v_{ej} = 1025 km s^{-1} and constant throughout the programme. Pacheco & Codina (1985) report an average expansion velocity from the widths of the emission lines as ~ 1080±80 km s^{-1}. They note that this velocity is consistent with those reported by Krautter at al. (1984) for earlier evolutionary stages. Thus we can feel justified in assuming a constant 1025 km s^{-1} velocity as the average ejection velocity.

Modelling the electron density and the ion density posed a slight

Table 6.1

Model Parameters.

D	3.27kpc
T_e	20000K
v_{ej}	$1025 kms^{-1}$
$(n_e)_o, (n_i)_o$	$3 \times 10^{10} cm^{-3}$
$(r_e)_o, (r_i)_o$	$1 \times 10^{13} cm.$
secondary	M0V

Input parameters for the free-free model of GQ Mus 1983. (See text for details).

problem. Krautter et al. (1984) noted that from the appearance of [OIII] lines in a low resolution IUE spectrum obtained of GQ Mus on 1983 February 20, the electron density was $\leq 6.5 \times 10^{5} cm^{-3}$. On the other hand Pacheco & Codina (1985) calculated that in 1983 May 10 the electron density was $\sim 3 \times 10^{7} cm^{-3}$ from the strengths of the [OI] and [NII] lines. Clearly these results contradict each other. We can attribute the higher densities obtained by Pacheco & Codina to their use of a homogeneous model for the shell which is unlikely to be an accurate representation of conditions in it. However the appearance of the [OIII] lines cannot be disputed and we suggest that the ejected shell from GQ Mus was not spherically symetric and thus these lines arose in those parts of the shell with the lowest density. Our model does not assume homogeneity but does assume spherical symmetry so we need to take some 'average' electron (and ion) density to describe conditions in the shell. We thus used that $(n_e)_o = (n_i)_o = 3 \times 10^{10} cm^{-3}$ and $(r_e)_o = (r_i)_o = 1 \times 10^{13} cm$. Such values result in densities midway between those obtained by Krautter et al. (1984) and Pacheco & Codina (1985). Given such gas density characteristics the ejected mass can be calculated from

$$M_{ej} = \int 4\pi r^2 (n_e)_o (r/(r_e)_o)^{-2} m_h \, dr \qquad (6.31)$$

thus $M_{ej} \sim 3 \times 10^{-5} M_o$, if most of the ejecta consisted of hydrogen which appeared to be the case in GQ Mus (Krautter et al., 1984). (This is ~ one order of magnitude lower than the ejected mass found by Pacheco & Codina, 1985 and obviously occurs as a consequence of using the lower electron densities that our values of $(n_e)_o$ and $(r_e)_o$ introduce to the model).

The secondary star was taken to be a late type main sequence star of radius $4.4 \times 10^{10} cm$ and blackbody temperature 3300 K which corresponds to a spectral type of M0V (Allen, 1973). Although we have no evidence for this spectral type of star, any late type main sequence star will emit

negligible infrared radiation compared to that arising from a hot plasma with the characteristics indicated above. Thus the exact spectral type of the secondary is irrelevant to the model fitting.

6.5 Results

The results from this programme for different infrared wavebands and at different times after outburst are given in Table 6.2, along with the corresponding observed fluxes at SAAO and by IRAS. (The near infrared data have been dereddened using E(B-V) = 0.45; Krautter et al., 1984).

The first thing we note is that if we compare the fluxes that we calculated analytically from equation 6.29 (see Table 6.3) with those obtained from the programme (Table 6.2) they are the same. This implies that the shell of GQ Mus is optically thin at infrared wavelengths and provides an adequate check on the reliability of the program.

The results are graphically represented in Fig. 6.8. and 4.5. From these graphs we can see that, apart from the J band fluxes, the model fluxes are consistent with the data (errors obtained from Whitelock et al., 1984 for the SAAO observations, and from the estimated median noise 1σ limits from the additional observations made by IRAS). The poor fit to the J fluxes is not surprising as the flux from this waveband does not only comprise free-free radiation. There is also significant emission from the strong emission lines HI P_β and P_γ (λ = 1.28μm and 1.09μm respectively), OI (λ = 1.129μm) and especially the HeI triplet (λ = 1.083μm) (Whitelock et al., 1984). Thus we would indeed expect the observed fluxes to fall well above the calculated free-free model flux predictions.

6.6 Conclusion

We have shown that the infrared flux observed from the nova GQ Mus 1983 during the period 27 - 310 days after outburst can be reasonally modelled by the free-free emission of a plasma at a temperature of

Table 6.2

Comparison of model and observed fluxes.

Date	27	42	64	96	140	141	179	215	217	225	268	310
J	5.50	3.24	2.32	1.08	1.14				1.01		0.44	0.41*
	1.24	0.80	0.53	0.35	0.24				0.16		0.13	0.11
H	1.55	0.85	0.64	0.30	0.31				0.25		0.13	0.12*
	1.37	0.90	0.59	0.40	0.27				0.18		0.14	0.12
K	1.79	0.94	0.72	0.37	0.37				0.31		0.15	0.14*
	1.46	0.97	0.64	0.43	0.29				0.19		0.15	0.13
L	1.60	0.88	0.68								0.11	0.12*
	1.48	1.04	0.70								0.17	0.15
I						0.35	0.23	0.23		0.23		*
						0.36	0.28	0.24		0.23		
II						0.32	0.31	0.29		0.21		*
						0.35	0.29	0.24		0.23		
III						0.42	0.36	0.38		0.23		*
						0.29	0.26	0.23		0.22		

In this table the date refers to the number of days after outburst of GQ Mus 1983. Observed fluxes and fluxes that have been calculated from the free-free model (in Jy) are given in the starred row and the next row respectively.

Table 6.3

Theoretical fluxes for optically thin gas shell.

	flux(Jy)	flux(Jy)
Date	140	217
J	0.24	0.15
H	0.27	0.18
K	0.29	0.19
L	0.32	0.22
Date	144	215
I	0.36	0.23
II	0.35	0.23
III	0.29	0.22

The free-free fluxes calculated analytically for an optically thin gas shell in GQ Mus 1983. The date gives the number of days after outburst and the fluxes are calculated for wavebands J - III (IRAS).

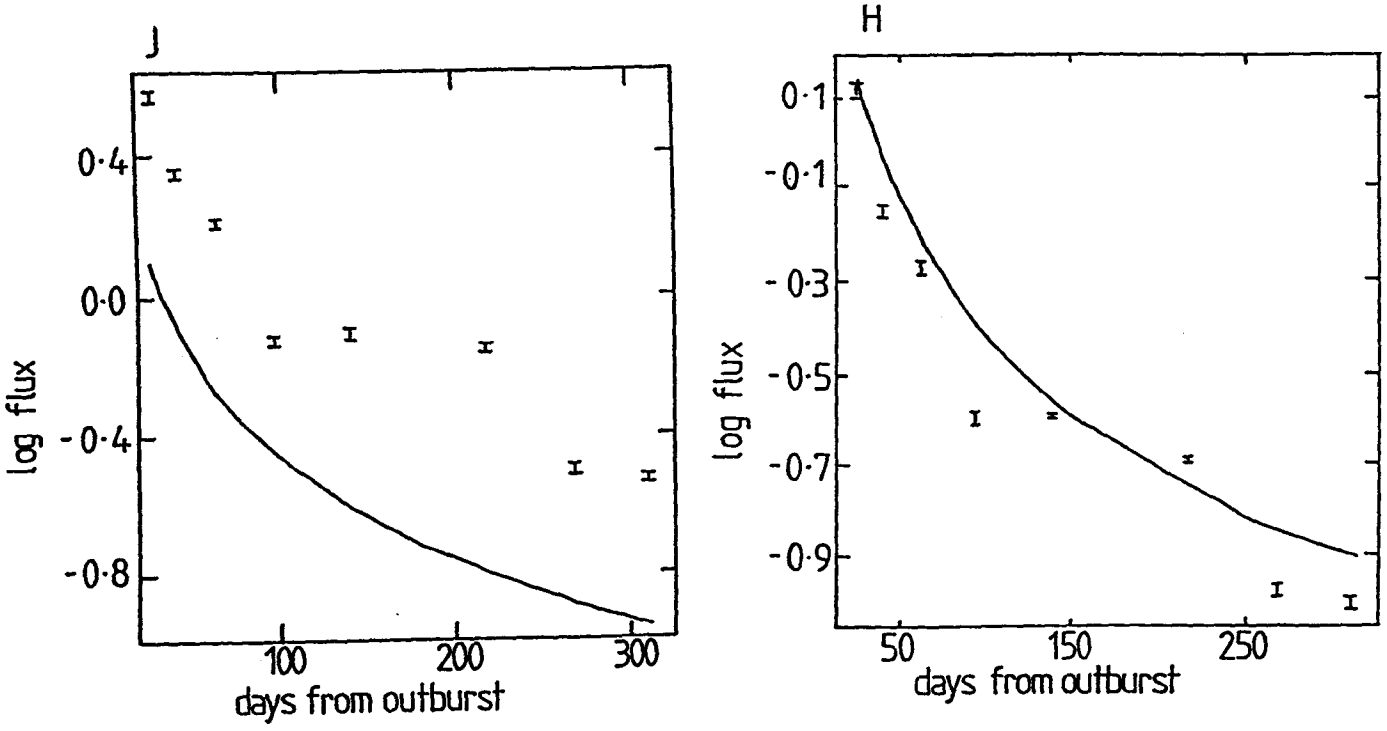
J
0·4
0·0
-0·4
-0·8
log flux
100
200
300
days from outburst
H
0·1
-0·1
-0·3
-0·5
-0·7
-0·9
log flux
50
150
250
days from outburst

(a) (b)

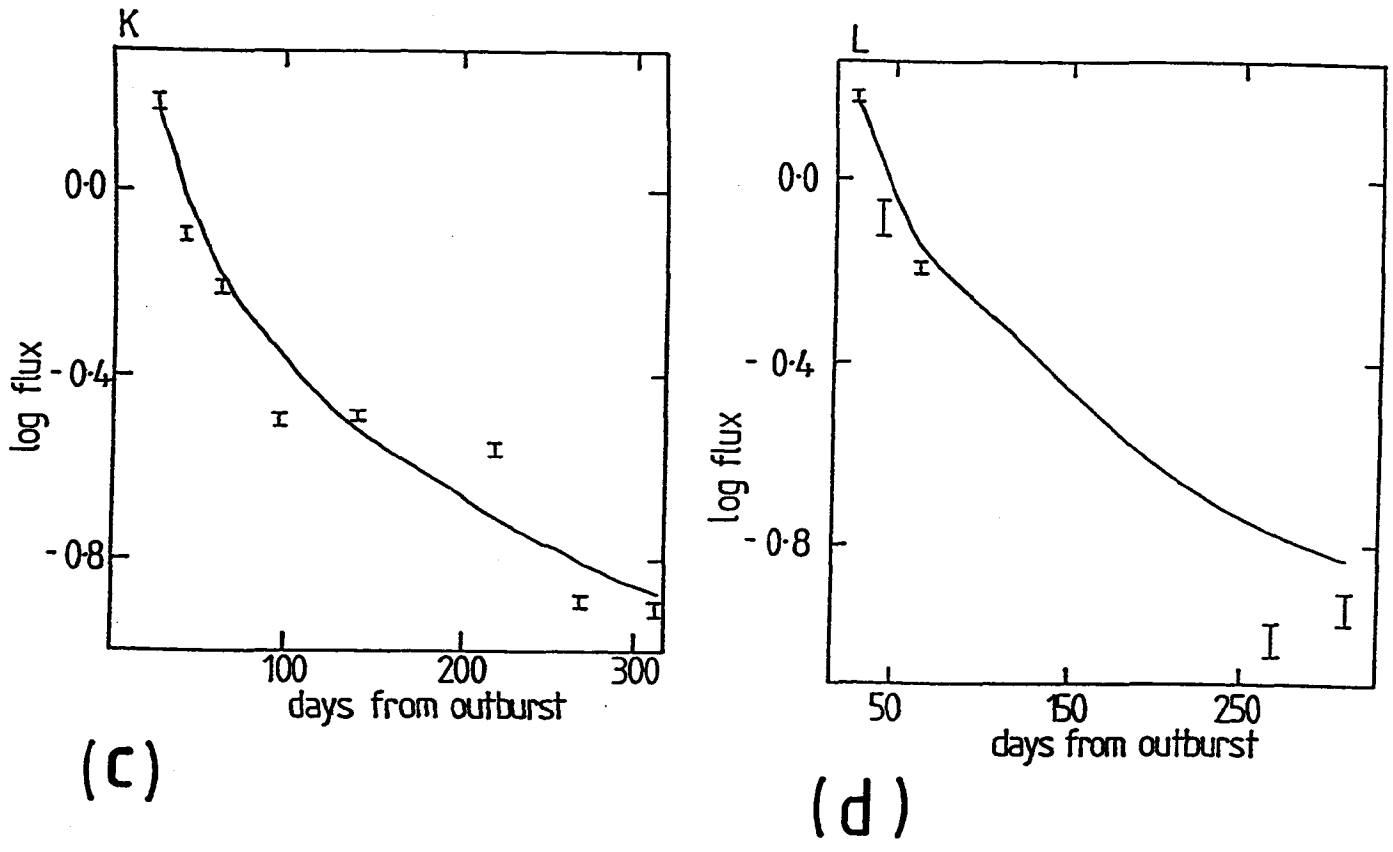

Figures 6.8a-d. The free-free model fits to the infrared light curves of GQ Mus 1983 (flux given in Jy). The range in observed values takes into account the errors in the data).

2.5×10^{4}K and $M_{ej} = 3 \times 10^{-5} M_{\odot}$, and which is optically thin in the infrared. This is indicated by the fact that the model fits the wavebands H, K, L, 12μm and 25μm well during a 250 day interval.

CHAPTER 7

THE RECURRENT NOVA RS OPHIUCHI

7.1 Introduction

On 1985 January 26, the recurrent nova RS Ophiuchi (RS Oph) underwent its fifth recorded outburst. This gave the astronomical community a remarkable opportunity to study such an object at all wavelengths simultaneously. In carrying out this study, RS Oph became the first recurrent nova to be detected in the radio and X-ray regions during outburst. During the previous outbursts of this object a 'first' had been discovered in that it was the first object other than the sun in which coronal lines were seen. It was also notable in that it displayed a visual light curve that was essentially the same over all outbursts. This light curve resembled that of a very fast classical nova. The outbursts, as well, gave good evidence for the presence of a stationary circumstellar envelope. It was indeed a very interesting object to study!

This chapter reviews all the outbursts of RS Oph both photometrically and spectroscopically. It also reviews the observations of this object at quiescence and lastly reports on a debate concerning the outburst mechanism for the star.

7.2 The 1898 Outburst

Observations of RS Oph before this century are very few but luckily we do have some data on the 1898 outburst. The variability of RS Oph was discovered in 1901 by Mrs. Fleming (Prager, 1940). The first study of the light variation was undertaken by Miss Cannon and consisted of Harvard photographs extending from 1888 to 1905. Cannon (1907) reported that, from 1888 - 1890, the photographic magnitude was steady at ~ 10.9 mags. Then it increased gradually until it reached ~ 10.4 mags and stayed at this

magnitude between 1893 - 1897. Observations taken in 1898 indicate that its magnitude was ~ 10.8 mags until May 31 of that year. RS Oph then underwent its first recorded outburst reaching a visual magnitude between 4 and 5 mags on June 19. The only actual observation reported was on June 30, when its photographic magnitude was recorded as 7.7 mags. The outburst spectrum was then said to resemble the novae AT Sgr 1900 and DM Gem 1903 at their maximum brightness. About this time emission lines of Hζ, Hε, Hδ, Hγ and Hβ were prominent and two bright emission lines were observed at ~ 4656A ,4691A (probably due to NIII 4640A and HeII 4686A). The visual flux then decreased at the rate of about 1 mag per month until October 8 when its magnitude was again 10.8; the star was then observed to fluctuate irregularly. In April 1900 its photographic magnitude was ~ 9.3 while in September of that year it was ~ 10 mags. Wendall (Cannon, 1907) observed the object 54 times during 16 nights in 1903 and 1904 and noticed a 0.76 mag variation.

At the time of these observations the spectrum of the star was thought to be of the type K and it was noted that there had been no evidence of the bright lines except at the 1898 outburst.

7.3 The 1933 Outburst

7.3.1 The Light Curve

On 1933 August 12 Loreta reported that RS Oph appeared to be undergoing another outburst; this was independently confirmed by Peltier a few days later (Prager, 1940). Adams & Joy (1933a) reported that, when they first observed this object on 1933 August 16, it was a strong crimson in colour.

Bertaud (1947) collated 2023 observations of this nova from mid August 1933 until the end of 1939. The results of this collation are shown in Fig. 7.1. The maximum occurred on 1933 August 12 with a visual magnitude

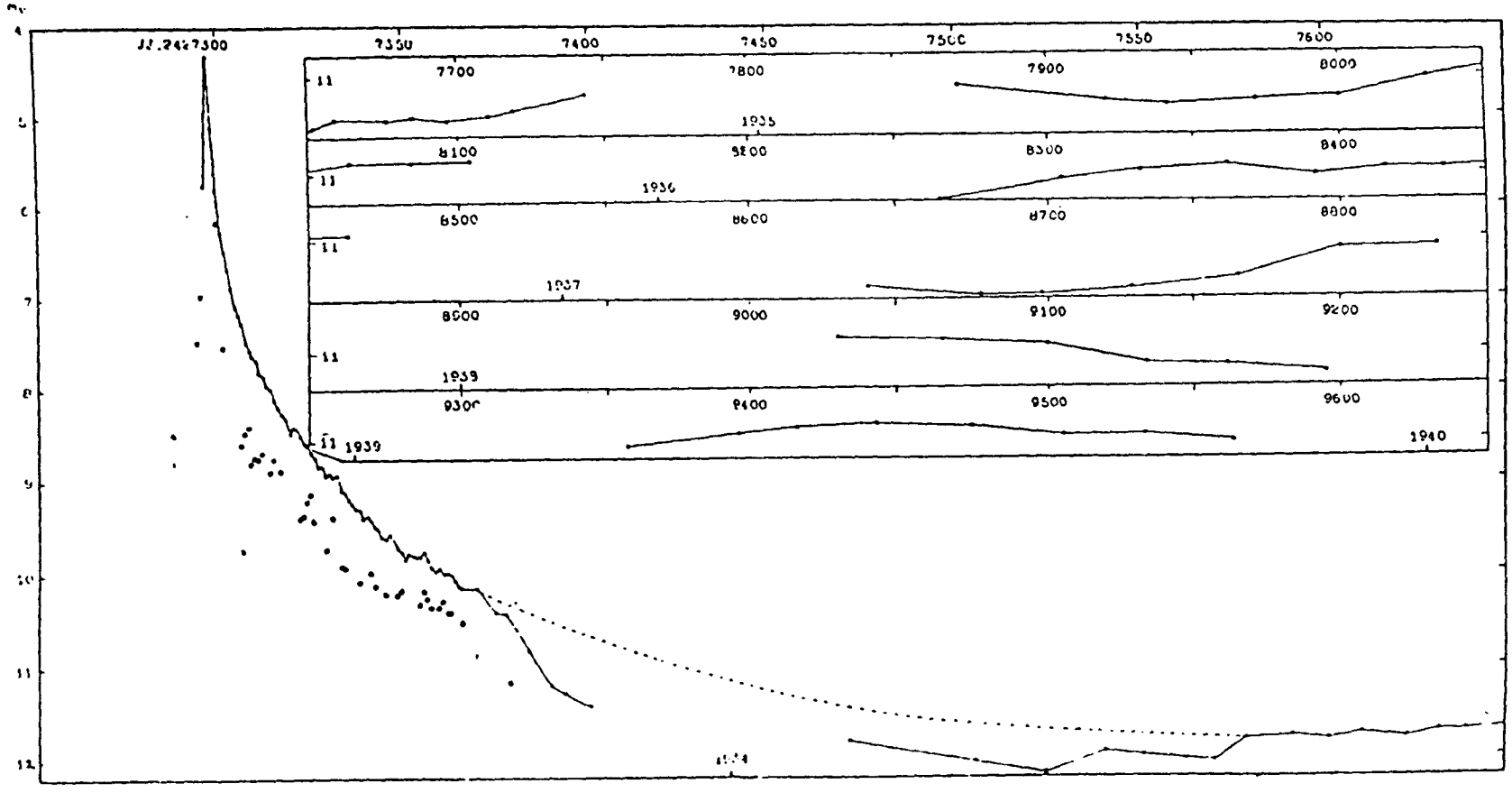

Figure 7.1. Visual light curve of RS Oph from 1933 to 1940. Reproduced from Bertaud (1947).

of 4.3. The time to fall by 3 mags from maximum was 9 days. After this time the visual light declined without noticable oscillations until it reached a minimum in late March of the following year. The light curve then oscillated around 11.5 - 10.9 magnitudes for the next five years. Table 7.1 gives the average magnitudes for each of the years 1934 to 1939. This author also measured the (B-V) colour index from 1933 August 15 until the end of October of that year. During this period the average was +0.67 although there was a range of values covering +0.4 → +0.94 (see Table 7.2).

Prager (1940) in his observations during this outburst, noted that the 1898 outburst observations coincided almost exactly with the light curve of 1933 (see later sections).

7.3.2 Spectroscopic Observations

Spectroscopy of RS Oph immediately after outburst was described by Adams & Joy (1933a). These authors observed the object from 1933 August 16 until 1933 September 2. On the first day of their observations they saw prominent lines of hydrogen with width $\Delta\lambda \sim 25 - 30$A, faint emission bands of helium and singly ionized iron on a strong continuous spectrum. The hydrogen lines exhibited P Cygni profiles and the hydrogen absorption bands had radial velocity ~ 60 km s^{-1}. Of the FeII lines those at λ4924 and λ5018 were the strongest. Faint emission lines were seen in the positions of the calcium H & K lines upon which were superimposed absorption lines. These features were probably interstellar in origin.

Two days later, on August 18, the strong absorption lines of hydrogen were less prominent, the continuous spectrum weaker and the lines of helium and FeII slightly stronger. It is at this point that the [OIII] nebular line at λ4363 was first seen as a faint sharp emission feature.

The next observation on August 29 showed strong emission bands at λ4039 (NIII) and λ4686 (HeII). The former band was ~ 25A wide and showed several maxima and absorption lines, suggesting the superposition of a

Table 7.1

Average yearly magnitudes of RS Oph from 1934 - 1939.

Year	Average Mag	Year	Average Mag
1934	11.69	1937	11.50
1935	11.05	1938	11.03
1936	10.99	1939	10.92

Reproduced from Bertaud (1947).

Table 7.2

(B-V) colour index of RS Oph during its 1933 outburst.

Date (1933)	(B-V)	Date (1933)	(B-V)
Aug 15	+0.71	Sept 28	+0.56
Aug 26	+0.94	Oct 13	+0.40
Sept 8	+0.68	Nov 2	+0.74
Sept 16	+0.70		

Reproduced from Bertaud (1947).

number of bands. The latter band was double, with an absorption line displaced slightly toward the red. Several other of the observed lines showed this saddle shaped profile. The next day the HeII λ4686 line was much fainter.

Five nebular lines were seen on August 31. These were [NeII] λ3868, [OIII] λ4363, [OIII] λ4959, [NeIII] λ3967 and [OIII] λ5007. The radial velocity measured from these lines was ~ -42 km s^{-1}. [OIII] λ4363 was the strongest line and the HeII λ4363 again became prominent. It appeared that the HeI lines became stronger when the HeII λ4686 line became faint and vice-versa.

The last spectrogram that these authors took on September 2 showed little continuum and strong bright hydrogen emission bands. These were much more condensed than at the beginning of the observations, with a slight absorption on the violet side. The NII λ4639 and HeII λ4686 lines were strong and there were moderately bright bands of neutral helium and singly ionized iron. The authors noted that 'the spectrum gives the impression of possible superpositions of two spectra, one perhaps arising from an extensive atmosphere produced by the outburst and the other from the star itself'.

Adams & Joy (1933b) then go on to make the first observations of coronal lines in an object other than the sun, when they noticed such lines in the spectrum of RS Oph on 1933 October 2; they observed the green line [FeXIV] λ5303 and [FeX] λ6374. Subsequently they observed [FeXI] λ3987, [CaXIII] λ4086 and [NiXII] λ4231 and Bowen and Swings (1947) identified the [KXI] λ4258 line. These lines were spilt into two very close components. Joy & Swings (1945) suggest that it was probable that the [FeX] λ6374 line had been present since ~ 1933 September 7 so enhancing the strength of the SiII λ6371 line above that of the SiII λ6347 line and thus indicating that a coronal line had appeared less than a month after outburst. The lines [FeXIV] λ5303 and [FeX] λ6374 changed very little up to 1933 November 10.

At the end of October 1933 the intensity of the [FeXIV] λ5303 line was comparable to that of Hβ and [FeX] λ6374 was more than twice as strong as HeI λ5875. The coronal lines had disappeared completely by March 1934, when the intensity of the continuous spectrum was greatly increased (Swings & Struve, 1941).

Wilson & Williams (1934) monitored the hydrogen lines throughout the outburst. Prior to August 18 the lines were asymmetrical; a sharp absorption line appeared to the violet of the band centre and they thought that the intensity in the violet side was less than that in the red side. Later on the sharp absorption component faded and the asymmetry became less noticable.

The narrowing of the line width with time is noteworthy. Generally the band widths decreased very rapidly for a time after maximum then the rate of decrease became gradually smaller until ~ September 1, and for at least two months after that changes in the bands were not observed. Wilson & Williams suggest that their observations of narrowing band width was an indication of deceleration of the ejected material.

These authors also measured the Balmer decrement of this nova and found it to correspond to a colour temperature of ~ 4000 K, which they considered to be too low for an object of this kind. Stebbins (Wilson & Williams, 1934) reported that by means of photoelectric colour determination he had estimated the spectral type of RS Oph to be gG3; however this result included the hydrogen emission lines and when allowance was made for them the resulting spectral type is earlier. This classification did at least confirm the low colour temperature obtained. Wilson & Williams (1934) calculated that if the nova was at a distance of 1200 pc interstellar reddening could probably account for the low colour temperature.

7.4 The 1958 Outburst

7.4.1 The Light Curve

On 1958 July 14 Fernald observed RS Oph to be undergoing a third outburst (Wallerstein, 1958). This information was circulated quickly and many observers had the opportunity to observe the nova throughout the 1958 outburst.

Cragg (1958) observed the nova during the first 75 days of its decline (see Fig. 7.2). He observed three 'stand stills' on day 8, 16 and 51. From the nova's maximum apparent magnitude of 5 mags Cragg, from his light curve, determined the nova amplitude to be 6.5 - 7 mags. He observed that the nova was 'white' in its appearance, until seven days after maximum when it abruptly changed to 'red'. He noted the similarity to the light curve of the previous outburst.

The light curve was followed using professional equipment (unlike Cragg's) by Connelley & Sandage (1958) and Svolopoulos (1966). The first authors' observations were made on 9 successive nights after the nova's discovery and suggested that B-V ranged from 0.74 mags just after outburst to 0.61 mags. On day 9 Svolopoulos's observations confirmed these findings, his values differing by no more than a few hundreths of a magnitude. He made much out of this apparent colour excess exhibited by RS Oph. He suggested that there might be an obscuring dust cloud in the vicinity of RS Oph, located between the solar Galactic arm and the inner Galactic arm; or alternatively that there could even be two clouds one connected with each arm. However Svolopoulos based his suggestion of a highly reddened star on the assumption that RS Oph was of spectral type B8, which subsequently has been foung not to be the case (see below).

Eskioglu (1963) made extensive visual and photographic observations of RS Oph between July 17 and October 31 1958. He too drew attention to the

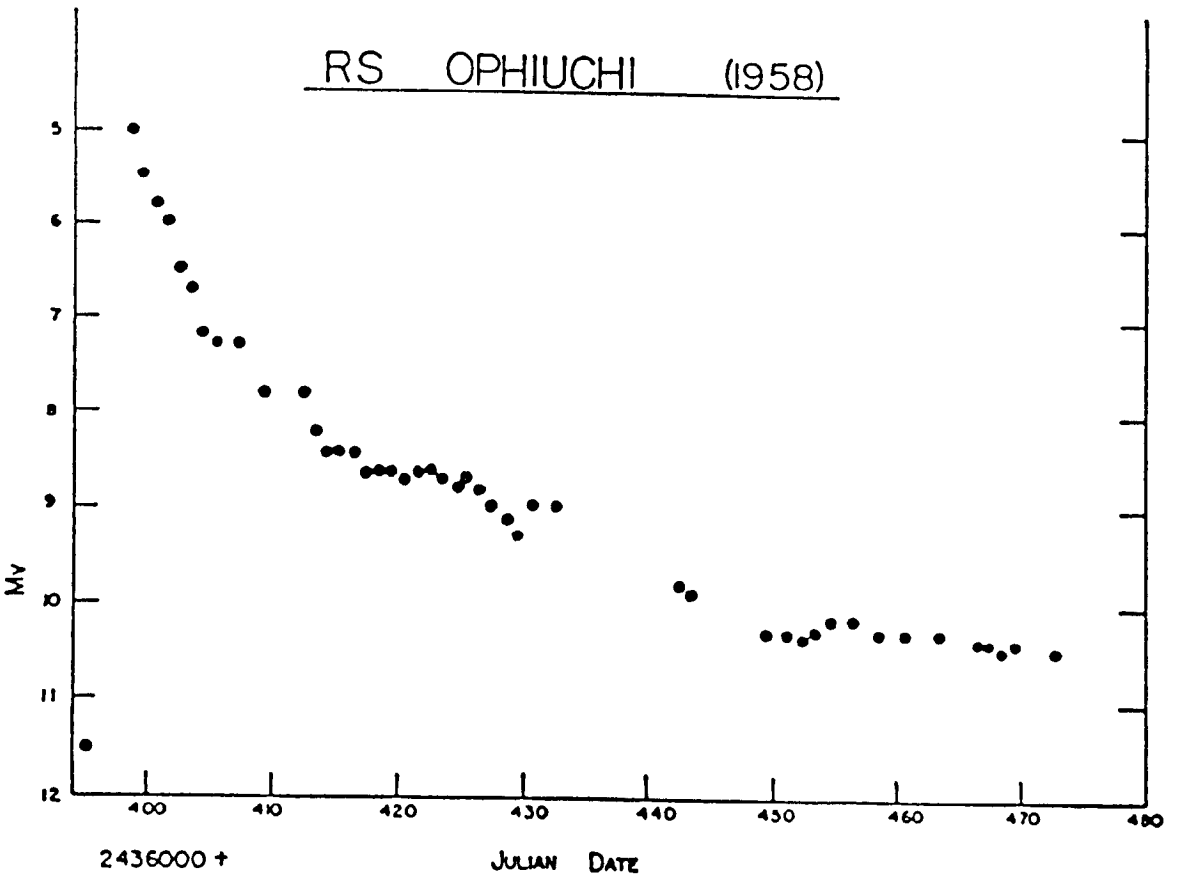

Figure 7.2. Visual light curve of the first 75 days of the 1958 outburst of RS Oph. Reproduced from Cragg (1958).

similarity between the 1958 light curve and that of the 1933 outburst but noted that, in fact, this outburst was less rapid than the previous one (see Fig. 7.3).

7.4.2 Spectroscopic Observations

Spectroscopic observations, as with the photoelectric ones, were obtained very soon after the nova's discovery. The evolution of the line profiles was described by Tolbert et al. (1967) and expanded upon by other authors. He decribes the spectra just before maximum as appearing flat and featureless, even the hydrogen lines being flat and broad. After maximum the emission lines grew considerably in intensity while still remaining very broad. The line profiles were irregular, being somewhat cut off on the violet side. On the violet wing at day 0.5 narrow lines appeared. The spectral lines then continued to grow in strength until about the third day and then both the intensity and width declined. After day 7 the line profiles did not change but the lines did become fainter (see Fig. 7.4).

Dufay et al. (1964) gave information on the development of individual lines with time. They described observations taken from July 14 - November 3 1958 covering the wavelength region 3500 - 8800A. At day 1 the most intense lines were the hydrogen Balmer series (Hα - H$_8$). They appeared to have a diffuse absorption component on the violet side which gave radial velocities of ~ 3620 km s^{-1}. HeI λ5876 was also strong and had an almost identical structure to that of the hydrogen lines. The interstellar H & K lines of CaII were present and in the near infrared, lines of NI and OI were observed. The spectroscopic evolution was such that emission lines of increasing excitation began to appear, followed by the forbidden lines of [OII], [NeIII], [OIII], [NII], [FeII], [FeIII] and later, [OI], [FeVII], and [ScVII]. Then about 30 days after maximum brightness the narrow emission line of [OIII] disappeared to reappear immediately afterwards as broad diffuse lines. Dufay et al. (1964) interpreted this as the arrival

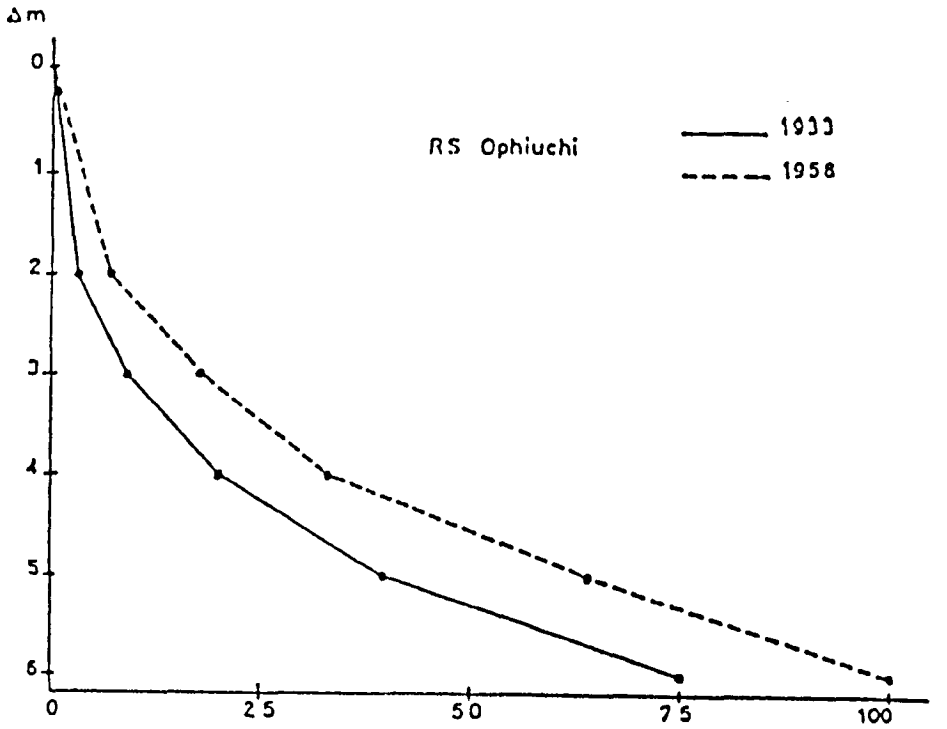

Figure 7.3. Comparison of the decline in the visual light curves of the 1933 and 1958 outbursts of RS Oph. Reproduced from Eskioglu (1963).

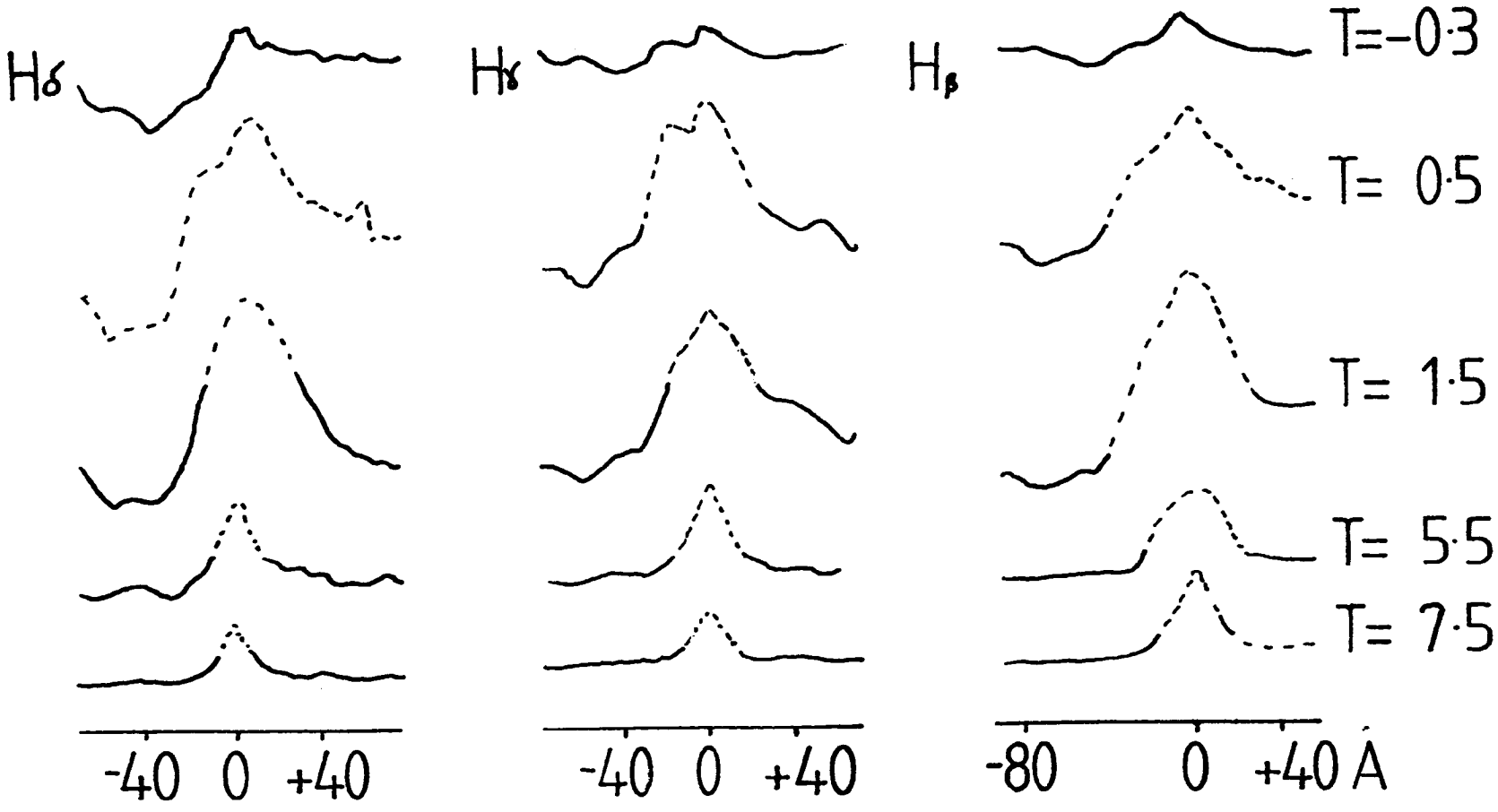

Figure 7.4. Profiles of the hydrogen lines over the first few weeks of the 1958 outburst of RS Oph. The dashed portions are based on non-linear sections of the calibration curves. 'T' gives the time after outburst in days when the line profiles were obtained. Reproduced from Tolbert et al. (1967).

of the ejecta at a preoutburst circumstellar envelope, which was the original site of the fine [OIII] emission. Coronal lines [FeX], [FeXI], [FeXIV], [AX], [NiXII] and [NiXV] appeared in late August and soon became very intense, being the dominant lines at the beginning of November. In the spring of 1959 the coronal lines had disappeared but forbidden lines of low excitation potential persisted. The multiplet OI λ8446 dominated the near infrared along with the hydrogen Paschen lines. Besides diffuse interstellar absorption bands the continuum showed a large number of metallic absorption lines corresponding to a 'fairly advanced spectral type'. As with the light curve, these authors note the spectral similarity between this and the previous outburst remarking that on some occassions the appearance of a particular line coincided to within a day.

Wallerstein (1958) made observations of this nova for the first 16 days after the 1958 outburst. He made extensive observations of the numerous narrow lines he found superimposed upon both the broad emission and possible absorption features. On the first night the broad hydrogen emission also had a very sharp emission component and an equally sharp absorption core. As these lines increased in strength the sharp lines weakened. However these sharp components were visible in other lines throughout the period of observation, the sharp absorption component of HeI λ3889 persisting until July 27. The velocities of these lines were determined and found to range between -10 km s^{-1} and - 62 km s^{-1} (see Table 7.3). Wallerstein suggested that the origin of the sharp absorption lines was in a slowly expanding envelope that surrounded the whole system, apart from the NaI and CaII lines at ~ -10 km s^{-1} which were probably interstellar. This was because the velocity of these sharp absorption lines did not change in the 17 nights of observation which strongly suggested that they were not formed in the violently expanding nova shell. Wallerstein noted that the sharp emission lines had velocities of ~ +20 km s^{-1} more than the sharp absorption lines and he doubted whether they

Table 7.3
Sharp lines in the 1958 outburst spectra of RS Oph.

Feature	E/A	1st	Last	Velocity (kms^{-1})
Hα	E	14.3	20.3	-13
Hα	A	14.3	20.3	-61
Hβ	E	14.3	17.3	-24
Hβ	A	14.3	17.3	-64
Hγ	E	14.3	16.3	-15
Hγ	A	14.3	17.3	-57
Hδ	E	14.3	15.3	-18
Hδ	A	14.3	17.3	-57
H > Hδ	A	14.3	17.3	-55
MgII 4481	A	14.3	14.4	(-53)
HeI 4471	A	14.3	14.4	(-44)
HeI 3889	A	14.3	27.4	-57
HeI 6678	A	14.3	15.3	(-58)
HeI 5876	E	15.3	15.3	(-45)
HeI 7065	E	16.3	17.3	(-34)
HeII 4686	E	23.3		(-35)
OI 7773	A	16.3	17.3	(-64)
OI 8446	E	16.3	17.3	(-58)
FeII	E	15.3		-39
[FeII]	E	17.3		-43
[FeIII]	E	20.3	24.3	-34
[OIII]	E	17.3		-40
[NeIII]	E	20.3		-37
[NII]	E	20.3		-51
[SIII]	E	20.3		-43
NaI	A	14.3		-11
		14.3		-62
CaII	A	14.3		-10
		14.3		-62

E/A represents the type of lines seen i.e. emission or absorption. The third and fourth columns give the date of the first and last appearance of the line (July 1958). Reproduced from Wallerstein (1958).

both came from the same region.

Around this time the idea that all novae might be in a binary system was surfacing (Kraft, 1963). Wallerstein made the first suggestion of the spectral type of the secondary from the photographic absolute magnitude of the system as deduced by Connelly and Sandage (1958). Thus he estimated that the secondary (if it had one) was of spectral type M similar, he noted, to that of the other recurrent nova T CrB.

Twelve low dispersion spectrograms of RS Oph were obtained by Joy (1961) between August 5 and October 10 1958. He saw no absortion lines at all during this period. Like Dufay et al. (1964) he saw, soon after outburst, strong emission from the Balmer lines of hydrogen together with lines of helium. These lines showed comparatively little change in width or intensity during the period of observation. He remarked on the appearance and number of lines of highly excited ions, some of which had excitation potentials of several hundred eV! All in all he was able to identify 165 lines, 30 due to hydrogen and helium, 42 due to iron and 26 due to forbidden iron lines; 38 different ions and 2 neutral atoms of 13 different elements were represented (see Table 7.4).

He compared his observations with those of the previous outburst and found only minor differences. These were, in 1958, the sharp auroral lines of [OI] λ6300 and λ6363 were enhanced and [OI] λ5577 appeared in great strength but they were not seen at all in 1933; also the bright NaI D lines and the [OIII] nebular lines, N_1 and N_2, and λ4363 were somewhat weaker in 1958.

Pottash (1967) attempted to interpret the spectra taken during the 1958 outburst assuming spherical symmetry. He explained the narrowing of the very large line widths in terms of an expanding, decelerating shell. Determination of the mass of this shell showed that it continuously increased with time. He explained these observations, as had other authors, by postulating a pre-outburst circumstellar envelope, completely

Table 7.4
Identified lines in the 1958 outburst spectra of RS Oph.

Element	No. of lines
H	15
HeI	10
HeII	5
CIII	3
NII	8
NIII	6
[NII]	3
OIII	5
[OI]	3
[OIII]	3
[NeIII]	2
[NeIV]	2
SiII	8
[SII]	2
[SIII]	1
[AV]	1
[AX]	1
[AXI]	1
[AXIV]	1
[KV]	4
[KVI]	1
[KXI]	1
[CaV]	3
[CaVI]	2
[CaVII]	1
[CaXIII]	1
[CaXV]	1
FeII	42
[FeII]	10
[FeV]	5
[FeVI]	3
[FeVII]	5
[FeX]	1
[FeXI]	1
[FeXIV]	1
[NiXII]	1
[NiXIII]	1
[NiXV]	1

Reproduced from Joy (1961).

distinct from the emitted shell and with which the shell interacted. Thus the shell was slowed down and added the envelope to its mass. He quantitatively checked this by calculating the momentum of the shell with time and found it to be a constant (see Table 7.5). He also found that the average state of ionization of the shell continued to increase with time by considering the intensities of lines at various states of ionization from different elements at stages in the nova's evolution (see Table 7.6).

Tolbert et al. (1967) attempted to find the form of the continuum for this nova. In the range 3800A - 5000A they calculated from plates taken in the first two weeks after outburst that the gradient of the continuum was 4.24 ± 0.22 and constant for at least the first 45 days. This gradient implied a colour temperature of ~ 3500 K. In the 5000A - 7000A range they calculated a gradient of +3.47 ± 0.5. It is interesting to note that the deduced colour temperature is that of a late type giant star.

As mentioned in section 7.3.1, Wilson & Williams (1934) calculated the colour temperature of RS Oph in the 1933 outburst by measurement of the Balmer decrement and found it to be ~ 4000 K. In the 1958 outburst Dufay & Bloch (1964) and Tolbert et al. (1967) both measured this quantity. They found good agreement between their own results and with the values obtained in the previous outburst (see Table 7.7). These measurements implied colour temperatures of ~ 3400 K. Dufay & Bloch (1964) attempted to determine whether interstellar absorption could explain this 'low' colour temperature. From absorption coefficient calculations they found the quantity of interstellar matter necessary to reduce the Balmer decrement to a value 'more suitable' for a planetary nebula. They found that that if a colour excess of E(B-V) = 0.75 was interpreted as being due to interstellar extinction the colour temperature increased from ~ 3400 K to a more 'appropriate' temperature of ~ 8400 K.

Table 7.5

Calculated momemtum of ejected shell of RS Oph.

Date	Momentum
1.5	2.5×10^{36}
2.5	2.2×10^{36}
4.0	2.2×10^{36}
7.0	2.0×10^{36}
10.0	2.1×10^{36}
15.0	2.1×10^{36}
25.0	2.2×10^{36}
40.0	2.3×10^{36}
60.0	2.2×10^{36}
90.0	2.1×10^{36}

Reproduced from Pottasch (1967), this table shows the constant ejected shell momentum with time after the 1958 outburst. (Date is given in days after outburst, momentum in g cm s^{-1}).

Table 7.6

Oxygen ionization state.

Date	N(OI)/N(H)	N(OII)/N(H)	N(OIII)/N(H)	Higher stages
2.5	-	52	-	-
4.0	30	31	5	-
7.0	30	25	10	-
10.0	25	22	15	3
15.0	15	18	20	12
25.0	8	15	21	21
40.0	5.0	12	22	26
60.0	3.4	8	16	37
90.0	2.7	6	11	45

This table shows the oxygen ionization state and abundance on various days after outburst for the 1958 outburst of RS Oph. Reproduced from Pottasch (1967). This demonstrates the increased level of ionization with time in the nova ejecta.

Table 7.7

The Balmer Decrement.

Line	1958 (TPP)	1958 (D&B)	1933 (W&W)
H α	2130	-	-
H β	389	407	398
H γ	100	100	100
H δ	50	45	40
H ε	18	25	20
H 8	10	16	25
H 9	7	8	(16)
H 10	-	7	-

This table gives the Balmer decrement as obtained by Tolbert et al., 1967 (TPP); Dufay & Bloch, 1964 (D&B); Wilson & Williams (1934) from the hydrogen Balmer lines. This shows the good agreement for this value from the 1933 and 1958 outbursts of RS Oph.

7.5 The 1967 Outburst

This outburst of RS Oph unfortunately was not as well researched as it could have been. This was mainly because the star was in conjunction with the sun for two months only about six weeks after outburst. A secondary reason was that, although the star was constantly monitored since it had been established that it was a recurrent nova, it was not expected to go into outburst for another ten years or so and thus caught observers unawares.

7.5.1 The Light Curve

Isles (1974) collated photometric data from 1963 February 24 until about 200 days after outburst. Between 1963 February 24 until 1967 October 22 RS Oph was faint, the observed visual magnitudes ranging between 9.5 - 12.2 mags. It was noted that, as the star declined, the scatter in the observations increased but it was difficult to know if this was real or due to different observers and/or to trouble with comparison stars. Hence a continuous light curve could not be drawn with any certainty. The slow variation which occurred seemed to have a typical length of about 1000 days, with minima around 11.9 - 11.6 mags and maxima around 10.4 -10.5 mags. On 1967 October 22 RS Oph was at 10.8 mags and, four nights later, was independently detected by several observers to be undergoing outburst.

The light curve is plotted in Fig. 7.5 from just before maximum (which occurred on 1967 October 27 at a magnitude of 5.4) for about 40 days, when the star was lost in the twilight. The most rapid decline was seen in the initial stage, the drop from 5.4 mags to 7 mags taking 8 days at a rate of 0.2 mag d^{-1}. During the next 25 days a steady fall of 2 mags occurred at a rate of 0.08 mag d^{-1}. After the object had reappeared from behind the sun it was at a visual magnitude of 10.8 on 1968 March 28. Thereafter the character of the light curve was similar to that before the

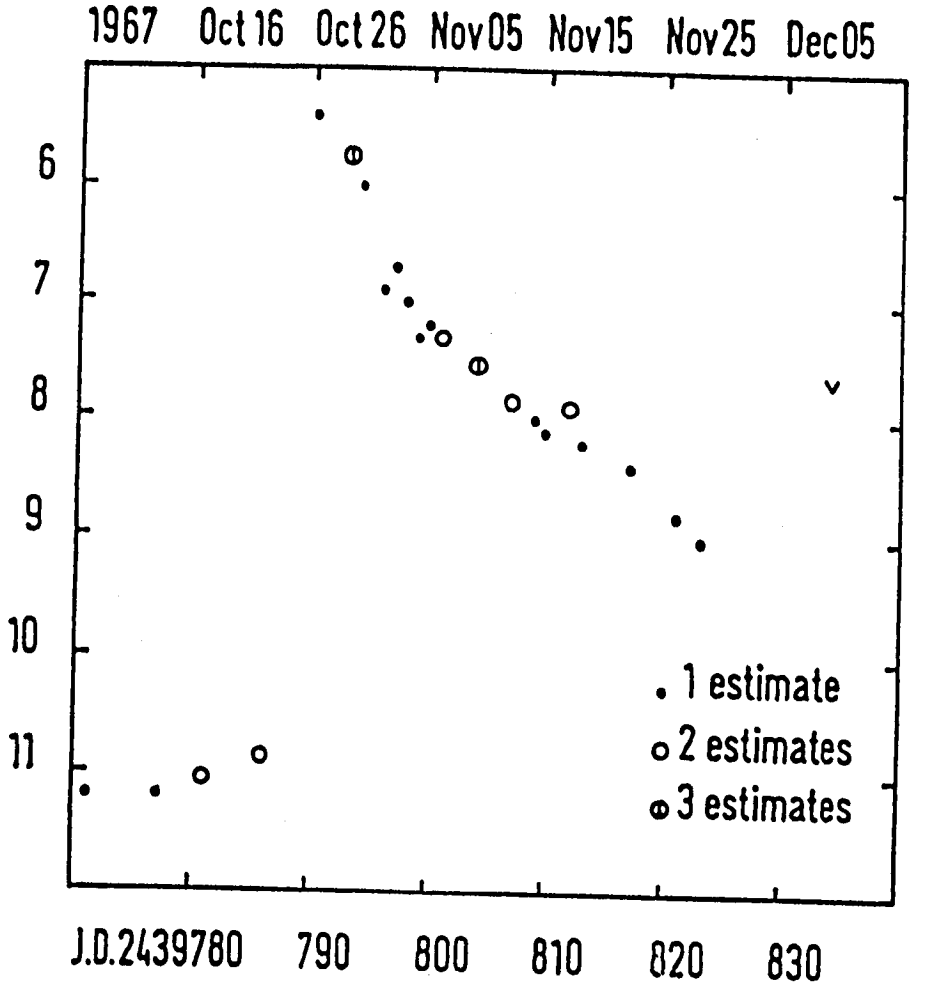

Figure 7.5. Visual light curve of the 1967 outburst of RS Oph. Reproduced from Isles (1974).

outburst. Isles (1974) noted that, as far as the visual light curve was concerned, RS Oph was 'back to normal' by 200 days after outburst.

7.5.2 Spectroscopic Observations

As mentioned before, this outburst was not as well monitored as it might have been. However we do have some spectroscopic observations of this outburst covering most times apart from those when the nova was behind the sun.

Wallerstein & Cassinelli (1967) and Barbon et al. (1968) had been constantly observing RS Oph since the previous outburst. They both obtained spectra about 4 months before this outburst. The first authors saw at this time a shell of moderate excitation with emission lines of hydrogen, helium and FeII. They noted that, throughout their observations, there had been no unambiguous spectral changes that would indicate the likelihood of another outburst. Barbon et al. (1968) saw much the same, i.e. an intense continuum with emission lines of neutral helium and FeII moderately strong. These authors then made extensive observations of the star from October 27 to December 2 1967.

On October 27 the spectrum was characterized by wide emission lines, which were bordered on the blue side by two systems of broad absorptions corresponding to velocities of ~ 2700 km s^{-1} and 3900 km s^{-1}. Visible at the centre of the emission bands was a narrow absorption line, bordered on the red by a sharp emission. As in the previous outbursts the radial velocity of these sharp lines was ~ 40 km s^{-1}. This was the value measured by Sandford (1947) for the radial velocity of the star hence virtual confirmation that the narrow lines arose in a stationary envelope surrounding the nova. In the next few days the absorption systems faded and eventually disappeared. In the time interval October 27 - November 7 the HeI emission lines became stronger than all the others with the exception of Hα and N_2. As the excitation increased the neutral helium

lines weakened and by November 8-9 some lines of highly ionized species were seen and rapidly increased in intensity.

As in previous outbursts coronal lines appeared in the spectrum of this star. Barbon et al. (1968) suggested that the first coronal line to appear was [FeX] λ6374 which was present on November 3, six days after outburst, in a blend with [OI] λ6364. By December 3 this line was stronger than Hβ.

RS Oph was also observed by Code (1968) on 1967 November 7 and 9 and he recorded in great detail the appearance of the spectra at these times. He found much the same as the previous authors. Even on November 8 the spectrum (as before outburst) was characterized primarily by strong broad emission lines of hydrogen, HeI and FeII. Code (1968) found no obvious displaced absorption components although he observed that the violet wings of the hydrogen emission bands were more diffuse and extended than they had been before. The [SII] λ4068.6, 4076.2 lines along with the SiII lines rivalled in strength and width those of hydrogen, HeI and FeII at this time. Present also as weak broad lines were those of MgII λ4481 and CII λ4267. Broad lines of higher ionization stages were present but extremely weak; HeII λ4686, λ4200 and NIII λ4640 - λ4634 were also visible.

Code also noticed the sharp emission lines observed by Wallerstein & Cassinelli (1967); the forbidden lines [OIII] λ4363, [NeIII] λ3869 and λ3968 were the strongest. He also observed some sharp FeII lines. The only absorption features he saw were sharp CaII H and K lines, the radial velocities of which were ~ -50 km s^{-1}, comparable with the velocities measured by Barbon et al. (1968). Code found that the only significant difference between his two spectra was a small increase in the intensity of the HeI lines relative to those of hydrogen and FeII, and a weakening of the sharp emission lines.

When RS Oph had reappeared from behind the sun Barbon et al. (1968) recommenced observations. On 1968 February 3 the HeI lines (except at

λ5876) and FeII lines had faded away, the observed lines were now of extremely high excitation. The strongest lines were the Balmer lines and HeII λ4866, after which came λ6827, seen in previous outbursts but possibly due to [KrIII], [FeX] λ6374 still stronger than Hβ, [AX] λ5535, [FeXIV] λ5303, [OIII] λ 4363, [NiXIII] λ5116 and [NiXIII] λ4231. The [OIII] lines were 'fuzzy' in appearance which was quite different from the other lines. By March, when the star was at its minimum, the excitation began to decrease. The coronal lines weakened with [AX] λ5535 and [FeXIV] λ5303 gone, although [FeX] λ6374 was still conspicuous. At this point [OIII] λ4959 - λ5006 became extremely strong. NII λ5755 was then stronger than HeI λ5876 and [FeVII] λ 5160, which was barely visible in February, became conspicuous. On the penultimate spectrum obtained by these authors, taken on May 7, the nova was fainter than its 'normal' brightness at ~ 13.3 mags. The coronal lines had disappeared, while [OIII] λ5006 with HeII λ4686, HeI λ5876, and in the ultraviolet the two [NeIII] lines λ3967 and λ3689 were all stronger than Hγ at this time. On the last spectrum obtained, taken in August, all these lines were still present although they were very weak.

Wallerstein (1969) obtained two spectrograms of this object on 1969 February 18, 110 days after outburst. His identifications of the emission lines are listed in Table 7.8. They showed coronal lines with [FeX] at nearly the same strength as Hβ, with most other emissions due to hydrogen, HeI or FeII. From the nine emission lines most easily measured he derived a radial velocity of ~ 47 km s^{-1}. He noted that this was quite close to the velocities of the lines measured in the premaximum spectrum (Wallerstein & Cassinelli, 1968) and spectulated that this may have indicated that the explosion could have been quite symmetric.

He also observed the continuum and any absorption lines that were present. A weak continuum was seen that increased in intensity up to ~ 6400A. From his spectra he compared the intensity at 5560A to that at 6670A and matched the continuum distribution with that of standard stars.

Table 7.8

Line identifications in the 1967 postmaximum spectra of RS Oph.

λ(A)	Identification	λ(A)	Identification
4861	Hβ	6086	-
4922	FeII + HeI	6106	-
4959	[OIII]	6181	-
5007	[OIII]	6236	FeII + ?
5015	HeI	6248	FeII
5018	FeII	6300	[OI]
5169	FeII	6348	SiII
5303	[FeXIV]	6374	[FeX]
5317	FeII	6417	FeII
5347	FeII	6433	FeII
5362	FeII	6456	FeII
5411	HeI	6516	FeII
5535	[AX]	6563	Hα
5577	[OI]	6678	HeI
5616	[CaVII]	6758	-
5630	[FeIV] + [CaV]	6826	[KrIII]
5694	[CaXV]		
5755	[NII]		
5876	HeI		
5991	FeII		

These lines were identified in the postmaximum spectrum of RS Oph obtained 110 days after the 1967 outburst. Reproduced from Wallerstein (1969).

He found that the continuum corresponded to a star later than G0 and earlier than K5 when taking into account the uncertainties in the reddening. The spectral type agreed with the 16 absorption lines that he identified as being due to FeI, CaI, SiI and BaII. The intensities of the BaII lines indicated that the star was at least as luminous as a giant. Wallerstein suggested that the star was in fact a K0III star.

On measurement of the radial velocities implied by the absorption lines he found them to be about 10 km s^{-1} more negative than the absorption line velocities observed between outburst at ~ -54 km s^{-1} (Wallerstein & Cassinelli, 1968). In view of this discrepancy he was undecided as to the origin of these lines, however whether or not this velocity difference was real is debatable due to the observational errors.

Barbon et al. (1968) also attempted to classify the star using data obtained between outbursts. Spectra taken in 1962 showed wide absorption bands of moderate strength at λ6350 - λ6158, λ6030 - λ5890, λ5780 - λ5635, λ5460 and λ5107 also the NaI doublet λ5890 - λ5896 was prominent. On comparison with standard spectra of advanced type stars the authors suggested a stellar classification of M2III, although they did admit some of the lines may have been due to interstellar absorptions. This result was in constrast to the classification of Wallerstein (see above).

7.6 The 1985 Outburst

7.6.1 The Light Curve

The most recent outburst of this object was discovered by Morrison (1985) on 1985 January 26 when the star, which had been at a visual magnitude of ~ 10.6 on the previous days, was found at a visual magnitude of 6.8 and still rising. It was thought that the star obtained its maximum flux the following day. On 1985 January 28 the visual magnitude of RS Oph was 5.2 (Rosino, 1986).

Fig. 7.6 shows the visual light curve as composed of all the data in the IAU Circulars for this object over the period January 22 until May 30. It shows the usual steep decline, the time taken to fall by the first 2 mags was 7 days, while the time taken to fall by the first 3 mags was 22 days. This initial decline was at a rate of 0.375 mag d^{-1}. From January 31 until March 6 the light curve appeared to be behaving in an oscillatory manner. The oscillations were of order 0.5 mag over a six day period although the curve was still in decline, falling by 0.8 mag until these oscillations stopped around April 8. After this date the little data obtained showed quite large variations. On April 17 the star was at 10.7 mags whilst on April 20 it was at 9.6 mags. By May 20 it had fallen to 12.3 mags although on June 27 this had risen to 11.5 mags. These observations were taken by a variety of observers so the variations may not have been quite as large in reality but it did appear that the star did not settle down to a constant magnitude after outburst. Fig. 7.7 shows a combined light curve of all the outbursts and emphasizes their remarkable similarity regardless of the time between outbursts.

Throughout the 1985 outburst astronomers were able to follow RS Oph at many frequencies, due to advances in astronomical technology. As a consequence, as well as a visual light curve, radio, X-ray and infrared light curves were obtained. These, with the exception of the infrared light curve, will be discussed now (infrared observations of RS Oph are discussed in chapters 8 & 9).

7.6.2 Radio Light Curve

RS Oph was the first recurrent nova to be detected at radio frequencies when Padin et al. (1985) detected it at 5GHz on 1985 February 13, 18 days after the optical maximum. On this day they recorded a flux density of ~ 23 mJy and subsequent observations on February 15 revealed an increase in flux density. Fig. 7.8 shows observations of the radio light

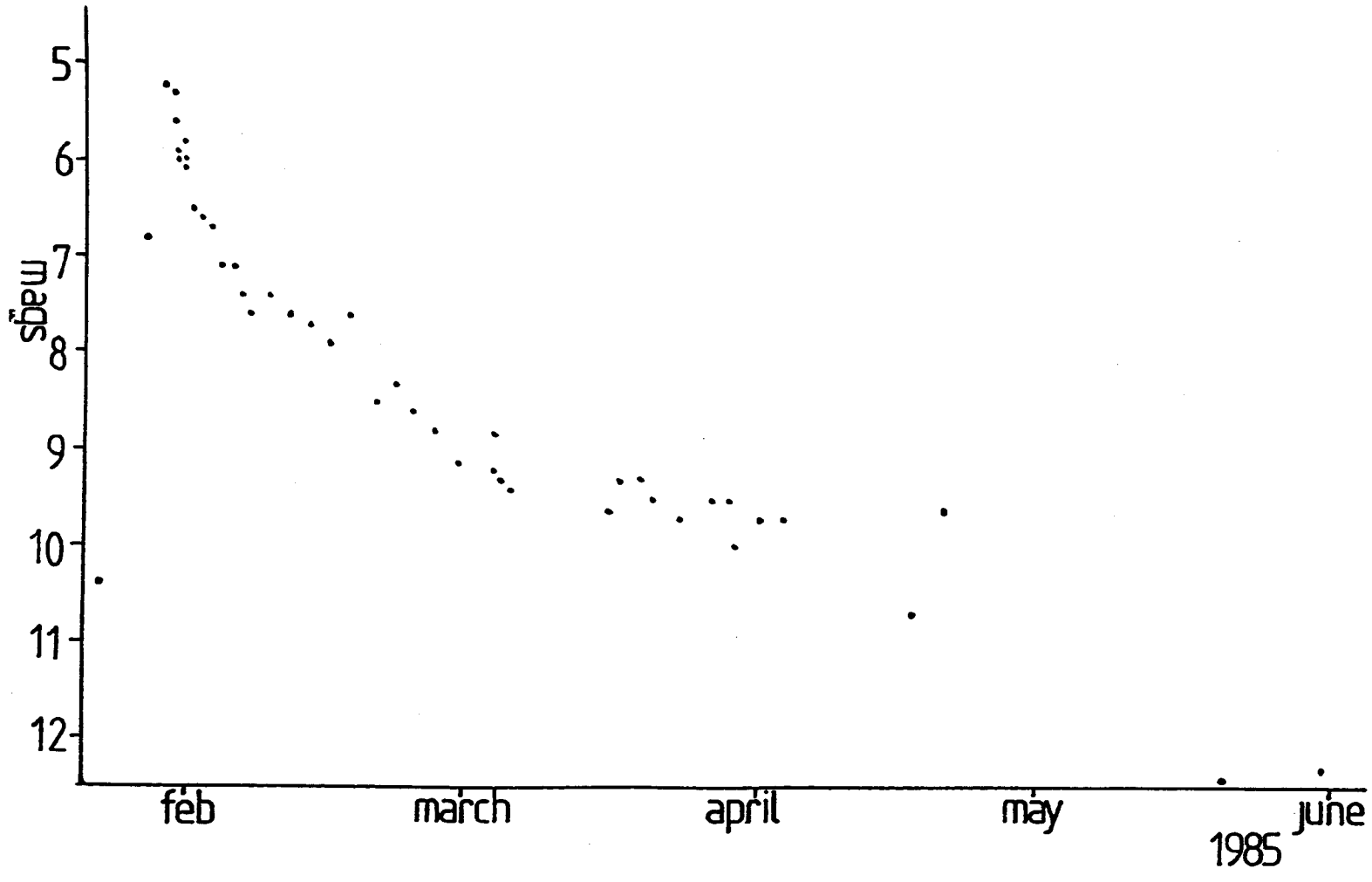

Figure 7.6. Visual light curve of the 1985 outburst of RS Oph. (From IAU Circulars).

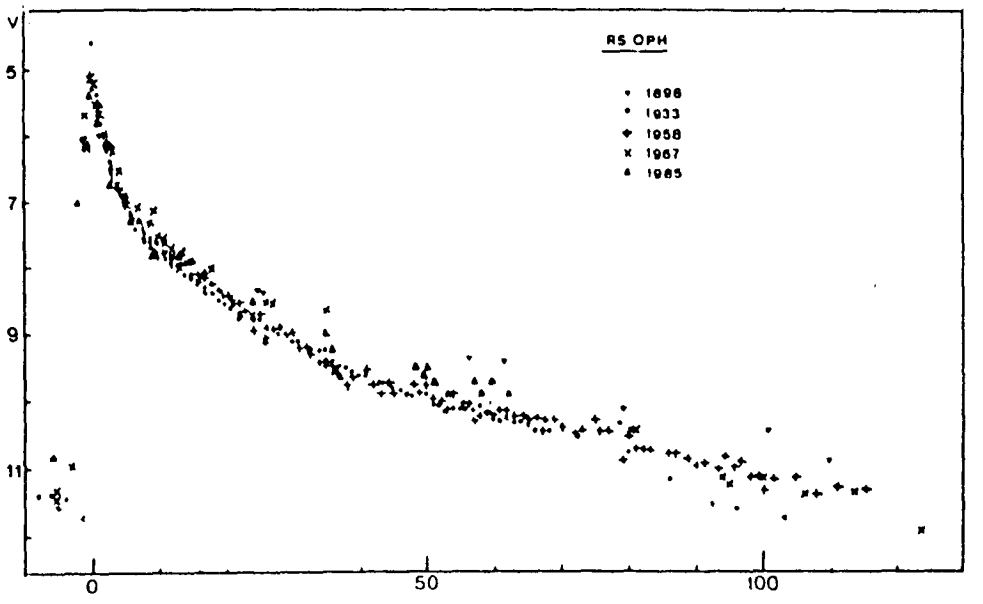

Figure 7.7. Combined visual light curve of all the recorded outbursts of RS Oph. Note the remarkable similarity of the curves. Reproduced from Rosino (1986).

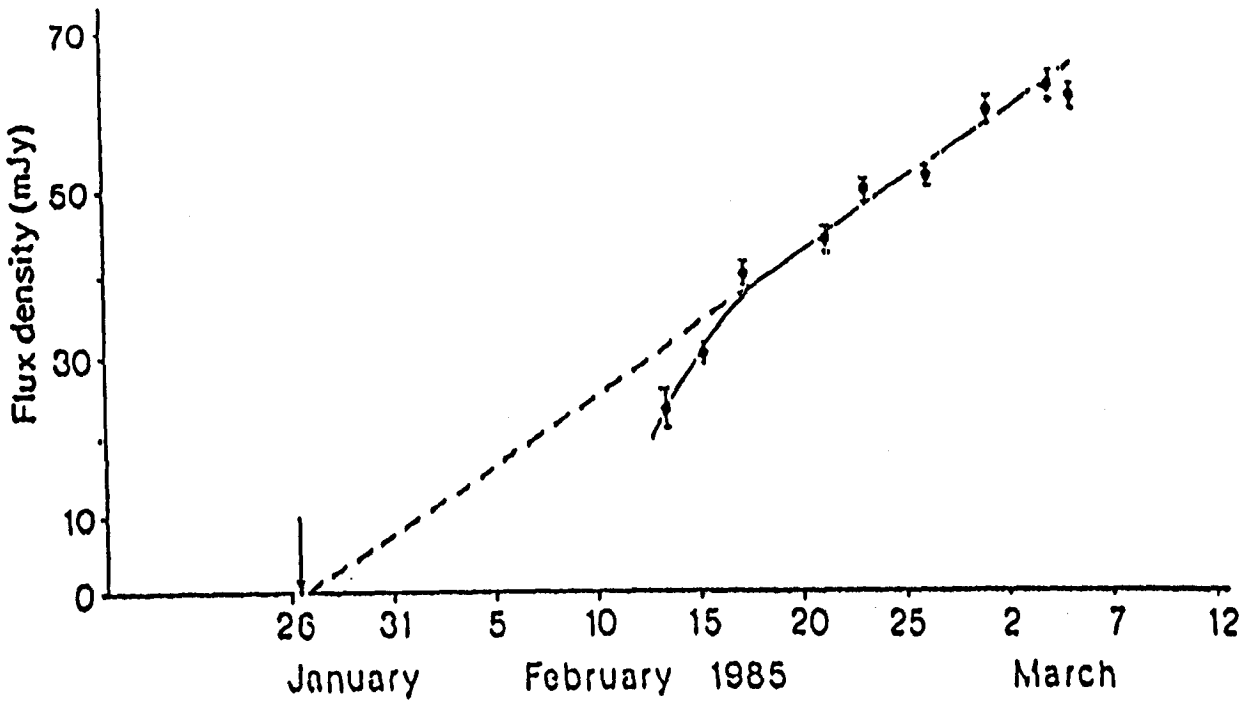

Figure 7.8. Radio light curve for RS Oph (1985) measured at 5 GHz with left-hand circular polarization. The vertical arrow indicates the time of the optical outburst. Reproduced from Padin et al. (1986).

curve between 1985 February 13 and March 5. It reveals two phases in the radio development of this object. Initially there was a rapid increase in flux density of ~ 4 mJy d^{-1} until February 18; this then gave rise to a slower linear increase which projected back to the time of the initial outburst and gave a $(t-t_0)$ dependence which had a constant of proportionality ~ 1.7 mJy d^{-1} (this is characteristic of classical radio novae). The authors suggested that the intial rapid rise indicated that the radio emission 'turned on' about 14 days after the nova explosion, but in a further 10 days it had reached the $(t-t_0)$ curve. Thus, they argued, although the radio emission was 14 days late in turning on, after 24 days the curve proceeded as if the emission had started at time t_0. Assuming a distance of 2 kpc and an average expansion velocity of 1000 km s^{-1}, they calculated a brightness temperature $T_b \sim 10^7$K.

Further observations relevant to this work were discussed by Davis (1986). At 5GHz the outburst reached its peak after 37 days and then decayed to half power (30 mJy) after a further 40 days (see Fig. 7.9). The decay curve was fitted by a $(t-t_0)^{-1.3}$ expression. Fig. 7.10 shows the spectral behaviour of a low frequency spectral index between 1.5 - 5GHz and a high frequency spectral index between 15 - 22GHz near the peak of the outburst. (The spectral index α is defined as $S \propto \nu^{+\alpha}$, where S is the flux density). The low frequency index started off inverted and became flat after the peak, whereas the high frequency index started off flat and became significantly inverted. Davis suggested that these results indicated a two component spectrum with an optically thick high frequency component emerging after the peak of the event.

In classical novae the radio emission detected is thermal and exhibits a brightness temperature $T_b \sim 10^4$K. During the optically thick phase they typically have a spectral index of ~ +1.5 (Hjellming et al. 1979). Such a difference in RS Oph's radio light curve led Padin et al. (1985) and Davis (1986) to suggest a non-thermal mechanism for the low frequency emission.

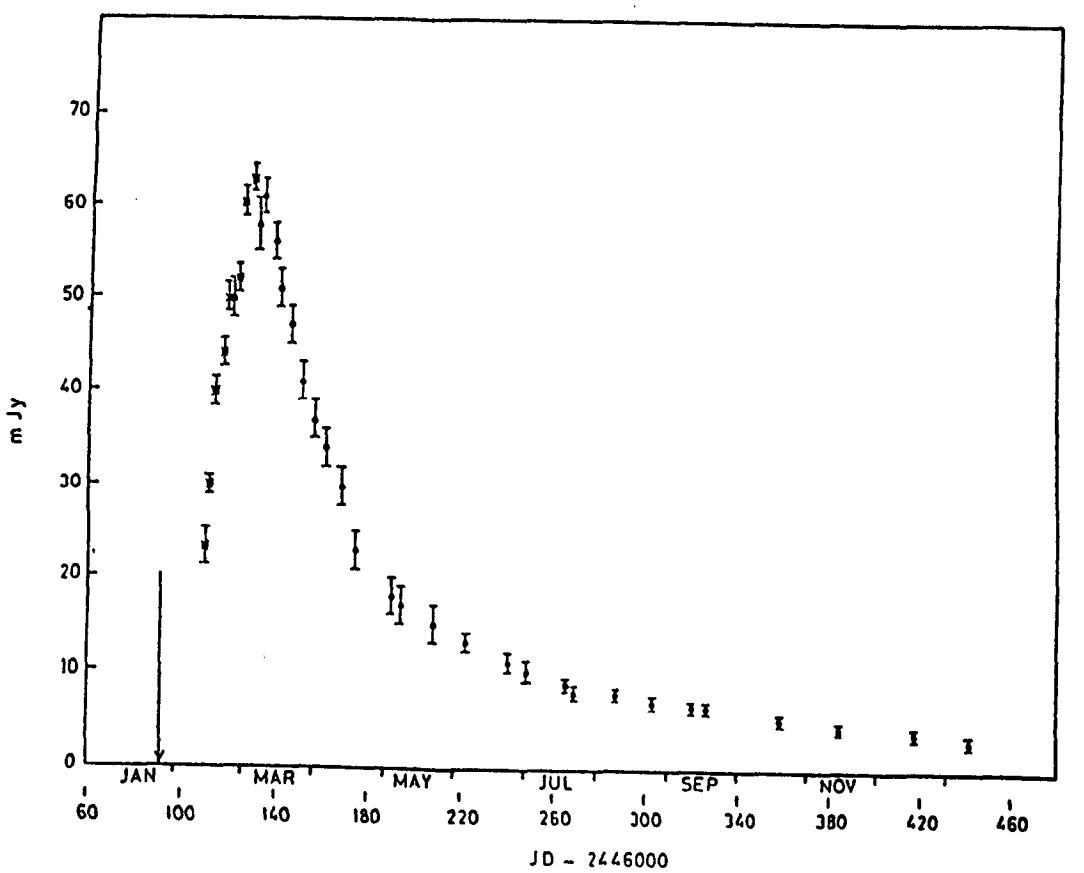

Figure 7.9. 4.9 GHz light curve of RS Oph at the 1985 outburst. The arrow marks the time of the outburst. • represents the data obtained at the VLA, and x represents data obtained at Jodrell bank. Reproduced from Davis (1986).

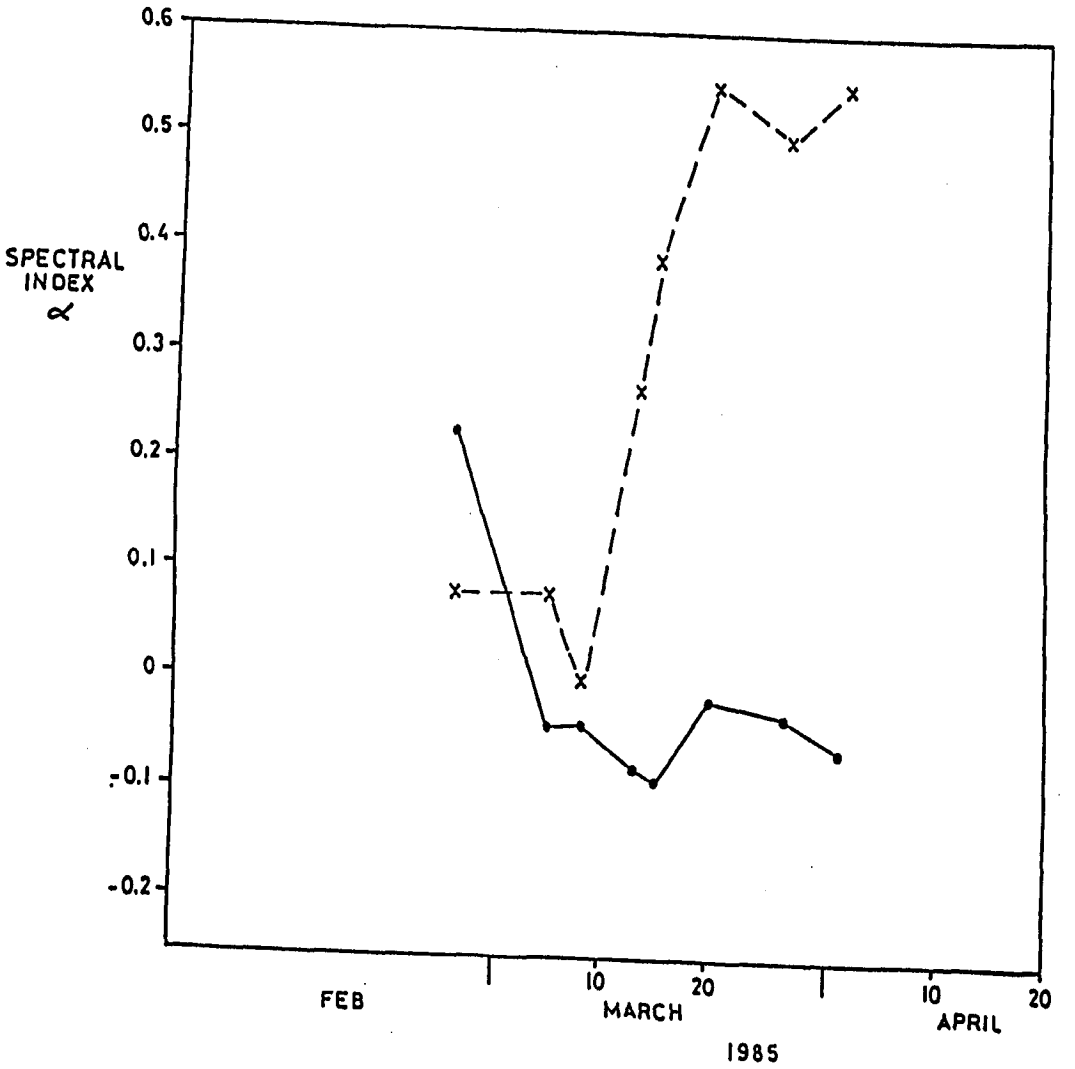

Figure 7.10. Spectral index α defined as $S \propto \nu^{+\alpha}$ for intial phase of the 1985 outburst. • gives α at 1.9GHz and 5GHz; x gives α at 15GHz and 22.5GHz. Reproduced from Davis (1986).

Their idea for the origin of this non-thermal emission was that it was caused by the interaction of the ejecta with the preoutburst envelope.

Extensive radio observations were undertaken by Hjellming et al. (1986). They observed RS Oph between 1985 February 24 - 1986 January at frequencies of 1.49, 4.85, 4.885, 14.94 and 22.46GHz. Fig. 7.11 plots these radio light curves. The radio source flux peaked at March 8 for 1.49GHz, March 3 for 5GHz, on or before March 5 for 15GHz, whilst the peak at 22GHz may have occurred before March 5 or was roughly constant at maximum between 5-15 March. At 1.49GHz a power law with spectral index α = -1.68 was present during day 60 - day 220 (after outburst); thereafter α = -1.02. At 4.9GHz α = -1.26 between days 80 - day 340; whereas at 15GHz α = -1.1 at day 60 but changed to -2.09 after ~ 140 days. Hjellming et al. found that at least two radio components existed from roughly March - July 1985, one with a negative spectral index between 1.4 - 5GHz and the other which had a positive spectral index at frequencies above 5GHz. In August the component with the positive spectral index became completely dominant in the decaying spectrum. The spectral index between 4.9 - 15GHz rose linearly from ~ 0.1 on March 5 to ~ 0.5 60 days after the outburst and then declined until it reached ~ 0 on day 270. The spectral index between 1.49 - 4.9GHz stayed at ~ -0.08 from the peak on March 5 until day 100, then it rose linearly in time reaching 0 at ~ day 130. At day 200 α ~ 0.2 and after that it declined roughly linearly with time until ~ 0.1 at day 330.

The data at 15GHz suggested that the radio source was both resolved and expanding at high velocities. The authors calculated a velocity of ~ 2100 km s^{-1} when assuming that its distance was 1.7 kpc and it was expanding symmetrically. There were however indications of asymmetry with the source more resolved in the EW direction.

Like Padin et al. (1985) and Davis (1986), Hjellming et al. (1986) also measured the brightness temperature and found the averaged T_b at 15GHz ~ 10^5K with inferred or probable values of 10^6K - 10^7K if the radio sizes

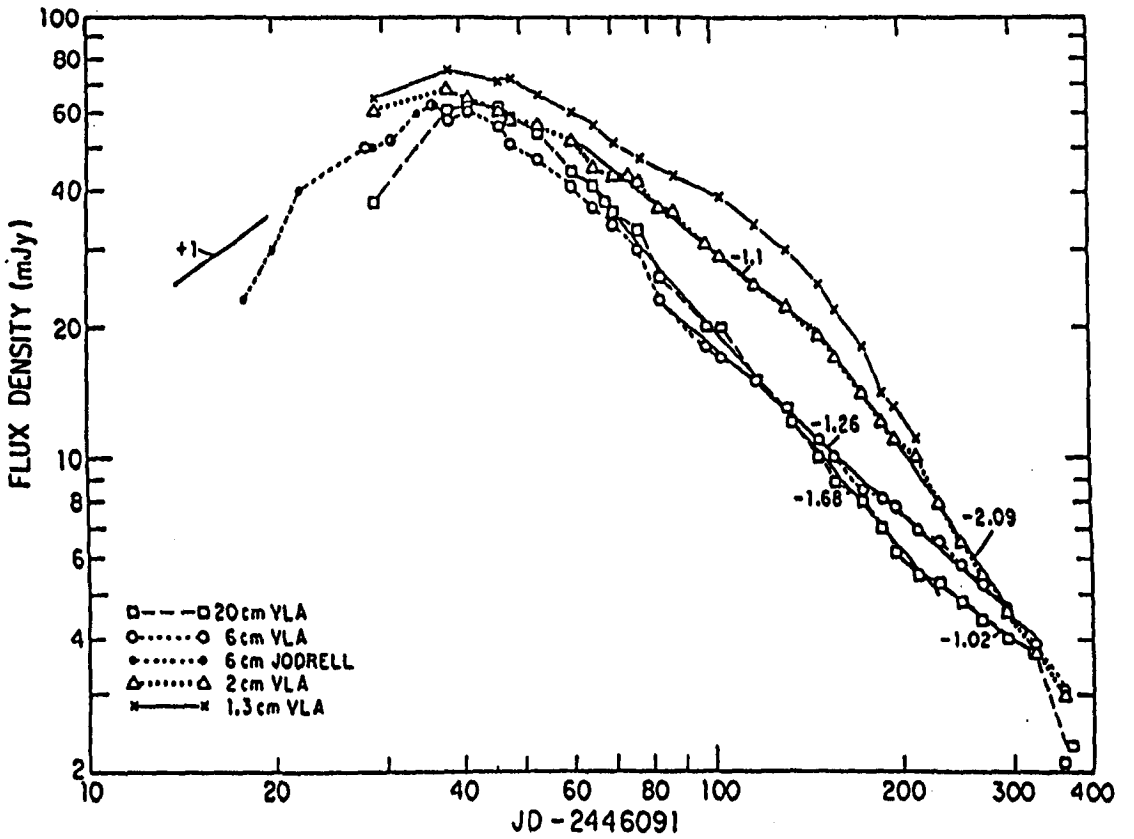

Figure 7.11. Radio flux densities of RS Oph plotted as a function of time since the 1985 outburst for the period between 1985 February 24 and 1986 January 31 at frequencies between 1.49GHz and 22GHz. The data for each frequency are connected with dashed lines, whilst solid lines indicate power-law segments with nearby numbers corresponding to the power-law exponent. Reproduced from Hjellming et al.(1986).

were the same at all frequencies. From the strength of the 21cm absorption line the distance to RS Oph was inferred to be ~ 1.6 kpc.

Although the basic trends found in these observations were like those in the previous data, the two sets of authors do not agree on the origin of the radio emission. They both agreed that it was non-thermal but Hjellming et al. disagreed that it was due to a self-absorbed synchrotron radio source related to a shock. This was because they considered that, for such a model, the decay of a single power law with a clearly defined spectral index, would be expected and not the complicated set of frequency dependent decays observed. Instead they suggested that it was likely that the material ejected with velocities $\geqslant$ 2000 km s^{-1} was associated with a non thermal component prominent in the radio spectra for the first 150 days, similar to that which arises from radio jets. The inverted spectrum component that decayed by a factor of ~ 20 whilst its spectral index changed from ~ 0.5 to 0 was attributed to a self absorbing synchrotron radio source, or, if the observed high frequency component was optically thin, the emission could have been gyrosynchrotron radiation. In this case the gyrosynchrotron emission of 300 - 500KeV electrons radiating in a magnetosphere in the binary system with magnetic fields upto 5000G could explain the complex spectral developement of the system.

Using VLBI Porcas et al. (1986) on 1985 April 13 compiled a radio map of RS Oph at 1.7GHz. The total flux density was ~ 30 mJy. This map is shown in Fig. 7.12. They found that more than 80% of the total flux of the source was seen in this structure. The emission was elongated in position angle ~ 84^{0} and possibly unresolved perpendicular to this direction. The extensions (probably symmetric) reached a distance of 200AU and had an average expansion velocity of ~ 4000 km s^{-1} 77 days after outburst, on assuming a distance of 2 kpc. The average brightness temperature over the structure was calculated to be ~ 1.5 x 10^{6}K in the central regions, consistent with the other radio work.

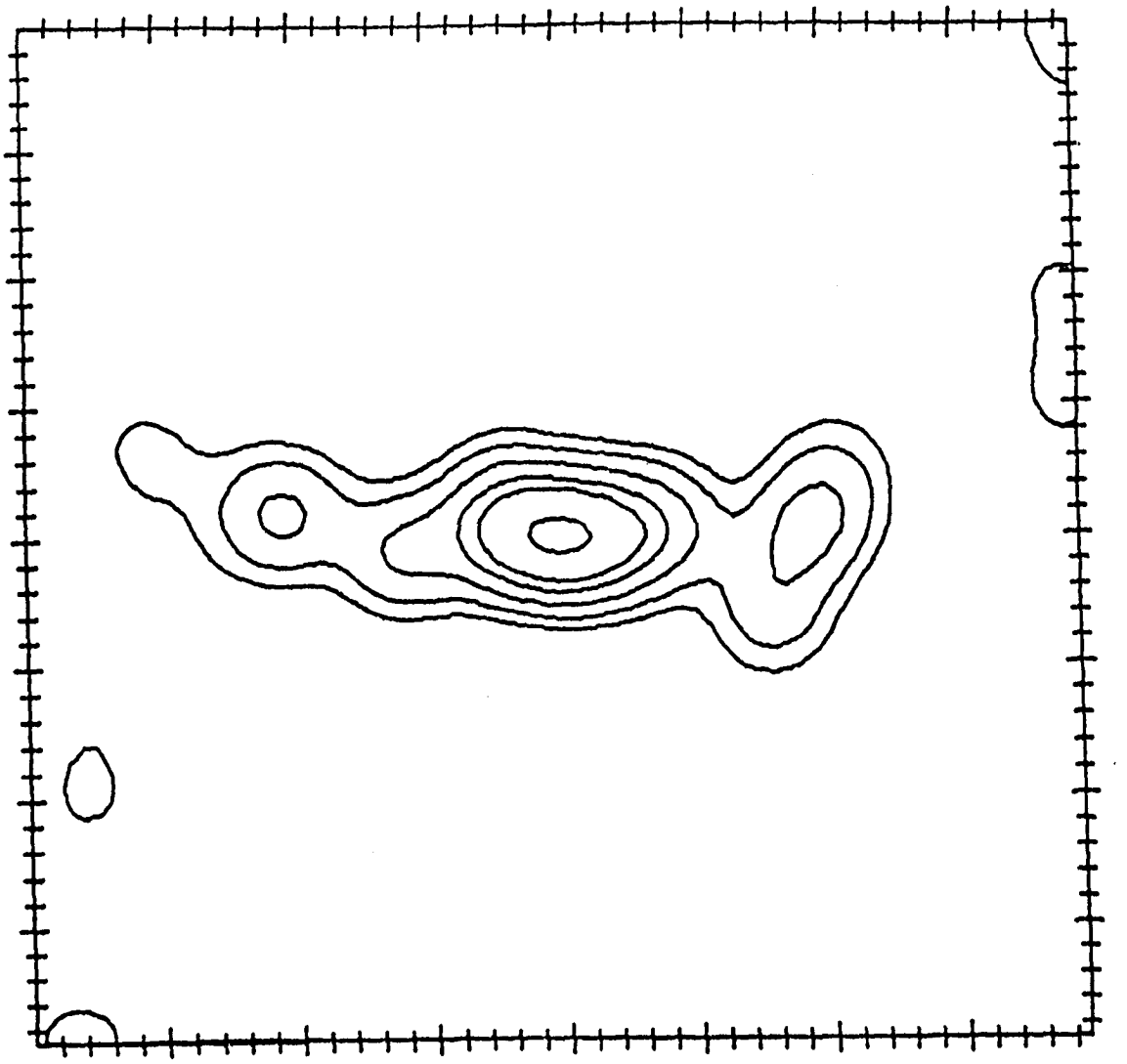

Figure 7.12. VLBI map of the structure of RS Oph, with resolution 35 m.a.s. Tick intervals = 10 m.a.s. Contour intervals are, 5, 10, 20, 35, 50 & 90% of peak brightness. Reproduced from Porcas et al. (1986).

One of the most surprising observations of this nova was a detection of a 'radio flare'. Spoelstra et al. (1987) discussed the conditions in the remnant that could have given rise to this phenomenon, which was seen at 5GHz on 1985 March 7 at a flux of 82 mJy, 20 mJy above the average level before and after the event. Fig. 7.13 shows the 'radio flare' that was thought to have lasted no longer than 24 hours. The authors have modelled this event as a region of magnetic field line reconnection, rather similar to that of a solar flare.

7.6.3 X-ray Light Curve

X-ray data were collected by EXOSAT as soon as RS Oph was far enough away from the sun to start observations, thus observations were started on 1985 March 22, 54 days after the peak of the optical outburst. Spectral information was obtained in the range 0.04KeV to 2.0KeV and the range 1.5KeV to ~ 15KeV. An X-ray light curve in the lower frequency range was obtained by Mason et al. (1986) and is shown in Fig. 7.14. They detected a count rate of almost 0.5 count s^{-1} at these frequencies, which made it one of the brightest sources ever detected by EXOSAT. The source then decayed over the next two months, slowly at first and then more rapidly, however despite this steep decline in April and May a significant residue emission was still detected during the final observation in October 1985, 250 days after optical maximum. On March 22 they found that the count rate rose steeply towards low energies and that the source was only detected below ~ 5KeV implying a very soft spectrum. When they attemped to fit the data from the low energy range with various simple spectral models, including hydrogen free-free emision, a power law spectrum, a blackbody spectrum and the spectrum of an optically thin line emitting plasma, they came to the conclusion that none of these provided an acceptable fit. A combination of two hydrogen free-free models with temperatures of 3.5×10^6K and 9.0×10^6K did fit, but this model required an unacceptably

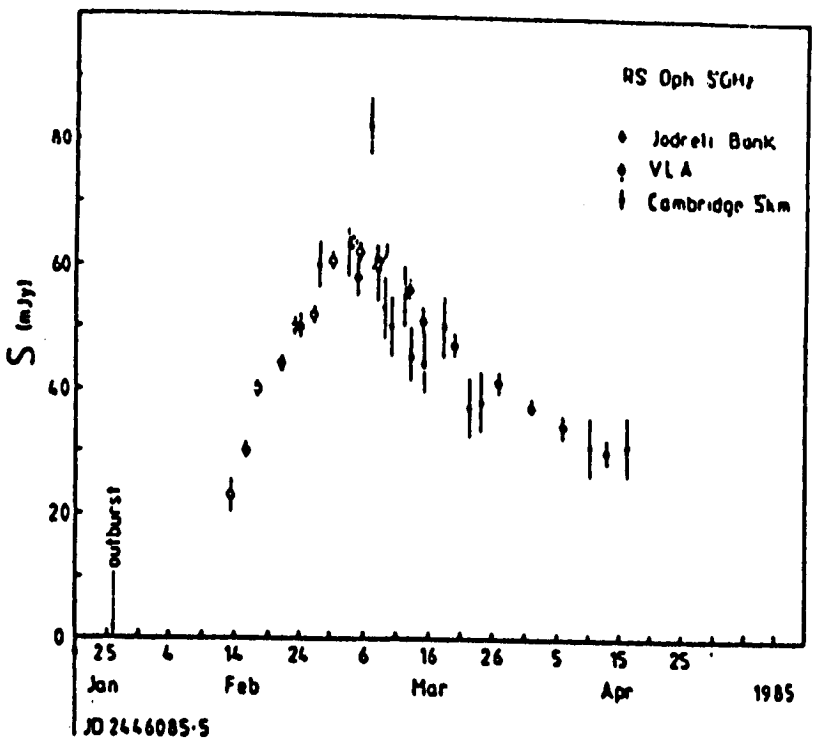

Figure 7.13. The 5GHz light curve for RS Oph with the 'radio flare'. Reproduced from Spoelstra et al. (1986).

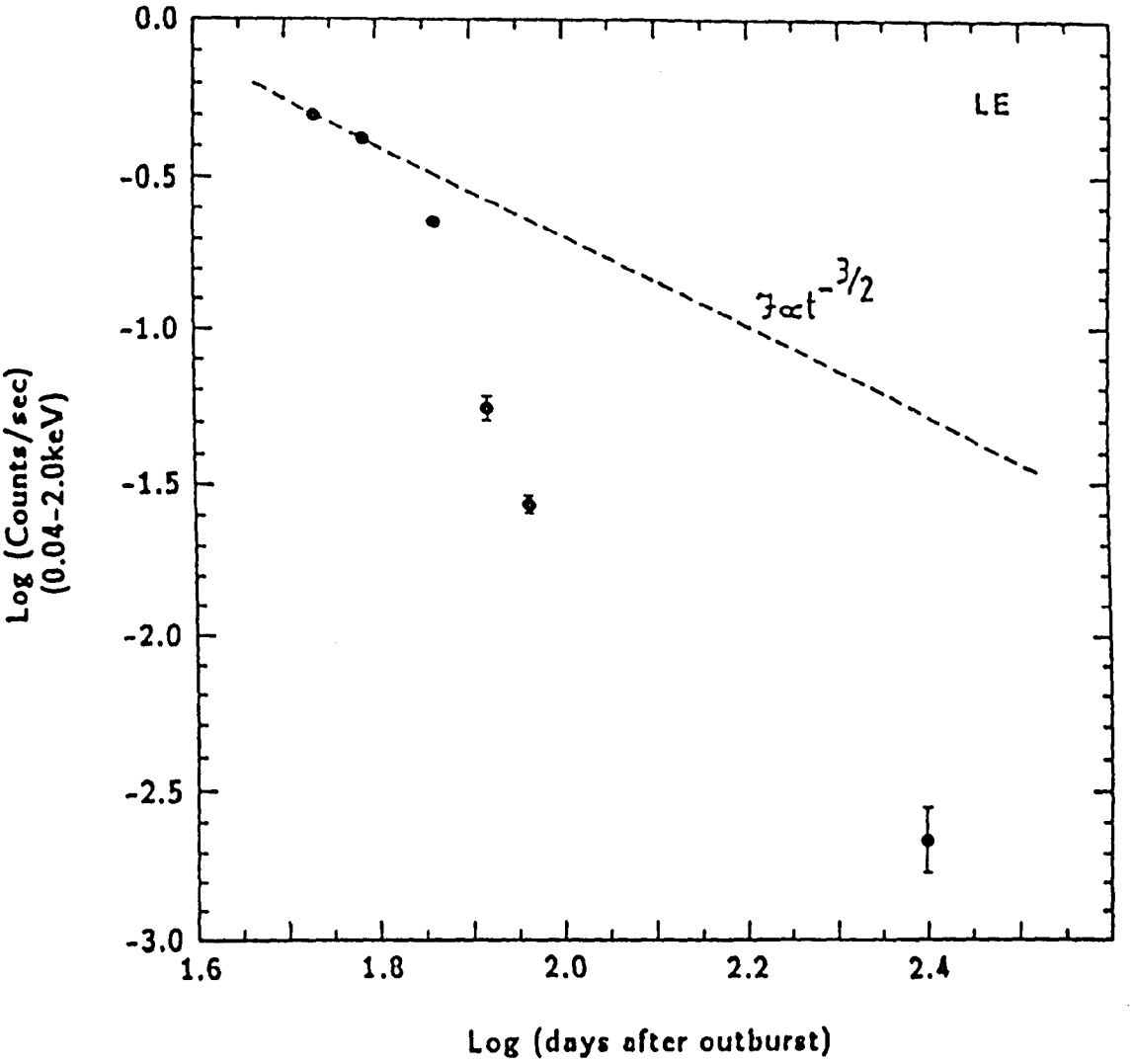

Figure 7.14. X-ray light curve for the 1985 outburst of RS Oph. The dashed line is the expected decay rate of the x-ray flux according to the model of Bode & Kahn, 1985 (see text). Reproduced from Mason et al. (1986).

low value of the interstellar absorbed. However they used this fit to estimate the total flux detected between ~ 1KeV - 6KeV to be about 1.5×10^{-10} erg $cm^{-2}s^{-1}$ on this date. However because the source was so soft they thought that this was no more than ~ 10% of the flux emitted in this band by RS Oph as the remainder would be absorped in the interstellar medium.

Using the data from the first 5 observations by EXOSAT the count rate in the two energy ranges was plotted. The results were consistent with there being a constant ratio between the count rate in the two ranges which suggested that there was no substantial change in the overall spectrum of the x-ray source as it decayed.

The authors suggested that the X-ray emission arose from shocked gas as the ejecta slammed into the pre-existing circumstellar shell, this pre-existing shell already being deduced from optical observations (see section 7.4.2). The reasons for this suggestion were that strong X-ray emission was seen a long time after the optical outburst (although it was somewhat unfortunate that X-ray detections could not have been made immediately after outburst); there was no short timescale variability detected in the X-ray flux which was consistent with emission from an extended source; the expected theoretical temperature from shock heated gas was consistent with the observed temperatures and their preliminary comparison indicated the flux and evolution of the optical coronal emission lines was consistent with them originating in the same hot gas that produced the X-ray emission. The X-ray emission that was left after 200 days was suggested to originate from the surface of the white dwarf primary where the thermonuclear burning was still thought to be persisting.

Bode & Kahn (1985) and O'Brien et al. (1986) attempted to model such X-ray emission assuming the shock origin of the X-rays. By assuming that the energy in the remnant was constant they showed that the shock radius varied with time as $r_s \propto t^{2/3}$. They then calculated the expected behaviour

of a shock wave expanding into the pre-existing circumstellar envelope (which they assumed was formed by the stellar wind of the secondary). They assumed spherical symmetry and found that, after 34 days, the inner parts of the remnant were cold, leaving a hot shell of constant thickness just in front of the shock and the luminosity of this shock heated envelope fell as $t^{-3/2}$.

This model was consistent with the first two X-ray observations (as shown in Fig. 7.14) but the subsequent points fell away much more steeply than a $t^{-3/2}$ relationship. This may be because, after this time, the blast wave had reached the edge of the preoutburst envelope. The assumption of spherical symmetry also over-simplified the situation as in the light of the radio observations (see previous section), this was clearly not the case.

7.6.4 Visual Spectroscopy

As mentioned before, advances in astronomical technology during the time preceding the 1985 outburst of RS Oph meant that this outburst was monitored in most available wavebands. Such extensive spectral coverage has enabled a greater understanding of this object.

Rosino & Iijima (1986) observed this star extensively from 2 weeks after maximum on 1985 February 10 until November of that year. The observations were carried out in the optical region of the spectrum from λ3900 - λ6600 and in the near infrared from Hα to λ9000 (these observations will be included here for completeness).

The spectra on February 10 were characterized by the presence of broad emission bands of hydrogen (Hα - Hζ), and narrow emissions of FeII, NiII, SiII and OI λ8446. The strongest Balmer and neutral helium lines were accompanied by two weak diffuse systems of blue-displaced P Cygni absorptions having mean radial velocities of -3500 km s^{-1} to -1650 km s^{-1}. Hα was extremely strong, with a complex asymmetric profile, which was

steeper on the blueward side, possibly due to superposed diffuse P-Cygni absorptions. Three days later emerged the NIII-OIII blend at λ4640-50, the HeII λ4686 line and, weakly, the coronal line [FeX] λ6374. During February 13 - February 21 the HeII λ4686 line rapidly strengthened whilst various other coronal lines emerged. Anupama & Prabhu (1985), on February 27, observed strong Hα, P_{11}-$_{15}$, and lines due to HeI with weaker, but still noticeable, coronal lines of [FeX] λ6374 and [FeXI]. Subsequently all the lines became narrower and the coronal lines strengthened. They observed [AXI] λ6919 in March and April while in the blue-green region during that time they saw Hβ, and lines due to HeI, HeII, NIII as well as coronal lines.

These observations were essentially similar to those of Rosino & Iijima (1986) which were taken almost simultaneously. They saw all the above mentioned lines and noted that the continuum was crowded by a multitude of emission lines, amongst which the strongest were of hydrogen and helium. Also prominent were the coronal lines and the forbidden lines of [OIII] λ5007 - λ4959, λ4363 and [NII] λ5755. In the near infrared the strongest lines were [FeXI] λ7891, OI λ8446 and HeI λ7065, followed by the hydrogen Paschen lines.

At this time Krautter (1986) also obtained visual spectra of RS Oph. He found much the same as the previous two authors, i.e. apart from the interstellar absorption lines the spectra were dominated by emission lines. The most prominent were the hydrogen Balmer lines, HeI, HeII, FeII and those due to other singly ionized metals. Very conspicuous were the coronal lines due to highly ionized states of iron which were amongst the strongest lines in the spectrum. Generally much weaker than the coronal lines were the forbidden lines, which arose in neutral atoms or ions of the lower ionizational states such as [OI], [OIII] and [NII].

Fig. 7.15 shows tracings of two characteristic emission lines HeI λ5876 and [FeX] λ6374. The line profiles were very complex and seemed to

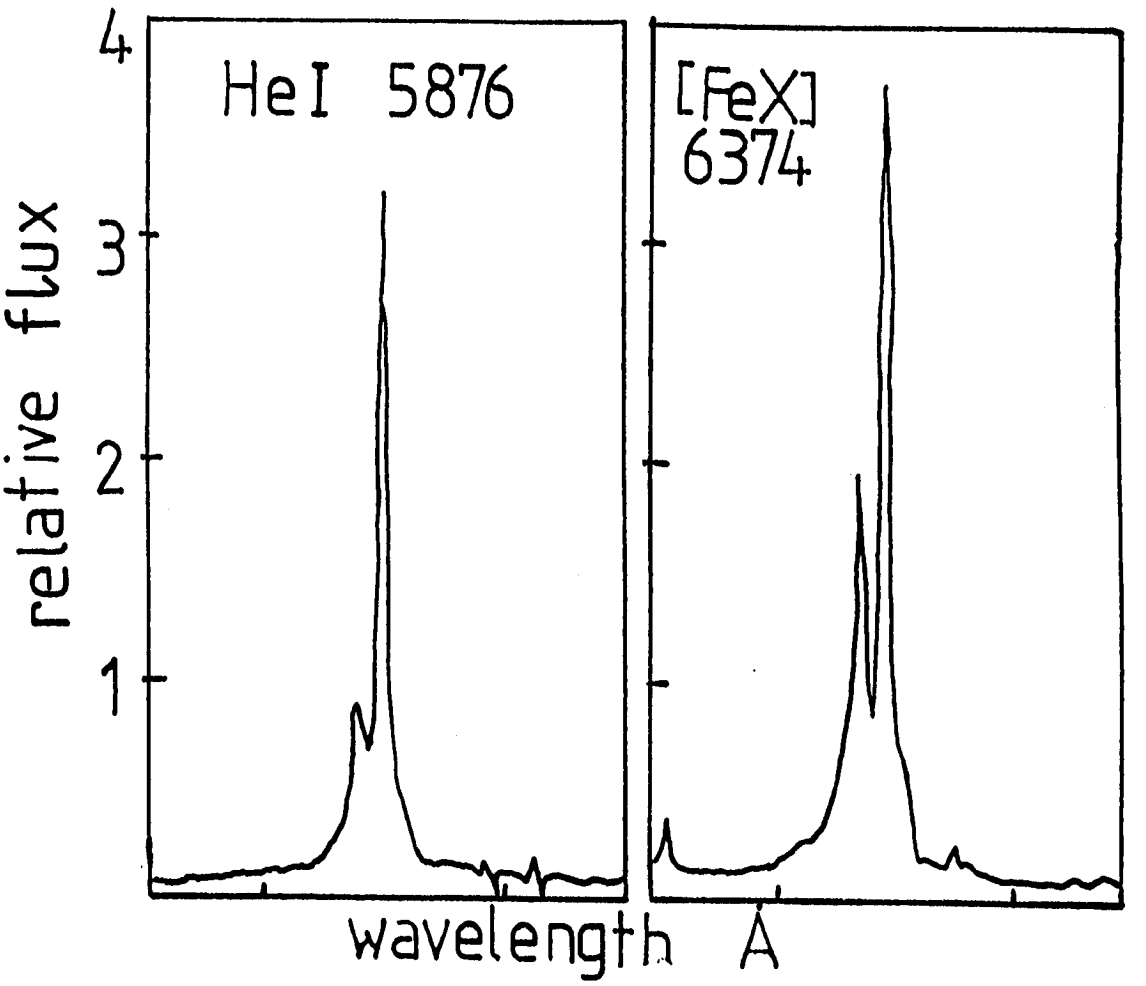

Figure 7.15. Tracings of the HeI λ5878 and [FeX] λ6374 emission lines in the spectrum of RS Oph after the 1985 outburst. Reproduced from Krautter (1986).

consist of several components. Krautter (1986) fitted two Gaussian components. The stronger component was slightly blue-shifted with a heliocentric radial velocity of ~ -17 km s^{-1}; the weaker component was also blue-shifted and had a mean radial velocity of ~ -170 km s^{-1}. Redshifted emission components were observed in both emission lines and the best fits resulted when 5 components were used. Krautter measured the line wings of Hα to have a total width corresponding to velocities of ± 2700 km s^{-1}.

At the end of April when the nova was approaching its 'average' minimum, Rosino & Iijima (1986), saw the degree of excitation decreasing. The coronal lines weakened when compared to the hydrogen and helium lines but at the same time, the spectrum showed an increase in strength of the nebular lines. (The nebular lines of OIII and NII had been broad diffuse and nebulous since April). In the second half of May the spectral changes became pronounced: all the coronal lines except [FeX] and [FeXI] had disappeared, and most of the high excitation lines were fading.

Between June and October 1985, the star had reached its minimum, yet Rosino & Iijima (1986) noted that there were still some signs of the recent outburst. There were still prominent lines of hydrogen, HeI and HeII, and noticable were the nebular lines of OIII & NII which were still broad and diffuse; the coronal lines, except [FeX] λ6374, had all gone. During this time the general degree of excitation was decreasing, although many weak emission lines of highly ionized atoms were observed.

Bruch (1986a,b) obtained spectra in July 1979, June 1984 and 1985 August 21, 207 days after the outburst. He found that the Hα emission line width varied considerably over the years and was twice as large after the 1985 outburst as it was in 1984, and five times as large as in 1979, although all spectra showed this line to be structured. In the same period the width of the helium lines remained essentially constant.

The author's main objective was to determine the character of the secondary. He observed that a late type absorption component was readily

visible in all spectrograms. Present in absorption was CaI λ4227 and the G band. To the yellow and red numerous absorptions that are typical for a cool star were seen. The strongest lines were those due to MgI, TiO and NaI. From this he came to the conclusion that the spectral type of the secondary was of M2. From assumptions of the reddening in the direction of the star and hence of the distance he concluded that the luminosity class of the star was III (giant).

7.6.5 Ultraviolet Spectroscopy

IUE spectra taken in quiesence of RS Oph in 1979, 1980, 1981 and 1982 revealed that it was not a high ionization object in general, although it did exhibit some lines of quite high ionization (Snijders, 1986; Rosino et al. 1982). It also showed a strong NIII] line which suggested that material transferred from the red giant was already enriched in nitrogen.

After the 1985 outburst of this object IUE observed it at various times between 13 - 253 days after outburst. Snijders (1986) has described the IUE observations. In the spectra the peak of the continuum flux moved to shorter wavelengths and the ionization level increased as a function of time (similar to all novae, see Chapter 1). The line profiles became narrower with time. On day 26 the full width of OI λ1304 was ~ 7000 km s^{-1} while on day 111 it was ~ 970 km s^{-1}. Fig. 7.16 shows the development of some of the lines with time. Low ionization lines like OI and MgII were already in decline on day 19, NIII] reached its maximum on that day whilst lines from higher ions were still increasing in strength. The next lines to reach their peak strength were the HeII, NIV] and NV lines; lastly [FeXI] and other coronal lines. Snijders remarked that such development was not only due to an increase in radiative ionization but could have also been caused by a drop in the density . In the case of the coronal lines their formation was governed by the shocks set up when the ejecta meet the stellar wind.

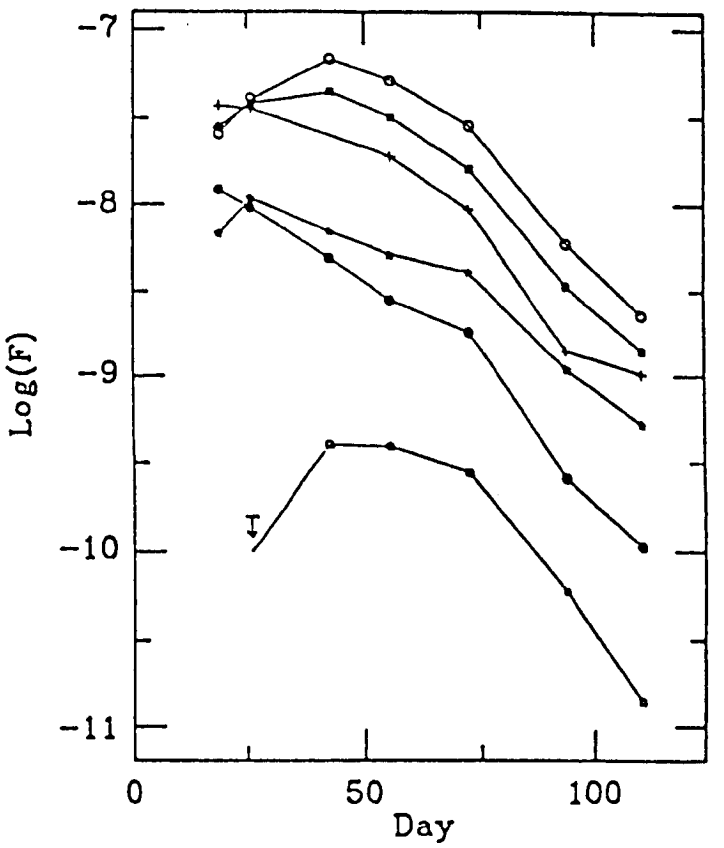

Figure 7.16. Ultraviolet emission line strength as a function of days after the 1985 outburst of RS Oph. Reproduced from Snijders (1986).

▫[FeXI] 2648
•OI 1304
☆HeII 1640
+ NIII] 1750
▪ NIV] 1486
∘ NV 1240

From such observations Snijders attempted to calculate the reddening and the distance of RS Oph. Using the HeII λ1640/HeII λ3203 line ratio he determined an E(B-V) of 0.73±0.06 and by the removal of the 2175A extinction feature and the Seaton (1978) extinction law he calculated E(B-V) to be 0.73±0.1. On examining the velocities of the rich interstellar line spectrum in the data he concluded that they were all typical of velocities in our local spiral arm and so an upper limit on the distance was set to ~ 2 kpc. By plotting the bolometric luminosity curve and recording the luminosity at the 'plateau stage' and assuming this to be 90% of the Eddington luminosity for a white dwarf of mass 1.38 $M_{\odot}$ he determined the distance to be 1.44 kpc.

7.7 Pattern of Outbursts

Both in photometry and spectroscopy the five outbursts of RS Oph have followed the same basic pattern. The light curve similarity is shown in Fig. 7.7 whilst the spectroscopic pattern is described by Rosino (1986) and his descriptions are repeated in Table 7.9.

7.8 Observations of RS Oph During Quiescence

Although studies of RS Oph during outburst have proven to be most interesting, studies during quiescence can also be of great value. Described here is a brief account of some of the observations obtained during quiescence.

After its first outburst there were few observations but in September 1907 the star was noticed to undergo a sharp minimum to 12.6 mags. Observations of its light curve from 1916 - 1933 showed small and irregular fluctuations (Prager, 1940).

The first serious attempt at spectroscopy on this object was made by Adams et al. (1927). On 1923 July 20 they saw very strong Hβ emission and fainter emission at Hγ, and several of the most prominent lines of FeII

Table 7.9
General developement of the outbursts of RS Oph.

DAYS AFTER OUTBURST	VISUAL MAG	REMARKS
0 - 2	4.8 - 5.8	WIDE EMISSION BANDS OF H, HeI, FeII WITH CENTRAL SHARP EMISSION AND NARROW P CYGNI ABSORPTION (V ~ -60 kms^{-1}). BROAD BLUE-SHIFTED ABSORPTION BANDS (V ~ -3900 kms^{-1} - -2700 kms^{-1}).
2 - 15	5.8 - 8.3	HeI FLARING. EMERGE AND STRENGTHEN HeII λ4686 AND THE FORBIDDEN LINES OF OI, OIII, NeIII, NII, SII THEN FeX λ6374.
16 - 30	8.4 - 9.2	HeII AND NIII λ4640 VERY STRONG. FeX INCREASING IN STRENGHT.
31 - 50	9.3 - 10.1	THE CORONAL LINES APPEAR AND STRENGTHEN. THEY BECOME OUTSTANDING NEAR DAY 50.
51 - 130	10.15 - 12	STILL PROMINENT: BALMER LINES, HeI λ5875, THE CORONAL LINES FeX, AX, FeXIV, FeXI; NII λ5755 & OIII.
131 - 200	11.5 - 13	FADING AND DISAPPEARANCE OF THE CORONAL LINES & HeII λ4686. WEAKENING OF HeI & FeII LINES. OIII FLARING, THE NEBULAR LINES HAZY AND DIFFUSE.

Reproduced from Rosino (1986).

were present as weak emissions. The radial velocity as measured from the hydrogen lines was ~ -35 km s^{-1}. There were many absorption lines present and from this absorption spectrum they classified the star as G5. A second spectrum obtained on 1926 July 3 revealed strong narrow bands of Hβ, Hγ, Hδ, and Hε projecting beyond the continuous spectrum of a Wolf-Rayet type star.

Observations obtained on 1936 August 16 were reported by Humason (1938). He saw emission lines of OIII λ5007 and λ4959, Hβ, Hγ, and Hδ. He noted that the continuous spectrum was much stronger relative to the emission lines than in 1923 and extended well into the violet. No absorption lines were seen at this time.

Swings & Struve (1941) obtained a spectrum in May 1941. It showed a very strong continuous spectrum. They suggested that in fact it was a composite spectrum, one component being K8 - M0 in type while the other component was emitting a weak but definitely blue continuum. There were bright lines present of Hα - H_8, many HeI and FeII lines as well as lines due to HeII, [OIII], OIII, NIII, [NeIII], [SII] and [FeII]. This bright line spectrum became much more pronounced in July 1942 (Swings & Struve, 1943). On 1942 July 19 they found a very conspicuous emission line at λ6374 which coincides with the position of the coronal line [FeX]. Subsequent spectra obtained on 1942, 10 and 12 days later, showed a considerable number of emission lines. The Balmer series Hα - H_{11} was observed and many lines of HeI, HeII, TiII, CrII, FeII and [FeII] were also seen. Other emission lines included those due to CII, CIII, NII, NIII, [OIII], [NeIII], MgII, SiII, [SII] and CaII.

When Sandford (1947) observed the star on 1947 July 27, he saw an absorption spectrum that was dominated by lines of FeII and TiII with stronger lines of FeI. He found that the best match for the continuous spectrum was a star of spectral type cA7se (a shell spectrum type star). He determined the radial velocity from 76 lines of FeI, FeII and TiII and

found the average to be ~ -38.8 km s^{-1} which was in agreement with the few lines of CrII, SrII and BaII that he also saw. At this time in emission the only conspicuous lines were those of hydrogen. They were divided into two components, the redward component being slightly stronger, and had an overall width of ~ 200 km s^{-1}. A few [FeII] lines were just about visible. Some of the strongest absorption lines of FeII appeared to be accompanied by weak emissions. The radial velocities were ~ -100 km s^{-1} and ~ +7 km s^{-1} for the hydrogen emission lines and ~ 47 km s^{-1} for the absorptions. Two of the [FeII] lines gave a radial velocity of ~ 44 km s^{-1}.

Observations by Merril & Bowen (1951) taken on 1951 May 18 showed a fairly strong continuous spectrum which extended from λ5400 - λ6860; emission lines were visible from λ5169 - λ6678. Of the Balmer lines Hα - H_{14} were seen in emission, each had a narrow dark core that was displaced slightly shortward of the peak of emission. Strong HeI lines were seen whilst more than 40 lines of FeII were seen in emission particularly in the blue and they also had nearly central dark cores of low intensity. TiII was represented by 26 narrow dark lines whilst other metals also represented by absorption lines were FeI, CrI, ScII, and possibly MgI and VII. Nine strong lines of [FeII] were visible, as well as two of [OI] at λ6300 and λ6363. Interstellar lines were also seen in the spectrum. The authors remarked that, in 1951, the emission lines were generally stronger and the absorption cores generally weaker than in 1947.

Rosino et al. (1968) reported observations between 1959 - 1962. At this time the average visual magnitude was ~ 11.5 and the star exhibited slow irregular fluctuations of luminosity from 10.5 - 12.5 mags. Spectra obtained showed a gradual decline in the degree of excitation, a progressive fading of the blue visual continuum and finally, a decisive strengthening in the red. In spectra obtained between 1959 - 1960, Balmer Hα - H_6, HeI λ6678, λ5876, [NII] λ5755, FeII and very faint [OIII] λ5007 were all seen in emission. Between 1961 - 1962 they saw a general

weakening of the emission lines. Most faded and disappeared leaving just Hα, Hβ and HeI λ5876. However wide absorption bands of moderate strength were seen with the NaI doublet prominent. Comparison with stars of known spectral type gave the best match for a M2III type.

Almost simultaneous observations were made by Wallerstein (1963) who observed the star from mid 1960 for two years. He interpreted the spectra in terms of a shell because of the strength of the TiII in absorption, the FeII in emision (which Rosino et al, 1968 had not detected) and the Hα - H_{30} in absorption. He also saw a few emission lines of [FeII] although no nebular lines were seen. The hydrogen emission lines were observed to have central absorption cores. From the spectra he obtained, Wallerstein estimated that the average E(B-V) was ~ 1.1.

In 1965 a 'mini-outburst' was observed in the visual by Rosino et al. (1968). Activity was seen on 1965 March 26 when the star was at 9.7 mags. Spectra obtained on April 2 showed a net increase of the degree of excitation and strong emission lines of hydrogen, HeI and FeII. During the following weeks the degree of excitation further increased and HeII λ4686 appeared about as strong as Hβ. By May 14 this line had faded away whilst hydrogen, HeI and FeII emission lines still appeared rather strong. Faintly forbidden lines of [FeII] and [SII] and the blend NIII λ4640 were also weakly recorded.

Between the last two outbursts in August 1981, Blair et al. (1983) obtained a spectrum of the star in the visual. As ever hydrogen Balmer and HeI dominated the emission line spectrum and there was a weak indication of HeII λ4686. The authors attributed the ragged appearance of the continuum to FeII lines. They found that the continuum energy distribution was very red with evidence of TiO absorption bands (obviously an indication of the late type secondary).

All these observations taken of RS Oph during quiescence obviously indicate a two component system. This is witnessed by the strong emission

lines (arising from the circumstellar gas shell) and the red continuum and absorption lines (arising from the secondary star).

7.9 Mechanism of Outburst

Before the conclusion of this chapter we devote some time to the mechanism of outburst for RS Oph. Recently Livio et al. (1986) challenged the well held belief that most recurrent novae underwent outburst as a result of thermonuclear runaway (TNR) on the surface of a white dwarf primary (see Chapter 1) and, indeed, in the case of RS Oph , debated the nature of the primary itself.

For RS Oph they found that the high accretion rate demanded to reconstitute a sufficient envelope to trigger TNR on the short recurrence timescale implied a luminosity and effective temperature of the primary white dwarf which were incompatible with observations of the system at quiescence. They also suggested that the extremely sharp rise to maximum and the large velocities of ejection seen were indicative of an extremely dynamic event and that the system at quiescence was more consistent with accretion onto a main sequence star. Thus their model is one of episodic accretion which involves the direct impact of the accretion stream with the primary which they assumed to be a bloated main sequence star. (This main sequence star must be in an expanded configuration, as the high mass transfer rate required implied a large total mass accreted so leaving the star in a 'bloated' state). Their model did explain the short recurrence timescale and was compatible with the radio observations of asymmetry in the RS Oph system.

However observations of the recent outburst obtained in the ultraviolet and X-ray suggested that the TNR model may be the correct model after all. In the X-ray there was a weak, but significant, residual emission detected from the object more than 200 days after outburst (Mason et al., 1986). The amount of residual flux was consistent with an origin

on the surface of a white dwarf where a TNR was still taking place. Turning now to the ultraviolet data of Snijders (1986), he found that it suggested abundances very similar to those found in classical novae (and these certainly undergo TNR). However it must be noted that both pre-outburst and post-outburst spectra of RS Oph indicated an overabundance of nitrogen because of the strong NIII] line and so this evidence on its own cannot point conclusively to a TNR event. What the ultraviolet data did show however was that, although the optical outburst was over in 10 days it took 57 days for the source to drop by a factor of two below the plateau luminosity and hence in view of this an episodic event appeared unlikely. Also the plateau luminosity compared well with the Eddington luminosity of a white dwarf at 1.6 kpc. This implied that RS Oph should have had a peak luminosity of four times this limit so explaining the high ejection velocities seen at outburst and so necessitating a TNR.

In conclusion the TNR model seems to be the most acceptable at present although it has difficulty in explaining the short recurrence time. Snijders (1986) suggested that RS Oph may be hiding a high energy source that is required to produce the high luminosities required for a TNR to work on these short timescales.

7.10 Conclusion

From data obtained at all wavelengths we have come to a bettter understanding of the RS Oph system. The distance, which is a vital parameter to obtain, was calculated as ~1.6±0.3 kpc from both ultraviolet and x-ray studies and the secondary star has been classified as M2III from visual spectroscopy (but see Chapter 8). The narrow lines seen pre and during outburst have been interpreted as arising from a pre-existing circumstellar envelope surrounding the star, probably originating from the stellar wind of the secondary. The narrowing of the optical lines has been suggested to be due to the deceleration of material as it ploughs into this

envelope (although it could also be due to the uncovering of slower moving layers of ejecta). There is further evidence for this in the detection of ultraviolet and optical coronal lines and x-rays, all of which require temperatures that could be produced in a shocked gas.

However despite what has been learnt about the system from its five outbursts and during quiescense there still remains unanswered questions, e.g. that of the outburst mechanism (see previous section) and the interpretation of the asymmetries discovered by the radio observations. It is hoped that further observations at all wavelengths will constantly be made of this system and by the time that it undergoes its sixth outburst most of the problems will have been addressed.

CHAPTER 8

INFRARED OBSERVATIONS OF RS OPHIUCHI

8.1 Introduction

This chapter is concerned with both the infrared photometry and spectroscopy obtained of RS Oph during its last outburst in 1985. Here, from the photometry, we attempt to interpret the colour-colour diagrams for this object. From the spectroscopy we try to determine the form of the continuum at various stages in the post outburst evolution of RS Oph in order to estimate the temperatures in the line forming region(s) of the remnant. We also attempt to determine the nature of the secondary. Preliminary work on these infrared data has already been reported by Evans (1986), and where necessary this work will be referred to here.

8.2 Preoutburst Infrared Observations

Near infrared (i.e. wavelengths < 1.25μm, the J band) preoutburst observations were discussed in Chapter 7. Most of these observations were spectroscopic and revealed the presence of the hydrogen Paschen series from $P\gamma$. Unfortunately the literature made little reference to preoutburst spectroscopic observations in infrared wavebands longward of J, so here we will concentrate on the few available photometric observations obtained in these wavebands between the last two outbursts. A list of these observations is given in Table 8.1 where the wavebands run from J to IRAS band II (25μm).

Feast & Glass (1974) noted that in the (J-H)-(H-K) colour plot the position of RS Oph was similar to that occupied by some Mira variables, whilst in the (J-K)-(K-L) colour plot it lay in a position that was more characteristic of normal giants or supergiants. They explained this by

Table 8.1

Pre-outburst infrared photometry of RS Oph.

Date	J	H	K	L	N	I(Jy)	II(Jy)	
	1.25μm	1.65μm	2.2μm	3.5μm	10μm	12μm	25μm	
1970 Mar 22	-	-	6.8	-	5.1			(1)
1970 Mar 23	-	-	7.0	-	4.5			(1)
1971	-	6.90	6.61	-				(2)
1973 May 10	7.74	6.99	6.62	6.25				(3)
1973 May 26	7.61	6.81	6.50	6.35				(3)
1976 Aug 11	7.51	6.96	6.54	6.02				(4)
1981 Aug 06	7.69	6.84	6.51	6.15				(5)
1982	7.53	6.79	6.45	-				(6)
1983						0.42		(7)
1983 Sep 16						0.28	0.16	(8)
1983 Sep 19						0.31	0.15	(8)

Data obtained from:

1) Geisel et al. (1970)

2) Swings & Allen (1972)

3) Feast & Glass (1974)

4) Szkody (1977)

5) Whittet & Evans (unpublished).

6) Kenyon & Gallagher (1983)

7) IRAS PSC.

8) Kenyon et al. (1986)

invoking very heavy reddening, corresponding to an E(B-V) of ~ 1.8. However IUE observations both pre- and post-outburst (Snijders, 1986) have shown this not to be the case as the E(B-V) was determined to be ~ 0.73 from these observations. But plotting all the preoutburst observations on the colour-colour diagrams (see Fig. 8.1) leads to a rather random scattering of the points so no conclusions can really be drawn as to whether the two plots agree or disagree about the nature of RS Oph. In view of the fact that both the J and K bands are contaminated by hydrogen and helium lines (e.g. Krautter et al., 1984) and that the strength of the lines due to these elements have been known to change during quiescence (albeit in the visual wavelength range, see Chapter 7) it may be possible that the behaviour of RS Oph in these two colour diagrams is due to the varying strength of these infrared emission lines.

This pre-outburst photometry has given no indication of an infrared excess in the J - L wavebands, but the IRAS PSC observation and the N point observations of Geisel et al. (1970) may have suggested an excess at these longer wavelengths. Further IRAS observations of RS Oph, the IRAS pointed observations (AO's) are dicussed by Kenyon et al. (1986). After making corrections for interstellar reddening and free-free emission they note that its far infrared flux distribution closely resembles that of HR8775 (an M0III star) with modest excesses at 12μm and 25μm. They note that further observations at 60μm and 100μm are needed to constrain the extent of cool dust in the system. Evans (1986) attempted to interpret the IRAS PSC point in terms of emission by dust. He fitted the JHKL (1981) points with a late type secondary, plus a 350 K blackbody to represent the dust. From this he calculated that $\langle\tau\rangle$, the absorption optical depth averaged over the spectrum of the heating source was ~ 0.02, and that the amount of dust present ~ few x $10^{-9} M_{\odot}$. However this treatment was based on the blackbody fit of 350 K and thus can only be considered a valid approximation for carbon based grains. The fact that there was no excess

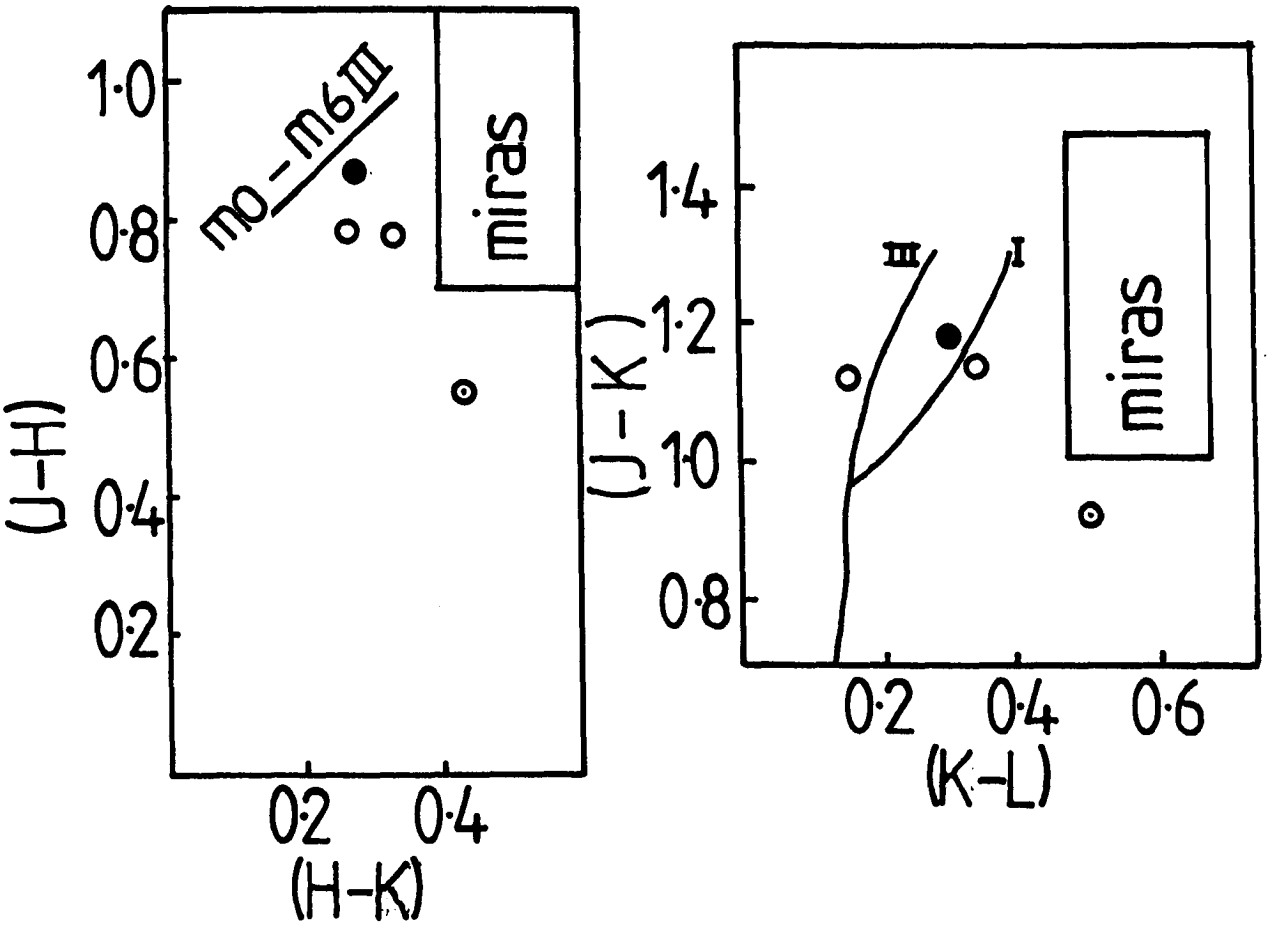

Figure 8.1. Shown here are the (J-H) - (H-K) and (J-K) - (K-L) colour-colour plots indicating the positions of the Miras, normal giants and supergiants. Reproduced from Evans (1986). Also shown are the points given by the pre-outburst photometry of RS Oph. Values taken from: o) Feast & Glass (1974), •) Szkody (1977) & ⊙) Whittet & Evans (unpublished).

at L, but perhaps an excess at longer wavelengths could point to the presence of a silicate based dust in the system and hence no conclusions can be made about its opacity and mass from a blackbody treatment. If we accept that there was silicate dust in RS Oph prior to outburst we would like to know the origin of this dust. Evans (1986) calculated that ~ $2 \times 10^{-11} M_0$ of dust could be formed in the wind of the secondary during a time period of 20 years (i.e. approximately the time between the last two outbursts), which may be a little on the low side considering the detections at the longer wavelengths. It is interesting to note that the secondary of this system is possibly oxygen rich (see section 8.5) and hence the formation of silicate based grains would appear the more likely (Yamamoto & Nishida, 1977). Alternatively the dust could have formed from the ejecta of the previous outbursts as it does in some classical novae (see Chapter 2). But the interaction between the ejecta and the wind and thus the resultant shocks could inhibit the formation of grains under these conditions (Evans, 1986). However if there were local density enhancements as a result of these shocks it might be that these were the sites of any grain formation.

8.2.1 The Accretion Disc

In order to solve the discrepancy in the preoutburst colours of RS Oph (see previous section), it had been suggested that the inclusion of the effect of the accretion disc might solve this problem (Evans, 1986). Indeed Berriman et al. (1985) had shown that the accretion disc in some dwarf novae and classical novae systems contribute considerably to the infrared flux of these objects.

The simplest configuration for the accretion disc in the RS Oph system is shown in Fig. 8.2. At a distance r from the white dwarf the observed locus of constant temperature T is an ellipse in the (x,y) plane with eccentricity $e = \cos i$, where i is the inclination to the line of sight.

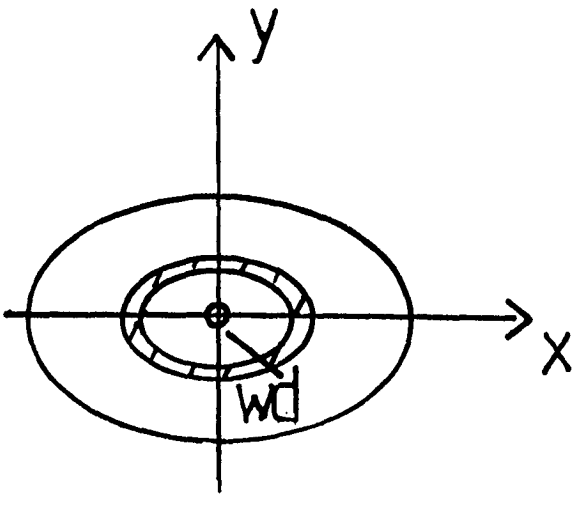

Figure 8.2. The accretion disc in RS Oph as we see it - i.e. at a distance r from the white dwarf the observed locus of constant temperature is an ellipse in the (x,y) plane with eccentricity e = cos i, where i is the inclination to the line of sight.

Hence the flux, f_ν, from an element is

$$f_\nu = B_\nu(T[x,y])\cos i \, dxdy \tag{8.1}$$

so that the total flux from a disc at inclination i is

$$F_\nu = 2\pi/D^2 \cos i \int 2h\nu^3/c^2 \, r/(\exp(h\nu/(kT(r)) - 1) \, dr \tag{8.2}$$

where D is the distance to RS Oph and R_1, R_0 are the inner and outer radii of the accretion disc respectively. Using the temperature variations in a steady state disc (e.g. Frank et al., 1985) we have

$$T(r) = (GMM/(8\pi r^3\sigma)[1 - (R_*/r)^{1/2}])^{1/4} \tag{8.3}$$

Here, M is the mass of the white dwarf and R_* is the white dwarf radius. σ is Stefans constant and M is the mass transfer rate.

Thus by the subsitution of equation (8.3), equation (8.2) was solved by using the NAG routine D01AGA, for frequencies corresponding to the JHKL bands. From equation (8.3) it can be seen that if the disc extends from the surface of the white dwarf the temperature becomes zero as the integrand tends to zero. In order to prevent this occuring the inner edge of the disc was placed at twice the radius of the white dwarf. This should not affect the results as the innermost edges of the accretion disc will radiate at much higher frequencies than those of the infrared.

The other parameters were chosen thus: Livio et al. (1986) estimated the mass of the white dwarf in the RS Oph system to be ~ $1.38M_0$ (they did this by taking into account the short recurrance time of this nova); at such a mass its radius is ~ 2×10^8 cm (e.g. Schwarzschild, 1958). The mass transfer rate was taken to be $M \sim 3.6 \times 10^{-8} M_0 \, yr^{-1}$ (Livio et al., 1986), and the outer edge of the accretion disc R_1, at a radius of

1×10^{11}cm (e.g. Frank et al., 1985). The distance was chosen as 1.3 kpc (see section 8.4).

The results of these calculations are shown in Table 8.2. This table also shows how reasonable changes in the 'free' parameters affect the fluxes from the disc at each infrared wavelength (M was not changed as the value we have used is the maximum reasonable value and any smaller value would lead to smaller fluxes). Clearly the accretion disc only has a negligible effect on the infrared fluxes of RS Oph. This could be due to the fact that its secondary is a red giant star, in constrast with the secondaries of dwarf novae and classical novae which in most cases are late type main sequence stars and thus do not dominate at infrared wavelengths. However P. A. Whitelock (private communication) notes that the average of the immediate post outburst magnitudes of RS Oph (obtained at SAAO from JD 2446200 - JD 2446400) i.e. J = 7.94, H = 7.07 and K = 6.75 (see next section), are dimmer than the average magnitudes obtained between JD 24465000 - JD 24469000 i.e. J = 7.67, H = 6.87 and K = 6.35 (these magnitudes compare well to the pre-outburst magnitudes given in Table 8.1). She suggests that the difference between the two sets of values may arise because the accretion disc, blasted away during the outburst, has reformed. She calculates it could have infrared magnitudes J = 9.3, H = 8.80 and K = 8.48. Our calculations (see above) predicted an accretion disc radiating considerably lower fluxes. Perhaps our assumption of a steady state disc radiating as a blackbody is invalid in the case of RS Oph. This would be especially so in the disc reformation period where conditions would be anything but steady state. So if the accretion disc were to emit significant infrared flux it would be unlikely that such a disc was in a steady state.

Table 8.2

Theoretical accretion disc magnitudes.

J	H	K	L	
12.28	12.23	12.21	12.19	$\dot{M}=2.3\times10^{18}$ g s^{-1} $R_1=1\times10^{11}$ cm
				$R_*=2\times10^{8}$ cm $M=1.38\ M_0$
11.55	11.17	10.77	10.07	$\dot{M}=2.3\times10^{18}$ g s^{-1} $R_1=5\times10^{12}$ cm
				$R_*=2\times10^{8}$ cm $M=1.38\ M_0$
12.45	12.39	12.36	12.32	$\dot{M}=2.3\times10^{18}$ g s^{-1} $R_1=1\times10^{11}$ cm
				$R_*=5\times10^{8}$ cm $M=1.00\ M_0$

Flux (in mags) of the accretion disc at infrared wavelengths.

8.3 Photometry

Photometry at J (1.25μm), H (1.65μm), K (2.2μm) and L (3.5μm) was obtained at SAAO within 5 days of the discovery of the outburst (Laney, 1985) and subsequent photometry was obtained on the 0.75m and 1.9m telescopes. The errors in the photometry were ± 0.04 mag at JHK and ± 0.06 mag at L. The dereddened data are given in Table 8.3, in which they have been dereddened using van de Hulst curve 15. (We gratefully thank P. A. Whitelock and her colleagues at SAAO for sending us these data).

The light curves at JHKL using the SAAO data are shown in Fig. 8.3. The rate of decline over the first two magnitudes are 0.081 mag d^{-1}, 0.070 mag d^{-1}, 0.071 mag d^{-1} and 0.071 mag d^{-1} at JHK and L respectively and so the decline by 2 mags in each waveband occurs over a period of ~ 30 days. The flux in the J band appears to decline at a greater rate than the flux in the other 3 bands, this is almost certainly due to the rate of decline in the very prominent HeI line at 1.083μm (see section 8.4).

In each wavelength it is noticeable that RS Oph had returned to its 'quiescent' value (as given in Table 8.1) by ~ day 85, and it is also apparent that the decline continued past these pre-outburst values. There is also a suggestion of a periodic variation in these light curves of ~ 35 days once this quiescent value is reached although later observations do not confirm this periodicity. Such a period, however, is much too short for late type giant pulsators (RS Oph has long been considered to have a late type giant as its secondary) since these variables have periods of a few hundreds of days (Allen, 1973). Neither does it tie in with the orbital period of 230 days of the RS Oph system (Friedjung, 1985).

Turning now to the colour-colour plots. The $(J-H)_0$-$(H-K)_0$ and the $(H-K)_0$-$(K-L)_0$ diagrams are shown in Fig. 8.4. During the first 35 days of the outburst the $(J-H)_0$ and $(H-K)_0$ colours are almost constant at 0.1 and 0.5 respectively. $(J-H)_0$ then increases rapidly until it becomes nearly

Table 8.3

Magnitudes of RS Oph during the 1985 outburst.

Julian Day (2440000+)	J	H	K	L
6100.65	3.49	3.61	2.84	2.51
6101.62	3.67	3.80	3.21	2.66
6107.61	4.23	4.38	3.79	3.16
6110.60	4.30	4.48	3.89	-
6113.62	4.75	4.95	4.36	3.78
6113.62	4.84	4.97	4.39	3.78
6114.61	4.73	4.92	4.32	3.65
6114.61	4.81	4.93	4.34	3.69
6116.63	4.76	4.88	4.09	3.62
6117.62	4.97	5.10	4.51	3.91
6120.62	5.23	5.39	4.83	4.26
6122.63	5.21	5.37	4.79	4.20
6131.59	5.55	5.69	5.15	4.65
6132.62	5.58	5.71	5.19	4.64
6133.64	5.66	5.79	5.29	4.74
6134.62	5.68	5.84	5.34	4.79
6135.63	5.72	5.85	5.29	4.80
6136.62	5.78	5.84	5.35	4.87
6152.65	6.11	6.07	5.59	(5.02)
6153.63	6.17	6.11	5.64	(5.20)
6166.58	6.55	6.40	5.97	-
6181.62	7.03	6.64	6.32	-
6182.62	7.09	6.69	6.36	-
6185.57	7.13	6.68	6.39	6.07

6203.57	7.33	6.77	6.46	6.18
6217.50	7.36	6.82	6.54	6.36
6221.51	7.34	6.78	6.52	-
6222.46	7.34	6.77	6.50	-
6223.40	7.34	6.77	6.50	6.38
6225.40	7.34	6.76	6.48	6.22
6244.43	7.21	6.70	6.42	6.26
6244.43	7.26	6.70	6.42	-
6256.46	7.39	6.80	6.50	-
6259.44	7.39	6.71	6.52	-
6261.47	7.40	6.80	6.52	-
6265.40	7.31	6.73	6.45	(6.44)
6270.36	7.30	6.71	6.44	-
6273.26	7.26	6.66	6.39	-
6276.25	7.25	6.63	6.36	-
6301.26	7.43	6.85	6.57	-
6303.27	7.41	6.81	6.54	-
6310.22	7.41	6.85	6.56	(6.36)
6313.30	7.39	6.77	6.53	-
6315.30	(7.31)	(6.73)	6.47	-
6347.28	7.46	6.88	6.60	-
6357.23	7.33	6.76	6.50	-
6536.62	7.10	6.59	6.32	-
6547.55	7.10	6.60	6.32	-
6569.59	7.17	6.65	6.32	-
6591.33	6.98	6.50	6.23	-
6595.48	6.89	6.42	6.15	-
6627.37	7.17	6.67	6.39	-
6638.36	7.18	6.67	6.42	-
6645.20	7.14	6.61	6.37	-

6652.42	7.14	6.60	6.32	-
6656.32	7.03	6.51	6.20	(5.90)
6662.28	7.28	6.70	6.43	-
6693.23	6.93	6.43	6.17	-
6760.28	6.93	6.41	6.13	-
6855.60	7.11	6.60	6.32	-
6862.66	7.06	6.58	6.30	-
6893.62	7.07	6.55	6.27	(6.00)

Dereddened magnitudes of RS Oph in bands JHK & L obtained at SAAO. Values in brackets show greater error bars than the average.

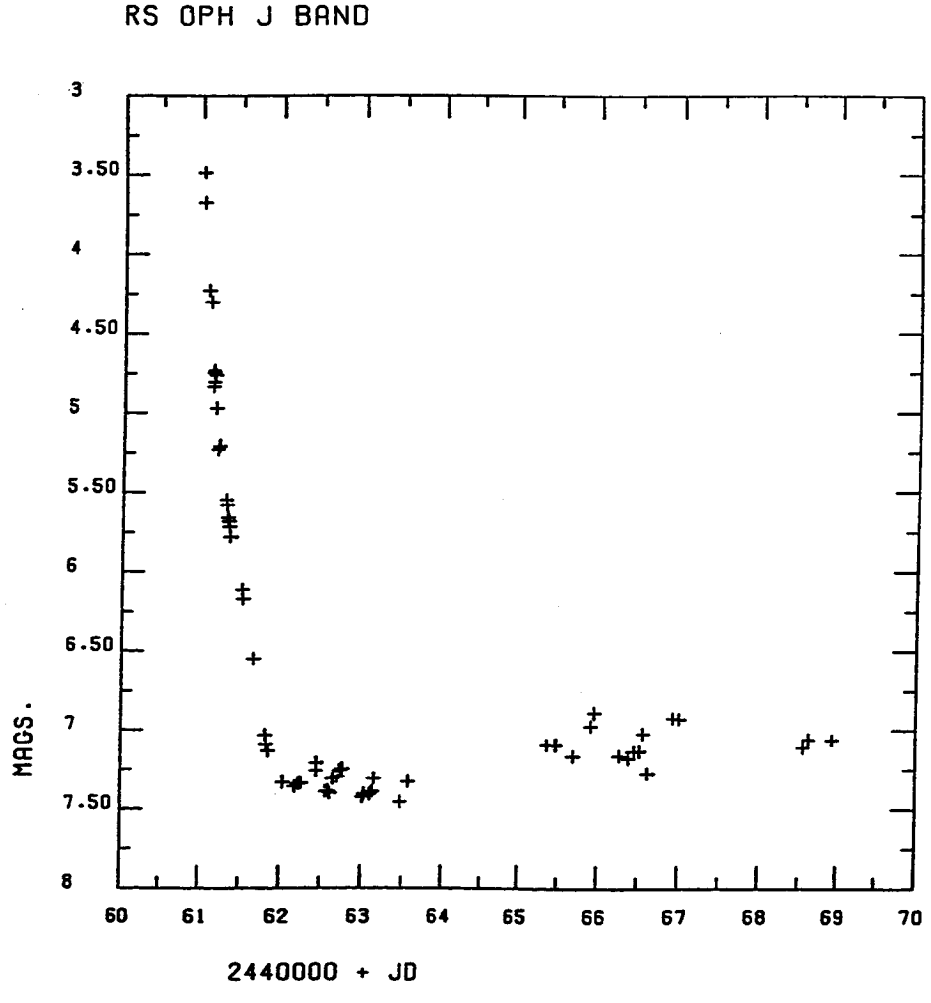
RS OPH J BAND
MAGS.
3
3.50
4
4.50
5
5.50
6
6.50
7
7.50
8
60
61
62
63
64
65
66
67
68
69
70
2440000 + JD

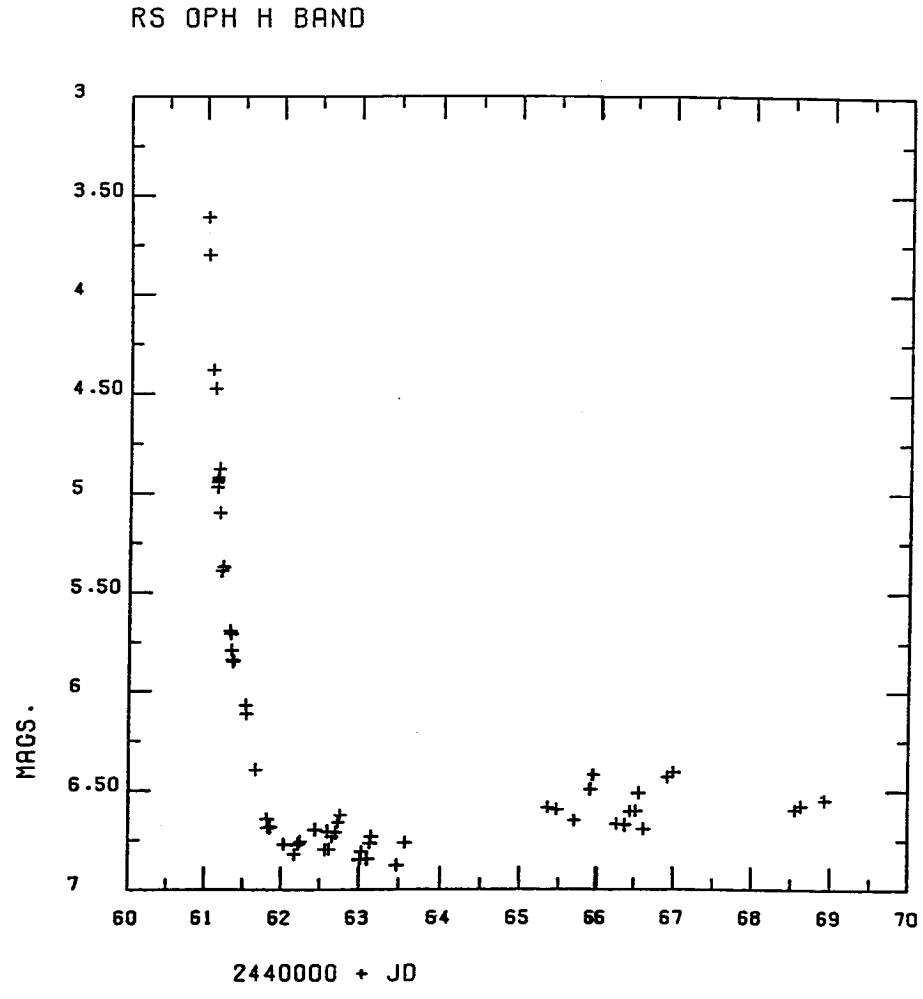
RS OPH H BAND
MAGS.
3
3.50
4
4.50
5
5.50
6
6.50
7
60
61
62
63
64
65
66
67
68
69
70
2440000 + JD

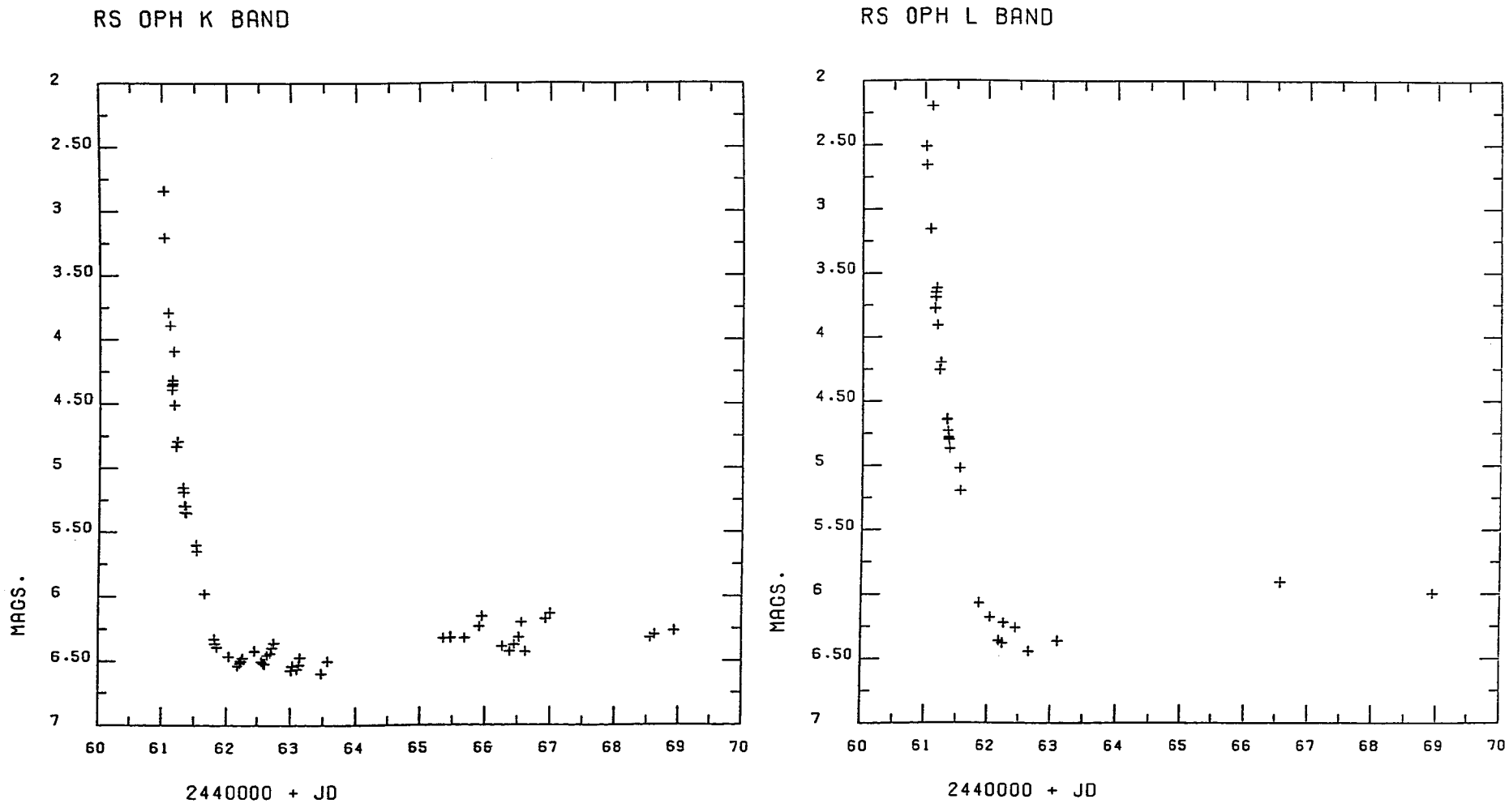

Figure 8.3. JHK & L light curves for RS Oph obtained at SAAO from 7 days after outburst. Data have been dereddened using van de Hulst curve 15 (see Table 8.3).

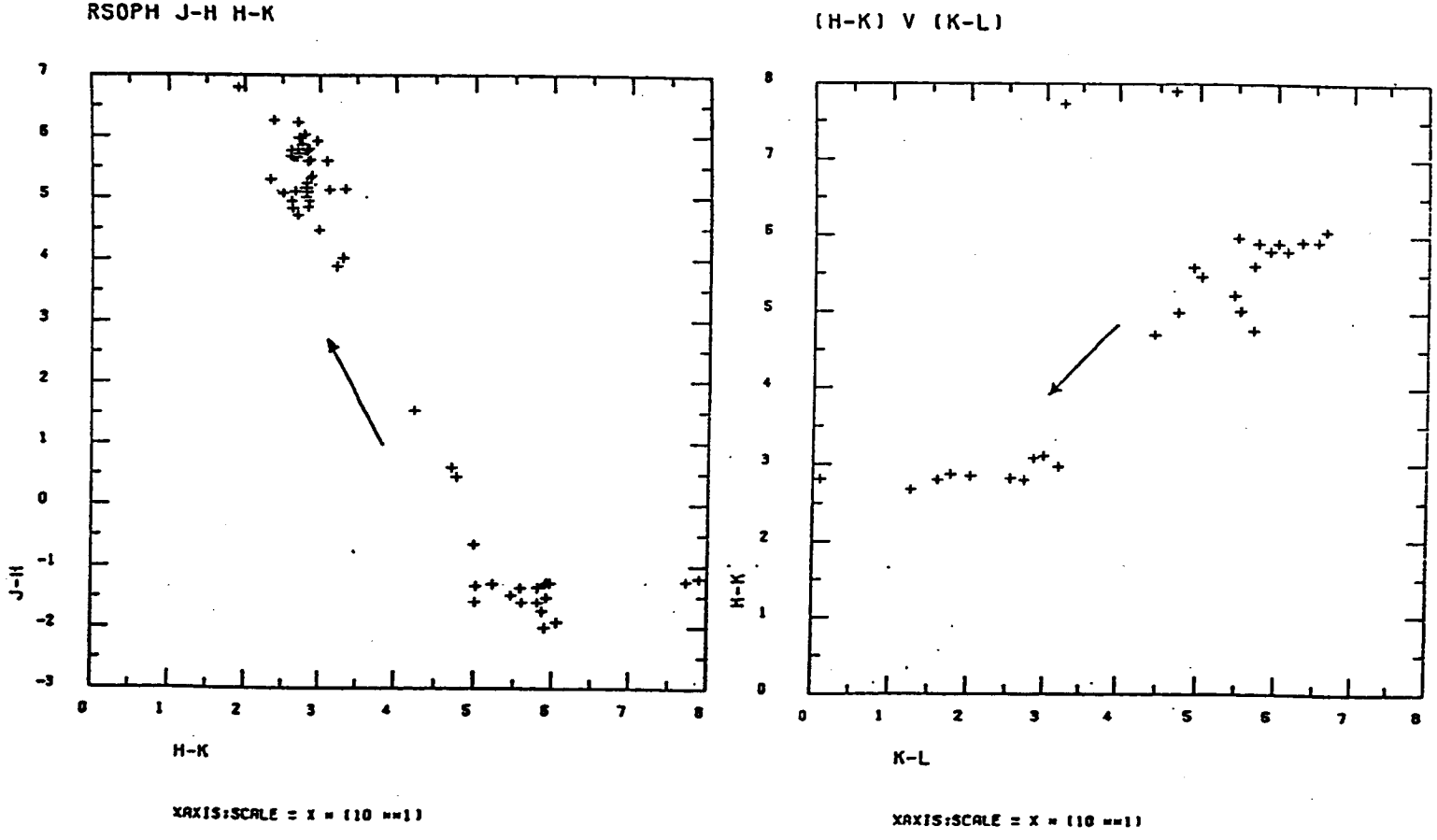

Figure 8.4. Post outburst $(J-H)_0$ - $(H-K)_0$ and $(H-K)_0$ - $(K-L)_0$ colour-colour plots for RS Oph. The arrows indicate the evolution with time during the 1985 outburst.

constant again at ~ 0.55 on day 103. The HeI line at 1.083μm is the culprit, the changes caused as it rapidly declines in strength (see section 8.4). After day 35 the $(H-K)_0$ colour declines until it too reaches a constant value of ~ 0.27 at day 107. This behaviour is probably due to the decline in intensity of the Br γ line at 2.166μm (see section 8.4). In the $(H-K)_0$-$(K-L)_0$ diagram, as well as $(H-K)_0$ becoming bluer with time so also does $(K-L)_0$, which is not to be expected if the only changing quantity was the Br γ line. In fact in this case the opposite would happen and $(K-L)_0$ should increase with time. If this diagram had been reversed in time, its behaviour could have been attributed to the formation of dust (Schmelz, 1984) so it is tempting to explain this diagram in terms of grain destruction (see Callus et al., 1986b). This is further suggested by the fit of Evans (1986) to this diagram that consisted of two components, one at 1500 K and the other at 4000 K. The cooler (presumably dust) component contributed less as time increased. However as mentioned in section 8.2 the amount of dust that could contribute at these wavelengths is fairly low.

8.4 Spectroscopy

Infrared spectroscopy was carried out on RS Oph on 1985 February 21, 1985 April 24 and 1985 June 21. The spectra were obtained in the JHK and L windows at UKIRT. Both high ($\lambda/\Delta\lambda \sim 10^3$) and medium ($\lambda/\Delta\lambda \sim 100$) resolution spectroscopy was carried out, the first being obtained with the UKIRT cooled grating spectrometer CGS2 whilst the latter was obtained with the circular variable filter (CVF).

The CVF spectrum obtained on February 21 is shown in Fig. 8.5. This spectrum (as with all the spectra) has been dereddened using the Savage-Mathis extinction law and E(B-V) = 0.73 (Snijders, 1986). In this spectrum most of the lines can be attributed to hydrogen. P α is the most dominant with Br γ-12 present. Also observable are HeI at λ = 2.058μm and

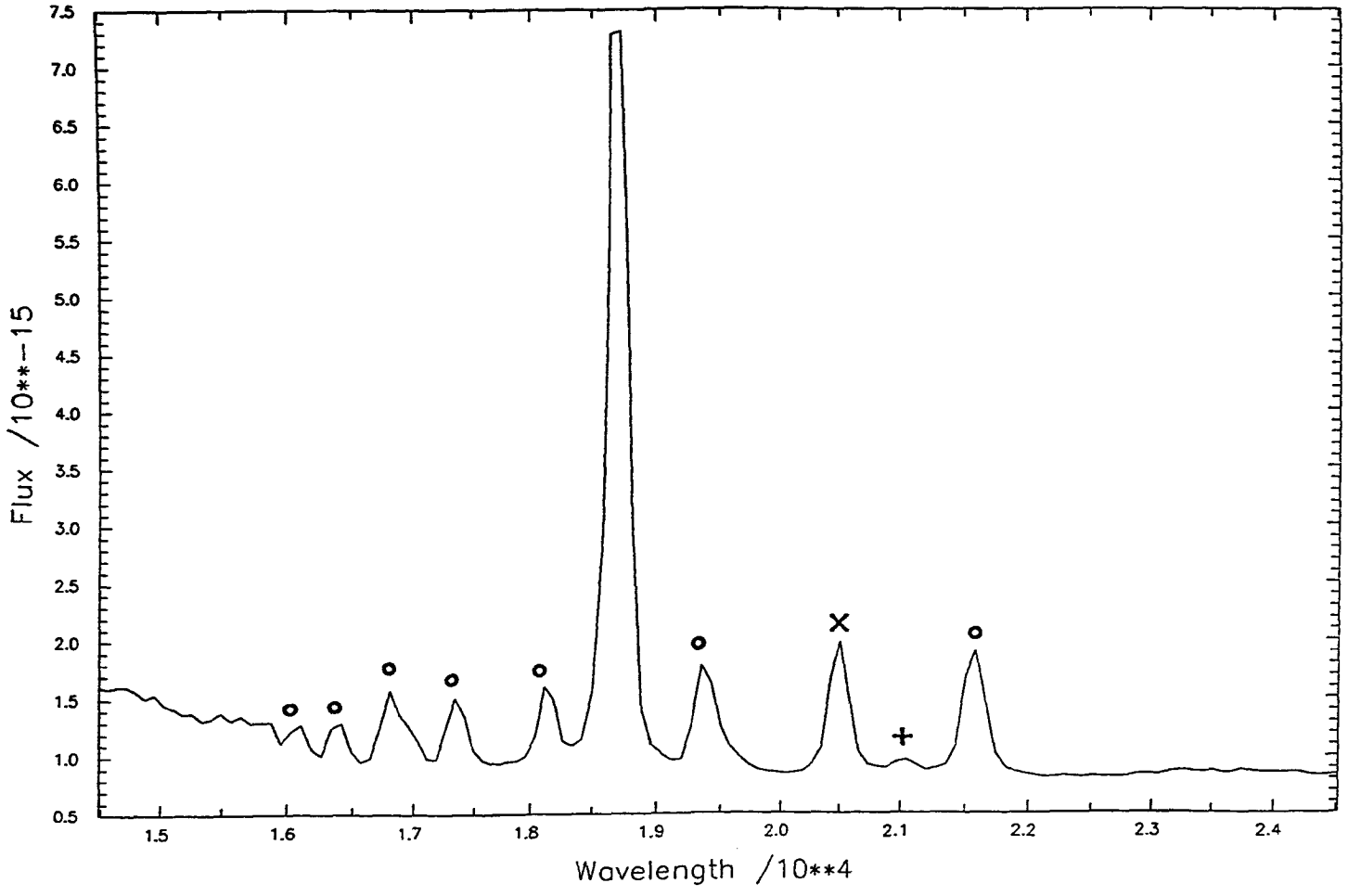

Figure 8.5. UKIRT CVF spectrum taken on 1985 February 21. Circles denote hydrogen Brackett lines, the cross HeI, and the plus sign CI. The most intense line is Pfund α. Units of flux are W cm^{-2} μm^{-1}.

CI at λ = 2.126μm. (Line identifications for all the spectra are given in Table 8.4).

We have attempted to determine the continuum of this spectrum in order to examine the properties of the region responsible for the line emission. The infrared continuum of RS Oph after outburst will probably consist of the continuum of the secondary and a nebular continuum. Evans (1986) fitted the pre-outburst near infrared photometry to an MOIII star at a distance of 1.3 kpc (see Fig. 8.6). Unfortunately due to variations in the infrared light curves both pre- and post-outburst, it is not certain if the secondary would have been this spectral type throughout the outburst. However for the purposes of fitting the continuum we assume that the secondary is indeed a MOIII star at the given distance. The first stage is to subtract this stellar continuum from our spectrum; hence all we have left are the lines sitting on top of a nebular continuum. As explained in Chapter 5, to properly fit a nebular continuum to a spectrum we need either the Hβ or HeII 1640A flux at the time the infrared spectrum was obtained. Fortunately we do have IUE spectra taken on February 21 (M. A. J. Snijders, private communication) and by ELF fits to the 1640A line the flux in this line was calculated. For the February spectrum, after the contribution of the secondary had been removed, the remainder of the continuum was fitted by a nebular continuum at a temperature of 1.65 x 10^5K and the IUE 1640A flux at this date. (The nebular continuum was found to be relatively insensitive to the values of electron density and the hydrogen/helium ratio assumed). This fitting depends on the assumption that the HeII 1640A line arises in the same region as the observed infrared nebular continuum, which may not be the case when considering the complexity of the circumstellar enviroment of RS Oph during outburst. However such a temperature of ~ 10^5K is not inconsistent with a strong HeII 1640A line as the ionization potential of helium is 24.6 eV.

This nebular continuum was then subtracted from the February spectrum

Table 8.4

Line identifications.

Date	Obs λ(μm)	Identifcation	Rest λ(μm)
Feb	1.609	H 13-4	1.611
	1.639	H 12-4	1.641
	1.679	H 11-4	1.681 (blend)
	1.734	H 10-4	1.737
	1.812	H 9-4	1.818
	1.868	H 3-4	1.876
	1.936	H 8-4	1.945
		+ ([SiVI])	1.961
	2.049	HeI	2.058
	2.104	CI	2.126
	2.157	H 7-4	2.166
April	1.635	H 12-4	1.641
	1.680	H 11-4	1.681
	1.730	H 10-4	1.737
	1.773	?	
	1.808	H 9-4	1.818
	1.867	H 4-3	1.876
	1.948	H 8-4	1.945
		+ [SiVI]	1.961
	2.047	HeI	2.058
	2.151	H 7-4	2.166
	2.313	?	
June	1.085	HeI	1.083
	1.096	H 6-4	1.094
	1.284	H 5-3	1.282
	1.536	H 18-4	1.534

1.549	H 17-4	1.544
1.554	H 16-4	1.555
1.574	H 15-4	1.570
1.589	H 14-4	1.589
1.613	H 13-4	1.611
1.642	H 12-4	1.641
1.685	H 11-4	1.681
1.739	H 10-4	1.737
1.966	H 8-4	1.945
	+ [SiVI]	1.961
2.005	possible molecular	
2.018	absorption ?	
2.057	HeI	2.058
2.168	H 7-4	2.166
2.3	CO features (see Table 8.9)	
2.465	[SiVII]	2.461
3.039	H 10-5	3.039
3.299	H 9-5	3.297

Line identifications in the 1985 February, April and June spectra of RS Oph. Columns give date when spectral features were observed, the observed wavelength of the feature, feature identification and the rest wavelength of these features.

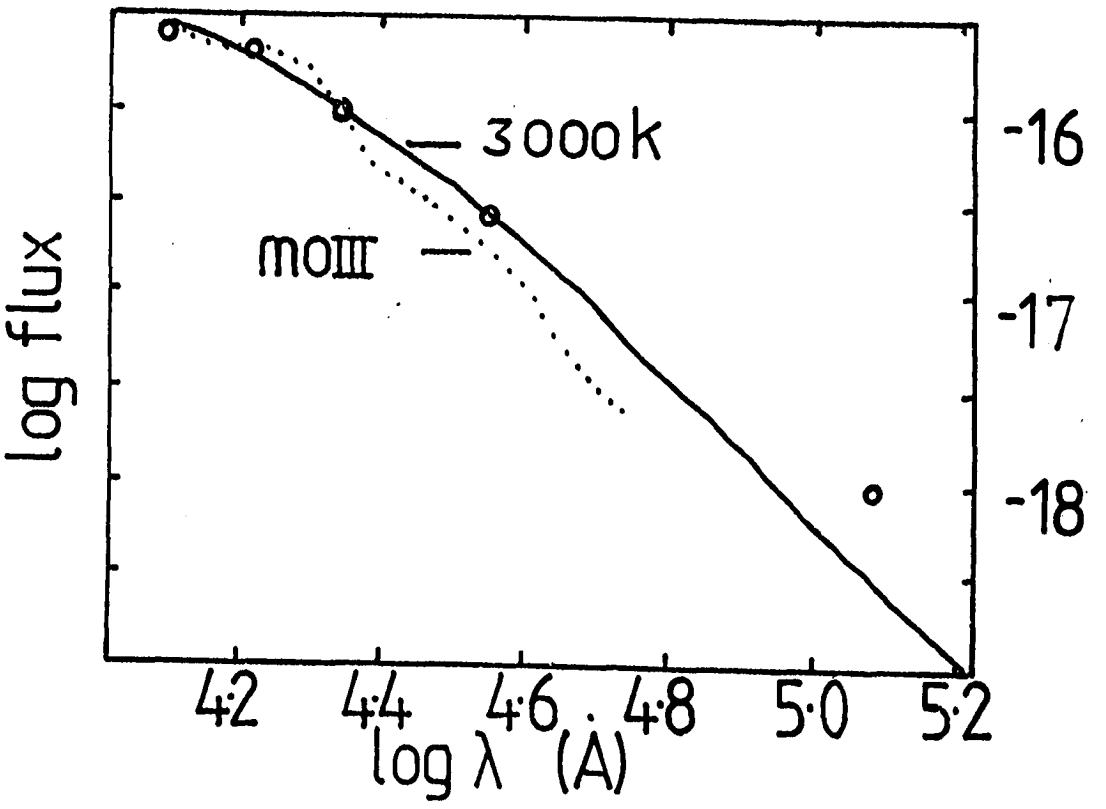

Figure 8.6. The pre-outburst infrared photometry with a MOIII star at 1.3kpc fitted to it. Flux in units of W $cm^{-2}\mu m^{-1}$. (Reproduced from Evans, 1986).

to leave just the lines. The most prominent hydrogen lines were fitted using the ELF routine in DIPSO. These fits were then added back to the nebular continuum so their equivalent widths could be found. Once these were found the temperatures implied by these lines were calculated using the procedure as described in section 5.3.2. The deduced temperatures were ~ 13000 ± 3500 K and are listed in Table 8.5. Another method of estimating the temperature in the region of the hydrogen lines is by determination of the height of the Brackett discontinuity at ~ 1.459μm. In February this gave a temperature of ~ 12000 K, however as this discontinuity is at the edge of the atmospheric window it can only be regarded as a lower limit.

When we superimpose the calculated nebular continuum for February on our spectrum we clearly notice the excess at longer wavelengths (see Fig. 8.7) over the fitted nebular continuum. As already noted emission by dust can be ruled out; apart from there being no evidence of dust at these wavelengths, extrapolating the excess to 3.5μm on the assumption of dust emission (i.e. a blackbody extrapolation) gives L ≃ 2.0 mags, compared with an observed value of ≃ 3.9 mags, which is consistent with the value of L ≃ 3.7 mags when the nebular continuum is extrapolated. Evans (1986) interpreted this excess as emission in the first overtone of the vibration-rotation transition in CO (λ = 2.3μm). Emission in this band has been reported in the Mira component of the symbiotic-like star BI Cru by Whitelock et al. (1983). CO is, of course, present in this system in the secondary as shown by the CO absorption bands in the high resolution spectrum in June (see below), and probably a stellar wind would transport CO out into the circumstellar enviroment. By February 21, if the ejected material was travelling at a velocity of ~ 1500 kms^{-1} (Rosino & Iijima, 1986) it would have reached a distance of ~ 3 x 10^{14}cm; whilst the stellar wind travelling at a velocity of ~ 20 km s^{-1} (Gorbatskii, 1972) would have reached a distance of ~ 10^{15}cm in the 18 years since the previous outburst. Hence the only region where CO emission would be possible is in the HII

Table 8.5

Temperatures implied by the H lines.

Date	Line	EW(nm)	Temp
Feb	Pasc α	180.0	20000
	Br γ	28.9	12600
	Br δ	17.5	12600
	Br ε	13.3	10350
	Br 10	10.5	10000
April	Pasc α	85.4	70000
	Br γ	12.7	44700
	Br δ	31.4	7950
	Br ε	7.3	25100
	Br 10	5.6	20000

The temperatures implied by the hydrogen lines as deduced from their equivalent widths in 1985 February and April.

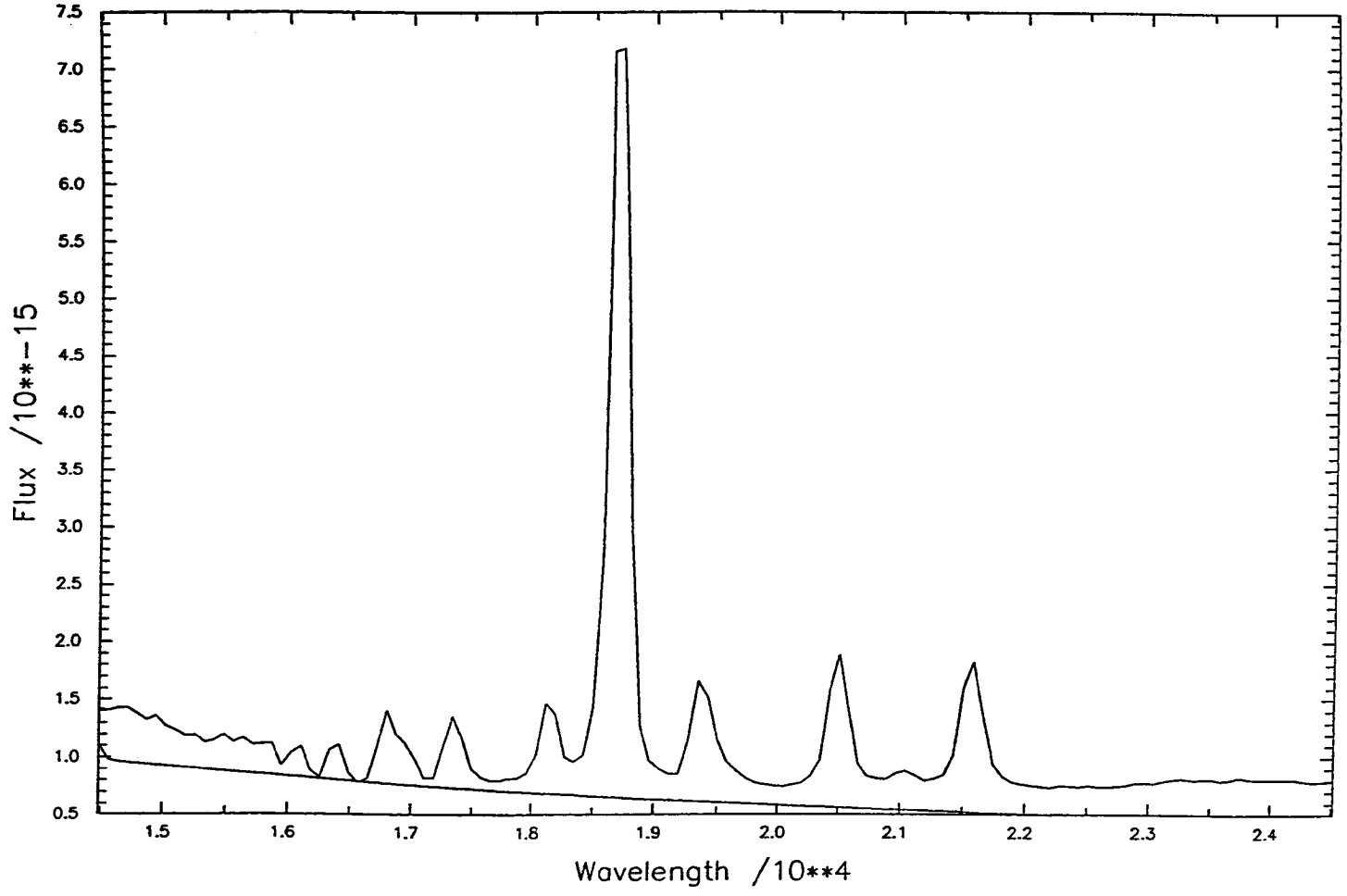

Figure 8.7. The 1985 February spectrum minus the stellar continuum, fitted with a nebular continuum at a temperature of 1.65×10^5K. Note the excess at longer wavelengths.

region set up by the radiation field of the nova at outburst; CO will not survive in the shock heated regions.

The CVF spectrum obtained on April 26 is shown in Fig. 8.8. The lines have not changed noticeably from February except that the CI feature at λ = 2.126μm has almost disappeared. The excess at longer wavelengths has also gone to be replaced by the now dominant continuum of the secondary. Again we have attempted to remove the continuum to find the temperature implied by the hydrogen lines. Unfortunately we do not possess an IUE spectrum for April 26 from which we could obtain the HeII 1640A flux. However we do have IUE spectra obtained at various times between 1985 February and May, so after determining the HeII 1640A flux at these times we interpolated to this date (see Fig. 8.9). Thus after the continuum of the secondary was removed a nebular continuum at a temperature of 10^5K fitted the remainder. Whether this temperature drop from February is real or not is debatable as a 40% decrease in the interpolated HeII 1640A flux for this time results in the nebular continuum at a temperature of 1.65×10^5K. Now following the same procedure as for February, the temperatures implied by the hydrogen lines is T = 40000 K ± 20000 K, excluding the Br δ line at λ = 1.945μm. Br δ gave a temperature of ~ 8000 K, which is clearly inconsistent with the other hydrogen lines. It is possible that another feature was contributing to this line so increasing the equivalent width, which in turn would imply a lower temperature. A possible candidate, particularly in view of later spectra (see below) is the [SiVI] λ = 1.961μm coronal line, although there is no evidence of any other coronal line in this spectrum.

As the continuum in the April spectrum is so close to that of the secondary's it is not possible to make any sensible measurement of the Brackett discontinuity and thus obtain independent evidence of the temperatures suggested by the hydrogen lines. The deduced temperatures for both February and April at these infrared wavelengths are discussed in

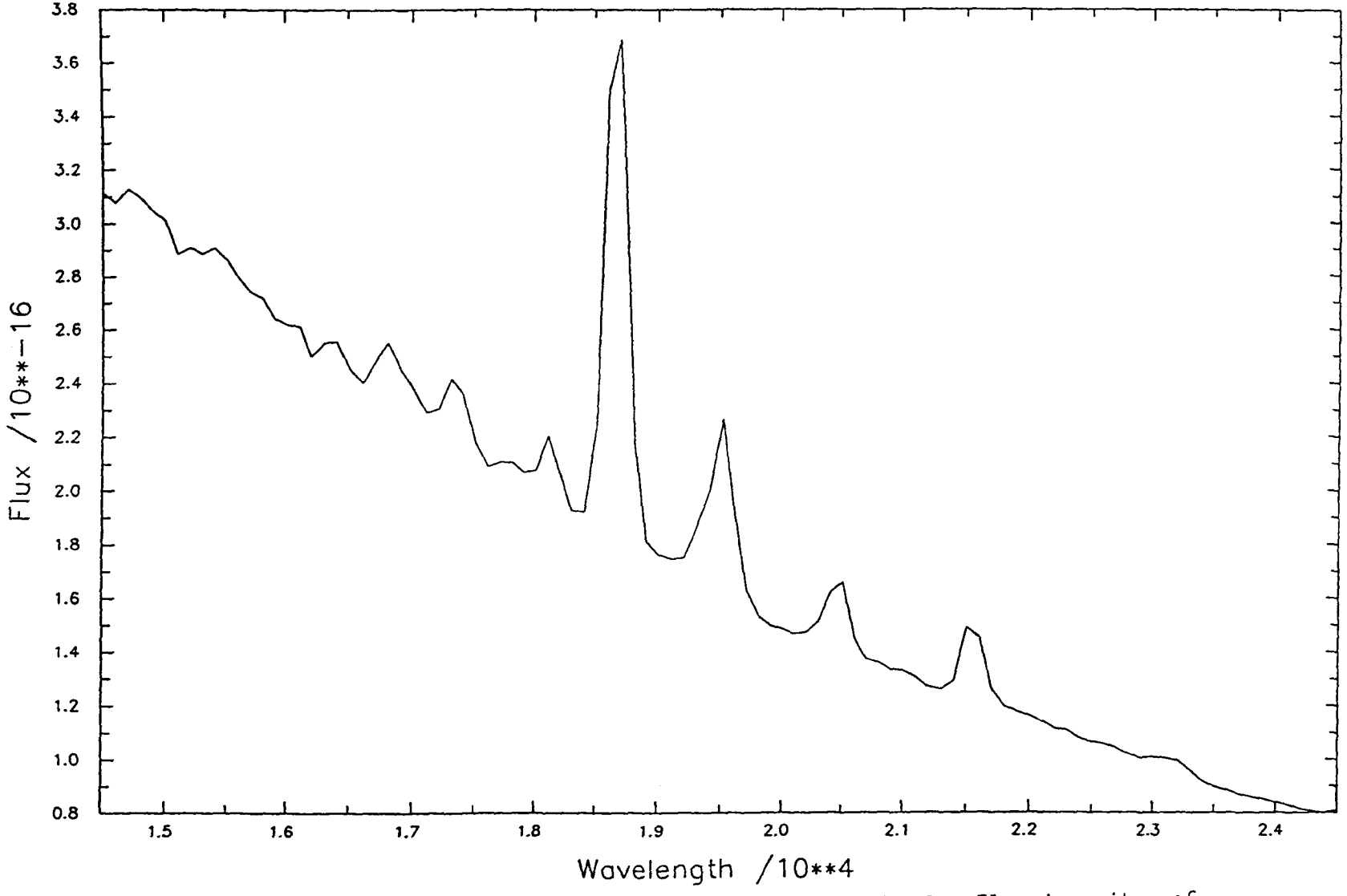

Figure 8.8. UKIRT CVF spectrum taken on 1985 April 26. Flux in units of W cm^{-2} μm^{-1}.

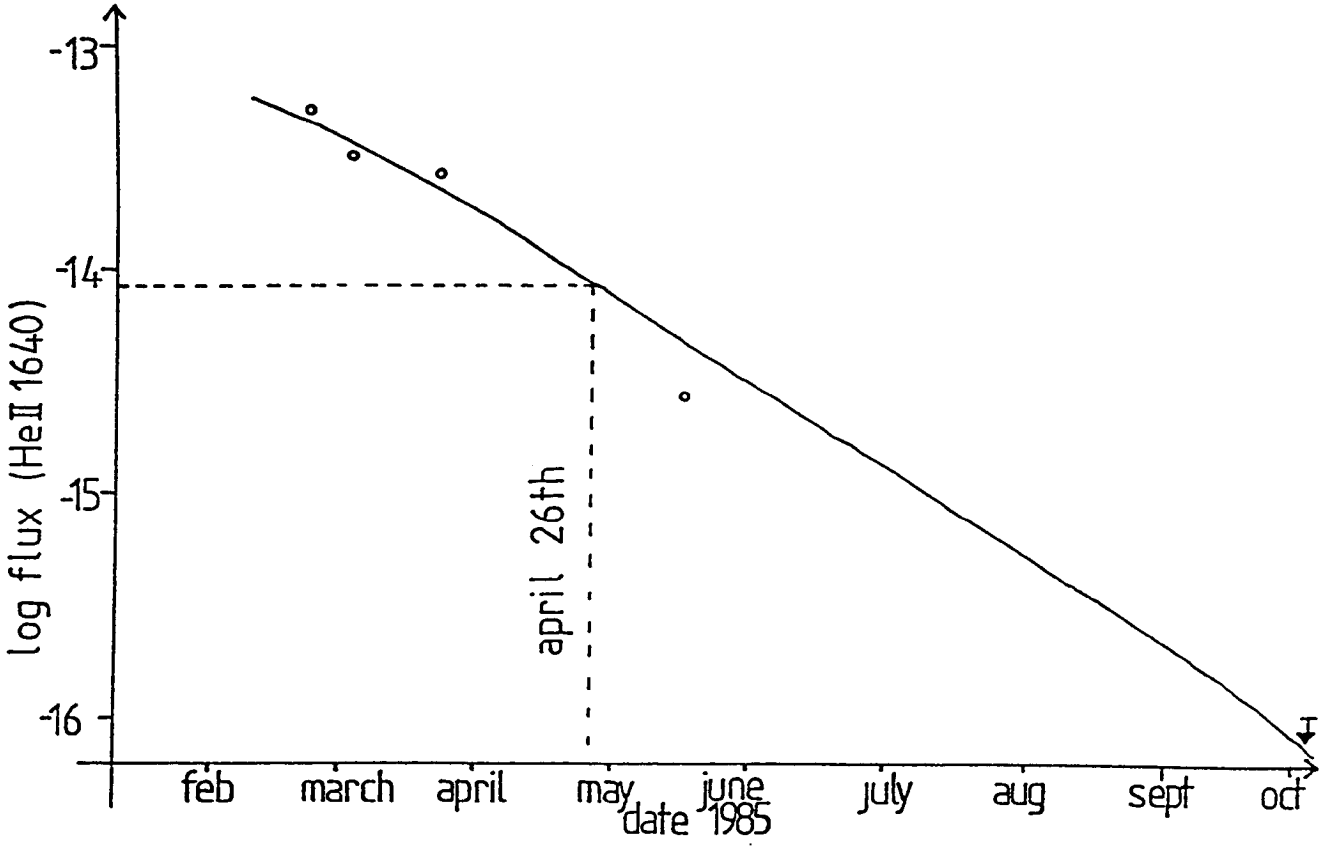

Figure 8.9. Graph of the flux in the HeII 1640A flux line as calculated by ELF from the IUE spectra, against time. This enabled us to determine the HeII 1640A flux at the time of the April spectrum (see text).

Chapter 9 where a model for the infrared behaviour of the nova is attempted.

Turning now to the high resolution June spectra, apart from the hydrogen P α-γ, Br γ-18, Pf δ-ε and helium lines, clearly identifiable in absorption in the K window at ~ 2.3μm are the first overtone vibrational rotational bands of CO. (The merged June spectrum is shown in Fig. 8.10 and the CO bands in greater detail in Fig. 8.11). These features can only arise in the giant secondary of RS Oph and are discussed in greater detail in section 8.5. Also present in these spectra are the coronal lines [SiVI] and [SiVII] at 1.961μm and 2.461μm respectively. In the optical and ultraviolet, coronal lines became prominent ~ 30 days after outburst and began declining ~ 40 days later (Rosino & Iijima, 1986; Snijders, 1986). February 21 is day 25/26, April 26 is day 90/91 and June 21 is day 146/147. Considering all the recorded outbursts of RS Oph, coronal lines have been known to appear as early as 6 days after outburst (Barbon et al., 1968) and persist until ~ day 200 (Rosino, 1986), so it is perhaps surprising that there was no evidence of coronal lines in the February spectrum. However listed in Table 8.6 are the product of the electron and the proton density as derived from the Brackett lines in the February spectrum by rearrangement of equation 8.7 (see next section) and assuming a temperature of 13000 K. Obviously we would expect this product to be the same regardless of which hydrogen line we were considering. We can see that this product as derived from the Br δ line gives us the greatest value. As $f \propto n_e n_p$, this may indicate that the flux in this line was too high suggesting that perhaps it was contaminated by another feature. It is therefore possible that the [SiVI] coronal line at 1.961μm was present in the February spectrum.

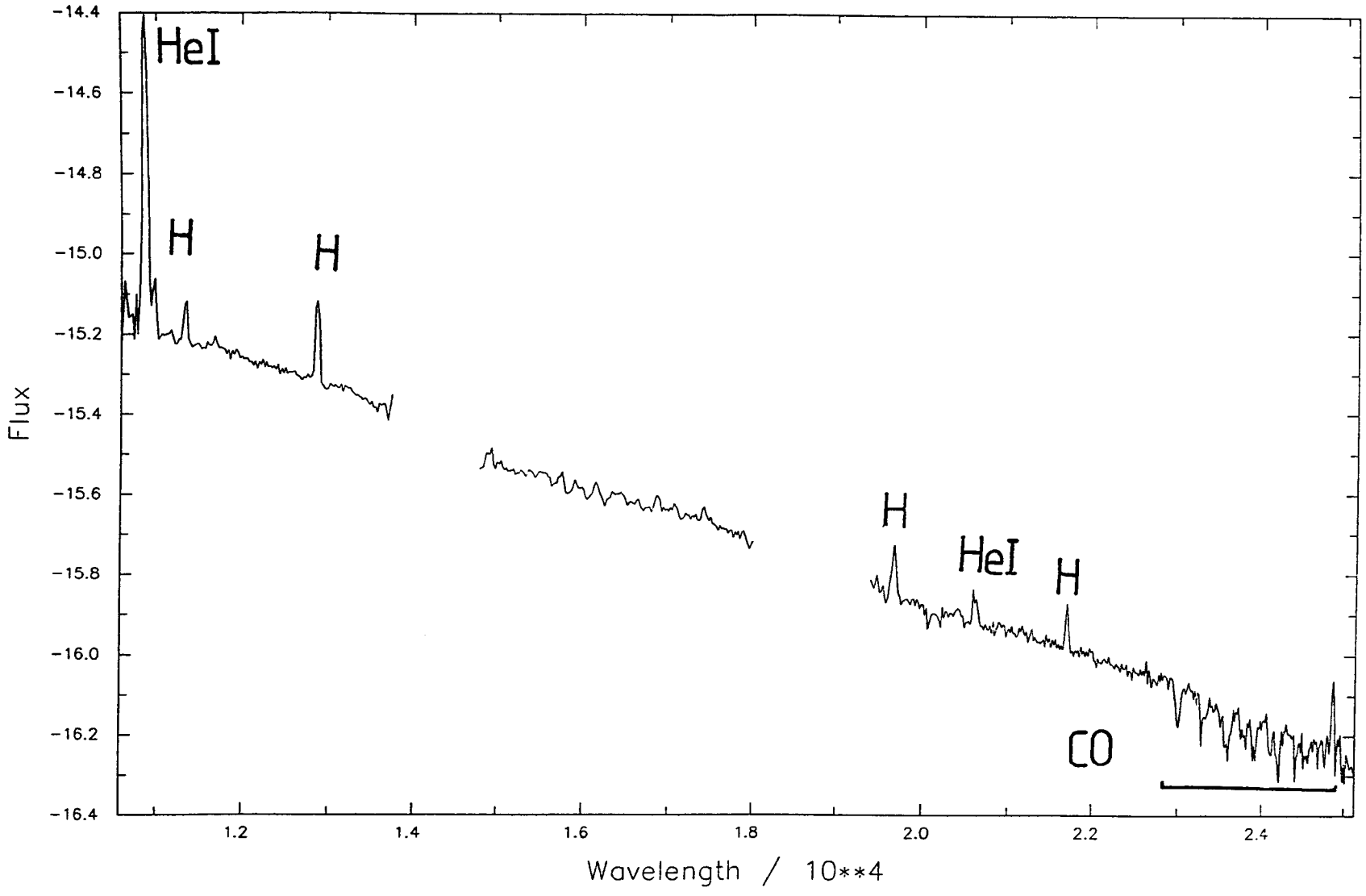

Figure 8.10. UKIRT merged spectrum obtained on 1985 June 21. Flux in units of W $cm^{-2}\mu m^{-1}$.

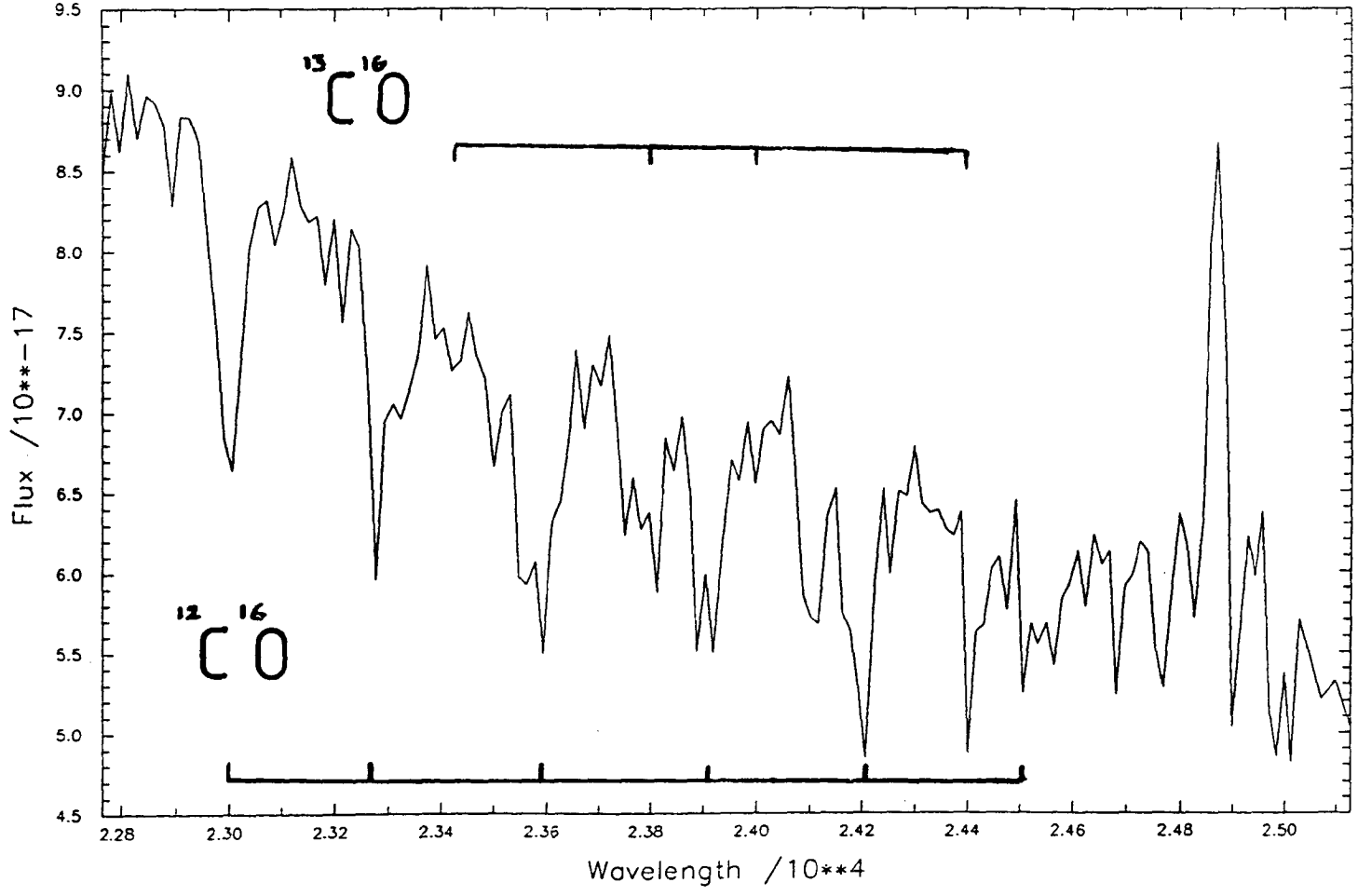

Figure 8.11. CO bandheads from the K window of the June spectra. Flux in units of W cm^{-2} μm^{-1}.

Table 8.6

Line	NeNi
Br γ	1.00
Br δ	1.11
Br ε	0.77
Br 10	0.72

The product of the electron density and proton density (relative to this quantity in the Br γ line) as deduced from the hydrogen Brackett lines in the February spectrum.

8.4.1 To Find the Reddening

It should be possible, knowing the fluxes in the infrared hydrogen lines, to determine the reddening if we assume that conditions in the nova remnant after outburst can be described by case B recombination theory. (Case B is described by Baker & Menzel, 1938). In this way we can calculate the relationship between the intensities of the hydrogen lines assuming no reddening, thus the departure from these intensities should lead to a reddening law.

If the lines are optically thin (which we assume is the case for the hydrogen lines in RS Oph) then the energy emitted in a transition from the upper (n) to lower (n') level is given by

$$E_{nn'} = N_n A_{nn'} h\nu_{nn'} \tag{8.4}$$

where N_n is the number of atoms in level n, $A_{nn'}$ is the Einstein A coefficient for transitions between states n and n', and $\nu_{nn'}$ is the frequency of the transition. Now

$$N_n = b_n N_p N_e \, h^3/(2\pi mkT)^{3/2} \, n^2 \exp(hRcZ^2/n^2kT) \tag{8.5}$$

(e.g. Baker & Menzel, 1938) where N_p is the number density of protons, N_e is the number density of electrons and b_n is a factor indicating the degree of departure from thermodynamic equilibrium at temperature T. All other symbols have their usual meanings. So combining equations (8.4) and (8.5) we get

$$E_{nn'}/(XN_pN_eT^{-3/2}) = b_n \exp(hRcZ^2/(n^2kT))A_{nn'}(n^2/n'^2 - 1) \tag{8.6}$$

where $X = h^3/(2\pi mk)^{3/2}$, a constant. So on the assumption that the quantities N_p, N_e and T are the same for all of the hydrogen lines then calculation of the RHS of equation (8.6) will lead to ratios between the intrinsic fluxes in each of the hydrogen lines since $E_{nn'} \propto$ flux.

Now the observed flux $f(\lambda)$ will be given by

$$f(\lambda) = f_0(\lambda)e^{-\tau} \tag{8.7}$$

where $f_0(\lambda)$ is the intrinsic flux and τ is the optical depth. Thus for any two hydrogen lines 1 and 2

$$f_1/f_2 = f_{01}/f_{02} \exp(-\Delta\tau) \tag{8.8}$$

where $\Delta\tau = [\tau_1 - \tau_2]$. On normalizing all line fluxes to that of the Br γ line the $\Delta\tau$ for each line was calculated using equations (8.6) and (8.8). The $A_{nn'}$, were obtained from Menzel & Pekeris (1935) and the b_n's were extrapolated from those given by Baker & Menzel (1938). This analysis was undertaken using the February data only, as at this time the temperature implied by the lines suggested that they originated from one region only, whereas the April data implied that the lines came from at least two regions (see Chapter 9). Thus $\Delta\tau$ was calculated for temperatures of 13000 K ±3500 K. In order to do this the flux from the lines was measured from the reddened spectra in two ways. Firstly the ELF routine in DIPSO was used and secondly by using the FLUX command (also in DIPSO). Thus, some estimate of the errors on the observed fluxes could be made.

Values of the two sets of observed fluxes and f_1/f_2 are given in Table 8.7. f_{01}/f_{02} and $\Delta\tau$ for temperatures ranging between the calculated February values are given in Table 8.8. A plot of $\Delta\tau$ against $1/\lambda$ is given in Fig. 8.12; also plotted on this graph is the line corresponding to an

Table 8.7

Fluxes in the hydrogen lines.

Line	Flux (ELF)	f/f(Brγ)	Flux (FLUX)	f/f(Brγ)
Pasc α	10.13	5.60	10.91	4.93
Br γ	1.81	1.00	2.21	1.00
Br ε	0.79	0.44	0.82	0.37
Br 10	0.57	0.32	0.77	0.35
Br 12	0.43	0.24	0.36	0.16
Br 13	0.40	0.22	0.27	0.12

This gives the observed reddened fluxes in the hydrogen lines in February as obtained fron the ELF and FLUX routines in DIPSO. Also given are the line fluxes normalised to that of the Brγ line. (1 unit of flux = 10^{-10} ergs cm^{-2} s^{-1}).

Table 8.8

Line	Temp	fo/foBr(γ)	Δτ(ELF)	Δτ(FLUX)
Pasc α	9500	10.49	0.63	0.76
	13000	10.60	0.64	0.77
	16500	11.21	0.70	0.82
Br γ	9500	1.00	0.00	0.00
	13000	1.00	0.00	0.00
	16500	1.00	0.00	0.00
Br ε	9500	0.53	0.19	0.35
	13000	0.50	0.14	0.30
	16500	0.50	0.14	0.30
Br 10	9500	0.41	0.26	0.16
	13000	0.39	0.20	0.10
	16500	0.37	0.17	0.06
Br 12	9500	0.24	0.00	0.37
	13000	0.22	-0.07	0.30
	16500	0.22	-0.08	0.28
Br 13	9500	0.19	-0.16	0.44
	13000	0.18	-0.21	0.39
	16500	0.17	-0.24	0.37

Intrinsic values of hydrogen line flux normalized to the intrinsic flux in the Brγ, at different temperatures. Also tabulated is the value of Δτ obtained using these intrinsic fluxes and the observed fluxes as read from ELF and FLUX (see text).

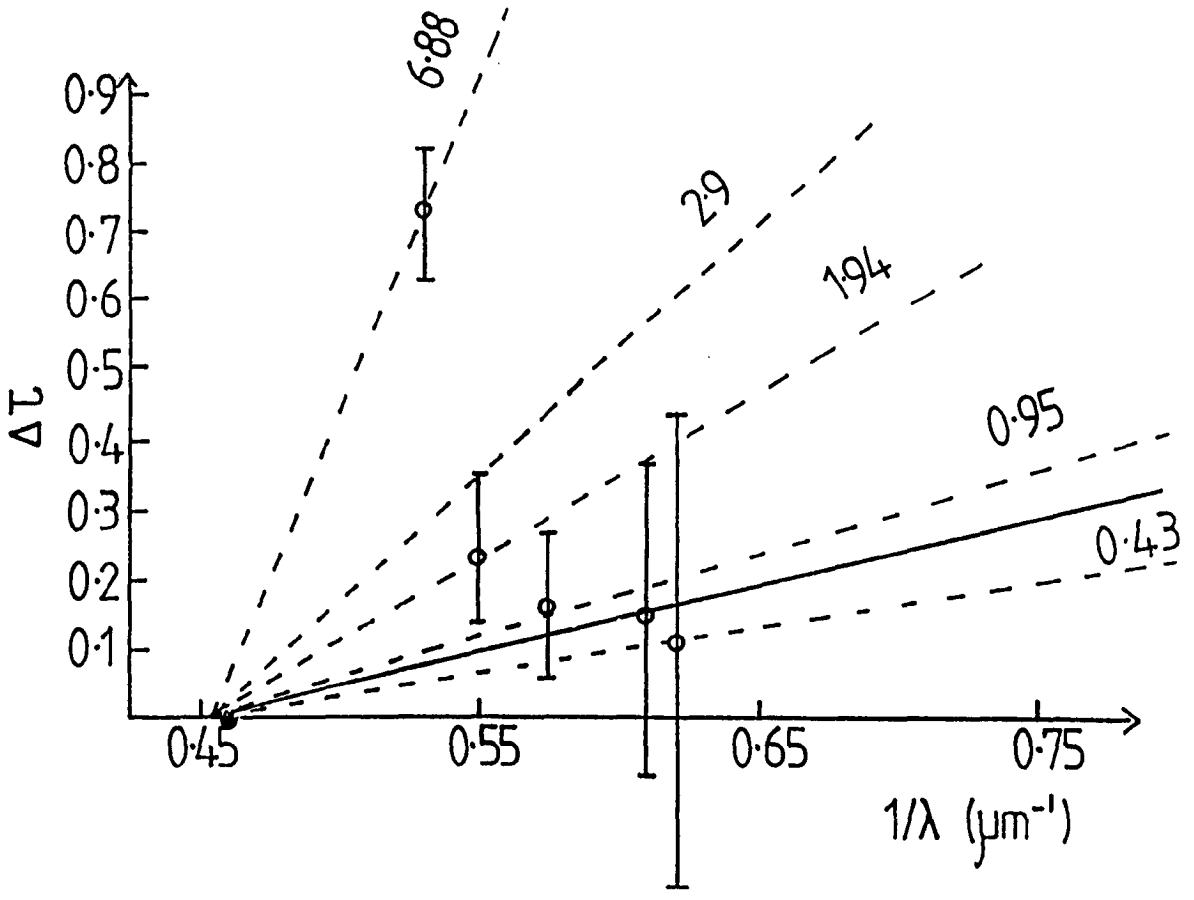

Figure 8.12. Graph of $\Delta\tau$ against $1/\lambda$ for the hydrogen lines in the February spectrum. This enables us to estimate the reddening in RS Oph at this time . The dotted lines represent different values of E(B-V), which are indicated by the numbers above each of the lines. The solid line represents an E(B-V) of 0.73, the value obtained by the ultraviolet studies of Snijders (1986).

E(B-V) of 0.73, the reddening obtained from ultraviolet studies (Snijders, 1986). Ignoring the P α point (which we will come to later) this reddening gives a reasonable fit to the Brackett lines. (The Br δ and 11-4 lines have been left out of this plot as they are both obviously contaminated by other lines and thus will not give a true indication of the reddening). However taking average values for the five plotted points and fitting a least squares fit to this gives a line with reddening law of E(B-V) ~ 0.95±0.5. So these results are consistent with the ultraviolet results.

Returning now to the P α line, the reddening deduced from this line, i.e. E(B-V) ~ 6.88, differed greatly from that deduced from the other lines. This implied that the flux in this line was greatly underestimated. (This was also hinted at by the determination of its equivalent width which seemed a little low in comparison with those of the other lines, see Table 8.5, thus suggesting a higher temperature). However it is very difficult to see why the flux in this line alone should be anomalously low.

8.5 The Secondary Star

Although in the above work we have considered the secondary star as being an MOIII star at a distance of 1.3 kpc as a reasonable approximation, we can further determine its nature by examination of the June spectrum. The continuum of these spectra is clearly that of the secondary star only. Already mentioned are the CO 2.3μm bands in absorption (section 8.4). Smoothing these features into 20A bins (the optimum resolution of the CGS2 at this wavelength) by use of the QSM routine on DIPSO, we have determined the wavelengths of the bandheads of this feature (given in Table 8.9). Some of these correspond to the 0-2, 1-3, 2-4,3-5, 4-6 and 5-7 levels of $^{12}C^{16}O$ and features due to the corresponding $^{13}C^{16}O$ are also present. Crude determination of the equivalent widths of these features (see Table 8.9) lead to an estimate of the C^{12}/C^{13} ratio in the secondary as equivalent width $\propto$ the number density of CO (e.g. Spitzer [1979], assuming

Table 8.9

Identified CO bandheads.

λ(μm)obs	Identification		λ(μm)rest	EW(nm)
2.300	$C^{12}O^{16}$	2-0	2.295	1.35
2.329	$C^{12}O^{16}$	3-1	2.325	1.19
2.342	$C^{13}O^{16}$	2-0	2.346	0.18
2.358	$C^{12}O^{16}$	4-2	2.353	1.34
2.379	$C^{13}O^{16}$	3-1	2.374	0.15
2.389	$C^{12}O^{16}$	5-3	2.385	1.08
2.411	$C^{13}O^{16}$	4-2	2.408	-
2.419	$C^{12}O^{16}$	6-4	2.417	1.16
2.441	$C^{13}O^{16}$	5-3	2.440	0.13
2.453	$C^{12}O^{16}$	7-5	2.448	0.80

The CO bandheads in the K window of the June spectrum. Given also are the equivalent widths of each feature.

that this region is optically thin). This ratio is ~ 8 which is consistent with that of an oxygen rich secondary (Knapp et al., 1985). It must be noted however that this CO may be material produced by the CNO thermonuclear runaway on the surface of the white dwarf which has been deposited in the atmosphere of the secondary during ejection and thus it is not necessarily a product of the secondary. But further evidence of the oxygen rich nature of the secondary is provided by the smoothness of the stellar continuum in the region of 3 - 3.3μm. This suggests that there are no hydrocarbon based molecules in the stellar atmosphere as are witnessed in carbon rich stars (Ridgway, 1984). Thus an oxygen rich star seems the more likely for the secondary in RS Oph.

Evans (private communication) has determined the spectral type of the secondary by use of the strength of the CO bands. He did this by determining the [2.35μm] - [2.2μm] colour as this gives a reasonable indication of spectral type as the depth of the CO bands is spectral type dependent (Kenyon & Gallagher, 1983). This method revealed the spectral type as being K8III (± 2 sub-divisions). The distance to RS Oph can be estimated once we know its spectral type, if we have its apparent visual magnitude at the time at which the data leading to the determination of this spectral type were obtained. Snijders (1986) has reviewed several methods of distance determination (see also Chapter 7) and concludes that $1.3 < D(kpc) < 2.0$ with a most likely value of 1.6 kpc. 2.0 kpc is considered a strict upper limit on the distance as this was determined from the absence of interstellar absorption in the Carina arm. Albinson et al. (1985) obtained simultaneous optical and infrared photometry at SAAO on 1985 June 27, just 6 days after the June spectrum was obtained. Taking E(B-V) to be 0.73 the distance to RS Oph was calculated for spectral types K6III - M0III using the distance modulus relationship (absolute magnitudes for standard stars were taken from Allen, 1973). Thus the range in distance in these instances is $0.77 < D(kpc) < 0.81$. These distances do

seem a little on the low side when considering Snijders' (1986) comments and perhaps suggest that it is not valid to use the apparent visual magnitude obtained 6 days after the spectral type was determined as the star may have fluctuated in this time. This is further borne out by the fact that Albinson et al. (1985) obtained a variation in the visual magnitude of 0.14 mags in just one day. However using both the optical and infrared data of Albinson et al. (1985) and comparing spectroscopy of standard stars (Strecker et al., 1979) it was found that the distance was 1.0 kpc for a M0III star and 1.8 kpc for a M2III star (as suggested by Barbon et al., 1968). (A later spectral type was excluded on the grounds that the distance then became greater than 2.0 kpc). These methods of distance determination all assume that the giant star in RS Oph will have the characteristics of a 'normal' field giant which maybe is not the case of giants in binary systems. However the spectral type of the secondary is thus probably within the range K6III - M2III. But it is just possible, given the binary nature of the system, that the secondary does exhibit irregular pulsations and thus its spectral type would change with the pulsations.

8.6 Conclusion

In this chapter we have shown how the infrared photometry and spectroscopy taken of RS Oph after its 1985 outburst can be a valuable source of information both by itself and in conjunction with data taken at other wavelengths. The nature of RS Oph as possessing a gas shell of many regions at different temperatures (as discussed by Bode & Kahn, 1985 when considering the x-ray data) has been confirmed. Fits to the infrared continuum revealed a nebular continuum at a temperature of $\sim 10^5$K whilst (at least in February) the hydrogen lines seemed to originate from a region at $\sim 10^4$K. The observations of infrared coronal lines suggested further regions with temperatures of $\sim 10^6 - 10^7$K.

The reddening of RS Oph as determined from the Brackett lines of hydrogen has been shown to be consistent with the ultraviolet value of E(B-V) ~ 0.73 and thus the earlier conclusion of Feast & Glass (1974) of high reddening from infrared photometry has been invalidated.

One obvious thing to search for in the infrared is for the existence of dust as it is most dominant here. There was little evidence for a hot carbon based dust in RS Oph, but the IRAS AO data hinted that there may be a cool dust component. The pre-outburst N point observation indicated that the presence of silicate dust could not be categorically ruled out. That such a type of dust may have existed was further indicated by the apparent oxygen rich nature of the secondary as determined from the June spectra. Spectroscopy at ~ 10μm during quiescence would thus be required to see when (and if) this dust forms so perhaps differentiating between dust formed from material in the ejecta and dust formed from the stellar wind of the secondary.

The secondary star in the RS Oph system had already been established to be a late type giant from optical data (Barbon et al., 1968; Wallerstein, 1969; Bruch, 1986a,b). Hence the obvious waveband to study the secondary is the infrared since it is most prominent at these wavelengths. Indeed the continuum in the June high resolution spectrum was that of the secondary's and its 2.3μm CO bands were clearly seen in absorption. From this spectrum the spectral type of the secondary was determined to lie between K6III - M2III. Thus, assuming these spectral types, the distance was estimated between 0.77 - 1.8 kpc. The nature of the secondary is perhaps one of the most interesting features of the RS Oph system and as such has not really been probed extensively. The infrared photometry showed variability after the star had returned to its pre-outburst colours. This variability may be connected with irregular pulsations in the secondary or perhaps the re-establishment of an accretion disc. Further long term infrared data on this object are clearly required

if we are to fully understand the nature of its secondary.

CHAPTER 9

A FREE-FREE MODEL FOR THE INFRARED EMISSION FROM RS OPHIUCHI.

9.1 Introduction

The recurrent nova RS Oph underwent its last outburst on 1985 January 26 (Morrison, 1985). As with the previous outbursts there was no evidence to suggest the presence of dust at JHKL wavelengths (see Chapter 8). We assume then that the infrared emission in these wavebands for the first months after outburst can be modelled in terms of thermal bremsstrahlung from an expanding gas. Unfortunately unlike the case of GQ Mus 1983 (see Chapter 6), the ejected gas in RS Oph is not freely expanding as it has been established that prior to outburst the nova is surrounded by a circumstellar envelope (Wallerstein, 1958; Pottasch, 1967) which probably originates from leakage from the giant secondary of the system (Evans, 1986). This complicates the model as now we will have to deal with deceleration and shocks as the ejecta collide with this circumstellar envelope.

In this chapter a basic model for describing the infrared emission for the first months after outburst of RS Oph is developed and compared to the actual observations (see Chapter 7 for a review of RS Oph).

9.2 The Model

This model for the infrared emission of RS Oph is essentially that of Bode & Kahn (1985) to explain the radio and x-ray emission of the star, taking account of the ideas of Spoelstra et al. (1987) to explain the radio 'flare' observed 41 days after outburst.

The Bode & Kahn (1985) model is spherically symmetric in which high velocity ejecta (initial velocity ~ 3000 km s^{-1}) interact with a slow moving preoutburst wind. The giant secondary has a wind mass-loss rate M

and terminal speed V_w whilst the nova explosion ejects mass M_e, initially in the form of a homogeneous sphere expanding with speed V. This sets up a double shock system in the gas i.e. a forward and reverse shock.

Now based on Bode & Kahn (1985) a shock with fixed speed larger than V, intially propagates into the wind; the postshock pressure is

$$P = 3\dot{M}/(16\pi V_w t^2) \tag{9.1}$$

at time t; this pressure also drives the reverse shock into the ejecta. The equation of motion of the reverse shock is

$$\rho_e(R_{rev}/t - \dot{R}_{rev})^2 = P \tag{9.2}$$

where $\rho_e = 3M_e/(4\pi V^3 t^3)$ is the density in the unshocked ejecta, so that

$$R_{rev} = Vt(1 - (t/t_*)^{1/2}) \tag{9.3}$$

is the radius of the reverse shock at time t and $t_* = M_e V_w/(\dot{M}V)$. In dealing with the reverse shock R_{rev} must always be positive or else the ejecta do not expand but contract which is clearly not the case, therefore $t/t_* < 4/9$ (from equation 9.3). The density immediately post-shock has been set equal to $4\rho_e$, valid for a strong adiabatic shock.

In dealing with the forward shock, the expanding ejecta do work on the stellar wind at a rate

$$W = 4\pi P r^2 \dot{r} = 3\dot{M}V^3/4V_w \times (1 - (t/t_*)^{1/2})^2 \times (1 - 1.5(t/t_*)^{1/2}) \tag{9.4}$$

Most of the energy transfer occurs at an early stage and the result can only be applied up to the instant when r becomes zero. Thus integrating equation (9.4) from $t/t_* = 0$ until $t/t_* = 4/9$ we find that the total energy communicated by the ejecta to the wind is $E = 0.0052 M_e V^2$. As the blast wave advances into the wind only an insignificant amount of energy is lost by radiation. The explosion is therefore modelled by Bode & Kahn as the instantaneous release of energy at a point and so they determine the outer shock radius to be

$$R_s = at^{2/3} \tag{9.5}$$

where $a = 6^{1/3}(EV_w/M)^{1/3} = 0.68 M_e^{1/3} V^{2/3} V_w^{1/3} / M^{1/3}$ (9.6)

In the Spoelstra et al. (1987) model they use the presence of a magnetic field to explain the radio flare in terms of magnetic flux reconnection. They point out that the cooled ejecta (and by implication, the cooled wind) will have been compressed in volume by a factor $\sim 10^4$ (the square of the Mach number in the reverse and forward shock) but calculate that the presence of a magnetic field will reduce this considerably to ~ 65 (varying by factors ~ 2, depending on the geometry of the magnetic field).

We combine these two models and thus suppose that the RS Oph remnant has the structure given in Fig. 9.1, where region A is the unshocked ejecta, region Aa is the hot shocked ejecta, region B is the cooled shocked ejecta, region C is the cooled shocked wind, region Ca is the hot shocked wind and region D is the unshocked wind (this is represented in plan in Fig. 9.2 for illustration only, planar geometry has not been used in the model).

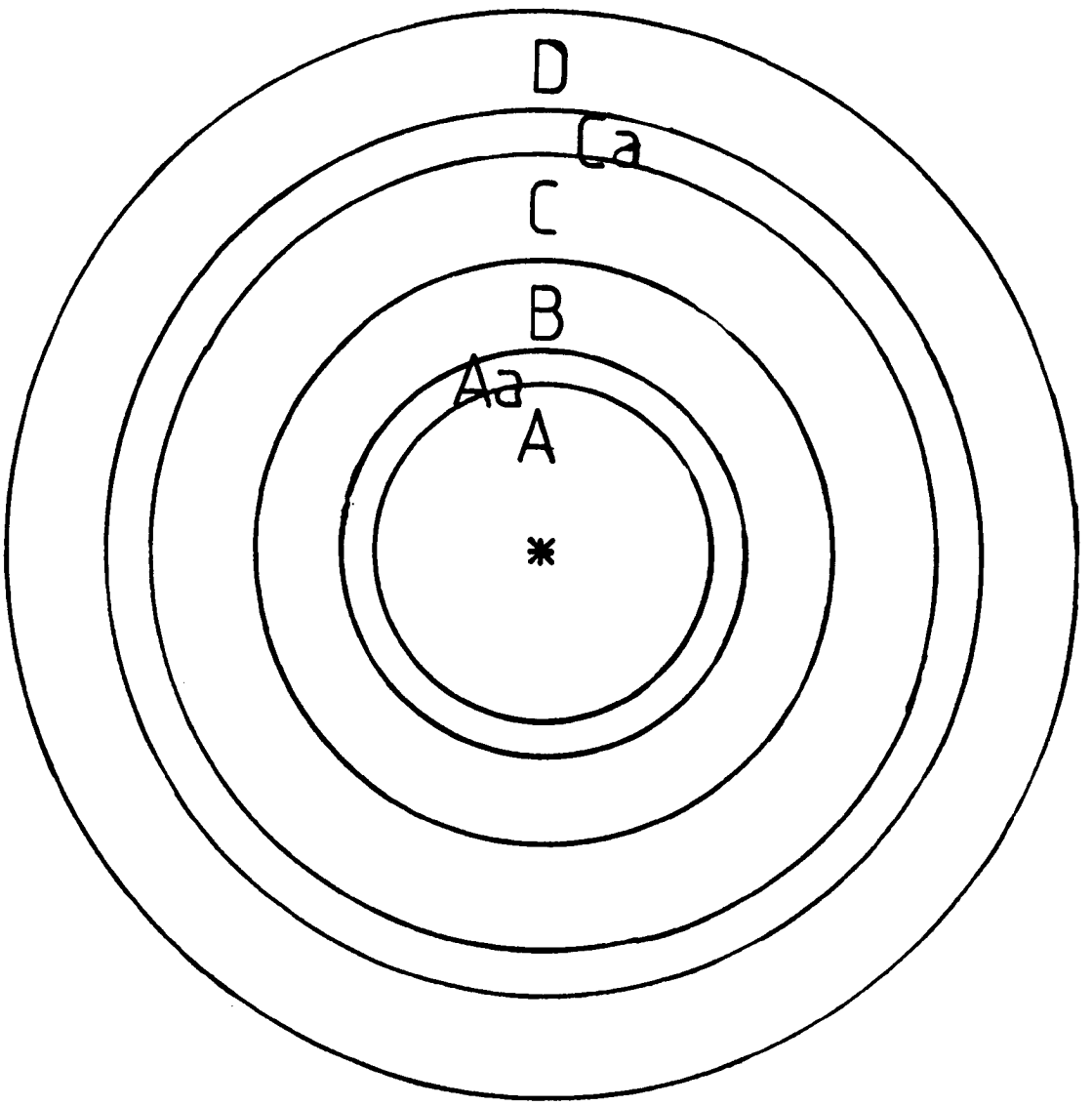

Figure 9.1. Suggested geometry of RS Oph for the first few months after outburst. Regions A, Aa, B, C, Ca and D are as explained in the text.

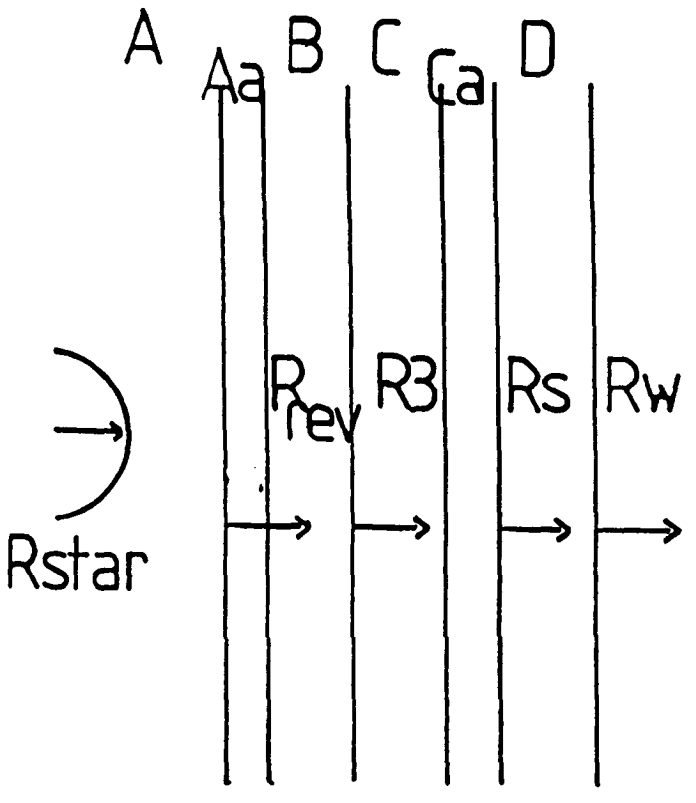

Figure 9.2. As previous figure but taking the situation in plan. (All symbols are explained in the text).

9.3 Extension of Models to the Infrared

What we need are conditions to describe the densities, temperatures and radii in each region to input into the model. Here we explain and justify these conditions.

9.3.1 The Star

The star (the secondary) is taken to be an MOIII giant because of the fit this gives to the infrared pre-outburst photometry (see Chapter 8). The radius of this star (needed to define the boundary of region 1) is taken to be 4.56×10^{12}cm, which is consistent with the radii of giant stars as taken from Allen (1973). The primary (white dwarf) is ignored as its contribution to the infrared will be negligible.

9.3.2 Regions Aa and Ca

In view of the fact that x-rays and coronal lines have been observed in RS Oph after outburst, we assume that the shocked ejecta and shocked wind regions (which will be the regions of highest temperature) reach temperatures of $\sim 5 \times 10^{6}$K. As f (the free-free flux) $\propto 1/T^{-1/2}\exp(h\nu/(kT))$ (see Chapter 6), at near infrared wavelengths, the flux will fall as the temperature increases. Thus we ignore the infrared flux from these regions as it will be small in comparison to the flux from regions of lower temperature.

9.3.3 Region A

We assume that for this region the density is uniform and thus falls as t^{-3} in keeping with the analysis of Bode & Kahn (1985). We discuss the validity of this assumption in section 9.7. The inner edge is taken to be the radius of the secondary and the outer edge R_{rev} equation (9.3). We also assume a temperature of $\sim 2 \times 10^{4}$K which is consistent with

temperatures calculated for nova ejecta (Gallagher & Starrfield, 1978).

9.3.4 Region B

Although in region A the density is uniform we assume an $1/r^2$ dependence in region B, which will probably more realistically describe a region of spherical symmetry and uniform outflow. Bode & Kahn (1985) note that material that has passed through the reverse shock is well cooled and subject to Rayleigh-Taylor instabilities, so it forms small condensations rather than a continuous shell. Obviously a density law such as we have taken is a continuous shell configuration, but we do this for simplicity and suggest that an overall low compression factor for this region will compensate for this and give the same result as several small condensations with large compression factors. The temperature we have taken is $T=10^5$K, which may seem a little on the high side in view of the short cooling time (Bode & Kahn, 1985). However during the evolution of the remnant new material continues to be shocked and subsequently to cool, as long as the shock has not passed the edge of the wind, and so some material must always be at a temperature of 10^5K. (We also try a temperature of 2×10^4K to determine the effect of a lower temperature on the results). The outer radius of this region, R3, is made a free parameter and is obtained by fitting the calculated flux to the observations.

9.3.5 Region C

As $R_s \propto t^{2/3}$ (equation 9.5) the density in this region will be proportional to $r^{-3/2}$. It will also be compressed in view of the fact that the shock has proceeded through it. Again we take the temperature to be 10^5K, and bear in mind the above comments.

9.3.6 Region D

The density and temperature in this region (as in region A) are taken to depend on r^{-2} and 2×10^4K respectively. The inner radius of this region will be the shock radius and the outer radius will be the radius of the wind. We take this radius to be constant throughout the model as the velocity of the wind << velocity of the ejecta and hence the overall velocity of the system.

9.4 Input Parameters

We shall endeavour to use values that have an observational or theoretical basis. Thus $V_w \sim 20$ kms^{-1} (Gorbatski, 1972) so in the 18 years since the last outburst $R_w \simeq 1.14 \times 10^{15}$cm. The velocity V, will not in reality be a constant as the ejecta will constantly be decelerated by the preoutburst envelope (Pottasch, 1967) but we take a median velocity of ~ 855 km s^{-1}; Rosino (1986) determined this average velocity to be ~ 960 km s^{-1} from the widths of the emission lines seen after the 1985 outburst.

The distance assumed is ~ 1.3 kpc. Hjellming et al. (1986) estimated the distance to be ~ 1.6 kpc from the interstellar CaII line, while Snijders (1986) estimated a distance of < 2 kpc from ultraviolet observations and we find ~ 1.3 kpc from fits of a MOIII star to infrared pre-outburst photometry of this star (see Chapter 8). The ejected mass is assumed to be $M_e \sim 6 \times 10^{27}$g. From the strength of the hydrogen and helium lines Pottasch (1967) derived the hydrogen and helium density and, assuming spherical symmetry to determine the volume, calculated a mass of 3×10^{28}g for a distance of 5.8 kpc. At the distance of 1.3 kpc that we have assumed Pottasch's estimate will be reduced to ~ 4.5×10^{27}g, so the value we have is reasonable. Finally the wind mass loss rate is assumed to be ~ $3.6 \times 10^{-8} M_\odot$ yr^{-1}, the value found by Livio et al. (1986) from theoretical considerations. It is known that there is an enhancement of metals in RS

Oph (Pottasch, 1967; Snijders, 1986) thus providing a situation in which the number density of electrons is not equal to the number density of ions. However these quantities have been assumed equal in our model. The free-free flux $\propto Z^2 n_e n_i$ (equation 6.9; in the optically thin case) where Z is the ionic charge. Thus in general the total free-free flux, F,

$$F \propto \sum_j Z_j^2 n_e n_j \tag{9.7}$$

where Z_j is charge and n_j is number density for ion j. Writing $\sum n_j Z_j^2 = X n_e$ (where X=1 for pure hydrogen, X=1.1 for a cosmic mixture of hydrogen/helium etc.) we have

$$F \propto X n_e^2 \tag{9.8}$$

So adjusting n_e by a factor of $X^{-1/2}$ will allow for the inequality in the electron and ion number densities.

9.5 The Equations

We follow the same set of equations as we did for GQ Mus 1983 (Chapter 6) and extend them to the four regions, taking into account the different density laws in regions A and C. However we assume that all parts of the configuration are optically thin at infrared wavelengths and so ignore the inclusion of the optical depth (this will be justified later). Taking the remnant to be further divided into regions as described by Fig. 9.3, the flux density f_n coming from region n can hence be calculated using

$$f_1 = \int_{\arcsin\left(\frac{R_{STAR}}{R_{rev}}\right)}^{\pi/2} \int_{\theta}^{\pi-\theta} \text{constl}\ 2\pi R_{rev}^3/D^2\ (\sin\theta/\sin\phi)^2 \cos\theta\ d\theta d\phi \tag{9.9}$$

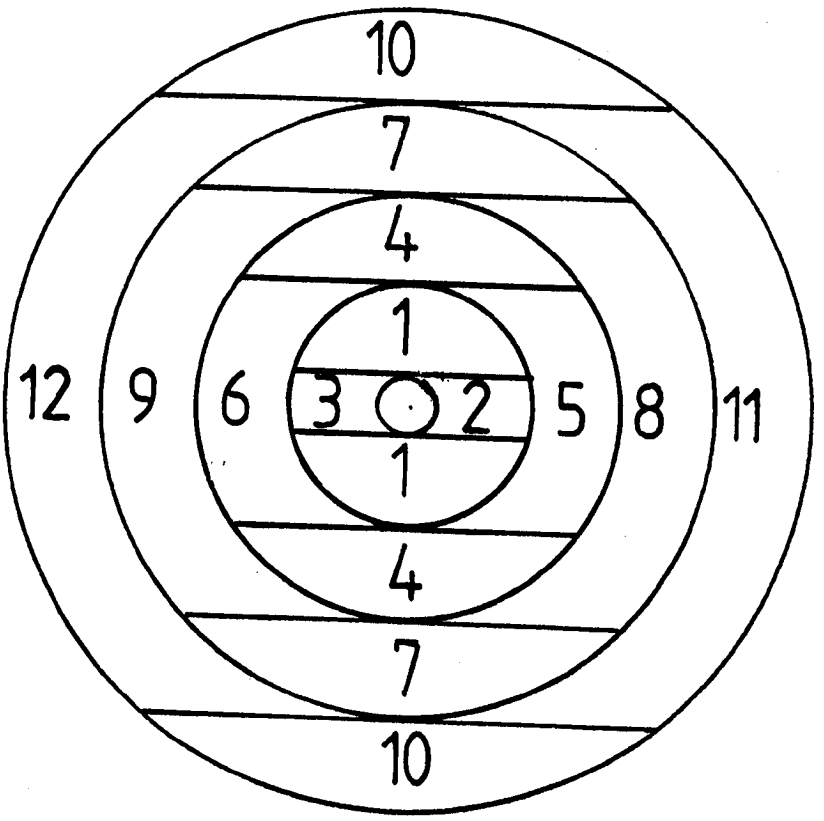

Figure 9.3. Further division of the regions in RS Oph. Flux is calculated from each of these regions (see text).

where

$$\text{const1} = 8/3(2\pi/3)^{1/2} e^6/(m^2c^3)(m/(kT))^{1/2}(n_e)_1^2 e\ xp(-h\nu/(kT)) \tag{9.10}$$

Here the symbols are defined as in Chapter 6, and $(n_e)_1$ is the electron density in region 1 which we have assumed is equal to the ion density. We have discussed in the previous section what happens if the electron density is not equal to the ion density i.e. if there is an enrichment of metals. Similarily

$$f_2 = \int_0^{\arcsin(\frac{RSTAR}{Rrev})} \int_\theta^{\arcsin(\frac{Rrev}{RSTAR}\sin\theta)} \text{const1}\ 2\pi R_{rev}^3/D^2\ (\sin\theta/\sin\phi)^2\cos\theta\ d\theta d\phi \tag{9.11}$$

$$f_3 = \int_{\pi/2}^{\pi} \int_\theta^{\pi-\arcsin(\frac{RSTAR}{Rrev}\sin\theta)} \text{const1}\ 2\pi RSTAR^3/D^2\ (\sin\theta/\sin\phi)^2\cos\theta\ d\theta d\phi \tag{9.12}$$

Thus the total flux density from region A is $f_A = f_1+f_2+f_3$. For region 4,

$$f_4 = \int_{\arcsin(\frac{Rrev}{R3})}^{\pi/2} \int_\theta^{\pi-\theta} \text{const2}\ 2\pi R3^3/D^2\ (\sin\phi/\sin\theta)^2\cos\theta\ d\theta\ d\phi \tag{9.13}$$

where

$$\text{const2} = 8/3(2\pi/3)^{1/2} e^6/(m^2c^3)(m/(kT))^{1/2}(n_e)_2^2(\ (r_e)_2/R3)^4$$
$$\exp(-h\nu/(kT)) \tag{9.14}$$

in which the density has been defined as $(n_e)_2(r/(r_e)_2)^{-2}$ and the electron density in region B is assumed equal to the ion density in region B. Also

$$f_5 = \int_0^{\arcsin(\frac{Rrev}{R3})} \int_\theta^{\arcsin(\frac{Rrev}{R3}\sin\theta)} \text{const2}\ 2\pi R3^3/D^2\ (\sin\phi/\sin\theta)^2\cos\theta\ d\theta\ d\phi \tag{9.15}$$

$$f_6 = \int_{\frac{\pi}{2}}^{\pi} \int_{\theta}^{\pi - \arcsin\left(\frac{R_{rev}}{R3}\sin\theta\right)} \text{const2}\ (R3/R_{rev})^4\ 2\pi R_{rev}^3/D^2\ (\sin\phi/\sin\theta)^2 \cos\theta\ d\theta d\phi \tag{9.16}$$

Thus the total flux density from region B is $f_B = f_4 + f_5 + f_6$. For region 7

$$f_7 = \int_{\arcsin\left(\frac{R3}{R_s}\right)}^{\pi/2} \int_{\theta}^{\pi-\theta} \text{const3}\ 2\pi R_s^3/D^2\ \sin\phi/\sin\theta\ \cos\theta\ d\theta d\phi \tag{9.17}$$

where

$$\text{const3} = 8/3(2\pi/3)^{1/2} e^6/(m^2c^3)(m/(kT))^{1/2}(n_e)_s^2((r_e)_s/R_s)^3 \exp(-h\nu/kT) \tag{9.18}$$

in which the density has been defined as $(n_e)_s(r/(r_e)_s)^{-3/2}$ and the electron density in region C is assumed to be equal to the ion density in region C. Similarly

$$f_8 = \int_{0}^{\arcsin\left(\frac{R3}{R_s}\right)} \int_{\theta}^{\arcsin\left(\frac{R3}{R_s}\sin\theta\right)} \text{const3}\ 2\pi R_s^3/D^2\ \sin\phi/\sin\theta\ \cos\theta\ d\theta d\phi \tag{9.19}$$

$$f_9 = \int_{\frac{\pi}{2}}^{\pi} \int_{\theta}^{\pi - \arcsin\left(\frac{R3}{R_s}\sin\theta\right)} \text{const3}\ (R_s/R3)^3\ 2\pi R3^3/D^2\ \sin\phi/\sin\theta\ \cos\theta\ d\theta d\phi \tag{9.20}$$

Thus the total flux density from region C is $f_C = f_7 + f_8 + f_9$. Finally

$$f_{10} = \int_{\arcsin\left(\frac{R_s}{R_w}\right)}^{\pi/2} \int_{0}^{\pi-\theta} \text{const4}\ 2\pi R_w^3/D^2\ (\sin\phi/\sin\theta)^2 \cos\theta\ d\theta d\phi \tag{9.21}$$

where

$$\text{const4} = 8/3(2\pi/3)^{1/2} e^6/(m^2c^3)(m/(KT))^{1/2} (n_e)_4^2((r_e)_4/R_w)^4 \exp(-h\nu/(kT)) \tag{9.22}$$

in which the density has been defined as $(n_e)_4(r/(r_e)_4)^{-2}$ and the electron density in region D is assumed to be equal to the ion density in region D.

$$f_{11} = \int_0^{\arcsin\left(\frac{R_s}{R_w}\right)} \int_{\theta}^{\arcsin\left(\frac{R_w}{R_s}\sin\theta\right)} \text{const4}\ 2\pi R_w^3/D^2\ (\sin\phi/\sin\theta)^2\cos\theta\ d\theta d\phi \tag{9.23}$$

$$f_{12} = \int_{\frac{\pi}{2}}^{\pi} \int_{\theta}^{\pi-\arcsin\left(\frac{R_s}{R_w}\sin\theta\right)} \text{const4}\ (R_w/R_s)^4\ 2\pi R_s^3/D^2\ (\sin\phi/s\ in\theta)^2\cos\theta\ d\theta d\phi \tag{9.24}$$

Thus the total flux density from region D is $f_D = f_{10}+f_{11}+f_{12}$. So the total observed flux, F, is

$$F = f_A+f_B+f_C+f_D+f_{star} \tag{9.25}$$

where f_{star} is the flux from the star.

We now deal with the compression factors that will enhance the density in regions B and C as a result of the shocks in the presence of a magnetic field. Let Z1 be the enhancement factor from region A to region B, and Z2 be the enhancement from region D to region C. Starting with Z1, the density in region B will be Z1 times the density in region A at the boundary of the two layers; thus continuity demands that

$$\begin{aligned} Z1(n_e)_1 &= (n_e)_2((r_e)_2/R_{rev})^2 \\ \text{so } (n_e)_2 &= Z1(R_{rev}/(r_e)_2)^2(n_e)_1 \end{aligned} \tag{9.26}$$

Similarly for Z2, the density in region C will be Z2 times the density in region D thus at the boundary of these two regions continuity gives

$$Z2(n_e)_4((r_e)_4/R_s)^2 = (n_e)_3((r_e)_3/R_s)^{3/2}$$

$$\text{so } (n_e)_3 = Z2(n_e)_4((r_e)_4)^2/((r_e)_3)^{3/2}R_s^{-1/2} \tag{9.27}$$

Here we make another assumption; obviously Z1 and Z2 are dependent on the time because of their dependence on the radii R_{rev} and R_s respectively and also because during this time after outburst, as the ejecta are being decelerated, we would expect the compression factor to decrease with time. But we assume for simplicity that they are constant. In the time period we are considering R_{rev} changes by a factor of ~ 3 and R_s also changes by about the same amount. For Z2, the expansion in R_s would only change its value by ~ 1.7, so we can feel justified in taking a constant value for this quantity. However the expansion in R_{rev} leads to a change in Z1 of ~ one order of magnitude. This dependence of Z1 on R_{rev} only arises because the density in region A was taken to obey a t^{-3} relationship (following Bode & Kahn, 1985) rather than a more realistic r^{-2} dependence, so the outcome is that this model overestimates the density in region B. Hence we can overcome this to a certain extent by taking a low value for Z1.

We now try different values of Z1, Z2 and R3 so that the model predictions fit the observational fluxes.

9.6 Results

Tables 9.1 and 9.2 show the predicted model fluxes along with the observed fluxes (the observed fluxes have been dereddened using E(B-V) = 0.73; Cassatella et al., 1985) for region B having a temperature of 2 x 10^4K and 10^5K respectively, for the time period 25 to 112 days after outburst. (Figs 9.4 & 9.5 show the fluxes graphically).

When considering the goodness of the fits to the observations we must take into account the fact that both the J and K bands are contaminated with emission lines. The J band is strongly contaminated by HI Pβ and Pγ (λ = 1.28μm & 1.09μm), OI (λ = 1.129μm) and especially the HeI triplet (λ =

Table 9.1

Temperature of region B is 2×10^4K.

time(days)	flux predicted / flux observed	J	H	K	L
25		7.31	8.82	9.02	9.25
		15.56	8.91	9.68	7.69
39		4.14	5.17	4.98	4.70
		9.15	5.16	5.42	3.90
44		3.57	4.51	4.24	3.88
		7.39	4.49	4.49	3.17
61		2.10	2.82	2.36	1.76
		5.15	3.51	3.41	(2.35)
74		1.71	2.37	1.87	1.20
		3.63	2.05	2.51	--
93		1.51	2.13	1.61	0.91
		2.13	2.07	1.72	(1.05)
112		1.42	2.04	1.50	0.79
		1.77	1.91	1.60	(0.95)

This table gives the infrared flux (in Jy) of RS Oph at different infrared wavebands on various days after outburst. The top row for each day is the flux predicted from the model (see text), and the bottom row gives the observed flux.

Table 9.2

Temperature of region B is 10^5K.

time(days)	flux predicted flux observed	J	H	K	L
25		8.01	8.81	8.41	7.86
		15.56	8.91	9.68	7.69
39		5.47	5.17	4.69	4.04
		9.15	5.16	5.42	3.90
44		3.83	4.51	4.01	3.35
		7.39	4.49	4.49	3.17
61		2.24	2.87	2.34	1.64
		5.15	3.51	3.41	(2.35)
74		1.76	2.37	1.83	1.12
		3.63	2.05	2.51	--
93		1.53	2.13	1.59	0.87
		2.13	2.07	1.72	(1.05)
112		1.47	2.09	1.56	0.85
		1.77	1.91	1.60	(0.95)

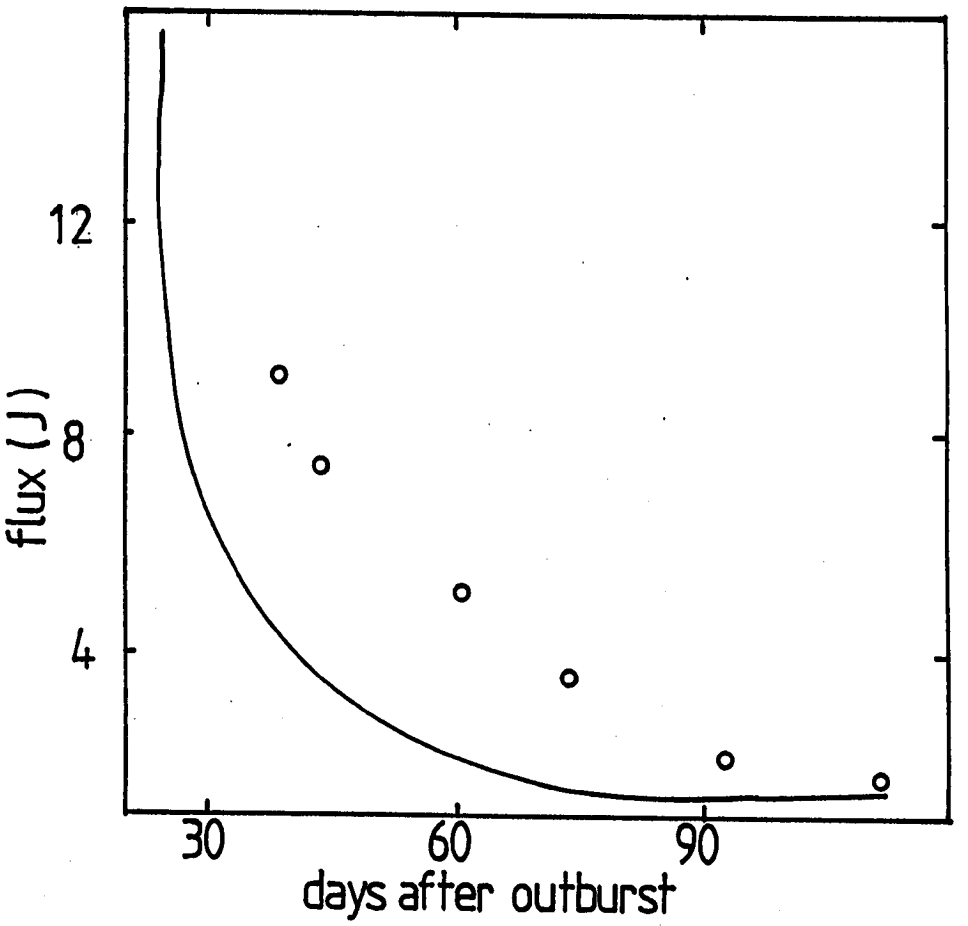

Figure 9.4a. Observed and model infrared light curves at the J waveband. Fluxes are given in Jy and time is given as days from outburst. The theoretical fluxes are plotted as a curve. The temperature in region B is 2×10^4K.

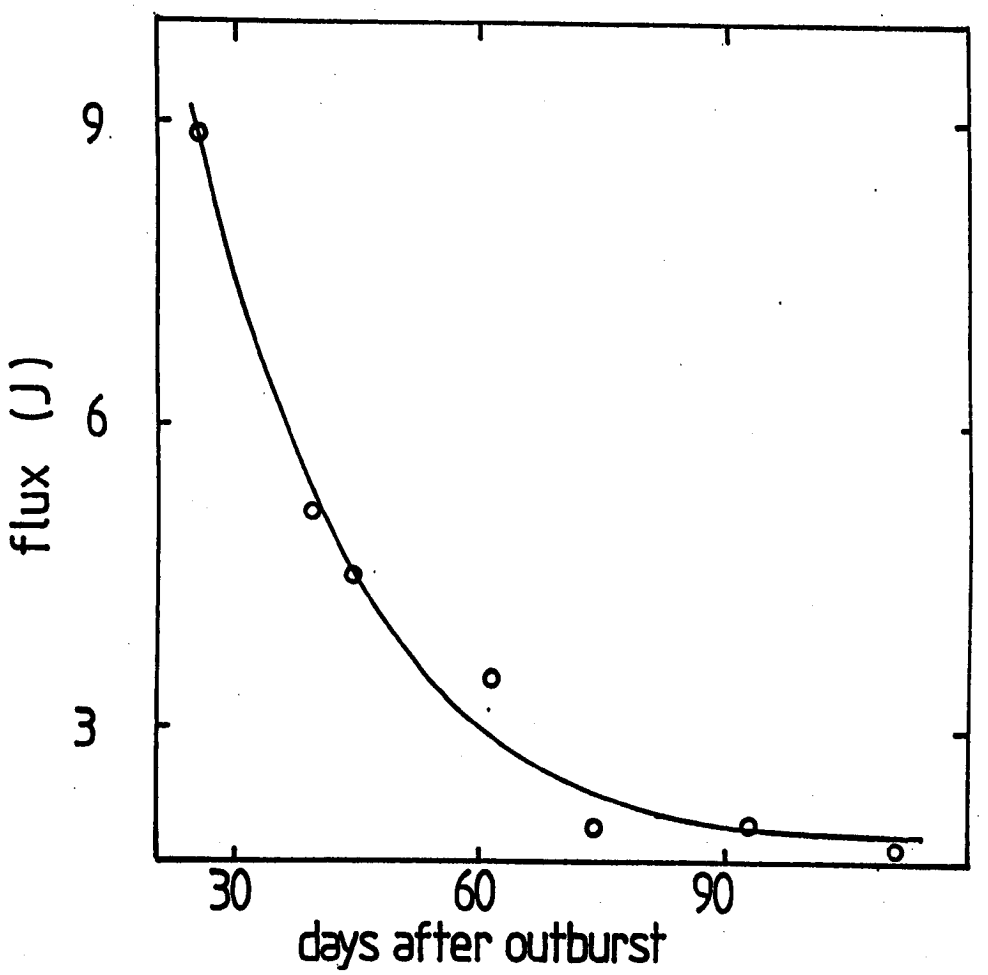

Figure 9.4b. As Fig. 9.4a but displaying the H light curve.

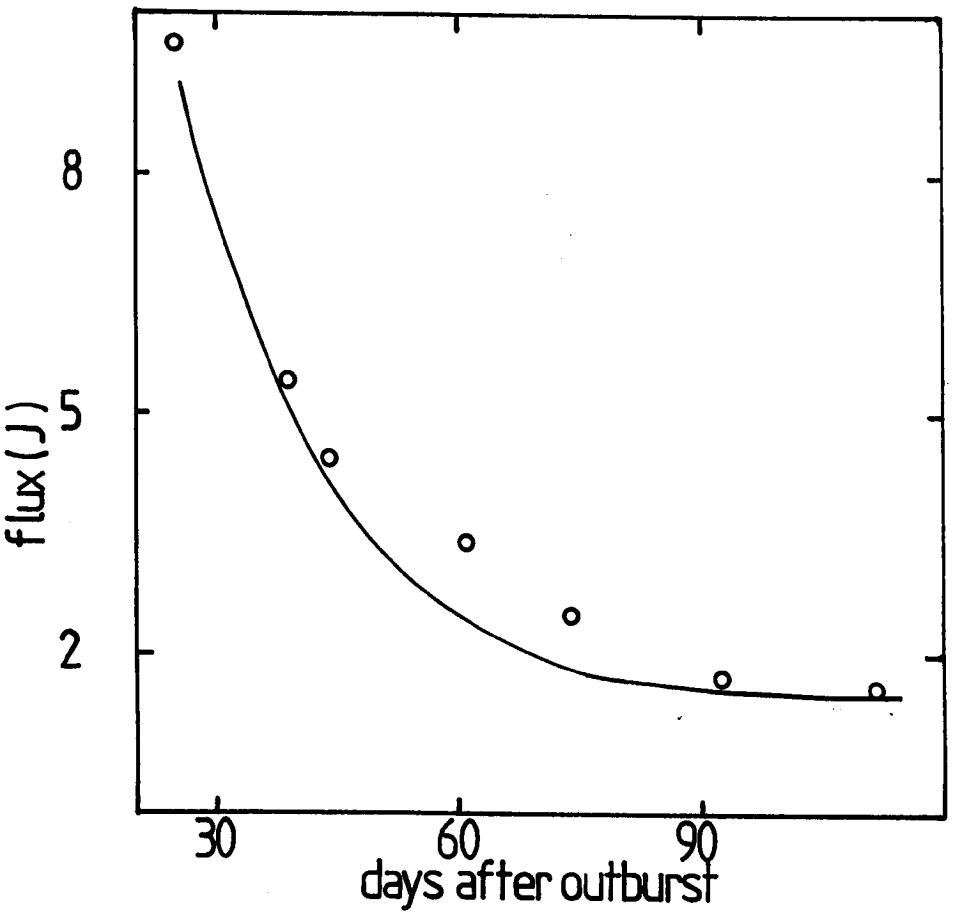

Figure 9.4c. As Fig. 9.4a but displaying the K light curve.

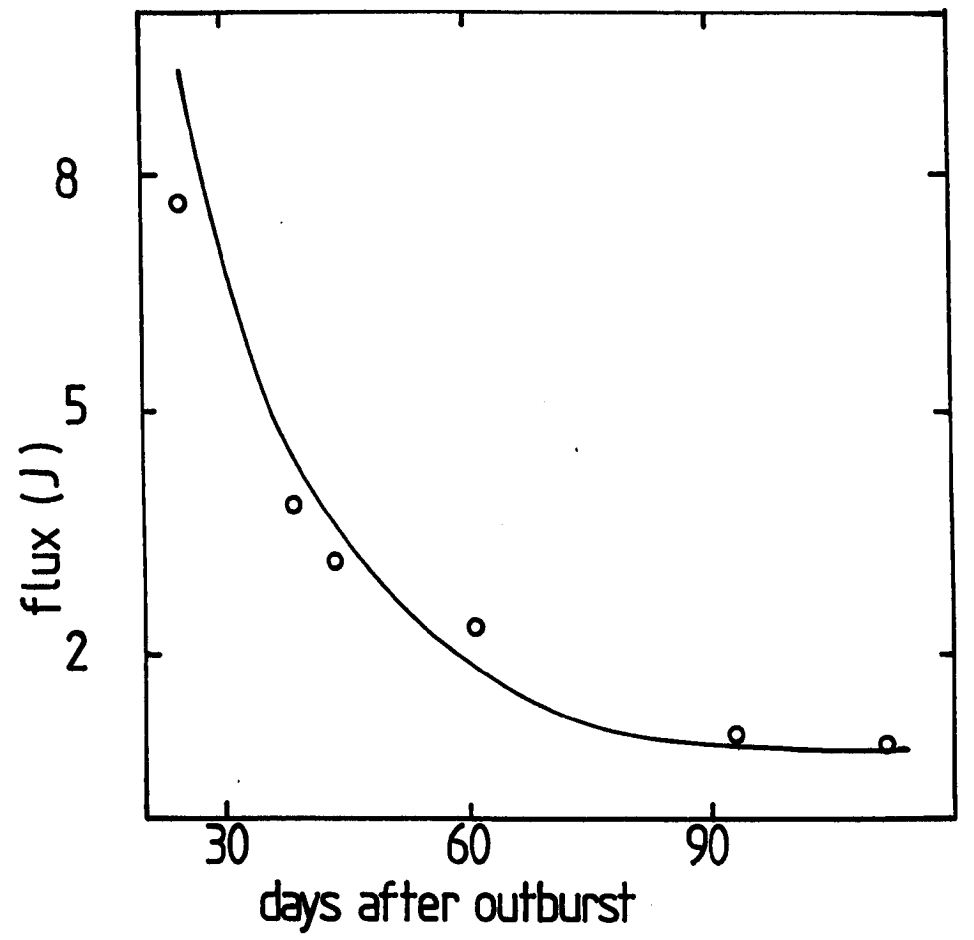

Figure 9.4d. As Fig. 9.4a but displaying the L light curve.

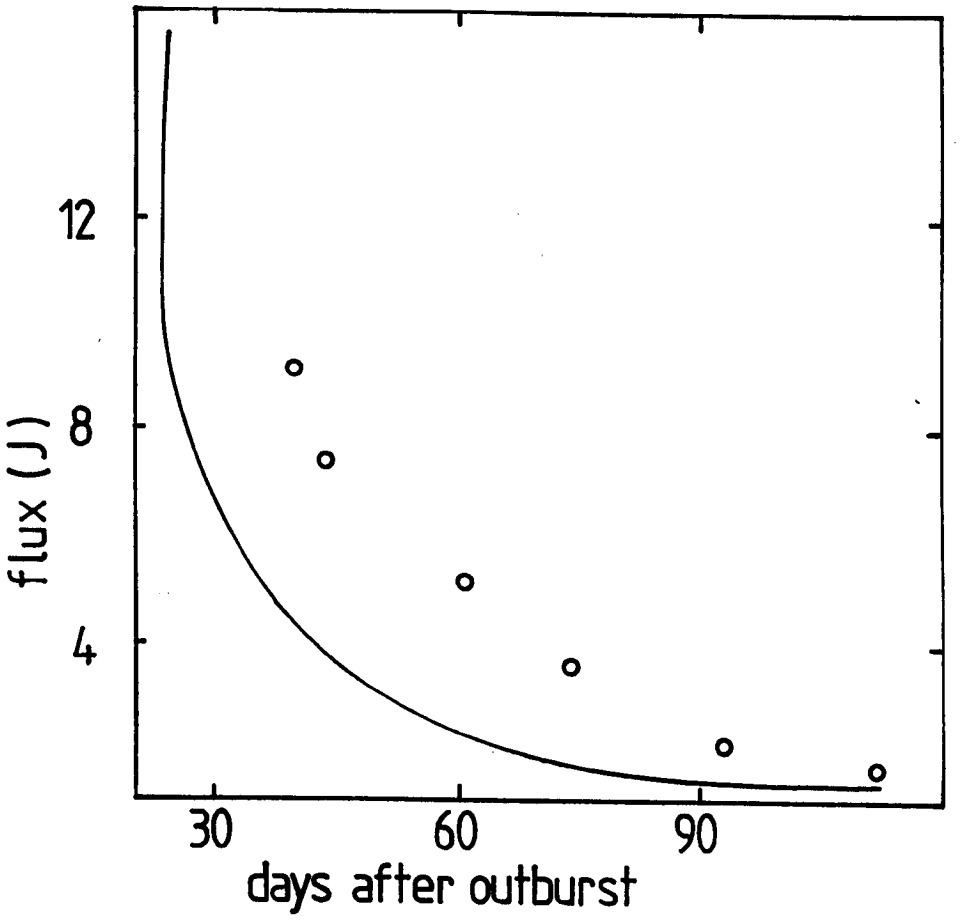

Figure 9.5a. Observed and model infrared light curves at the J waveband. Fluxes are given in Jy and time is given as days from outburst. The theoretical fluxes are plotted as a curve. The temperature in region B is 10^5K.

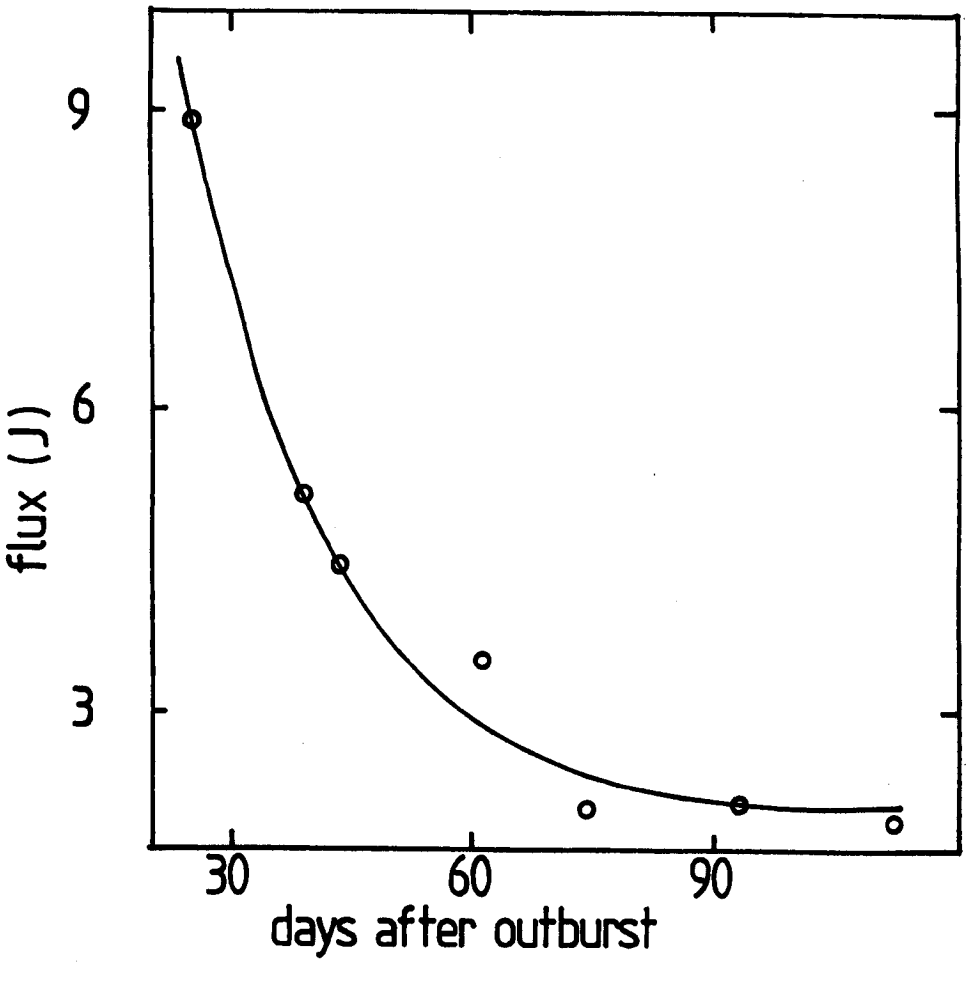

Figure 9.5b. As Fig. 9.5a but displaying the H light curve.

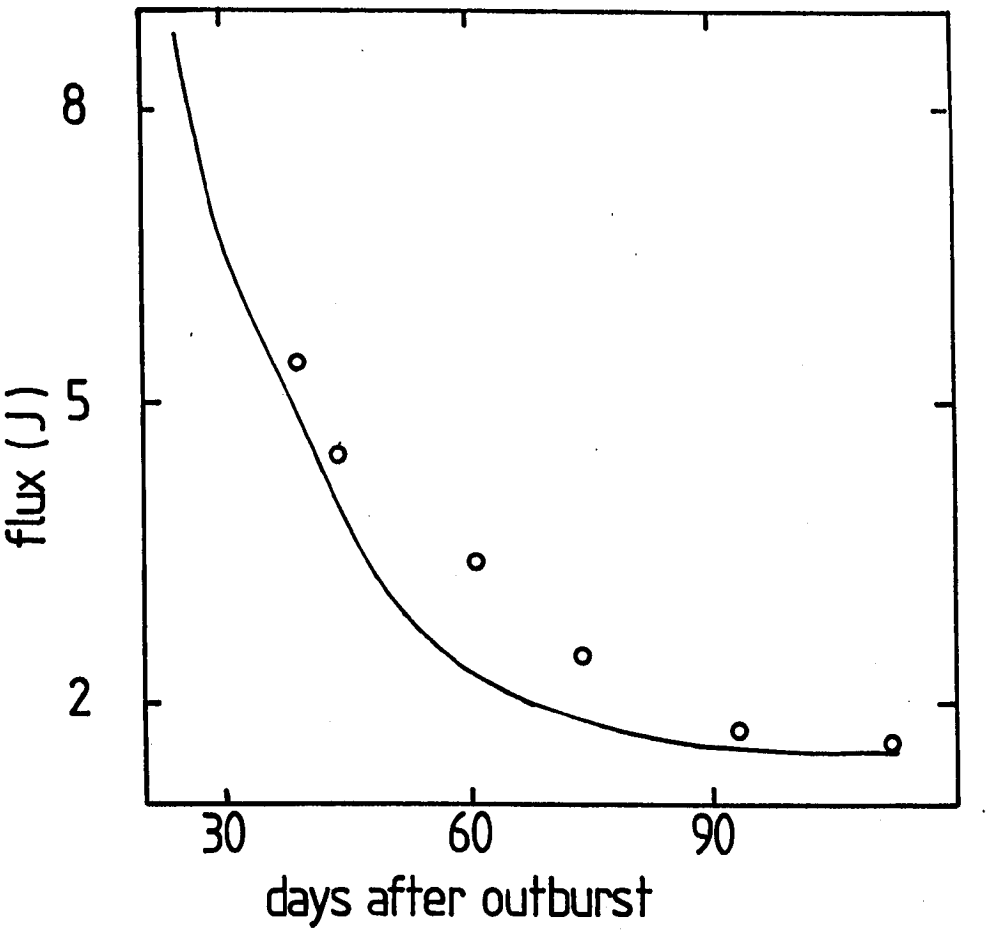

Figure 9.5c. As Fig. 9.5a but displaying the K light curve.

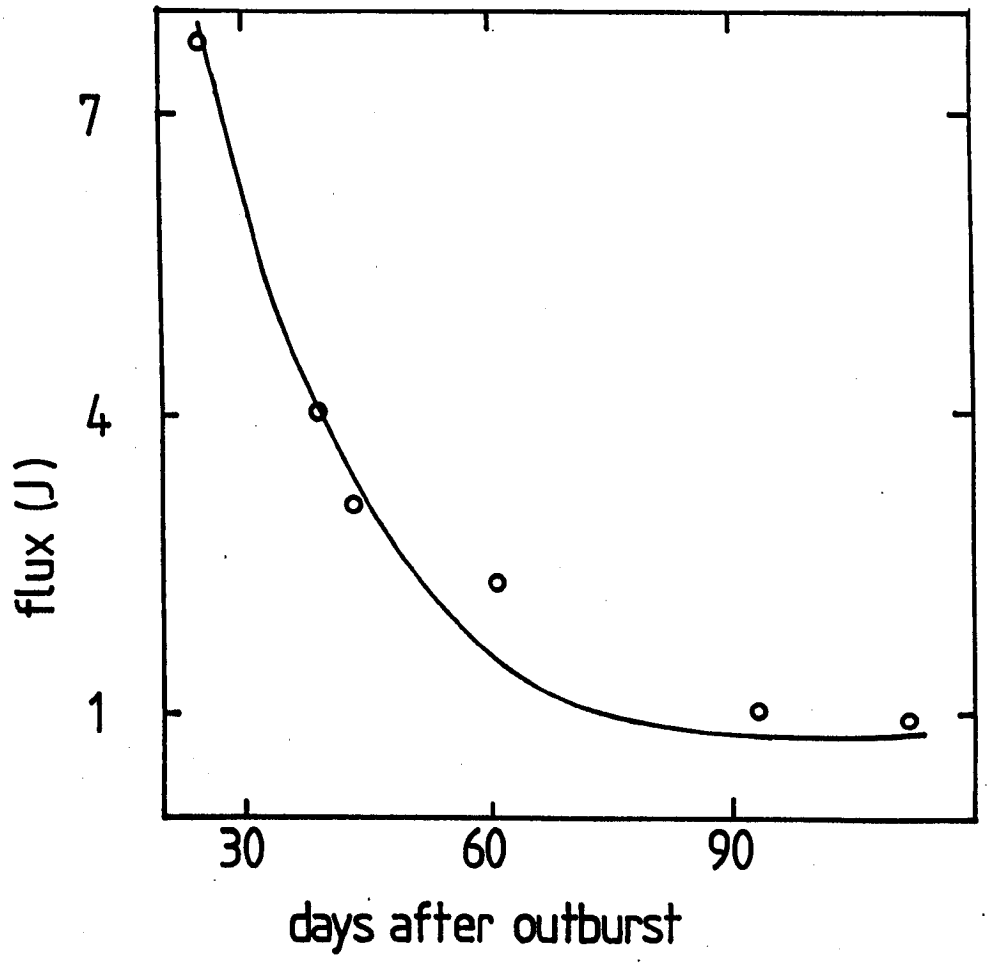

Figure 9.5d. As Fig. 9.5a but displaying the L light curve.

1.083μm); (see Chapter 8). The K band is contaminated by HI Bγ (λ = 2.166μm) and HeI (λ = 2.058μm); (also see Chapter 8). So for consistency the observed J and K fluxes should lie above the predicted ones. On the other hand, the wavebands H and L are uncontaminated by strong emission lines, so the flux in these bands should be almost entirely due to free-free radiation and flux from the secondary.

For region B having a temperature of 2×10^4K, the observed J and K band fluxes lie above the calculated ones as expected, whilst the H band fluxes match very well (i.e. to within the observational errors in most cases). However the L band fluxes, particularly at the earlier dates do not fit well. When the temperature of region B is raised to 10^5K, the fits for the J, H and K bands remain much the same as in the previous case but the L band fits are much improved. The exception to these results for both cases is the flux on day 61. On this day the predicted fluxes in bands H and L are ~ 25% lower than those actually observed.

The enhancement factors Z1 and Z2 for the regions B and C are 15 and 130 respectively if T_2 (temperature in region B) = 2×10^4K; and 19 and 130 respectively if $T_2 = 10^5$K.

Table 9.3 shows the fluxes coming from each of the four regions of the remnant (see Fig. 9.1), at different wavelengths at various stages of the nova evolution (days 25, 74 and 112). We see that the flux coming from region A << 1% of the total flux at any time.

We have ignored optical depth effects. We can deduce if this is a valid assumption by estimating the optical depth τ on the earliest day of our observations (when τ should be highest) using the approximation (e.g. Rybicki & Lightman, 1979)

$$\tau \sim 0.02 n_e^2 s/(\nu^2 T^{3/2}) \qquad (9.28)$$

Table 9.3

Calculated model fluxes (Jy) from each region.

λ	time(days) region	25	74	112
J	A	0.046	0.001	0.00021
	B	6.47	0.40	0.082
	C	0.10	0.0094	0.0055
	D	9.1(-6)	1.7(-6)	3.5(-9)
H	A	0.053	0.0012	0.00024
	B	6.66	0.41	0.084
	C	0.145	0.0096	0.0057
	D	1.1(-5)	1.9(-6)	4.0(-9)
K	A	0.058	0.0013	0.00027
	B	6.8	0.42	0.086
	C	0.148	0.0098	0.0058
	D	1.2(-5)	2.2(-6)	4.5(-9)
L	A	0.066	0.0015	0.00030
	B	6.97	0.43	0.088
	C	1.52	0.01	0.006
	D	1.3(-5)	2.5(-6)	5.0(-9)

where s is the width of the emitting region, n_e is the electron number density, ν the frequency and T the temperature. Using the worst possible parameters i.e. the highest value of n_e and the lowest value of ν for each of the regions, τ ranges between 10^{-5}-10^{-7} and hence any optical depth effects are indeed entirely negligible.

A graphical representation of R3, the boundary between the cooled shocked ejecta and the cooled shocked wind, is given in Fig. 9.6. We attempt to fit an equation of the form $R3 = \alpha t^{\beta}$, where α and β are constants, through the points using a least squares fitting routine. Thus the equation for the best curve through these points is $R3 = \alpha t^{0.9928}$ (where $\alpha = 1.12 \times 10^{13}$ cm day$^{-0.9928}$); this is essentially $R3 \propto t$, i.e. a constant velocity of value ~ 1400 km s^{-1}. Pottasch (1967) calculated values for the radius of the line emitting region from the widths of the emission lines in the 1958 outburst. These values are given in Table 9.4 along with our fitted R3 values for the same stages in the outburst. The values are dissimilar enough to suggest that the emission lines do not orginate in region B (see next section). The physical interpretation of these results will now be discussed.

9.7 Discussion

The temperature of region B which gives the best fits to the observational data sets is $T_2 = 10^5$K so we will base the discussion on this model (see later and Chapter 8 for deduced temperatures from spectroscopy). As mentioned earlier (section 9.3.4) such a temperature does not appear to be in agreement with Bode & Kahn (1985), who predict a rapidly cooling shocked ejecta. Again we suggest that this could be due to the fact that new material is continually being shocked to ~ 10^6K - 10^7K and hence some of the cooling material must be at the intermediate temperature. Also, as the predicted fluxes for day 61 do not fit the observational values at all

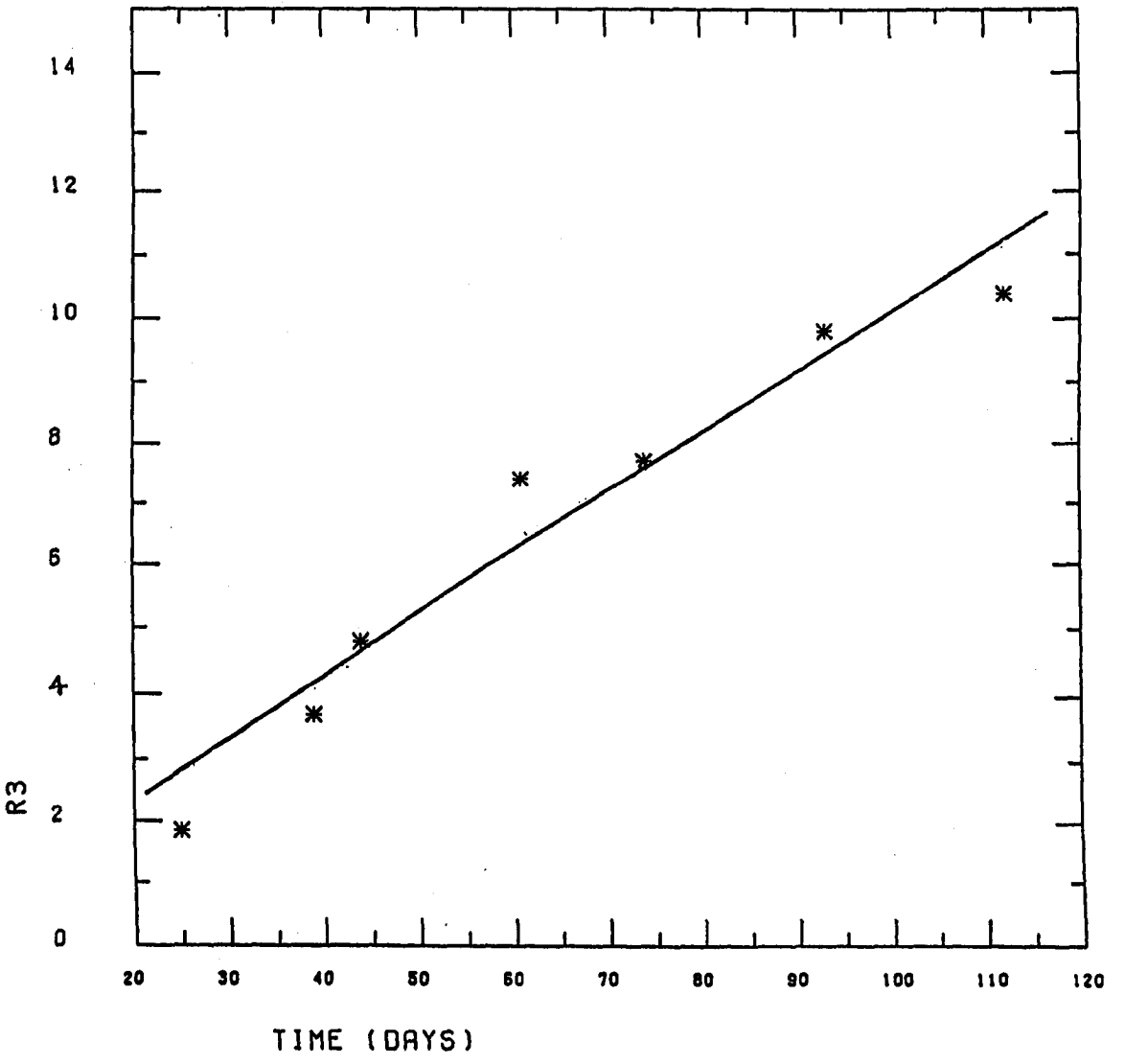

Figure 9.6. Graph showing the fitted evolution of R3 with time. R3 is given in cm x 10^{-14}, whilst the time is given as days after outburst.

Table 9.4

R3 and R (Pottasch, 1967).

		R3(model)	R(Pottasch)
time	25	1.85(14)	2.99(14)
	39	3.70(14)	3.88(14)
	61	7.40(14)	4.81(14)
	93	9.80(14)	5.93(14)

Time is in days from outburst, R in cm. (See text for details).

well (in contrast with the other days) we will ignore these results for the purposes of the general discussion but later discuss a reason why the fluxes on this day may be much higher than the model predicts.

Turning first to the density enhancement factors Z1 and Z2 for regions B and C respectively we have values roughly in agreement with Spoestra et al. (1987). They calculated enhancement factors of ~ 33 - 130, in the presence of a magnetic field of strength 4×10^{-6}T. As our enhancement factors are 19 and 130 we can say that the infrared model fit is consistent with the Spoestra et al. (1987) discussion. We expected a low enhancement factor in region B firstly because the material being subject to Rayleigh-Taylor instabilities will be in the form of dense clumps and thus we are really taking an average value for Z1 over the whole volume of this region. More importantly taking the density to follow t^{-3} in region A leads to an overestimation of the density in region B.

Table 9.5 gives the values of R_{rev}, R3, R_s, together with the number densities on either side of the contact discontinuity R3 on various days after outburst (in these regions the temperature is the same at 10^5K). Initially region C has a greater spatial extent than region B, but the latter has a number density ~ 10 times greater on its side of R3. As expected (because of this greater number density and hence pressure) the extent of region B soon exceeds that of region C. (Although this is a very simplistic approach to the physical situation as it does not take into account the density gradients in the two individual regions, the density gradients are not large enough to affect the qualitative discussion). At the end of the time period (day 112) the densities in the two regions are comparable and so the regions are then virtually indistinguishable from each other. This too is satisfyingly consistent with the model as a whole. It is at this time when the shock has reached the edge of the stellar wind ($R_s = at^{2/3} = 1.136 \times 10^{15}$cm, a ~ 2.5×10^{10}cm $s^{-2/3}$) so that at ~ 112 days this condition holds. Thus we would expect the number densities on both

Table 9.5

Number density on either side of R3.

		R_{rev}	R3	Rs	no. den(B)	no. den(C)
time	25	1.5(14)	1.85(14)	4.18(14)	1.76(9)	1.39(8)
	39	2.2(14)	3.70(14)	5.62(14)	2.51(8)	4.24(7)
	44	2.5(14)	4.80(14)	6.09(14)	1.28(8)	2.76(7)
	61	3.2(14)	7.40(14)	7.57(14)	3.42(7)	1.29(7)
	93	4.4(14)	9.80(14)	1.00(15)	4.40(7)	7.37(6)
	112	5.0(14)	1.13(15)	1.14(15)	5.85(6)	5.60(6)

Time in days, radii in cm and densities in cm^{-3}.

sides of R3 to become equivalent soon after this time, as there will be no shocks and hence no density enhancements.

As mentioned in Chapter 8, the 1985 February 21 UKIRT spectrum of RS Oph posed a problem. The hydrogen emission lines, by virtue of their equivalent widths, all appeared to be originating from a region having a temperature ~ 10^4K, but the fit to the nebular continuum pointed to a temperature of ~ 10^5K. The solution to this discrepancy is indicated by our model. Returning to Table 9.3 we can see that ~ 80% of the flux on day 25 (1985 February 20) comes from regions B and C which are both at a temperature of 10^5K, hence the continuum should be dominated by material at this temperature. However the strength of the emission lines is proportional to $T^{-3/2}\exp(h\nu/(kT))$ (see equations 8.5 & 8.6), so those emission lines orginating from the regions at 2 x 10^4K will be ~ 10 times stronger than those arising from the middle two regions at ~ 10^5K assuming equivalent number densities in the regions. What we will see then are emission lines at ~ 10^4K sitting on a continuum at ~ 10^5K.

On 1985 April 26 (the date a second UKIRT spectrum was obtained) the contribution to the flux from the regions at ~ 10^5K is ~ 25% (the rest of the flux at this time comes from the secondary) so again we would expect the nebular continuum to be at this temperature which indeed it was (see Chapter 8). However the average temperature implied by the lines is higher than that in the earlier spectrum (~ 4 x 10^4K; Chapter 8). This is probably caused by the number densities in the 10^5K regions becoming such that the line flux from both the 2 x 10^4K and 10^5K regions are similar. Thus when we calculate the temperature of the line emitting region from equivalent widths we obtain a temperature between the two extremes. This can be explained by Rayleigh-Taylor instabilities in the cooled shocked regions (10^5K regions). These give rise to dense clumps of material so that emission lines from denser regions (but regions of higher temperature) may be able to rival in flux those emission lines from regions of less

density but at cooler temperature. This of course is a neccessarily simplistic view of the situation in the nova remnant. It does not take into account the density gradients across region B and the relative volumes of regions A and B with time (which would also tend to make the contribution of the lines from region B greater as time passes). With a more realistic density law in region A these observations may be more fully explained.

In this model we wish to know the region from which the 5GHz radio 'flare' seen by Spoelstra et al. (1987) could originate. They observed this flare on day 41, and required the density to be enhanced and the shocked gas (ejecta) to cool quickly to generate the magnetic field of the predicted strength. Thus in such instances the flare probably arose from one of the cooled dense condensations in region B, the region of the cooled shocked ejecta.

One further point of interest is the role that the secondary plays in the model (which we have assumed here to be a MOIII type; Chapter 8). Table 9.6 shows the flux at the JHK and L wavelengths originating from such a star at a distance of 1.3 kpc and the fluxes at these wavelengths observed from RS Oph after day 112. This reveals that the secondary produces virtually all the infrared flux after day 112. (The J and K fluxes being a little above those predicted from this 'typical' star because of strong emission lines). As noted in Chapter 8 the infrared light curves show variations. These variations have amplitude of typically ~ 0.3 mags. This might explain the poor fits to the day 61 data if the star was then at a maximum in its fluctuating cycle, as an addition of ~ 0.15 mags to the H and L observations on that day would mean about a 60% reduction in the differences between the observed and the model fluxes.

Table 9.6

Observed infrared flux after day 112.

		J	H	K	L
Flux from a typical MOIII at 1.3kpc (in Jy).		1.34	1.95	1.40	0.67
Flux from RS Oph					
time (days)	126	1.72	1.82	1.50	(0.81)
	132	1.76	1.91	1.54	(0.79)
	165	1.67	1.87	1.54	
	210	1.62	1.78	1.45	
	256	1.57	1.73	1.42	

9.8 Conclusion

The infrared flux originating from RS Oph in the first months after outburst can be reasonably modelled by free-free radiation plus the contribution from a MOIII secondary, where we have modelled the effect of the ejecta colliding with the preoutburst circumstellar envelope. Regions of hot shocked ejecta and hot shocked wind are presumably where the x-rays and coronal lines seen in RS Oph after outburst originate; such regions do not contribute to the infrared flux because of their high temperature. We suggest that the radio 'flare' seen by Spoelstra et al. (1987) 41 days after outburst arises from a region of cooled shocked ejecta and that the February and April UKIRT spectra can be reasonably explained if most of the flux is originating from regions with temperatures ~ 10^5K, which is indeed what the model predicts. Thus it all seems very self consistent.

There are however some factors that have not been modelled explicitly and instead taken in their simplest 'average' form. These are: assuming that the enhancement values for the density in the regions of cooled shocked ejecta and cooled shocked stellar wind are constants, and modelling the former region as a continuous shell rather than dense condensations of material embedded in a more rarified medium.

The factor that we have approximated which will probably have the greatest effect on the results is the modelling of the density in region A as having a t^{-3} dependence. This was used in accordance with the model of Bode & Kahn (1985) so a simple solution for the radius of the reverse shock could be obtained. Such a law increases the flux coming from region B in relation to that coming from region A (because of the form of the density enhancement Z1, see section 9.5). What seems likely if the density in region A was set to follow a r^{-2} dependence is that the overall flux from these two region would remain the same but a greater proportion of this flux would be coming from region A. It will only be by the inclusion of

these factors that we will get a totally realistic model of the infrared flux from the RS Oph system.

CHAPTER 10

CONCLUSIONS AND FURTHER STUDIES.

10.1 Classical Novae.

This work has been divided into two halves. In the first half we looked at the infrared behaviour of classical novae, paying particular attention to their grain forming ability and the novae GQ Mus 1983 and PW Vul 1984 and the second halve dealt with the recurrent nova RS Oph.

10.1.1 Grain Nucleation.

Ever since the infrared became available as an astronomical tool astronomers had been studying novae as possible sites of grain formation as it was observed that a visual minimum was accompanied by an infrared maximum in the light curves of these objects. We have thus explored a possible mechanism for the formation of carbon grains in these systems: namely nucleation on ions. This formation mechanism has never (to our knowledge) been applied to nucleation in novae. The results that emerged from this model were extremely encouraging. It appeared to be a very likely method of grain formation. Firstly the nucleation rate as estimated from the observations of classical novae was close to the calculated nucleation rate for nucleation onto ions (~ $10^{-10}cm^{-3}s^{-1}$ and ~ $6 \times 10^{-11}cm^{-3}s^{-1}$ respectively), in constrast with the extremely low nucleation rate calculated for homogeneous nucleation (~ $5 \times 10^{-24}cm^{-3}s^{-1}$). Also there were regions in the nova ejecta that contained neutral carbon and other ionized elements, and it could even explain why some novae formed dust and others did not. The work done previously seemed to suggest that the most important nova parameter in determining whether or not a nova would produce dust was the nova speed class, faster ones being less able to form dust. Our model has reinforced this but the nova ejected mass and the

ejecta elemental abundances are equally important in determining the nova's dust forming capibilities. For example a nova of a slow speed class might not be able to produce dust if the ejected mass is so high that by the time enough nucleation centres are available the carbon number density is too low for the onset of grain condensation, or a nova with a relatively low abundance of carbon may not produce grains as the carbon will be completely ionized before most of the other suitable elements.

This model is obviously worth pursuing and perhaps the next direction to follow is the actual chemistry of the situation. We have considered nucleation to occur if carbon is neutral and any other element ionized. However in reality condensation of neutral carbon may be more favourable on particular ions. A. P. Jones (private communication) considers that iron or silicon ions will be the most likely to act as nucleation centers for neutral carbon atoms. Another path to explore is the application of the model to the formation of silicate based dust as this type of dust has also been observed in some novae.

The validity of this grain nucleation model to systems other than classical novae is another avenue for future developement. Wolf-Rayet stars are a small group of very luminous stars which have temperatures ~ 30000 K (Willis & Wilson, 1978). They show very strong broad emission lines of helium, carbon, oxygen and nitrogen but few absorption lines (Conti, 1978). The emission lines are thought to arise in an expanding stellar atmosphere moving at very high speed (~ 2000 km s^{-1}) so the star is continuously losing mass (Conti, 1978). Some are known to be in a binary configuration (Cohen & Kuhi, 1977; Cohen & Vogel, 1978), and some have been observed as dust sources (Gehrz & Hackwell, 1974). Due to their very high effective temperatures and considerable mass loss it would be well worth examining the possibility that dust is formed in these systems by some type of ion nucleation process.

Planetary nebulae are isolated nebulae that consist of shells of gas

that have been lost in the fairly recent past by their central stars (Osterbrock, 1974). They are thought to be the precursors of white dwarfs (Cahn & Wyatt, 1976). The central stars of planetary nebulae are old stars and have temperatures of ~ 5 x 10^4K - 3 x 10^5K (Osterbrock, 1974), whilst temperatures in the gas shells have been calculated at 6000 K - 20000 K (Kitchin, 1982). Infrared studies of these objects have revealed the presence of dust of both a graphite and silicate nature (Barlow, 1983). With such conditions in planetary nebulae it would be worth considering whether nucleation on ions could lead to the formation of grains in these objects.

Most other systems that are known to produce dust (e.g. long period variables, N type giants, some irregular variables) probably do not use this mechanism of dust production as their effective temperatures are too low to bring about the necessary ionization of the required elements in a reasonable time.

10.1.2 IRAS.

We now move on to the IRAS observations of classical novae. These allowed us to develop the ground based data already available on these objects. In some cases information derived from the ground based data was confirmed e.g. V4077 Sgr was found to possess a dust shell and the nova GQ Mus did not; whilst for the older novae studied the IRAS observation gave us an indication of their evolution since outburst. However some of the IRAS results require further investigation. In some cases it was impossible to differentiate between emission by dust and emission by fine structure lines. High resolution spectroscopy at far infrared wavelengths (H. Dinerstein, private communication) will hopefully remove any ambiguities about the nature of the infrared emission. It is hoped that when the ISO satellite becomes operational in 1992 it will improve on the IRAS studies since it will provide a greater wavelength coverage

(3 - 200μm) and has a sensitivity many orders of magnitude greater than that of IRAS (ISO INFO, 1986).

10.1.3 GQ Mus.

The nova GQ Mus did not reveal any dust when it was observed at ground based sites or by IRAS. On applying its observed and calculated parameters to our grain nucleation model it was found that it was not expected to form dust because any carbon in the ejecta was completely ionized before the condensation distance was reached. Bearing this in mind we attempted to reproduce the infrared fluxes from this nova in terms of free-free emission. This model fitted the data well and it was hence concluded that its infrared emission was due to an optically thin gas emitting thermal bremstrallung.

10.1.4 PW Vul.

One of the most interesting characteristics of the nova PW Vul was its production of silicate dust some months after outburst. Now we know that some novae do produce this type of dust, it must be considered an advantage to monitor any future novae at 2 - 4μm, 10μm and 20μm and over a reasonable (at least a year) timebase. In this way we will be able to discover if novae forming silicate dust are indeed rarer than novae forming carbon based dust or if it is just an artefact of the infrared wavelength range that the observations have previously been made in. With (hopefully) a greater sample of silicate dust producing novae we should be in a better position to deduce their similarities and this will lead to a better understanding of why (and how) this type of dust is produced in novae.

10.2 RS Oph.

Turning now to the latter half of this study, this dealt with the infrared observations of the recurrent nova RS Oph at its 1985 outburst. This nova was found to exhibit a very complicated infrared behaviour. The infrared spectroscopy revealed that there were many regions of differing temperature in the remnant, as witnessed by the distinct temperature of the nebular continuum, the temperature as deduced from the hydrogen lines, and the existence of infrared coronal lines. These regions are probably a consequence of the nova ejecta interacting with a pre-outburst envelope and giving rise to shocks. The later spectra were almost entirely dominated by the continuum of the secondary. This was deduced to be a star of type in the range K6III - M2III. Obviously more high resolution infrared spectroscopy at quiescence is required if we are to narrow this range down further. There was also observed, from spectroscopy obtained in 1985 June, CO absorptions at 2.3μm which obviously arose from the secondary. However it was not clear if this CO originated in the secondary or was material produced by a thermonuclear runaway on the white dwarf that had been deposited in the atmosphere of the secondary during ejection. It would be extremely useful if, in addition to 2.3μm spectroscopy during quiescence, we could also obtain millimeter CO observations. Such observations would complement each other and would thus indicate the origin of the CO absorptions seen after the 1985 outburst. The infrared photometry, at the time when the secondary's continuum was dominant in the spectra, showed distinct variations in magnitudes in all infrared wavebands. It is not known (yet) if these variations were due to processes going on in the system as a whole or were solely due to the secondary. If they were due to the secondary it implies that it is no 'normal' giant star, which is perhaps not surprising bearing in mind the effects that interaction with its primary will have on it. It is therefore essential that infrared photometry and spectroscopy is continued over a long time period in order

to look for evidence of pulsations in the secondary.

The infrared light curves of RS Oph during the 1985 outburst were successfully reproduced using a free-free emission model in the presence of shocks and the consequent density enhancements. This model was based on the model that Bode & Kahn (1985) used to interpret the x-ray data. Their model does have a few problems especially with regard to modelling the region of the unshocked ejecta as one of constant density. Further work on this model should therefore include a more realistic representation of this region. As such, dust emission in the J - L bands was not required to reproduce the infrared emission and so the likelihood of there being any carbon based dust in this system seems remote. However there is a chance that there may be silicate based dust in the system because of the detections at 10μm and 12μm. It seems unlikely that, if there is dust, it were to be formed in the ejecta (because of the strong shocks), but it is possible that it could be formed in the wind from the secondary. It must be considered a priority to undertake high resolution spectroscopy at 10μm and 20μm of this object in a few years time to clear up any remaining uncertainty to whether silicate dust does form in this system.

Unfortunately RS Oph is the only recurrent nova that has been studied in great detail at most wavelengths, but it would be an advantage if we could compare these data to those of other recurrents. The other recurrents must therefore be constantly observed in order to catch further outbursts, and extensive wavelength coverage must be undertaken as soon as an outburst is reported. Even in quiescence studies of recurrent novae could provide useful information regarding their secondaries and such studies should be undertaken. Recurrent novae have been noted to be a very heterogeneous group and further studies may be able to find other similarities between them other than their recurrence time that may help to determine unambiguously their mechanism of outburst.

10.3 Final Conclusion.

This work has demonstrated the worth of studying novae at infrared wavelengths, especially with regards to their dust forming abilities. However it has also indictated the importance of obtaining simultaneous observations of these objects at many wavelengths as witnessed by the information obtained on RS Oph by using such data. It is hoped that such observations will be, in future, given priority.

APPENDIX

THE SYMBIOTIC STAR RR TELESCOPIUM

A.1 Introduction

The object RR Telescopium is a very unusual star. It has sometimes been referred to as a symbiotic star, at other times a very slow classical nova. Fleming (1908) discovered the variability of RR Tel and since then it has been regularly monitored in the visual and more recently at infrared and ultraviolet wavelengths.

We discuss here simultaneous UBVRIJHLMN photometry obtained at SAAO, and IRAS observations of this object. But first we take a brief look at the general characteristics of symbiotic stars and of the known history of RR Tel itself.

A.2 Symbiotic Stars

Symbiotic stars were originally defined as those having an optical spectrum which represented a combination of absorption features of a low temperature star, with emission lines of high excitation (Boyarchuk, 1968). With the progress in astronomical techniques over the recent years other spectral components to symbiotics have been found. In the infrared some of the stars have been shown to have a dust excess (Swings & Allen, 1972), whilst ultraviolet studies of symbiotics have revealed the presence of strong emission lines and ultraviolet continua (Slovak, 1982). Some symbiotics have even been observed in x-rays (Allen, 1984) and free-free radio emission at 15GHz has been detected from ~ nine symbiotic stars (Allen, 1984). Thus symbiotic stars are not a very homogeneous group and many stars are not classified as exclusively symbiotic but may belong to another group as well (e.g. RS Oph and T CrB usually classed as recurrent novae are also referred to as symbiotic stars).

Irregular variations of brightness is one of the most characteristic features of symbiotic stars. Their light curves can be considered as a whole series of small flares (see Fig. A.1), although different stars have rather different light curves. Symbiotic stars have been divided into two classes. Type I symbiotics (e.g. Z And) have quasi-periodic changes in brightness with a timescale of a few months. At minimum their spectra combine those of a cool giant with a high excitation spectrum. Type II (e.g. V1016 Cyg) look like long-period variables (many symbiotics are known to contain Mira stars), with low excitation emission lines. In the infrared symbiotics can further be divided (e.g. Feast et al., 1983). S-type symbiotics have colours that match those of late type stars, whilst in D-type symbiotics there is a conspicuous excess at the longer wavelengths indicating the presence of dust.

There have been many explanations for the phenomenon of symbiotic stars. The earliest hypotheses were of a single star system. In one scenario the star was of high temperature and surrounded by an optically thick extended envelope, whilst a further model consisted of a cool star surrounded by a very high temperature corona. However both these models have been discounted as the observations just do not match the theoretical behaviour of such systems (Boyarchuk, 1986). The presently favoured explanation is that of a binary star system involving a cool giant and a dwarf enveloped by an accretion disc. Infrared observations confirmed the existence of a cool component in all symbiotic stars (usually a M type giant; Allen, 1982) whilst ultraviolet observations gave direct indications of the presence of a hot component in these stars (Nussbaumer, 1982). This hot component is often a subdwarf similar to the central star of a planetary nebula or maybe even a white dwarf. Whether it is the hot star or the accretion disc which is the source of the high temperature emission has been debated. Boyarchuk (1986) describes a situation in which it is the accretion disc that is responsible for the high temperature component.

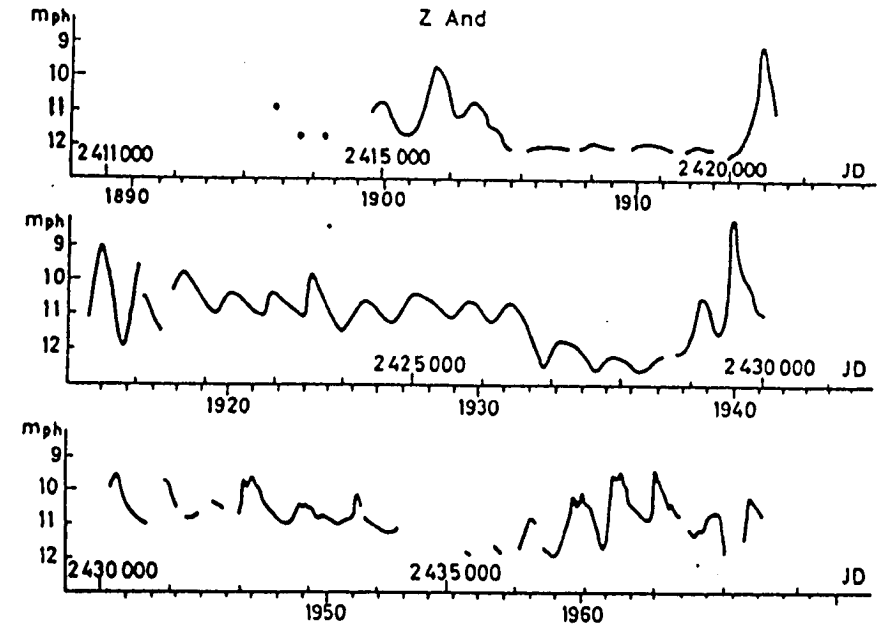

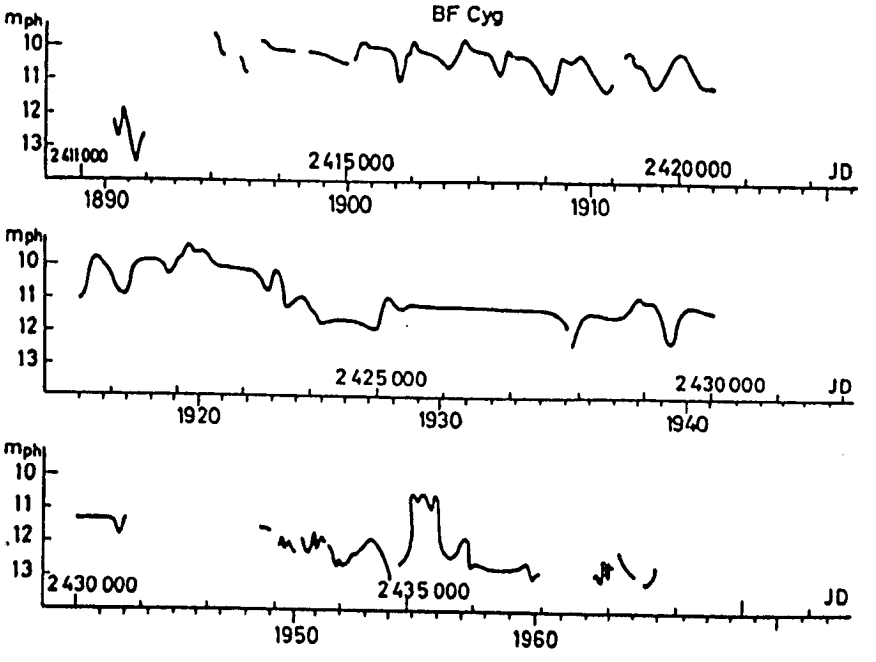

Figure A.1 The light curves of the symbiotic star Z And and BF Cyg. (Reproduced from Boyarchuk, 1968).

The cool component fills ~ 60% of its Roche lobe and thus the star can lose matter which will lead to the formation of an accretion disc around the hot component. Thus the high temperature emission with T ~ 10^5K - 10^6K will be emitted from the boundary and internal layers of the disc and will give rise to excitation of the surrounding nebula. In any case whatever it is that gives rise to the high temperature component it is clear that the observational characteristics of symbiotic stars can be best explained by *invoking a binary system.*

A.3 RR Tel

This star was discovered as a variable by Fleming (1908). From then on it was almost constantly monitored and a visual period of 386.73 days was derived by Gaposchkin (1945). In 1944 November it underwent a nova-like outburst when it rose from ~ 14 mags - ~ 6 mags. Fig. A.2 shows the visual light curve of this star from 1933 - 1950. The star remained at a maximum from 1944 to 1949 and only began to fade in June 1949 making it an extremely slow nova. The first suggestion that RR Tel might be of a symbiotic nature was made by Henize & McLaughlin (1951) who thought that the star consisted of a long period variable and a slow nova.

Subsequent observations at most wavelengths have done much to elucidate the true nature of this object. Feast & Glass (1974) suggested that the infrared flux coming from RR Tel indicated both the presence of a cool star and a heated dust shell. The cool star was later classified as a M giant because of the TiO bands discovered by Webster (1974). Further infrared studies by Feast et al. (1977) revealed the presence of large brightness variations, which lead these authors to suggest that the cool component was a Mira type variable. This suggestion was reinforced by the studies of Allen et al. (1978), whose low resolution scans in the 1.9μm - 2.6μm atmospheric window revealed steam (H_2O) and CO absorption bands in RR Tel. Such observations are characteristic of many oxygen-rich Mira

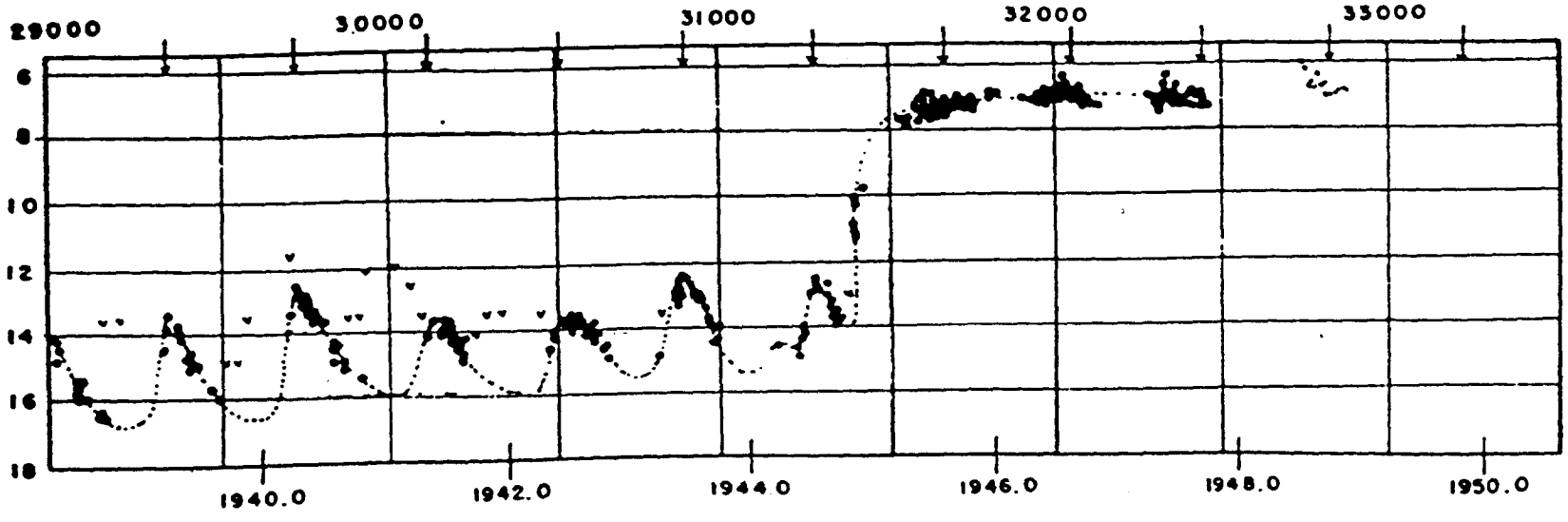

Figure A.2. The visual light curve of RR Tel from 1933 to 1950. (Reproduced from Heck & Manfroid, 1982).

variables and the intensities of the bands in RR Tel pointed to the Mira being at minimum when these data were collected. Extensive JHKL infrared photometry obtained by Feast et al. (1983) over the years 1972-81 revealed a period of 387 days, which is almost identical to that obtained in the optical region. (Fig. A.3 shows the infrared periodicity of RR Tel). Their studies also showed that the infrared excess (that had already been attributed to dust) increased towards Mira minimum. This implied that the dust could not be wholly heated by the Mira component but at least partly heated by the hot component and/or ionized gas in the system. Roche et al. (1983) obtained a 2μm - 13μm spectrum of RR Tel and concluded that there was both silcate and smooth dust emission (probably carbon based dust).

Turning now to the ultraviolet data on this object, Penston et al. (1983) obtained extensive IUE observations of RR Tel from 1978 June until 1979 February. Their ultraviolet spectra were dominated by hundreds of emission lines. These were generally resonance, semi-forbidden or forbidden lines but some recombination lines were also identified. They attempted to find a fit to the ultraviolet continuum. They found that the continuum could be modelled with a hot ionizing source (either a hot blackbody or an accretion disc), a gaseous emission continuum and a cool (M) type star. There was also a further source of continuum that they suggested was a star of spectral type near AOV, or optically thick circumstellar emission from a 'chromosphere'. Hayes & Nussbaumer (1986) investigated the time variability of RR Tel in the stronger ultraviolet emission lines. They found that there was a decrease in the ultraviolet line fluxes over the period 1978-84, but they could find no correlation with any infrared or optical periodicity.

Some of the most recent observations of RR Tel were obtained in the far infrared by the IRAS satellite. Kenyon et al. (1986) describe the pointed observations of this star and note that its infrared energy distribution is only consistent with that of a Mira if the star is very

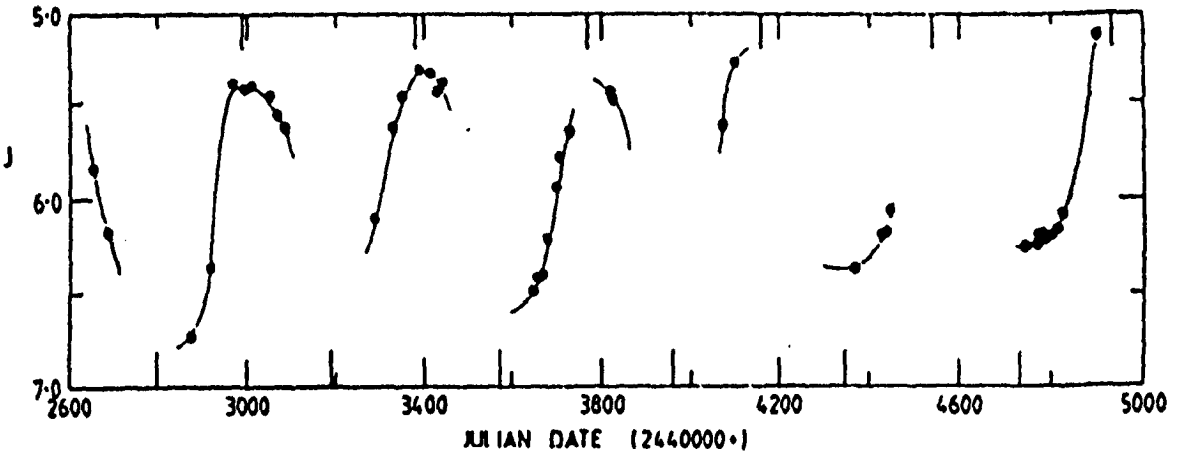

Figure A.3. The infrared periodicity of RR Tel. Here the J magnitude is plotted against Julian date. The periodicity can be judged from the vertical lines at 387 day intervals along the top and bottom of the figure. (Reproduced from Feast et al., 1983).

heavily reddened ($A_K \sim 0.65$). However this is contrary to the reddening found by Penston et al. (1983) ($A_K \sim 0.05$) and may be due to the fact that Kenyon and his co-authors matched their observations of RR Tel to the continuum of a particular Mira (o Ceti) rather than to the continuum of an arbitrary Mira. Keeping these previous observations and conclusions about the nature of RR Tel in mind, we now describe our observations of this object.

A.4 SAAO Observations

Our observations were carried out at SAAO, where simultaneous photometry at UBVRIJHKLMN wavelengths was obtained on 1985 June 28 (Albinson et al., unpublished). The data were dereddened using E(B-V) = 0.1 (Penston et al., 1983) and we hence attempted to reproduce the data points using various sources of emission.

A.4.1 Results

The dereddened data points are shown in Fig. A.4 along with our model fit to the points. This fit consists of a blackbody at 9000 K; a blackbody at 2000 K; a nebular continuum with temperature 2×10^4K, electron density $3 \times 10^6 cm^{-3}$ and a flux in the HeII 1640A line of 2.5×10^{-10}erg $s^{-1} cm^{-2} A^{-1}$ (this is comparable with the flux in this line as determined by Hayes & Nussbaumer, 1986) and finally a blackbody at 600 K. Such components lead to a fit that slightly underestimates the ultraviolet points, underestimates the N point and severely overestimates the I point (by a factor of ~ 2). This model will now be discussed.

A.4.2 Discussion

We will assume that the blackbody components to the model can be physically described thus. The 9000 K blackbody is the hot blue component which corresponds to a star of spectral type AOV (Allen, 1973). The 2000 K

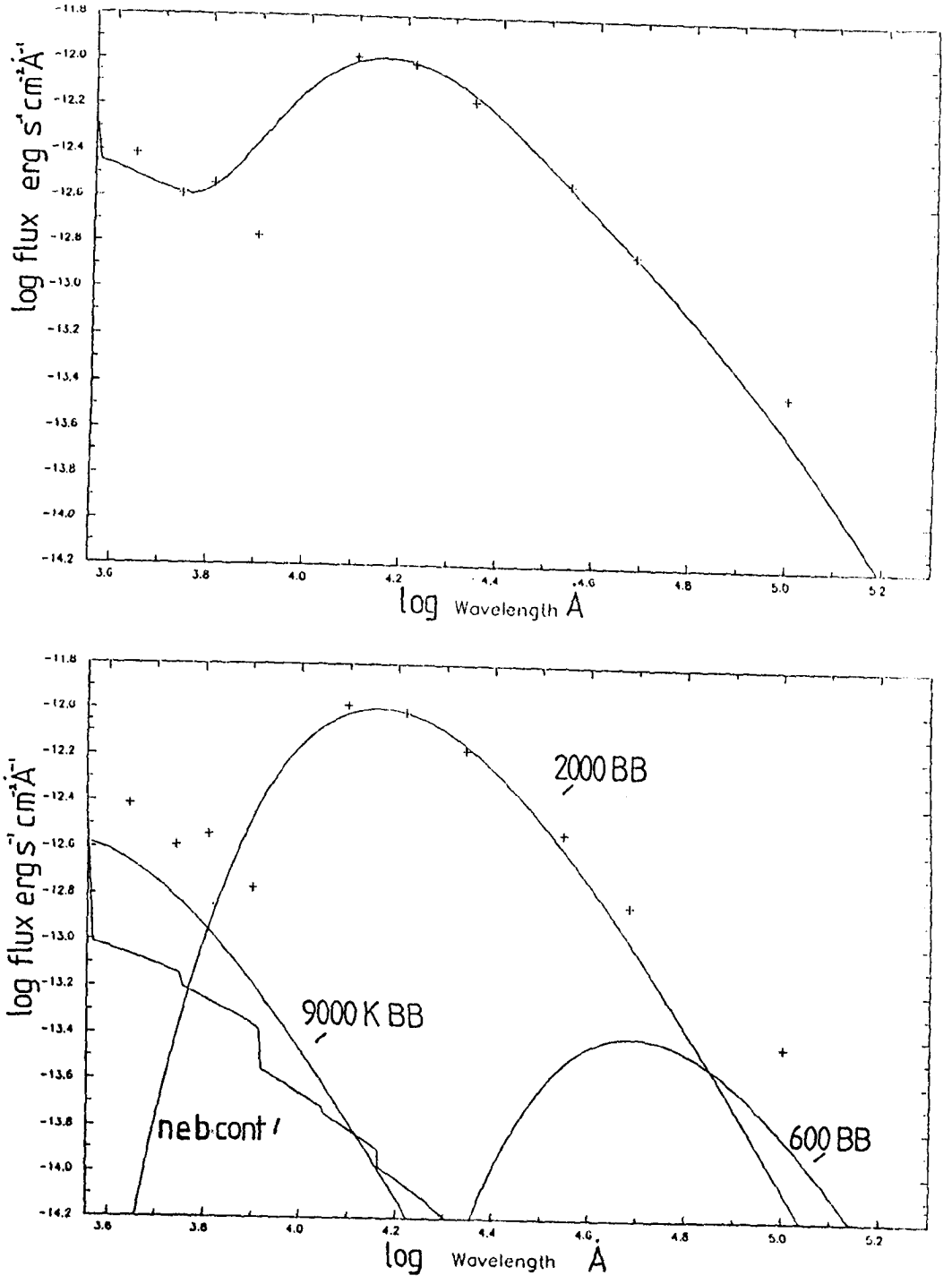

Figures A.4 The infrared photometry obtained at SAAO on 1985 June 28. On the top figure the solid line represents the best fit to the data, whilst the individual components that compose this fit are shown in the bottom figure (see text for details).

blackbody is the cool Mira component (Allen, 1973); such a star could range in spectral type from M5e to M8e. Lastly the 600 K blackbody describes a conducting dust component. The radii of the stars and the dust shell can hence be calculated by using the amount by which the blackbodies have to be scaled to fit the data (see equation 5.8). So assuming a distance of 2.5 kpc to RR Tel (Thackeray, 1977), the AOV star has a radius of ~ 4.6×10^{11}cm, the Mira has a radius of ~ 3.8×10^{13}cm whilst the inner edge of the carbon (conducting) dust shell is at a distance of ~ 3.1×10^{14}cm from the geometrical center of the system (assuming that such a shell is spherical). Comparing the star radii to those of typical stars of their class (Allen, 1973) we find that the radii are ~ 2.3 times too big. This could be due to an inaccurate distance assumption (Thackeray, 1977 assumed that M_V(max) was -6 mags and that the visual extinction was 0.5 mags when determining the distance) and/or the fact that the star is in a multiple system and the quantities given by Allen refer to single stars only. It is reassuring however that the radii of the hot and cool components are in about the right ratio for stars of their type and that the dust shell is larger than either of the two stars. If the distance is indeed ~ 1 kpc, as indicated by the above work, there is no discrepancy. We will return to the discussion of this dust presently.

Mentioned previously (section A.4.1) were the problems with this fit. We now discuss the reasons for these problems. Due to the fact that the ultraviolet region is crowded with emission lines (Penston et al., 1983) it does not seem unreasonable to attribute the excess at the U and B wavelengths to emission lines. The overestimation at I could be due to the H^- continuum which is present in the continuum of in such a Mira. This continuum peaks in the H band and causes the flux shortwards of this band to drop more steeply than would a blackbody. This leaves us with the excess over the modelled N point. There can be no doubt that this is caused by silicate dust which peaks at 9.7μm.

Table A.1 lists all the available photometric data obtained between 5μm and 100μm (these data have not been dereddened as an E(B-V) ~ 0.1 will not have a significant effect at these wavelengths). The most noticeable change in flux with time occurs around 10μm. This is probably due to changes in the flux emitted by the silicate dust as well as to changes in flux from the Mira itself. As noted before, Feast et al. (1983) showed that the Mira did not make a significant contribution to the heating of the dust, but as their data was obtained only at JHKL wavebands any conclusions they drew may only be applied to the carbon dust as the silicate dust will not manifest itself at these wavelengths. Is it perhaps possible that the Mira is heating the silicate dust but not the carbon dust? The only reasonable way in which this could be achieved is if the carbon dust is dispersed throughout the system whereas the silicate dust is indeed associated with the Mira. As the Mira in RR Tel is oxygen rich (Allen et al., 1978) it is possible that the silicate dust is associated with the Mira, whilst the carbon based dust is dust that has been formed after the nova explosion and has hence expanded out of the close vicinity of the Mira. Unfortunately apart from the occurrence of the nova explosion, which would suggest that there is a white dwarf in the system, there is no direct evidence to show the presence of a white dwarf. Bearing in mind the O-rich nature of the Mira it seems likely that a thermonuclear runaway on a white dwarf would be required to produce an overabundance of carbon which could then condense to form a carbon based dust.

The presence of a nebular continuum at a temperature of 2×10^4K is interesting. It is unlikely that the AOV star at a blackbody temperature of 9000 K could excite to such a continuum. Penston et al., (1983) from their ultraviolet studies, note that their estimate of the flux ($\lambda < 912$A) to the flux ($1200 < \lambda < 3250$A) suggests an exceedingly hot component in the system. Indeed for a blackbody this ratio would give $T > 7 \times 10^4$K. It is probably this hot ionizing source that is exciting the nebular continuum.

Table A.1

Infrared Photometric Observations of RR Tel.

λ(μm)	MAGNITUDE	FLUX (Jy)	COMMENTS	
4.9	2.6	14.41	-	(1)
4.9	2.85	11.09	SAAO 28/6/85	
8.6	1.9	9.3	-	(1)
10.0	0.41	25.35	28/6/72	(2)
10.0	1.21	12.13	SAAO 28/6/85	
11.3	0.6	18.3	-	(1)
12.0		23.22	IRAS AO's 4/4/83	(3)
12.0		19.00	IRAS AO's 13/10/83	(4)
12.0		20.00	IRAS AO's 19/10/83	(4)
12.0		20.00	IRAS AO's 24/10/83	(4)
12.0		20.00	IRAS AO's 13/11/83	(4)
12.0		19.88	IRAS PSC	
12.0		27.58	IRAS LRS	
18.0	-0.8	29.35	-	(1)
20.0	-0.75	19.36	28/6/72	(2)
25.0		27.34	IRAS AO's 4/4/83	(3)
25.0		16.00	IRAS AO's 13/10/83	(4)
25.0		17.00	IRAS AO's 19/10/83	(4)
25.0		15.00	IRAS AO's 24/10/83	(4)
25.0		15.00	IRAS AO's 13/11/83	(4)
25.0		16.42	IRAS PSC	
60.0		9.53	IRAS AO's 4/4/83	(3)
60.0		3.00	IRAS AO's 13/10/83	(4)
60.0		2.80	IRAS AO's 19/10/83	(4)
60.0		2.80	IRAS AO's 24/10/83	(4)
60.0		2.80	IRAS AO's 13/11/83	(4)

60.0	2.62	IRAS PSC	
100.0	<1.05	IRAS PSC	
100.0	0.89	IRAS AO's 13/10/83	(4)
100.0	0.93	IRAS AO's 19/10/83	(4)
100.0	1.00	IRAS AO's 24/10/83	(4)
100.0	0.77	IRAS AO's 13/11/83	(4)

Data taken from:

(1) Gehrz et al. (1973), (2) Glass & Webster (1973),

(3) Evans et al. (unpublished), (4) Kenyon et al. (1986).

A.5 IRAS

IRAS observed RR Tel both as part of the general survey and in its pointed observations (AO's). (See Chapter 4 for explanation of IRAS operations). All IRAS observations of this object are given in Table A.1. Figs. A.5 show the detections of RR Tel in IRAS bands I, II and III as observed on 1983 April 4. Fig. A.6 shows the IRAS LRS of RR Tel (IRAS Science Team, 1986). We can see that the silicate feature extends from ~ 8μm → ~ 13μm so any variability in band I is almost certainly caused by the changes in this feature. Because of the errors on the fluxes from IRAS (~ 10% on the AO's; Kenyon et al., 1986) it is difficult to tell whether or not there is indeed a significant variability at the other IRAS wavelengths. However due to the variability of the ultraviolet emissiom lines (Hayes & Nussbaumer, 1986) it is possible that in IRAS band III changes in flux may be caused by variable emission lines such as [OIII], which has features at ~ 52μm and 88μm.

A.6 Conclusion

The symbiotic star RR Tel has proved to be a most interesting object. The SAAO observations seem to confirm the presence of an early type main sequence star in the system, suggested by earlier ultraviolet studies, whilst the presence of two types of dust in the system is also comfirmed. It is this dust that poses the greatest problem. Previous infrared studies had indicated that the carbon based dust is not heated by the Mira component but the variability of the system at ~ 10μm implied that the silicate dust is. It is therefore suggested that the carbon based dust was formed in the nova ejecta of 1944 and has since dispersed around the entire system whilst the silicate dust is formed by the Mira itself. Since the nova explosion in 1944 the silicate dust has been re-established around the secondary. In such a scenario the presence of a white dwarf is desirable

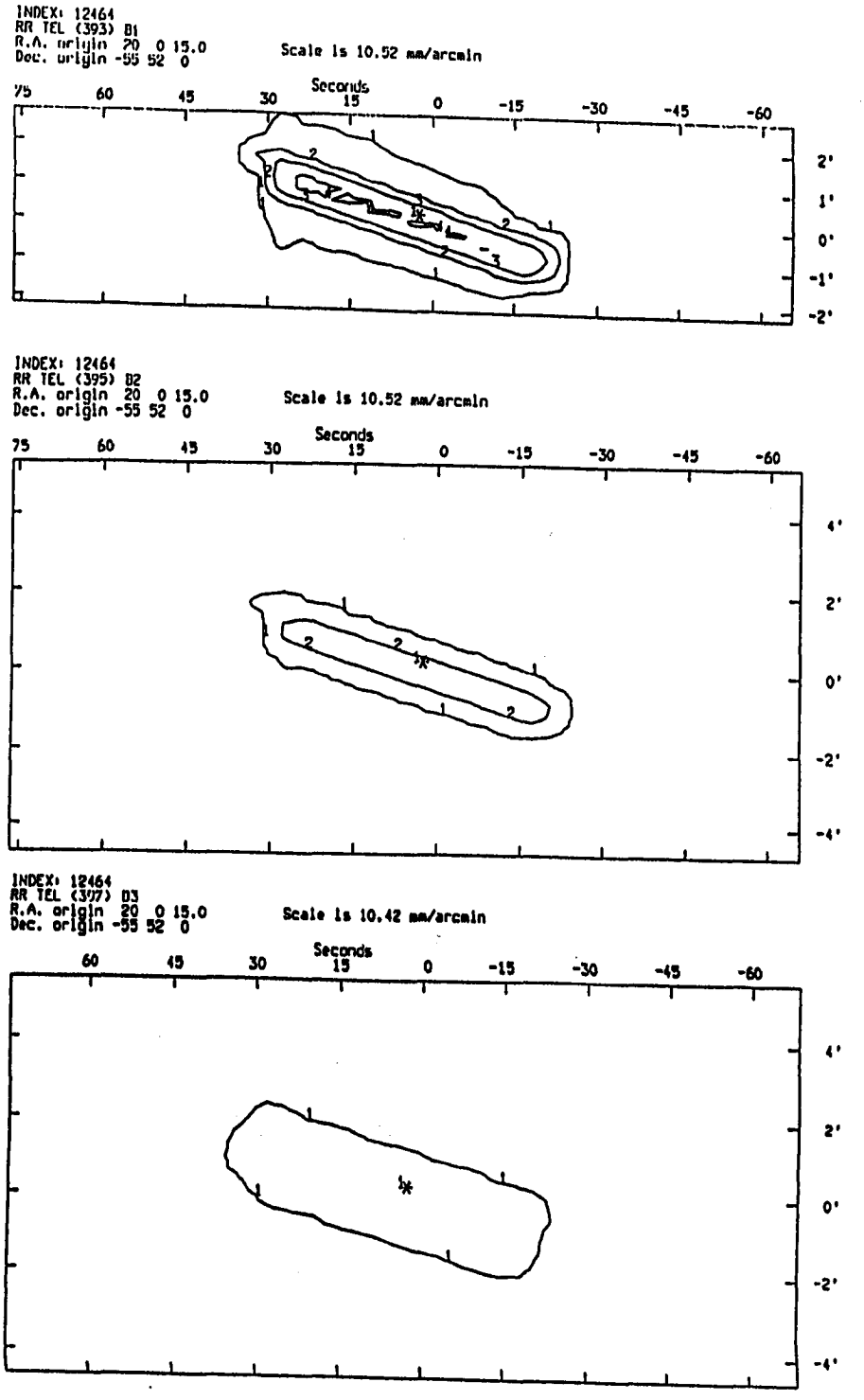

Figures A.5 IRAS detections of RR Tel in bands I, II & III.

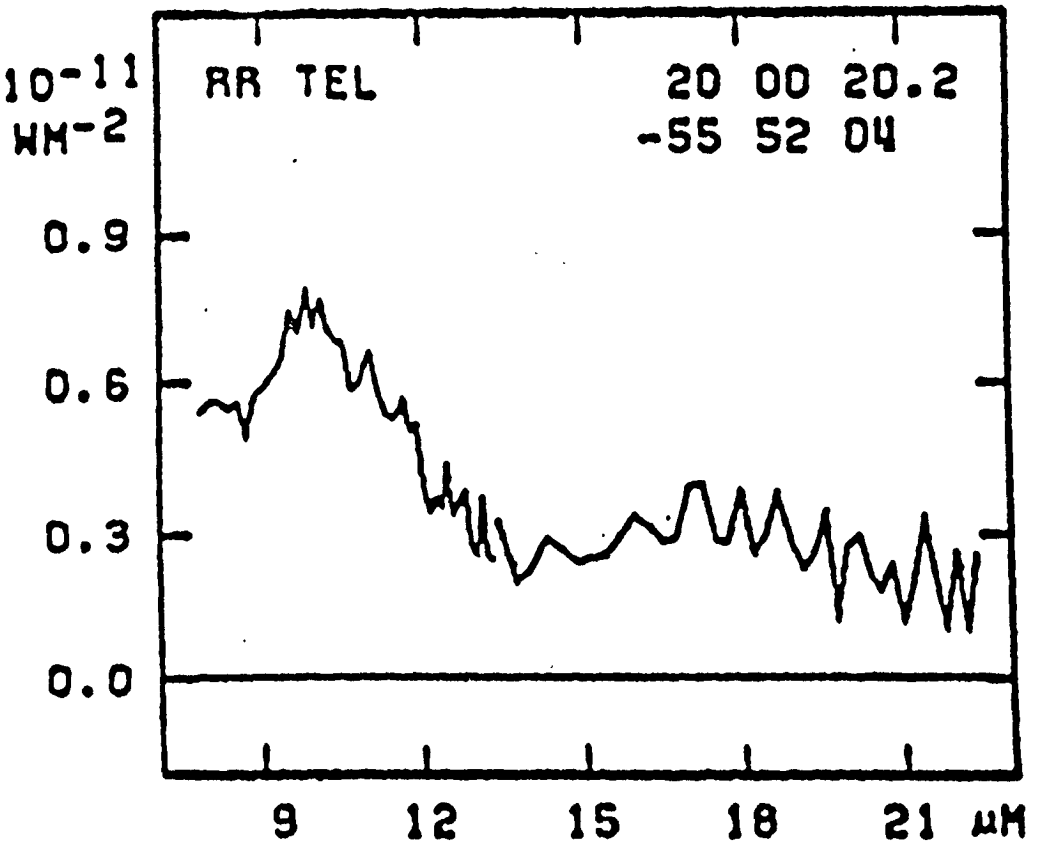

Figure A.6 IRAS LRS of RR Tel.

as a TNR is required to produce the necessary amount of carbon that will produce the dust. As yet the presence of a white dwarf has not been directly confirmed. It would therefore be extremely useful if this star could be monitored in x-rays where an accretion disc (if there is one) will exhibit the greatest effect and thus suggest parameters for the type of primary star. It is essential that the star is regularly monitored at all wavelengths if we are to truly understand its nature.

APPENDIX II

LIST OF PUBLICATIONS.

Callus C. M., Albinson J. S., Evans A. & Bode M. F., in 'Light on Dark Matter', ed. F. Israel, D. Reidel, Holland, p149, 1986.
"IRAS Observations of Classical Novae".

Callus C. M., Evans A. & Albinson J. S., Irish A. J., **17**, 330, 1986.
"Circumstellar Matter in the Recurrent Nova RS Ophiuchi".

Callus C. M., Albinson J. S. & Evans A., Astrophys. Space Sci., **131**, 437, 1987.
"Nucleation in Novae".

Callus C. M., Evans A., Albinson J. S., Mitchell R. M., Bode M. F., Jameson R., King A. R. & Sherrington M. R., MNRAS, in press.
"IRAS Additional Observations of Classical Novae".

REFERENCES

Adams W. S., Humason M. L. & Joy A. H., PASP, **39**, 365, 1927.

Adams W. S. & Joy A. H., PASP, **45**, 249, 1933a.

Adams W. S. & Joy A. H., PASP, **45**, 301, 1933b.

Aitken D. K. , Roche P. F. & Allen D. A., MNRAS, **200**, 69P, 1982.

Albinson J. S., Bode M. F., Evans A. & Goldsmith M. J., IAU Circ., no. 4091, 1985.

Allen C. W., Astrophysical Quantities, The Athlone Press, University of London, 1973.

Allen D. A., Beattie D. H., Lee T. J., Stewart J. M. & Williani P. M., MNRAS, **182**, 57P, 1978.

Allen D. A. in 'The Nature of Symbiotic Stars', eds. M. Friedjung & R. Viotti, D. Reidel Dordrecht, p27, 1982.

Allen D. A., Proc. ASA, **5**, 369, 1984.

Andrillat Y. & Houziau L., IAU Circ., no.3969, 1984.

Anupama G. C. & Prabhu T. P., in 'RS Ophiuchi (1985) and the Recurrent Novae Phenomenon', ed. M. F. Bode, VNU Science Press, p17, 1986.

Arsenijevic' J. & Vince I., Sov. Astron., **21**, 370, 1977.

Baas F., Allamandola L. J., Geballe T. R., Persson S. E. & Lacy J. H., Ap. J., **265**, 290, 1983.

Baker J. G. & Menzel D. H., Ap. J., **88**, 52, 1938.

Barbon R., Mammano A. & Rosino L., in 'Non-Periodic Phenomena in Variable Stars', ed. L. Detre, Academic Press, Budapest, p257, 1968.

Barlow M. J. in 'Planetary Nebulae', ed. D. R. Flower, D. Reidel, p105, 1983.

Bath G. T. & Shaviv G., MNRAS, **175**, 305, 1976.

Bath G. T. & Shaviv G., MNRAS, **183**, 515, 1978.

Beichman C. A., Neugebauer G., Habing H. J., Clegg P. E. & Chester T. J., IRAS Explanatory Supplement, 1984.

Berriman G., Szkody P. & Capps R. W., MNRAS, **217**, 327, 1985.

Bertaud P. M. C., Bull. Astronomique (Paris), **14**, 61, 1949.

Blades J. C. & Whittet D. C. B., MNRAS, **191**, 701, 1980.

Bode M. F., Vitas in Astronomy, **26**, 369, 1982.

Bode M .F. & Evans A., Astron. Astrophys., **89**, 158, 1980.

Bode M. F. & Evans A., MNRAS, **197**, 1055, 1981.

Bode M. F., Evans A., Whittet D. C. B., Aitken D. K., Roche P. F., & Whitmore B., MNRAS, **207**, 897, 1984.

Bode M. F. & Evans A., MNRAS, **200**, 175, 1982a.

Bode M. F. & Evans A., Ap. J., **254**, 263, 1982b.

Bode M. F. & Evans A., Q. Jl. RAS, **24**, 83, 1983.

Bode M. F. & Evans A., MNRAS, **203**, 285, 1983b.

Bode M. F. & Evans A., Astron. Astrophys., **151**, 452, 1985.

Bode M. F. & Evans A., in 'The Classical Nova', eds. M. F. Bode & A. Evans, Wiley, in press.

Bode M. F. & Kahn F. D., MNRAS, **217**, 215, 1985.

Bowen I. S. & Swings P., Ap. J., **105**, 92, 1947.

Boyarchuk A. A., in 'Non-Periodic Phenomena In Variable Stars', ed. L. Detre, D. Reidel Dordrecht, p395, 1968.

Boyarchuk A. A., Irish Astron. J., **17**, 392, 1986.

Bruch A., Astron. Astrophys., **167**, 91, 1986a.

Bruch A., in 'RS Ophiuchi (1985) and the Recurrent Nova Phenomenon', ed. M. F. Bode, p13, 1986b.

Cahn J. H. & Wyatt S. P., Ap. J., **210**, 508, 1976.

Callus C. M., Albinson J. S., Evans A. & Bode M. F., in 'Light on Dark Matter', ed. F. Israel, D. Reidel, Holland, p149, 1986.

Callus C. M., Evans A. & Albinson J. S., Irish A. J., **17**, 330, 1986b.

Carter B., MSc Thesis, University of Cape Town, 1985.

Cassatella A., Hassell B. J. M., Harris A. & Snijders M. A.J., in 'Recent results on Cataclymic Variables', ESA SP236, p281, 1985.

Cassinelli J. P., Wegner G. A. & Wallerstein G., preprint.

Catchpole R. M., Glass I. S., Roberts G., Spencer Jones J. & Whitelock P. A., South African Astron. Obs. Circ., 9, 1, 1985.

Clayton D. D. & Hoyle F., Ap. J., **203**, 490, 1976.

Clayton D. D. & Wickramsinghe N. C., Astrophys. Space Sci., **42**, 463, 1976.

Code A. D., Ap. J., **151**, L145, 1968.

Collins P., IAU Circ., no. 4023, 1984.

Collin-Souffrin S., in 'Novae and Related Stars', ed. M. Friedjung, D. Reidel, Holland, p123, 1977.

Cohen M. & Kuhi L. V., MNRAS, **180**, 37, 1977.

Cohen M. & Vogel S. N., MNRAS, **185**, 47, 1978.

Connelley M. & Sandage A., PASP, **70**, 600, 1958.

Conti P. S., Ann. Rev. Astron. Astrophys., **16**, 371, 1978.

Cragg T. A., PASP, **71**, 47, 1958.

Davis R.J., in 'RS Ophiuchi (1985) and the Recurrent Nova Phenomenon', ed. M. F. Bode, p187, 1986.

Dinerstein H., Astron. J., in press, 1986.

Donn B., Wickramasinghe N. C., Hudson J. P. & Stecher T. P., Ap. J., **153**, 451, 1968.

Draine B. T., Ap. J., **245**, 880, 1981.

Draine B. T. & Lee H. M., Ap. J., **285**, 89, 1984.

Duerbeck H. W., Geffert M., Nelles B., Dummler R. & Nolte, IBVS, no. 2641, 1984.

Dufay P. J. & Bloch M., Annales d'Astrophysics, **27**, 462, 1964.

Dufay P. J., Bloch M., Bertaud C. & Dufay M., Annales d'Astrophysics, **27**, 555, 1964.

Ennis D., Becklin E. E., Beckwith S., Elias J., Gatley I., Matthews K., Neugebauer G. & Willner S. P., Ap. J., **214**, 478, 1977.

Eskioglu A. N., Annales d'Astrophysics, **26**, 331, 1963.

Evans A., in 'RS Ophiuchi (1985) and the Recurrent Nova Phenomenon', ed. M. F. Bode, VNU Science Press, p117, 1986.

Feast M. W. & Glass I. S., MNRAS, **167**, 81, 1974.

Feast M. W., Whitelock P. A., Catchpole R. M., Roberts G. & Carter B. S., MNRAS, **202**, 951, 1983.

Ferland G. J. & Shields G. A., Ap. J. (Lett)., **224**, L15, 1978.

Ferland G. J., Lambert D. L., Netzer H., Hall D. N. B. & Ridgeway S. T., Ap. J., **227**, 489, 1979.

Ferland G. J., Williams R. E., Lambert D. L., Shields G. A., Slovak M., Gondhalekar P. M., & Truran J. W., Ap. J., **281**, 194, 1984.

Flannery B. P., MNRAS, **170**, 325, 1975.

Fleming W. P., Circ. Harv. Coll. Obs., no. 143, 1908.

Franciosi, C., IAU Circ., no. 4033, 1985.

Frank J., King A. R., & Raine D. J., Accretion Power in Astrophysics, Cambridge University Press, 1985.

Friedjung M., in 'RS Ophiuchi (1985) and the Recurrent Nova Phenomena', ed. M. F. Bode, VNU Science Press, p77, 1986.

Friedjung M., in 'The Classical Nova', ed. M. F. Bode & A. Evans, Wiley, in press.

Fujimoto M. Y., Publ. Astron. Soc. Japan, **32**, 463, 1980.

Gallagher J. S., Astron. J., **82**, 209, 1977.

Gallagher J. S. & Code A. D., Ap. J., **189**, 303, 1974.

Gallagher J. S. & Ney E. P., Ap. J. (Lett)., **204**, L35, 1976.

Gallagher J. S. & Starrfield S., Ann. Rev. Astr. Astrophys., **16**, 171, 1978.

Gaposchkin S, Harv. Ann., **115**, 22, 1945.

Gehrz R. D., Ney E. P., Becklin E. E. & Neugebauer G., Ap. J. Lett, **13**, 89, 1973.

Gehrz R. D. & Hackwell J. A., Ap. J., **194**, 619, 1974.

Gehrz R. D., Grasdalen G. L. & Hackwell J. A., Ap. J., **237**, 855, 1980a.

Gehrz R. D., Hackwell J. A., Grasdalen G. L., Ney E. P., Neugebauer G. & Sellgren K., Ap. J., **239**, 570, 1980b.

Gehrz R. D., Hackwell J. A. & Grasdalen G. L., IAU Circ., no. 3711, 1982.

Gehrz R. D., Ney E. P., Grasdalen G. L., Hackwell J. A. & Thronson H. A., Ap. J., **281**, 303, 1984.

Gehrz R. D., Grasdalen G. L. & Hackwell J. A., Ap. J. (Lett)., **298**, L47, 1985a.

Gehrz R. D., Grasdalen G. L. & Hackwell J. A., IAU Circ., no. 4065, 1985b.

Gehrz R. D., Grasdalen G. L. & Hackwell J. A., IAU Circ., no. 4111, 1985c.

Glasby J. S., 'Variable Stars', Constable, 1968.

Glass I. S., MNRAS, **164**, 155, 1973.

Glass I. S & Webster B. L., MNRAS, **163**, 277, 1973.

Glass I. S., Mon. Notes Astron. Soc. S. Africa, **33**, 53, 1974.

Gorbatskii V. G., Sov. Astron. A. J., **16**, 32, 1972.

Greenhouse M., IAU Circ., no. 4065, 1985.

Grotrian W., Z. Fur. Astrophysik., **13**, 215, 1937.

Hatfield B. F. & Brodzik D., IAU Circ., no. 3082, 1977.

Hayes M. A. & Nussbaumer H., Astron. Astrophys., **161**, 287, 1986.

Heck A. & Manfroid J., ESO Messenger, **30**, 6, 1982.

Henize K. G. & McLaughlin D. B., Ap. J., **114**, 163, 1951.

Henning T. & Svatos J., Astron. Nachr., **307**, 49, 1986.

Hirst C. J. & Cudlip W., Starlink User Note 60.1, RAL, UK, 1984.

Hjellming R. M., Wade C. M., Vandeberg N. P. & Newell N. T., Astron. J., **84**, 1619, 1979.

Hjellming R. M., van Gorkom J. H., Taylor A. R., Seaquist E. R., Padin S., Davis R. J. & Bode M. F., Ap. J. Lett, **305**, L71, 1986.

Hoffmeister C., Richter G. & Wenzel W., Variable Stars, Spinger-Verlag, 1985.

Hoyle F., MNRAS, **106**, 343, 1946.

Hoyle F., MNRAS, **107**, 231, 1947.

Humason M. L., Ap. J., **88**, 228, 1938.

Hyland A. R. & Neugebauer G., Ap. J. (Lett), **161**, L101, 1970.

Iljima T. & Rosino L., PASP, **95**, 506, 1983.

IRAS Survey Team, Nature, **303**, 287, 1985.

IRAS Science Team, Astron. Astrophys. Suppl. Ser., **65**, 607, 1986.

Isles J. E., J. Brit. astr. Ass., **84**, 203, 1974.

ISO INFO, no. 1, ESA, 1986.

Jennings R. E., SRC IRAS Newsletter no. 1, 1980.

Jennings R. E., Cudlip W. & King K. J., SERC IRAS Newsletter no.10, 1983.

Joy A. H. & Swings P., Ap. J., **102**, 353, 1945.

Joy A. H., Ap. J., **133**, 493, 1961.

Kenyon S. J. & Gallagher J. S., Astron. J., **88**, 666, 1983.

Kenyon S. J., Fernandez-Castro T. & Stencel R. E., Astron J., **92**, 1118, 1986.

Kenyon S. J. & Wade R. A., PASP, **98**, 935, 1986.

Kitchen C. R., Early Emission Line Stars, Adam Hilger Ltd, 1982.

Knapp G. R., Chang K. M. & Morris M., in 'Mass Loss from Red Giants', eds. M. Morris & B. Zuckerman, D. Reidel, Holland, p159, 1985.

Kosai H., IAU Circ. no. 3963, 1984.

Kovetz A. & Prialnik D., Ap. J., **291**, 812, 1985.

Kraft R. P., Ad. Astron. Astrophys., **2**, 43, 1963.

Krautter J., Beuermann K., Leitherer C., Oliva E., Moorwood A. F. M., Deul E., Wargau W., Klare G., Kohoutek L., van Paradjis J. & Wolf B., Astron. Astrophys., **137**, 307, 1984.

Krautter J., Beuermann K. & Ogelman H., ESO Messenger, **39**, 25, 1985.

Krautter J., in 'RS Ophiuchi (1985) and the Recurrent Nova Phenomenon', ed. M. F. Bode, p23, 1986.

Lamb D. Q & Van Horn H. M., Ap. J., **200**, 306, 1975.

Laney D., IAU Circ. no. 4036, 1985.

Lang K. R., Astrophysical Formulae, Springer-Verlag, New York, 1974.

Livio M., Truran J. W. & Webbink R. F., Ap. J., **308**, 736, 1986.

MacDonald J., Fujimoto M. Y. & Truran J. W., Ap. J., **294**, 263, 1985.

Malakpour I., Astrophys. Space Sci., **47**, 49, 1977.

Martin P. G., in 'The Classical Nova', eds. M. F. Bode & A. Evans, Wiley, in press.

Mason K. O., Cordova F. A., Bode M. F. & Barr P., in 'RS Ophuichi (1985) and the Recurrent Nova Phenomenon', ed. M. F. Bode, 167, 1986.

Mathis J. S., Rumpl W. & Nordsieck K. H., Ap. J., **217**, 425, 1977.

Mazeh T., Netzer H., Shaviv G., Drechsel H., Rahe J., Wargau W., Blades J., Cacciari C. & Wamsteker W., Astron. Astrophys., **149**, 83, 1985.

McLaughlin D. B., Pub. Am. Ast. Soc., **8**, 145, 1935.

McLaughlin D. B., PASP, **61**, 74, 1949.

McLaughlin D. B., Stars & Stellar Systems, **6**, 585, 1960.

McLean I. S., MNRAS, **176**, 73, 1976.

Menzel D. H. & Pekeris C. L., MNRAS, **96**, 77, 1935.

Merrill P. W. & Bowen I. S., PASP, **63**, 255, 1951.

Mitchell R. M. & Evans A., MNRAS, **209**, 945, 1984.

Mitchell R. M., Evans A. & Bode M. F., MNRAS, **205**, 1141, 1983.

Mitchell R. M., Evans A. & Albinson J. S., MNRAS, **221**, 663, 1986.

Mitchell R. M., Robinson G., Hyland A. R. & Neugebauer G., MNRAS, **216**, 1057, 1985.

Ney E. P. & Hatfield B. F., Ap. J. (Lett)., **219**, L111, 1978.

Noskova R. I., Zaitseva G. V. & Kolotilovea, Sov. Astron. Lett., **11**, 257, 1985.

Nussbaumer H. in 'The Nature of Symbiotic Stars' eds. M. Friedjung & R. Viotti, D. Reidel Dordrecht, p85, 1982.

Ogelman H., Beuermann K. & Krautter J., Ap. J. (Lett)., **287**, L31, 1984.

Osterbrock D.E., Astrophysics of Gaseous Nebulae, Freeman, 1974.

Pacheco J. A. & Codina S. J., MNRAS, **214**, 481, 1985.

Paczynski B., Ann. Rev. Astron. Astrophys., **9**, 183, 1971.

Padin S., Davis R. J. & Bode M. F., Nature, **315**, 306, 1985.

Payne-Gaposchkin C., The Galactic Novae, Amsterdam, 1957.

Penston M. V., Benvenuti P., Cassatella A., Heck A., Selvelli P., Macchetto F., Ponz D., Jordan C., Cramer N., Rufener F. & Manfroid J., MNRAS, **202**, 833, 1983.

Phillips J. P., Wade R., Selby M. J. & Sanchez Magro C., MNRAS, **187**, 45p, 1979.

Piirola V. & Karhonen T., Astron. Astrophys., **79**, 254, 1979.

Porcas R. W., Davis R. J. & Graham D. A., in 'RS Ophiuchi (1985) and the Recurrent Nova Phenomenon', ed. M. F. Bode, VNU Science Press, p203, 1986.

Pottasch S. R., Bull. Astr. Inst. Netherlands, **19**, 227, 1967.

Prager R., Harvard Bulletin, **912**, 15, 1940.

Ridgway S. T., in 'Galactic and Extragalactic Infrared Spectroscopy', ed. M. F. Kessler & J. P. Phillips, D. Reidel, p309, 1984.

Robbins R. R. & Sanyal A., Ap. J., **219**, 485, 1978.

Roche P. F., Aitken D. K. & Whitmore B., MNRAS, **211**, 535, 1984.

Roche P. F., Allen D. A. & Aitken D. K., MNRAS, **204**, 1009, 1983.

Rosino L., in 'RS Ophuichi (1985) and the Recurrent Nova Phenomenon', ed. M. F. Bode, p1, 1986.

Rosino L., Bianchini A. & Rafanelli P., Astron. Astrophys., **108**, 243, 1982.

Rosino L., Iijima T. & Rafanelli P., IAU Circ., no. 3978, 1984.

Rosino L. & Iijima T., in 'RS Ophuichi (1985) and the Recurrent Nova Phenomenon', ed. M. F. Bode, p27, 1986.

Rosino L. & Iijima T., Astrophys. Space Sci., **130**, 157, 1987.

Rybicki G. B. & Lightman A. P., 'Radiative Processes in Astrophysics', John Wiley & Sons Ltd., 1979.

Sandford R. F., PASP, **59**, 331, 1947.

Sanyal A., Astrophys. J. Supp., **28**, 115, 1974.

Sayer A. R., Harvard Annals, **105**, 21, 1937.

Schatzman E., Bul. Ac. Roy. Belg. Cl. Sci., **34**, 828, 1948.

Schatzman E., Annules d'Astrophysique, **12**, 281, 1949.

Schmelz J. T., Ap. J., **89**, 108, 1984.

Schmidt T., Z. Astrophys., **41**, 182, 1957.

Schwarzschild M., Structure and Evolution of the Stars, Dover, 1958.

Seeliger, A. N., **130**, 393, 1892.

Shara M. M., in 'Novae, Dwarf Novae and Other Catalysmic Variables', University of Rochester, p526, 1980.

Shara M. M., Ap. J., **243**, 926, 1981.

Shylaja B. S., Astrophys. Space Sci., **104**, 163, 1984.

Slovak M. H. in 'Advances in UV astronomy: Four years of IUE Research', eds. Y. Kondo, J. M. Mesel & R. D. Chapman, NASA Conf. Publ., p448, 1982.

Snijders M. A. J., Batt T. J., Seaton M. J., Blades J. C. & Morton D. C., MNRAS, **211**, p7, 1984.

Snijders M. A. J., in 'RS Ophiuchi (1985) and the Recurrent Nova Phenomenon', ed. M. F. Bode, VNU Science Press, p51, 1986.

Snijders M. A. J., Astrophys. Space Sci., **30**, 243, 1987.

Sowell J. R., Laird J. B. & Thorstensen J. R., IBVS, no. 2700, 1985.

Sparks W. M., Starrfield S. & Truran J. W., in 'Novae and Related Stars', ed. M. Friedjung, D. Reidel, p189, 1977.

Spitzer L., 'Physical Processes in the Interstellar Medium', Wiley, 1978.

Spoelstra T. A. T., Taylor A. R., Pooley G. G., Evans A. & Albinson J. S., MNRAS, **224**, 791, 1987.

Starrfield S., Sparks W. M. & Truran J. W., Ap. J., **192**, 647, 1974.

Stratton F. J. M., Handbuch Der Astrophysik, **6**, 294, 1928.

Stratton F. J. M., MNRAS, **105**, 275, 1946.

Strecker D. W., Erickson E. F. & Witteborn F. C., Ap. J. Suppl., **41**, 501, 1979.

Svolopoulos S. N., PASP, **78**, 157, 1966.

Swings J. P. & Allen D. A., PASP, **84**, 523, 1972.

Swings P. & Struve O., Ap. J. **94**, 291, 1941.

Swings P. & Struve O., Ap. J., **97**, 194, 1943.

Szkody P., Ap. J., **217**, 140, 1977.

Szkody P., Dyck H. M., Capps R. W. & Becklin E. E., Astron J., **84**, 1359, 1978.

Tempesti P., Astron. Nachrichten Bd., 300, 51, 1979.

ter Haar D., MNRAS, 106, 283, 1946.

Thackeray A. D., Mem. R. astr. Soc., 83, 1, 1977.

Tolbert C. R., Pecker J. C. & Pottasch S. R., Bull. Astr. Inst. Netherlands, 19, 17, 1967.

Truran J. W., Starrfield S., Strittmatter P. A., Wyatt S. P. & Sparks W. M., Ap. J., 211, 539, 1977.

Truran J. W., in 'Essays on Nuclear Astrophysics, ed. C. A. Barnes, D. D. Clayton & D. N. Schramm, Cambridge University Press, p467, 1982.

Tucker W. H., Radiation Processes in Astrophysics, MIT Press, 1975.

Vogt N., in 'The Classical Nova', ed. M. F. Bode & A. Evans, Wiley, in press.

Vrba F. J., Schmidt G. D. & Burke E. W., Ap. J., 211, 480, 1977.

Wakuda M., IAU Circ., no. 3777, 1983.

Wakuda M., Hamamatsu & Shizuoka, IAU Circ., no. 3778, 1983.

Wallerstein G., PASP, 70, 537, 1958.

Wallerstein G., PASP, 75, 26, 1963.

Wallerstein G., PASP, 81, 672, 1969.

Wallerstein G. & Cassinelli J. P., PASP, 80, 1968.

Warner B., MNRAS, 162, 189, 1973.

Webster B. L. in 'Stellar Instability and Evolution', IAU Symp. 59, eds. P. Ledoux, A. Noels & A. W. Rodgers, D. Reidel Dordrecht, p123, 1974.

Whitelock P. A., Feast M. W., Roberts G., Carter B. S. & Catchpole R. M., MNRAS, 205, 1207, 1983.

Whitelock P. A., Carter B. S., Feast M. W, Glass I. S., Laney D., Menzies J. W., Walsh J. & Williams P. M., MNRAS, 211, 421, 1984.

Williams R. E., Sci. Am., 244, 96, 1981.

Williams R. E., Sparks W. M., Gallagher J. S., Ney E. P., Starrfield S. & Truran J. W., Ap. J., **251**, 221, 1981.

Williams P. M. & Longmore A., IAU Circ., 3676, 1982.

Williams R. E., Ney E. P., Sparks W. M., Starfield S. G., Wyckoff S. & Truran J. W., MNRAS, **212**, 753, 1985.

Willis A. J. & Wilson R., MNRAS, **182**, 559, 1978.

Wilson O. C. & Williams E. G., Ap. J., **80**, 344, 1934.

Wu C. C & Kester D., Astron. Astrophys., **58**, 331, 1977.

Yamamoto T. & Hasegawa H., Prog. Th. Phys., **58**, 816, 1977.

Yamamoto T. & Nishida S., Prog. Th. Phys., **57**, 1939, 1977.

Yamamoto T., Sato S. & Nariai K., Publ. Astron. Soc. Japan, **31**, 691, 1979.

Yamamoto T. & Seki J., Astrophys. Space Sci., **64**, 153, 1979.

Zellner B., Astron. J., **76**, 651, 1971.